

**CHARACTERIZATION OF URBAN CANOPY
PARAMETERS AND THEIR RELATIONSHIP WITH
SPATIALLY VARIABLE URBAN CLIMATE INDICATORS**

Ph. D. THESIS

by

KSHAMA GUPTA



**DEPARTMENT OF ARCHITECTURE AND PLANNING
INDIAN INSTITUTE OF TECHNOLOGY ROORKEE
ROORKEE – 247 667 (INDIA)
JUNE, 2019**

**CHARACTERIZATION OF URBAN CANOPY
PARAMETERS AND THEIR RELATIONSHIP WITH
SPATIALLY VARIABLE CLIMATE INDICATORS**

A THESIS

*Submitted in partial fulfilment of the
requirements for the award of the degree*

of

DOCTOR OF PHILOSOPHY

in

ARCHITECTURE AND PLANNING

by

KSHAMA GUPTA



**DEPARTMENT OF ARCHITECTURE AND PLANNING
INDIAN INSTITUTE OF TECHNOLOGY ROORKEE
ROORKEE – 247 667 (INDIA)
JUNE, 2019**



**©INDIAN INSTITUTE OF TECHNOLOGY ROORKEE, ROORKEE-2019
ALL RIGHTS RESERVED**



INDIAN INSTITUTE OF TECHNOLOGY ROORKEE ROORKEE

CANDIDATE'S DECLARATION

I hereby certify that the work which is being presented in the thesis entitled **“CHARACTERIZATION OF URBAN CANOPY PARAMETERS AND THEIR RELATIONSHIP WITH SPATIALLY VARIABLE CLIMATE INDICATORS”** in partial fulfilment of the requirements for award of the Degree of Doctor of Philosophy and submitted in the Department of Architecture and Planning of the Indian Institute of Technology Roorkee, is an authentic record of my own work carried out during the period from July, 2012 to June, 2019 under the supervision of Dr. Pushplata, Department of Architecture and Planning, Indian Institute of Technology Roorkee, Roorkee.

The matter presented in the thesis has not been submitted by me for the award of any other degree of this or any other Institute.

(KSHAMA GUPTA)

This is to certify that the above statement made by the candidate is correct to the best of my knowledge.

(Pushplata)
Supervisor

The Ph. D. Viva-Voce Examination of, Research Scholar, has been held on.....

Chairman, SRC

Signature of External Examiner

This is to certify that the student has made all the corrections in the thesis.

(Pushplata)

Head of the Department

Supervisor

Dated: _____

ABSTRACT

Urban areas occupy 3% of ice free land area but are cumulatively responsible for emission of 75% of Green House Gases (GHGs), therefore contribute significantly in global warming. Developing regions are expected to house nearly 90% of future growth by 2050 with 35% of the growth concentrated in just three countries – India, China and Nigeria. Apart from the high pressure of urban growth in these regions, inadequate infrastructure and lack of implementation of planned urban development is going to exacerbate a number of climatic and environmental problems such as heat stress, air pollution, global warming, and increased use of artificial energy, storm water runoff, and overall environmental degradation in these regions. Increased frequency of natural disasters and extreme weather events in these regions calls for scientific understanding of impact of urban areas on climate and vice versa to ensure sustainable development and to mitigate climate change impacts.

Lack of information on Urban Canopy Parameters (UCPs) is considered as one of the major reason behind limited urban climate research and modeling in developing regions. Availability of detailed information on UCPs is critical for urban climate studies as well as for implementation of recent Urban Canopy Models (UCMs) for scientific understanding of climatic phenomenon in these regions. Urban Canopy parameters define those characteristics of urban built form which has direct or indirect bearing on urban climate. Most of the studies in developed world have utilised 3D GIS database either developed from ground survey or remotely sensed data such as Aerial Photographs, Airborne LiDAR and high resolution InSAR data for retrieval of UCPs. However, nonexistence of 3D GIS database and non-availability of above RS datasets in developing regions necessitates to employ widely available alternative datasets for retrieval of UCPs. Hence, this study focuses on retrieval of UCPs by employing Very High Resolution Satellite (VHRS) optical stereo data in highly dense and complex urban environment of Delhi, India. Not many studies have explored the use of VHRS data for extraction of UCPs, however, the repeat availability, extensive coverage and low cost makes this data much suitable for generation of UCPs. It further dwells into the demonstration of retrieved UCPs for urban climatic applications in the study region.

Although, the impact of 3D UCPs on urban climate is significant and it is considered as one of the main contributor to UHI phenomenon. However, a very few studies have analyzed relationship of 3D UCPs such as building height, frontal area index, floor area ratio and sky view factor with spatially variable climate indicators such as RS derived Land Surface Temperature

(LST) and it remained largely unexplored even for the regions having highly planned urban infrastructure. Hence, the study also aims to analyze the relationship of generated UCPs especially 3D UCPs with spatially variable climate indicators.

The Delhi Urban Agglomeration (UA), which is the third largest UA of the world and largest UA of India, has been selected as the study area due to its sprawled, highly heterogeneous and complex development characteristics of urban built form, high air pollution levels, high anthropogenic pressure and challenging composite climate.

A novel step-by-step methodology has been developed in this study to extract key UCPs such as building height, building surface fraction and wall area ratio from VHRS optical stereo data in complex urban environment of study region. Photogrammetric processing of VHRS optical stereo data (Pleiades1A/1B) has been carried out to obtain Digital Surface Model (DSM), Digital Terrain Model (DTM), normalized DSM (nDSM) and ortho images which have been further employed to retrieve key UCPs. The nDSM contains the height of all above-ground objects that includes vegetation, building and all elevated objects. The key UCPs thus retrieved have been employed to compute other UCPs in complex urban environment of Delhi. The validation of key UCPs derived through VHR optical stereo images has shown good accuracy with ground measurements. The Mean error, RMSE and MAE for building heights has been found to be less than 1 m and Cumulative Random Error (CRE) ranged from 2.5% to 9.9% in high-rise to low-rise development respectively. The other key UCPs such as Land Use Land cover (Accuracy ~ 85%), Building Surface Fraction (BSF) (Accuracy ~84.27%) and SVF (RMSE-0.046 and correlation-0.94) also displayed reasonable accuracy. It renders VHR optical stereo data a good choice for generation of UCPs especially in a highly heterogeneous urban built-up environment.

Characterization of UCPs in the study region revealed highly dense, heterogeneous and sprawled character which has significant impact on urban climate. High Building Surface Fraction value (>0.6) in more than 35% of built-up area has shown high building density while distribution of Mean building height in study area revealed a highly sprawled character of the study region as nearly 96% of buildings falls in the height range of 3 -21m. Only 4% of buildings have height more than 21m and building with more than 30 m in height are very few and are mainly found in the peripheral region. Nearly 50% of built-up area has standard deviation of building height more than 2 which is indicative of highly heterogeneous and complex development in the study region.

Generated UCPs were further utilized to demonstrate few applications of UCPs such as Ventilation assessment and GIS based Local Climate Zone (LCZ) map which can be utilized to understand and characterize the urban climate phenomenon as well as for urban climate research and modeling. The pixel based classification methodology proposed by World Urban database and Access Portal Tool (WUDAPT), which have been widely applied to collect data on urban form and function by utilizing free RS datasets and GIS software, provided poor accuracy (overall accuracy -49.43% and kappa ~0.46) of LCZ classification in the complex urban environment of study area. However, GIS based LCZ maps generated from application of detailed UCPs displayed high accuracy of classification (overall Accuracy >85% and kappa ~0.86) not only for the entire classification but even for each LCZ class.

Analysis of ventilation path maps showed merely 17% of built-up area as ventilated area. More than 45% area falls under weak or blocked ventilation and nearly 38% area is partially ventilated. The ventilation map of Delhi clearly brings out the lack of adequate ventilation in the study area which makes the city prone to severe air pollution in winter season and high UHI conditions. The unavailability of proper ventilation corridors retards the air flow within the built-up area resulted in very weak circulation and thereby restricts the continuous flow and exchange of fresh air in these regions.

The spatially variable climate indicators (LST, temperature at 2m and wind speed at 10m) for the assessment of relationship with UCPs, ventilation assessment and LCZ map have been obtained from Landsat 8 and WRF simulations. The primary results of UCPs-LST relationship revealed strong correlation with 2D UCPS while 3D UCPs other than building height and surface roughness length did not show strong correlation. For 3D UCPs, complete temperature data cube in horizontal as well as vertical direction may help in analyzing the relationship. The key UCPs which exhibited strong relationship with LST were utilized to analyze the variability of Surface Urban Heat Island (SUHI) across all four seasons in a year. SUHI intensities was found to be maximum during winter season while lowest during post-monsoon season across all UCPs.

The ventilation–LST relationship in study area revealed an interesting finding that well ventilated area has mean lower temperature and higher mean wind speed as compared to weak ventilation area. The difference in the mean temperature of both the classes were highest in monsoon season which raises serious concerns regarding the thermal comfort in built-up area. Although, the study area is mostly dry during the year, but, in monsoon season humidity level is more than 80% and slight increase in temperature leads to substantial increase in thermal stress. Analysis of GIS

based LCZ map with LST of all four seasons revealed that all the built-up LCZ classes other than open low rise and sparsely built LCZ exhibited more temperature than mean LST is all seasons. However, out of all built-up classes' heavy industry, large low rise and compact low rise exhibited maximum deviations from mean LST for most of the seasons.

The study recommends the use of VHRS optical stereo data for retrieval of 2D as well as 3D UCPs in complex and heterogeneous urban environment of developing regions. This is the next best suitable alternative available in the absence of Airborne LiDAR and aerial images data in the developing regions. Similarly, study also recommends use of retrieved UCPs for ventilation assessment and GIS based LCZ map in developing regions. Availability of information on UCPs has substantial potential for understanding the climate characteristics of urban areas in developing regions, carrying out urban climate research, improved modeling of urban climate phenomenon and climate oriented urban planning to mitigate climate change impacts and to ensure sustainable development.

ACKNOWLEDGEMENT

The work presented in this thesis would not have been possible without the support and encouragement extended by many people throughout this journey. I take this opportunity to extend my sincere gratitude and appreciation to all those who made this Ph.D thesis possible.

First and foremost, I would like to extend my sincere gratitude to my research guide Dr. (Mrs.) Pushplata for being patient with me and extending me the complete freedom to explore the field of study at my own pace. I sincerely thank her for dedicated help, advice, inspiration, encouragement and continuous support, throughout my Ph.D. Her enthusiasm, integral view on research and her mission for providing high-quality work, has made a deep impression on me. I am really glad to be associated with her in my life. My special words of thanks should also go to my research committee members Dr. P S Chani, Dr. Mahua Mukherjee and Dr. R D Garg and earlier Dr. P K Garg for their continuous support, guidance and encouragement. Thanks are also due to Director/s, IIT, Roorkee for giving me this opportunity to carry out PhD research in their esteemed institution.

I would like to sincerely thank Dr. P S Roy, Former Director, IIRS and Dr. S K Saha, Former Dean Academics, IIRS who gave me permission to pursue PhD at IIT, Roorkee. My heartfelt thanks are due to Sh. PLN Raju, now Director, NESAC, Shillong and Former Group Head, IIRS who encouraged me and gave me the confidence to take up PhD at IIT, Roorkee. I sincerely thank Dr. YVN Krishna Murthy, Former Director, IIRS, Dr. A. Senthil Kumar, Former Director, IIRS and current Director, CSSTE-AP and Dr. Prakash Chauhan, Director, IIRS for facilitating me by providing all necessary infrastructure to carry out my research work. I would like to express my sincere gratitude to Dr. S K Srivastava, Dean Academics, IIRS for his faith and constant encouragement. I thank Sh. Pramod Kumar, Group Head, URSD for his constant support and facilitation.

I would also like to thank external examiners for their critical review and valuable suggestions. My sincere and heartfelt gratitude is due to Dr. Arijit Roy, Head, Disaster management Studies, IIRS for his scientific inputs, critical and constructive suggestions throughout my research work. Without his guidance, it would have been impossible for me to complete my PhD thesis. I would like to thank my immediate colleagues at URSD, IIRS especially Dr. Sandeep Maithani for sharing the workload and encouraging me to complete thesis writing. I sincerely thank Dr. Praveen Thakur, WRD, IIRS for his help to initiate the work in WRF model and Sh. Prasun Kumar Gupta, GID, IIRS for programming support. I would like to thank Regional Meteorological Centre, Delhi for providing the ground observation data of meteorological variables. I would also like to thank Dr. Yogita Shukla, who kindly consented to

read my thesis and provided moral support and valuable inputs for editing of thesis report. Thanks are also due to my friend Dr. Ashutosh Bhardwaj, IIRS and PhD research scholars of IIT Roorkee Dr. Tejas Rawal, Sh. Dinesh Singh, Ms. Harsimran Kaur, Dr. Mansha Swami and Sh. Suryendu for being a mainstay of moral support throughout the duration of PhD. I would also like to thank Sh. Aniruddha Debnath, Ms. A. Lalitha, Ms. M. Bhavana, Sh. Alok Jhaldiyal, Ms. Sumandeep, Ms. Sabi and Ms. Shweta with the lab work.

I am what I am today because of my parents who taught me upright values and always being a strong pillar of strength in my life. Their presence in my life and unconditional love had always inspired me to achieve big in life. Their patience and sacrifice will remain my inspiration throughout my life. I owe deepest gratitude to my children and my husband who had silently suffered throughout my journey of ups and downs and always being supportive whole heartedly. Without their help, it was almost impossible to achieve what I had achieved in my research work and PhD. I also like to thank sincerely all my teachers and colleagues who directly and indirectly supported me, had faith in my capabilities and being instrumental in enriching my personality and realizing my potential throughout my life specially Ms. Madhu Agarwal, Ms. Kalpana Pandit, Dr. Mahavir, Late Sh. Premnath Singh, Late Dr. S.K. Pathan, Dr. N. Sridharan, Late Dr. A K Tiwari, Sh. Sudhir Kumar, Sh. Kamal Pandey, Ms. Suji Mol, Dr. John Mathew and Sh. Balasubramani.

Last but not the least I thank GOD almighty for always being there throughout my ups and downs. I gratefully acknowledge ISRO for providing me opportunity and support and I am thankful to GIT&DL and CMA staff of IRS, library staff and administrative staff of IIRS and IIT, Roorkee for cooperation.

Kshama Gupta

Table of Contents

CHAPTER 1	INTRODUCTION.....	1
1.1	OVERVIEW	1
1.2	RESEARCH BACKGROUND.....	1
1.3	RESEARCH GAPS.....	6
1.4	RESEARCH QUESTIONS.....	7
1.5	AIM AND OBJECTIVES.....	7
1.6	RESEARCH METHODOLOGY	7
1.7	SCOPE AND LIMITATIONS	9
1.7.1	Scope.....	9
1.7.2	Limitations	9
1.8	ORGANIZATION OF THESIS.....	10
CHAPTER 2	LITERATURE REVIEW.....	13
2.1	INTRODUCTION.....	13
2.2	URBANIZATION AND CLIMATE CHANGE	13
2.3	URBAN CLIMATE	15
2.4	URBAN BUILT FORM AND URBAN MICRO CLIMATE	17
2.5	URBAN CANOPY PARAMETERS	18
2.6	METHODS FOR ESTIMATION OF AERODYNAMIC ROUGHNESS PARAMETERS	29
2.6.1	Reference (classification) based methods.....	29
2.6.2	Micrometeorological method.....	29
2.6.3	Morphometric methods.....	30
2.6.4	Micrometeorological vs. Morphometric methods	30
2.7	GEOSPATIAL TECHNOLOGIES FOR SPATIALLY VARIABLE URBAN CANOPY PARAMETERS.....	31
2.7.1	Surface cover characterization.....	32
2.7.2	3D Building database and urban canopy parameters.....	33

2.7.3	Sky View Factor	35
2.8	METHODS FOR SPATIALLY VARIABLE URBAN CLIMATE INDICATORS...	36
2.8.1	Thermal Remote Sensing.....	37
2.8.2	Numerical Modeling.....	38
2.9	RELATIONSHIP BETWEEN SPATIALLY VARIABLE URBAN CANOPY PARAMETERS AND CLIMATE INDICATORS.....	40
2.10	IMPLICATIONS AND APPLICATIONS OF URBAN CANOPY PARAMETERS FOR URBAN CLIMATE STUDIES.....	42
2.10.1	Ventilation assessment.....	42
2.10.2	GIS based Local Climate Zone.....	43
2.10.3	Urban climate maps	45
2.10.4	Urban Climate Research and modeling	46
2.11	SUMMARY	48
CHAPTER 3	STUDY AREA CONTEXT.....	49
3.1	INTRODUCTION.....	49
3.2	LOCATIONAL CHARACTERISTICS.....	49
3.3	HISTORICAL EVOLUTION AND URBAN BUILT FORM	51
3.4	DEMOGRAPHIC AND SPATIAL GROWTH OF DELHI URBAN AGGLOMERATION AND COMPOSITION OF INTERSTATE URBAN AREA	56
3.5	CLIMATE.....	58
3.5.1	Air Pollution	61
3.5.2	Urban Heat Island	61
3.5.3	Prevailing Wind Direction.....	62
3.6	SUMMARY	63
CHAPTER 4	CHARACTERIZATION OF URBAN CANOPY PARAMETERS	65
4.1	INTRODUCTION.....	65
4.2	DATA USED	66
4.3	METHODOLOGY.....	68
4.3.1	Data preprocessing.....	68

4.3.2	Land Use Land Cover Map.....	72
4.3.3	Road and Metro Rail network Map	73
4.3.4	Sky View Factor (SVF)	74
4.3.5	Building Height, Mean Building Height and Standard Deviation of Height Map.....	75
4.3.6	Surface Cover Characterization	76
4.3.7	Building Volume.....	78
4.3.8	Volumetric Averaged Height.....	78
4.3.9	Complete Wall Surface Area	79
4.3.10	Complete Aspect Ratio	80
4.3.11	Building Surface area to Plan Area Ratio	80
4.3.12	H/ W ratio	80
4.3.13	Zero Plane Displacement Height	81
4.3.14	Surface Roughness Length	81
4.4	RESULTS	82
4.4.1	Digital Surface Model Generation	82
4.4.2	Digital Terrain Model	82
4.4.3	nDSM (Normalized Digital Surface Model) Generation.....	84
4.4.4	Land use/Land Cover map.....	85
4.4.5	Building Height Map	86
4.4.6	Building Surface Fraction.....	90
4.4.7	Impervious Surface Fraction.....	92
4.4.8	Pervious Surface Fraction.....	93
4.4.9	Building Volume.....	95
4.4.10	Height-to-Width Ratio	96
4.4.11	Building Surface Area to Plan Area Ratio.....	98
4.4.12	Complete Aspect Ratio	99
4.4.13	Sky View Factor Map.....	100

4.4.14	Zero Plane Displacement Height	102
4.4.15	Surface Roughness Length	103
4.5	DISCUSSION	104
4.5.1	Validation of Digital Terrain Model and Building Heights.....	104
4.5.2	Retrieval of Urban Canopy Parameters	106
4.5.3	Characterization of Urban Canopy Parameters in study area	108
4.5.4	Effect of grid size.....	111
4.6	SUMMARY	111
CHAPTER 5 URBAN CANOPY PARAMETERS AND THEIR RELATIONSHIP WITH URBAN CLIMATE INDICATORS		113
5.1	INTRODUCTION.....	113
5.2	MATERIALS AND METHODS.....	115
5.2.1	Land Surface temperature	115
5.2.2	Weather Research and Forecasting Model Simulations	121
5.2.3	Relationship between Urban Canopy Parameters and urban climate Indicators	130
5.3	RESULTS	131
5.3.1	Land Surface Temperature.....	131
5.3.2	WRF Model Simulations	131
5.4	DISCUSSIONS.....	142
5.4.1	UCPs-LST relationship and seasonal variability	142
5.4.2	Spatio- seasonal variability of SUHI intensities	144
5.4.3	Diurnal- seasonal variability of Urban Heat Island Intensity	147
5.4.4	Methodological and operational concerns	150
5.5	SUMMARY	152
CHAPTER 6 APPLICATION OF URBAN CANOPY PARAMETERS FOR URBAN CLIMATE STUDIES		155
6.1	INTRODUCTION.....	155
6.2	METHODOLOGY	157

6.2.1	Ventilation assessment map.....	157
6.2.2	Local Climate Zone map.....	160
6.3	RESULTS	164
6.3.1	Ventilation Assessment.....	165
6.3.2	WUDAPT Local Climate Zone Map	166
6.3.3	GIS based Local Climate Zone Map.....	167
6.3.4	Accuracy Assessment	171
6.4	DISCUSSIONS	171
6.4.1	Criteria for Ventilation path assessment.....	171
6.4.2	Relationship of Ventilation assessment map with spatially variable climate indicators	172
6.4.3	Effect of Scale in LCZ classification	178
6.4.4	WUDAPT and GIS based Local Climate Zone	184
6.4.5	Role of seasonality in LCZ classification	185
6.4.6	Relationship of Local Climate Zone Map with Land Surface Temperature.....	186
6.5	SUMMARY	188
CHAPTER 7	CONCLUSION, RECOMMENDATIONS AND SCOPE FOR FURTHER RESEARCH	189
7.1	INTRODUCTION.....	189
7.2	KEY FINDINGS AND CONCLUSIONS	189
7.2.1	General Observations.....	189
7.2.2	Retrieval of Urban Canopy Parameters	191
7.2.3	Characterization of Urban Canopy Parameters in study region	191
7.2.4	Challenges faced in the retrieval of Urban Canopy Parameters	193
7.2.5	Application of Urban Canopy Parameters	193
7.2.6	Relationship of UCPs with Spatially variable climate indicators.....	194
7.2.7	Relationship of ventilation assessment and GIS based LCZ map with Climate indicators	195
7.3	MAJOR CONTRIBUTIONS OF THE RESEARCH STUDY	196

7.4	KEY RECOMMENDATIONS	198
7.4.1	Urban Canopy Parameters	198
7.4.2	Implications for urban climate studies, research and modeling.....	199
7.4.3	Implications for urban planning.....	200
7.5	SCOPE FOR FURTHER RESEARCH	201
7.5.1	Urban Canopy Parameters	201
7.5.2	Choice of Grid Size.....	202
7.5.3	Spatially Variable Urban Climate indicators	203
7.5.4	Application of Urban Canopy Parameters	204
7.5.5	Urban climate Research and Modeling.....	204
	BIBLIOGRAPHY	207
	Appendix A: Description of Local Climate Zone.....	231
	Appendix B: Bio Data of Candidate	235
	Appendix C: List of Publications.....	237
	Appendix D: Answers to the Examiners' comments.....	239

LIST OF FIGURES

Figure 1-1: Broad methodology flow chart for the research	9
Figure 2-1: Illustrated Calculation of Sky View Factor	26
Figure 2-2: Graphical Representation of Urban Canopy Parameters (1).....	27
Figure 2-3: Graphical Representation of Urban Canopy Parameters (2).....	28
Figure 3-1: Location of Study area	50
Figure 3-2: Geomorphological Characteristics of Study area	50
Figure 3-3: Old City of Delhi, 1857	52
Figure 3-4: British Capital of New Delhi	52
Figure 3-5: (A) Built-up Area of Delhi, 1942 (B): Built-up Area of Delhi, 1952.....	53
Figure 3-6: Population Density in Delhi, 1962.....	54
Figure 3-7: Development of Ring Towns	55
Figure 3-8: Growth Rate of urban area of Delhi and its peripheral towns	58
Figure 3-9: Climate zones of India	59
Figure 3-10: Graphical representation of Climate of Delhi	60
Figure 4-1: Methodology for generation of normalized DSM	69
Figure 4-2: Photogrammetric preprocessing.....	70
Figure 4-3: Digital Terrain Model generation tool	71
Figure 4-4: Methodology for generation of Land Use Land Cover.....	73
Figure 4-5: Sky View Factor Calculation tool.....	74
Figure 4-6: Methodology for the retrieval of building heights.....	76
Figure 4-7: Methodology for computation of surface cover fraction	77
Figure 4-8: Flow chart for the computation of complete wall area	79
Figure 4-9: Mosaicked Digital Surface Model of the study area.....	83
Figure 4-10: Mosaicked Digital Terrain Model of the study area	84
Figure 4-11: Normalized DSM of the study area	85
Figure 4-12: Land Use Land Cover map	86
Figure 4-13: Building Height distribution	87
Figure 4-14: Distribution of building heights in Delhi UA	88
Figure 4-15: Distribution of mean of building height in 30 m grid cell	88
Figure 4-16: Distribution of Standard Deviation of Building Height.....	89
Figure 4-17: Standard Deviation of Building height in each 30 m grid cell	90
Figure 4-18 : Building Surface Fraction	91

Figure 4-19: Distribution of Building Surface Fraction	92
Figure 4-20: Distribution of Impervious Surface Fraction	92
Figure 4-21: Impervious Surface Fraction.....	93
Figure 4-22: Pervious Surface Fraction	94
Figure 4-23: Percentage distribution of pervious surface fraction	94
Figure 4-24: Building Volume.....	95
Figure 4-25: Distribution of Building Volume	96
Figure 4-26: Wall Area Ratio (λ_w).....	97
Figure 4-27: Distribution of Height-to-Width Ratio in Delhi UA.....	97
Figure 4-28: Height- to-Width Ratio Map.....	98
Figure 4-29: Building Surface area to Plan Area Ratio	99
Figure 4-30: Complete Aspect Ratio	100
Figure 4-31: Continuous Sky View Factor Map.....	101
Figure 4-32: Distribution of Sky View Factor (Overall)	102
Figure 4-33: Percentage Distribution of Sky View Factor map (Built up area)	102
Figure 4-34: Zero Plane Displacement Height	103
Figure 4-35: Surface Roughness Length	104
Figure 4-36: Error bias in building heights with ground measurements	106
Figure 5-1: Broad Methodology for derivation of urban climate indicators	115
Figure 5-2: Methodology for Estimation of Land Surface Temperature.....	116
Figure 5-3: Methodology for WRF Simulations.....	122
Figure 5-4: Domain configurations of the study area	124
Figure 5-5: Flowchart for the preparation of upscaled 3-class urban LULC.....	128
Figure 5-6: Land Surface Temperature maps of the study region	132
Figure 5-7: Multi class (3- class) Urban Land Use Land Cover at 50 m grid resolution	133
Figure 5-8: Spatial Distribution of Temperature, Relative Humidity and Wind Speed in Domain 1 and Domain 2 of the study region (June 2017).....	134
Figure 5-9: Spatial Distribution of Temperature, Relative Humidity and Wind Speed in the study region (August 2017)	135
Figure 5-10: Spatial Distribution of Surface Temperature, Relative Humidity and Wind Speed in the study region (December 2017).....	135
Figure 5-11: Validation of Temperature at 2m with point observation data of IMD, Delhi	136
Figure 5-12: Correlation graphs for the Temperature at 2m with IMD, Delhi.....	137
Figure 5-13 Validation of WRF model results with MODIS LST for three seasons of Delhi .	138

Figure 5-14: Validation and Correlation graphs for Relative Humidity at 2m with point observation data of IMD, Delhi	140
Figure 5-15: Validation and Correlation graphs for Wind Speed at 10m with point observation data of IMD, Delhi.....	141
Figure 5-16: Building Surface fraction and SUHI Intensity.....	145
Figure 5-17: Pervious Surface fraction and SUHI Intensity.....	145
Figure 5-18: Impervious Surface fraction and SUHI Intensity.....	145
Figure 5-19: Building Height and SUHI Intensity.....	146
Figure 5-20: Surface Roughness and SUHI Intensity.....	146
Figure 5-21 : Sky View Factor and SUHI Intensity	146
Figure 5-22: Diurnal variability of Surface Urban Heat Island Intensity in Summer Season ..	148
Figure 5-23: Diurnal variability of Surface Urban Heat Island Intensity in Winter Season	148
Figure 5-24 : Diurnal variability of Surface Urban Heat Island Intensity in Monsoon Season	148
Figure 5-25: Diurnal variability of Canopy Layer Urban Heat Island Intensity in Winter Season	149
Figure 5-26: Diurnal variability of Canopy Layer Urban Heat Island Intensity in Summer Season	149
Figure 5-27 : Diurnal variability of Canopy Layer Urban Heat Island Intensity in Monsoon Season	149
Figure 6-1: WUDAPT methodology for Local Climate Zonation Classification	162
Figure 6-2: Methodology Flow Chart for GIS based Local Climate Zone.....	164
Figure 6-3: Ventilation Assessment Map	166
Figure 6-4: WUDAPT Local Climate Zone Classification	167
Figure 6-5: GIS based Local Climate Zone Classification	170
Figure 6-6: Class wise departure from Mean LST for each ventilation class.....	173
Figure 6-7: Diurnal variability from Mean LST of Ventilation class.....	179
Figure 6-8: Diurnal variability in bias from Mean temperature at 2m of Ventilation class	180
Figure 6-9: Diurnal variability in bias from Mean Wind Speed at 10 m of Ventilation class..	181
Figure 6-10: Diurnal variability in bias from Mean LST of Ventilation class in urban	182
Figure 6-11: Diurnal variability in bias from Temperature at 2m of Ventilation class in urban built-up.....	183
Figure 6-12: Diurnal variability in bias from Wind Speed at 10m of Ventilation class in urban built-up.....	184
Figure 6-13: Bias from Mean LST of Local Climate Zone classification	187



LIST OF TABLES

Table 2-1: Urban Canopy Parameters.....	20
Table 2-2: Definition of key UCPs and their impact on urban micro climate.....	23
Table 3-1: Urban Growth in Delhi (1951-2001).....	57
Table 4-1: Data used for retrieval of Urban Canopy Parameters.....	67
Table 4-2: Specification of Pleiades data	68
Table 4-3: Area statistics under different classes for Land Use Land Cover	86
Table 4-4: Distribution of Building Height and Mean Building Height.....	89
Table 4-5: Standard Deviation of Building height in 30 m Grid cell	90
Table 4-6: Percentage distribution of Height-to-Width Ratio	98
Table 4-7: Percentage distribution of Building Surface area to Plan Area Ratio	99
Table 4-8: Percentage distribution of Complete Aspect Ratio	100
Table 4-9: SVF Accuracy Assessment statistics.....	101
Table 4-10: Distribution of Zero Plane Displacement Height.....	103
Table 4-11: Percentage Distribution of Surface Roughness Length.....	104
Table 4-12: Validation of Digital Terrain Model with DGPS observations.....	105
Table 4-13: Validation of Building Heights obtained from nDSM against ground measurements	105
Table 5-1: Specification of Landsat 8 Operational Land Imager (OLI) and Thermal Infrared Sensor (TIRS)	116
Table 5-2: Details of downloaded Landsat data	117
Table 5-3: Details of atmospheric parameters	120
Table 5-4: Details of updated Land Surface Parameters	127
Table 5-5: Modified LULC codes for USGS classification	128
Table 5-6: Physics schemes used for WRF simulations	129
Table 5-7: Simulation Dates for WRF simulations	129
Table 5-8: Area statistics of 3-class Urban LULC at 50 m grid resolution	132
Table 5-9 Percentage of pixels in difference image with MODIS LST	138
Table 5-10: Statistical parameters derived from the observed (IMD) and simulated WRF outputs for three seasons of Delhi, 2017	139
Table 5-11: Correlation of Urban Canopy Parameters with Landsat LST	143
Table 6-1: z_0 and z_d classification for Ventilation assessment.....	160
Table 6-2: Area Statistics of Ventilation Assessment Map	165

Table 6-3: Percentage area of WUDAPT and GIS based LCZ classification	168
Table 6-4: Modified Criteria ranges for Local Climate Zone*	169
Table 6-5: Area statistics of built-up GIS based Local Climate Zone	171
Table 6-6: Accuracy Assessment of WUDAPT and GIS based Local Climate Zone	172
Table 6-7: Departure in Degree Celsius from Mean LST of each ventilation class	174
Table 6-8: Relationship of UCPs with ventilation assessment	175



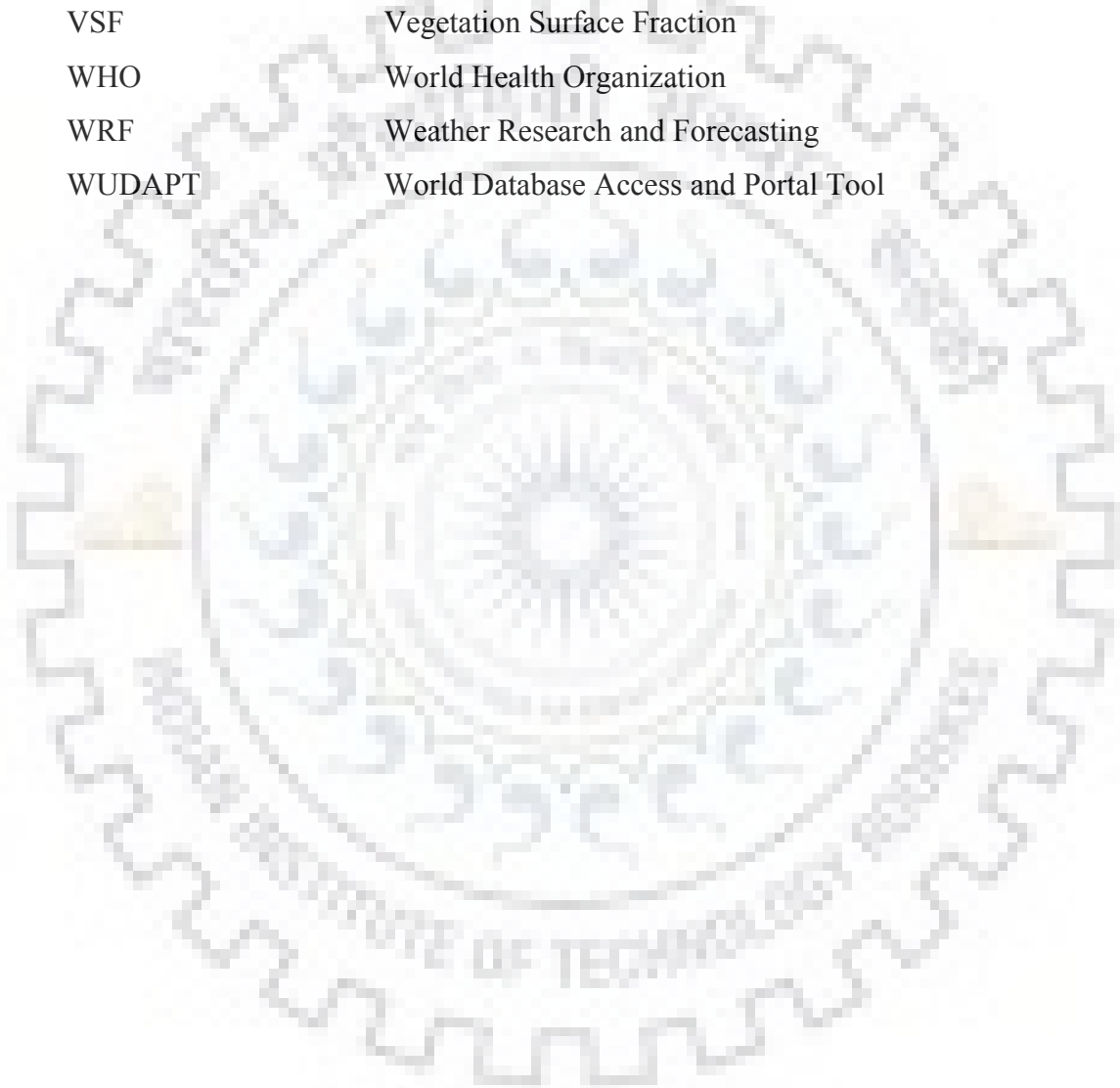
LIST OF ACRONYMS

ACRONYM	FULL FORM
3D	3- Dimensional
ASTER	Advanced Spaceborne Thermal Emission and Reflection Radiometer
AVHRR	Advanced Very High Resolution Radiometer
AWifs	Advanced Wide Field Sensor
BEM	Building Energy Modeling
BEP	Building Energy Parameterization
BSA-PAR	Building Surface area to Plan Area Ratio
BSF	Building Surface Fraction
BV	Building Volume
CAR	Complete Aspect Ratio
CFD	Computational Fluid Dynamics
CHR	Compact High-rise
CLR	Compact Low rise
CMR	Compact Midrise
COTS	Commercial of the shelf
CRE	Cumulative Random Error
DGPS	Differential Global Positioning System
DN	Digital Number
DSMs	Digital Surface Models
DTMs	Digital Terrain Models
EMS	Electromagnetic Spectrum
EOS	Earth Observation Satellite
ETM+	Enhanced Thematic Mapper
FAD	Frontal Area Density
fAPAR	Fraction of Absorbed Photosynthetically Active Radiation
FAR	Floor Area Ratio
Fcover	Fractional cover
GCPs	Ground Control Points
GE	Google Earth

GFS	Global Forecasting System
GHG	Green House Gas
GIS	Geographic Information System
GSL	Global Settlement Layer
HPC	High Performance Computing
H-W Ratio	Height-to-Width Ratio
IMD	Indian Meteorological Department
InSAR	Interferometric Synthetic Aperture Radar
IPCC	Intergovernmental Panel on Climate Change
ISA	Impervious Surface Area
ISF	Impervious Surface Fraction
LAI	Leaf Area Index
LCZ	Local Climate Zone
LiDAR	Light Detection and ranging
LISS	Linear Imaging Self Scanner
LSPs	Land Surface Parameters
LST	Land Surface Temperature
LULC	Land Use Land Cover
MAE	Mean Absolute Error
MBH	Mean Building Height
MLUCM	Multi-Layer Urban Canopy Models
MM5	Mesoscale Model 5
MODIS	Moderate Resolution Imaging Spectroradiometer
MX	Multi-Spectral
NCAR	National Center for Atmospheric Research
NCEP	National Centre for Environmental Prediction
NCR	National Capital Region
NCT	National Capital Territory
NDBI	Normalized Difference Built-up Index
NDMC	New Delhi Municipal Corporation
nDSM	normalized DSM
NDVI	Normalized Difference Vegetation Index
NIR	Near Infrared

NLCD	National Land Cover Dataset
NUDAPT	National Urban Database and Access Portal Tools
NV	Natural Ventilation
NWP	Numerical Weather Prediction
OHR	Open High-rise
OLI	Operational Land Imager
OLR	Open Low rise
OMR	Open Midrise
OSM	Open Street Map
pph	Person Per Hectare
PSF	Pervious Surface Fraction
PVC	Proportional vegetation cover
RH	Relative Humidity
RMSE	Root Mean Square Error
ROI	Region of Interest
RS	Remotely Sensed
RTE	Radiative Transfer Equation
SAR	Synthetic Aperture Radar
SLUCM	Single layer urban canopy model
SUHI	Surface Urban Heat Island
SUHII	Surface Urban Heat Island Intensities
SVF	Sky View Factor
T2	Temperature at 2m
TIRS	Thermal Infrared Sensor
TM	Thematic Mapper
TOA	Top of Atmospheric
UA	Urban Agglomeration
UAVs	Unmanned Aerial Vehicles
UC- map	Urban Climatic map
UCLHII	Urban Canopy Layer Heat Island Intensities
UCMs	Urban Canopy Models
UCPs	Urban Canopy Parameters
UHI	Urban Heat Island

UI	Urbanization Index
UME	Urban Morphology Extractor
UMEP	Urban Multi-scale Environmental Predicto
USGS	United States Geological Survey
VC	Ventilation Coefficient
VDI	Verein Deutscher Ingenieure
VHRS	Very High Resolution Satellite
VSF	Vegetation Surface Fraction
WHO	World Health Organization
WRF	Weather Research and Forecasting
WUDAPT	World Database Access and Portal Tool



CHAPTER 1

INTRODUCTION

1.1 OVERVIEW

The irreversible trend towards high density urbanization leads to a number of climatic and environmental problems such as heat stress, air pollution, global warming, increased storm water runoff, increased use of artificial energy, increased frequency of natural disasters and environmental degradation over urban areas (Grimmond *et al.*, 2010a; Mills *et al.*, 2010; Baklanov *et al.*, 2018). Although, urban areas occupy only 2-3 % of land area but they are responsible for more than 75% of Green House Gas (GHG) emissions that is one of the major contributor to altered climate patterns and current state of global warming (Revi *et al.*, 2014). It has significant impact on human health as well as sustainability of urban areas. With approximately 54% of world population living in urban areas in 2014 which is expected to increase more than 66% by 2050 (DESA/UN-WUP, 2018), it is inevitable to study and understand the impact of urban areas on climate and vice versa.

Urbanization not only change the land cover but it also alters the urban form and its roughness characteristics which has significant impact on urban climatic conditions (Oke, Mills, Christen, & Voogt, 2017). Urban form of any area evolves constantly and its spatial variability extends from sub meter (walls and facets) to tens of kilometers (whole cities). Urban areas with high density of built up and complex morphology exhibits higher temperatures and reduced wind flow (Chen and Ng, 2011; Ng *et al.*, 2011). The myriad urban surface and roughness characteristics leads to highly heterogeneous urban environment which significantly impacts urban micro climate.

1.2 RESEARCH BACKGROUND

In recent years there is significant development in Urban Canopy Models (UCMs) to obtain quantified information on urban climate, its impacts and vulnerabilities with a further aim to assist policy makers in climate mitigation and adaptation. However, the major constraint in the application of UCMs is the paucity of accurate spatial information on Urban Canopy Parameters (UCPs) which can aptly and accurately represent urban heterogeneity and network of local weather information that are imperative for utilization of these models (Carter *et al.*, 2012; Fei Chen *et al.*, 2011; Salamanca *et al.*, 2011). UCPs define the urban heterogeneity of urban built form by characterizing the change in 3D urban configuration, surface cover and materials. It has

been proven by researchers that the 3D configuration or geometry of buildings alters the temperature and wind flow patterns in urban canyons (Wong, Nichol and Ng, 2011; Stewart and Oke, 2012; Berger *et al.*, 2017). Numerical simulations with UCMs have also indicated that availability of accurate information on UCPs provides improved simulation results for understanding Urban Heat Island (UHI), air pollution and climate change scenarios (Chen *et al.*, 2011; Salamanca *et al.*, 2011; Brousse *et al.*, 2016; Bhavana, M., Gupta, Kshama, 2018; Hammerberg *et al.*, 2018). Hence, availability of information on UCPs is critical for urban climate studies.

Availability of reliable information on UCPs is lacking especially in developing region where existing 3D building database or UCPs information is almost non-existent. However, nearly 90% of future urban growth by 2050 is expected to take place in developing regions with 35% of the growth concentrated in just three countries – India, China and Nigeria (DESA/UN-WUP, 2018). Out of these countries also, India is likely to add largest number of urban dwellers in coming years. The cities of developing region not only have high density built-up and large sizes due to intense population pressure but they area also characterized with lack of planning controls which leads to complex urban development with high level of heterogeneity and huge variety in urban forms.

From last few decades, researchers have been trying to understand the impact of urban canopy properties (geometric, radiation, thermodynamic, and surface cover properties) on urban micro climate (Givoni, 1992, 1998; Grimmond & Oke, 1999; Landsberg, 1972; G. Mills *et al.*, 2010; Oke *et al.*, 2017; Stewart & Oke, 2012) through scientific observations and analysis and also tried to translate these into design practices. The urban canopy properties are described by a number of UCPs such as aerodynamic roughness properties (e.g., roughness length, zero plane displacement height), building height characteristics (e.g., mean building height and standard deviation of height), building geometry characteristics (e.g., height-to-width ratio, wall-to-plan area ratio, complete aspect ratio), building volume characteristics (e.g. building plan and frontal area densities), radiation trapping parameters (e.g., sky view factor), surface cover properties (e.g., impervious surfaces, albedo), surface material properties (e.g., heat storage capacity, emissivity), vegetation type, height and geometry, and more (Burian and Brown, 2003b; Burian, Han and Brown, 2003a; Burian, Stetson, Stephen W., Han and Ching, Jason, Byun, 2004; Burian and Jason, 2009; Jeyachandran, Burian and Stetson, 2010; Xu *et al.*, 2017).

National Urban Database and Access Portal Tools (NUDAPT) provides a comprehensive list of 24 UCPs in 132 layers that represent the heterogeneity of urban environment in the meteorological, urban dispersion and air quality models (Jason Ching et al., 2009). It hosts the high resolution gridded UCPs for more than 33 cities in USA. However, there is a lack of information on such robust UCPs especially in the developing region. World Database Access and Portal Tool (WUDAPT) is another initiative aimed at generating the information on urban form and function and defines a set of UCPs for each urban built form class (Bechtel et al., 2015, 2019; Gerald Mills et al., 2015). The studies on urban climate map (Ren, Ng, & Katzschner, 2011; Xu et al., 2017) and ventilation assessment also utilizes UCPs for preparation of urban climate and ventilation analysis (Gal and Sümeghy, 2007; Gál and Unger, 2009; Wong, *et al.*, 2010a; Wicht, Wicht and Osińska-Skotak, 2017). UCPs have been also applied for simulating effect of urbanization in Weather Research and Forecasting (WRF) and mesoscale models (MM5) and also for Urban Heat Island(UHI) modification studies (Jason Ching et al., 2009).

Several researchers over the years have been working for obtaining surface cover properties and morphological (UCPs) parameters over urban areas (Ellefsen, 1991; Grimmond *et al.*, 1998; Grimmond and Oke, 1999; Burian, Velugubantla and Brown, 2002a; Gál and Sümeghy, 2007; Wong, *et al.*, 2010a). A range of UCPs were computed for Oklahoma and Houston cities using 3D GIS databases (Burian, Han and Brown, 2003a ; Burian and Brown, 2003b). Remotely sensed data have been used extensively for extracting the information for 2D and 3D UCPs. Airborne Light detection and Ranging (LiDAR) systems have been used increasingly to derive the three dimensional building data sets and subsequently for retrieval of UCPs all around the world (Burian, Han and Brown, 2003a; Zhou and Neumann, 2008; Zhang, Awrangjeb and Fraser, 2011; Carter *et al.*, 2012; Wicht and Wicht, 2018). However, availability of Airborne LiDAR data in some of the developing countries is limited due to restrictions in data acquisition which in turn limits its use for derivation of 3D building database and subsequent computation of UCPs (Gupta *et al.*, 2015; Gupta *et al.*, 2017a).

Synthetic Aperture Radar (SAR) and Interferometric SAR(InSAR) satellite and airborne systems have also been used to map urban building form, distribution, density and roughness elements (Jeyachandran et al., 2010; Xu et al., 2017). However, the studies concluded that in areas with small building heights the accurate relationship between radar backscatter and UCPs could not be established. It was found that fusion of optical and SAR data provides better height estimates (Xu et al., 2017; Yong, Peifeng, Hui, & Edward, 2015). However, use of SAR technique is still limited due to high data cost and limited availability of very high resolution SAR data. Besides,

in an urban area with high built-up density and complex development, layover effects and volume scattering is too high and backscattered signal of individual building is difficult to obtain (Awrangjeb, Zhang, & Fraser, 2015; Thiele, Cadario, Schulz, Thonnessen, & Soergel, 2007).

The increased availability of very high resolution sub-meter optical stereo datasets, photogrammetric softwares and computing facilities in the last few years facilitates the generation of very high resolution Digital Terrain Models (DTMs) and Digital Surface Models (DSMs) that allow the extraction of building footprints and height information with reasonable accuracy (Fraser, Baltsavias and Gruen, 2001; Poli *et al.*, 2015; Gupta *et al.*, 2017a). Initially aerial photography have been used for manual collection of building footprints and height however, it was time consuming and resource intensive task (Steven J Burian, Velugubantla, *et al.*, 2002a). Very High Resolution Satellite (VHRS) stereo datasets (~0.5 m spatial resolution) have been used for extraction of building heights in complex urban environment with high building density (Tack, Buyuksalih and Goossens, 2012a; Dini, Jacobsen and Heipke, 2013; Gupta *et al.*, 2015; Gupta *et al.*, 2017a) with Root Mean Square Error (RMSE) of less than 1m. Hence, satellite stereo data may prove to be a good source of information for extracting the 3D information in urban areas with complex development.

In-situ measurements have been used for studying the relationship between urban climate and morphology since the inception of urban climate research (Landsberg, 1972; Oke *et al.*, 2017). Although, in-situ field observations have good temporal coverage, their spatial distribution is largely constrained and limited in urban areas. Besides, a vast network of observations is required to represent urban heterogeneity and to understand their relationship with UCPs. The spatially distributed in-situ observation data is either not available or inaccessible in most of the developing regions. Moreover, with the inception of Earth Observation (EO) programme in 1972, a paradigm shift was observed in studying the natural and manmade resources with the help of Remotely Sensed (RS) images. Satellite remote sensing images have tremendous capabilities to acquire spatially variable, area wide information in visible, infrared and microwave regions of Electromagnetic Spectrum (EMS) with repetitive coverage (Gupta and Jain, 2005; Gupta *et al.*, 2017a). It has great potential not only for providing the accurate and up-to-date information on UCPs (Xu *et al.*, 2017) but it can also provide information on emitted radiation by earth surface features which can be used to retrieve spatially variable Land Surface Temperature (LST) (Voogt & Oke, 2003; D. Zhou *et al.*, 2019) and related parameters.

Satellite remote sensing data have been widely utilized to investigate the linkages between UCPs and LST. Most frequently used UCP is the vegetation surface fraction (Hong-Mei, Xiao-Ling, Ping-Xiang, & Zhi-Yong, 2006; Liwen Huang, Shen, Wu, Zhang, & Zeng, 2015; Naeem, Cao, Waqar, Wei, & Acharya, 2018; Perera & Langappuli, 2013), surface albedo (Bonafoni, Baldinelli, Rotili, & Verducci, 2017; Salleh, Latif, Pradhan, Wan Mohd, & Chan, 2014) and impervious surface area (Kaspersen, Fensholt, & Drews, 2015; Perera & Langappuli, 2013; Weng, Lu, & Liang, 2006). In few studies, proportion of buildings, parking lots and roads, their coverage and density have also been used to study the relationship. Numerous studies have utilized urban LULC as descriptor of urban surface cover to study the relationship (J. Jiang & Tian, 2010; Jun, Kim, Kim, Yeo, & Hyun, 2017; Kotharkar, Ramesh, & Bagade, 2018; Perera & Langappuli, 2013). Although, the impact of 3D UCPs on urban climate is significant and it is considered as one of the main contributor to UHI phenomenon. However, there are a very few studies which have analyzed relationship of 3D UCPs such as building height, frontal area index, floor area ratio and sky view factor with LST and this area of research therefore remained largely unexplored even in the regions with planned infrastructure. (Chun and Guldmann, 2014; Scarano and Sobrino, 2015; Guo *et al.*, 2016; Berger *et al.*, 2017; Yin *et al.*, 2018). Hence, there is a need to explore the relationship of 2D/3D UCPs with spatially variable climate indicators.

On the other hand, Satellite remote sensing provides information on biophysical characteristics (Deng & Wu, 2012; Ridd, 1995; Weng *et al.*, 2006), materials (Heiden, Segl, Roessner, & Kaufmann, 2007; Herold, Roberts, Gardner, & Dennison, 2004), landscape patterns (Liu, Jia, Han, & Zhang, 2018; Shen, Ibrahim Abdoul, Zhu, Wang, & Gong, 2017; Tv, Aithal, & Sanna, 2012), Land Use Land Cover (LULC) (Ganguly *et al.*, 2017; Kotharkar *et al.*, 2014; Gerald Mills *et al.*, 2015), built-up density, surface cover fractions (Ridd, 1995; Wu & Yuan, 2011) and 3D configuration of earth surfaces (Burian, Han and Brown, 2003a; Xu *et al.*, 2017) which have been employed to derive various UCPs. The obtained information on earth surface characteristics therefore forms an important inputs for numerical simulations of climatic indicators such as temperature, wind speed, humidity, pressure etc. and have been ingested in numerical models to downscale climate indicators to micro scale and simulate the impact of urban area on climate (Ching *et al.*, 2009; Brousse *et al.*, 2016; Hammerberg *et al.*, 2018). The simulated climate indicators at micro scale together with remotely sensed derived LST provide spatially variable information which can also be utilized to understand the relationship of UCPs with urban micro climate (Salamanca *et al.*, 2011; Berger *et al.*, 2017; Hammerberg *et al.*, 2018) in a complex urban environment.

1.3 RESEARCH GAPS

Recent trends in urbanization indicate future urban growth is bound to happen in the developing world mainly in Asian and African countries at an unprecedented rate. This rapid urbanization is characterized with high density of built-up area forming large urban agglomeration in low and middle income countries in these continents. The huge population pressure, lack of infrastructure and coping mechanisms, unplanned growth, formation of slums, lack of vegetation, high levels of air pollution and many more social and environmental issues makes urban communities highly vulnerable to extreme weather conditions. These regions holds the key to the future strategies for climate change mitigation and adaptation and it becomes important to study and regularly monitor them in the current dynamic scenario.

Lack of detailed information on urban morphological characteristics or UCPs in these regions is considered to be one of the major constraint in implementation of recently developed UCMs, application of UCPs for urban climate research and to investigate the relationship between UCPs and climate indicators. Many research studies have utilized 3D Geographic Information System(GIS) cadastral databases for the derivation of UCPs in American and European countries (SJ Burian et al., 2003; Jason Ching et al., 2009; Wicht & Wicht, 2018). Remotely sensed data such as Aerial Photographs, Airborne LiDAR and high resolution InSAR data have been extensively used for the development of 3D GIS database. However, in most of the developing countries 3D GIS cadastral database is almost non-existent. Furthermore, availability of airborne data (stereo and LiDAR) and high resolution InSAR data is limited, hence, new alternatives needs to be explored for obtaining the information on urban morphological characteristics in these regions. The vast range of widely sub-meter high resolution optical stereo data therefore needs to be explored for retrieval of UCPs in these regions.

Satellite Remote Sensing mainly LST from Landsat and Aster thermal bands have been utilized extensively for investigating the relationship of UCPs with LST. However, relationship with 3D UCPs is less explored in developing countries one of the primary reason being the non-availability of spatially variable information on 3D UCPs. Spatially variable climate indicators such as Temperature at 2m, wind speed, pressure, humidity other than LST is generally available at coarse resolution. The best available resolution in free domain is 12.5 km which is too coarse to be utilized for assessment at urban scale (Anon, n.d.a). Mesoscale models such as WRF can be utilized for downscaling the climate indicators to 0.5-1km resolution and can be applied to understand the relationship of climate indicators with urban morphology at micro scale.

1.4 RESEARCH QUESTIONS

Research gaps identified based on preliminary understanding of literature posed following research questions in order to address the requirement of retrieval of UCPs in a complex and high density urban environment of developing world:

1. Can high resolution optical satellite stereo images be effectively utilized for retrieval of UCPs in high density complex urban environment?
2. What are the suitable sources for spatially variable climate indicators to assess the relationship with spatially variable UCPs?
3. What are the potential applications of UCPs for urban climate studies in complex urban environment?

1.5 AIM AND OBJECTIVES

Research gaps highlighted the need to develop novel approaches to retrieve UCPs in highly dense and complex urban environment and to further investigate their relationship with climate indicators.

Therefore, the study aims to retrieve and characterize urban canopy parameters and analyze their relationship with spatially variable urban climate parameters. In order to achieve the research aim, following objectives have been formulated:

1. To retrieve and characterize Urban Canopy Parameters (UCPs) spatially in a highly complex and dense urban environment using VHRS optical stereo data.
2. To develop relationship between UCPs and spatially variable urban climate indicators.
3. To demonstrate application of UCPs for urban climate studies in complex urban environment.

1.6 RESEARCH METHODOLOGY

The broad methodology to carry out this study can be divided into three major segments. First segment addresses the first objective i.e. retrieval of UCPs from high resolution optical satellite stereo. The retrieved UCPs have been utilized further to analyze relationship with spatially variable climate indicators which have been generated as part of second objective. Third segment of methodology addresses the application of retrieved UCPs (first objective) for urban climate studies i.e. ventilation assessment and GIS based Local Climate Zone (LCZ) mapping and

analysis of their relationship with spatially variable climate indicators generated as part of second objective.

The sequential steps to carry out this research (Figure 1-1) includes procurement of high resolution satellite stereo data, photogrammetric preprocessing to obtain Digital Surface Model (DSM), Digital Terrain Model (DTM) and normalized DSM (nDSM). Ortho images generated from high resolution multispectral data and DSM have been classified to obtain Land Use Land cover with broad level 1 classes for example, water, vegetation, built-up, bare soil and bare rock. LULC and normalized DSM have been processed further to obtain building height (Burian, Han and Brown, 2003a; Oke *et al.*, 2017; Xu *et al.*, 2017), wall area ratio and building (Stewart & Oke, 2012; Xu *et al.*, 2017), pervious and impervious surface fractions (Stewart & Oke, 2012) which have been further utilized to compute other 2D and 3D UCPs. The generated UCPs have been further employed to demonstrate the applications of UCPs such as ventilation assessment and GIS based Local Climate Zone (LCZ) map for urban climate research and modeling in the study area.

Land Surface Temperature (LST) have been retrieved through processing of thermal remote sensing data of Landsat 8 Thermal Infrared Sensor (TIRS) to analyze the relationship between UCPs and spatially variable climate indicators. The major steps includes conversion of digital numbers to Top of Atmospheric (TOA) radiance and estimation of land surface emissivity both of which have been utilized to obtain spatially variable LST. Model simulations have been carried out to obtain the spatially variable climate indicators at high resolution (~500m) as the other spatially variable climate indicators are not available through remote sensing at urban scale. To carry out model simulations, first of all updated land surface parameters such as albedo, vegetation fraction, leaf area index etc., a high resolution 3-class urban LULC obtained from remote sensing data and Meteorological data have been ingested in the numerical model (Weather Research and Forecasting model). Climate indicators such as LST, temperature at 2m, wind speed, relative humidity, pressure etc. have been downscaled to 500 m grid resolution through model simulations. The outputs obtained from numerical model simulations have been validated with point observation data of Indian Meteorological Department (IMD) and Moderate Resolution Imaging Spectroradiometer (MODIS) LST. The spatially variable climate indicators thus obtained from Landsat 8 and model simulations have been employed to assess the relationship with UCPs. The detailed methodology for all steps as discussed above have been provided in respective chapter 4, 5 and 6.

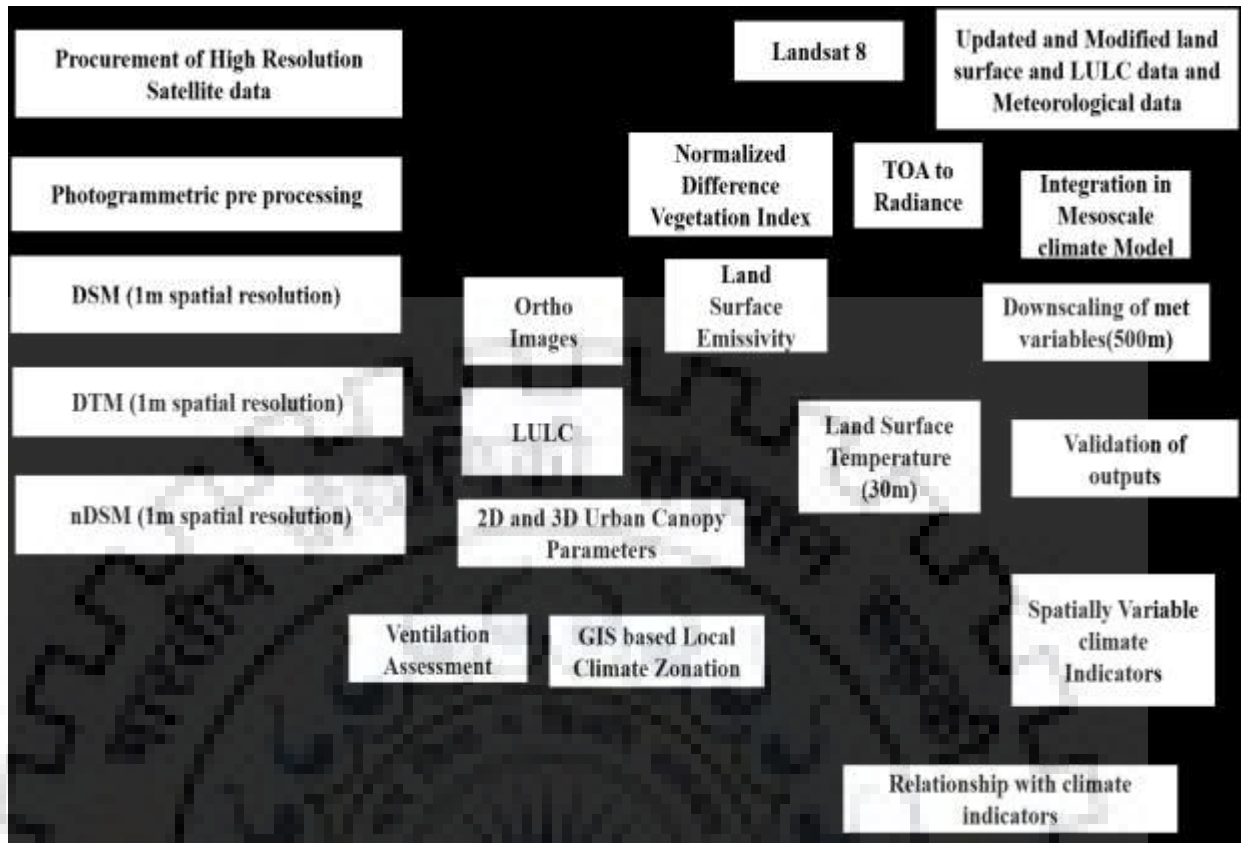


Figure 1-1: Broad methodology flow chart for the research

1.7 SCOPE AND LIMITATIONS

1.7.1 Scope

This study focuses on retrieval of spatially variable 2D and 3D UCPs by utilizing high resolution optical stereo data and the application of UCPs in a highly dense and complex urban environment of developing regions. The study also analyses the relationship of UCPs with spatially variable climate indicators derived from remote sensing data and numerical model simulations.

1.7.2 Limitations

Some of the UCPs such as frontal area index and frontal area density could not be computed as the automated tools for the computation of these parameters could not yield satisfactory results in a large and complex built-up area.

Some of the spatially variable climate indicators such as LST derived from satellite remote sensing (30 m Resolution) and LST, temperature at 2m and wind speed obtained from WRF

simulations (500m resolution) were only utilized for the assessment of relationship, since other parameters could not provide significant spatial variability at the resolution of 500m. So the main limitation is the availability of climatic parameters at higher resolution for the establishment of relationships between UCP and micro-scale climatic variability.

Obtaining cloud free data in the study region was a challenge as monsoon season is mostly cloudy and winter season suffers intense fog due to composite climate of study region. Hence, one LST scene from each season could only be analyzed to understand the relationship of UCPs with LST.

Due to limitation of available computational resources, a few days' simulations could only be carried out with WRF–urban at high resolution (~500 m grid size) as high resolution model simulations are computational resource intensive.

1.8 ORGANIZATION OF THESIS

The thesis have been organized in seven chapters out of which first three chapters are dedicated to research background (Chpater1), review of existing literature (Chapter 2) and study area context (Chapter 3). The next three chapters (Chapter 4-6) details out the research work carried out in this study that includes retrieval and characterization of UCPs in selected study area (chapter 4), relationship of UCPs with spatially variable climate indicators (Chapter 5) and application of UCPs in the study region (Chapter 6). Last chapter is the concluding chapter (Chapter 7) which outlines the key finding, recommendations, contributions of the study and scope for further research.

Chapter 1 is the introductory chapter and starts with a discussion on the research background. It outlines the research gaps which assist in framing of research questions. To obtain the answer to the research questions, 3 research objectives and broad methodology have been formulated. The chapter also highlights scope of the study and limitation faced while executing the study and a brief introduction to the organization of the thesis.

Literature Review, which have been studied to frame and understand this study, is summarized in chapter 2. The chapter outlines the research requirements in this area through a discussion on potential of geospatial technologies for retrieval of UCPs using various remote sensing data sets and their limitations. It is found that due to various limitations, use of airborne LIDAR, aerial photography and high resolution InSAR is not feasible for the study region. Hence, it recommended exploring the use of sub-meter optical satellite stereo data due to wider and easy

availability for the retrieval of UCPs in the complex urban environment of the study region. The application of retrieved UCPs includes ventilation assessment, GIS based local climate Zone, urban climate map (UC-map) and urban climate research and modeling. Discussion on worldwide trends of urban climate revealed increased temperature and precipitation intensity and decreased ventilation in urban areas, which necessitates the detailed study of urban climate to mitigate the negative impacts of changing climate scenario. However, it requires spatially variable high resolution information on urban climate variables which cannot be obtained through field based in-situ measurements and physical modeling. Remote sensing and numerical modeling are the methods which can be employed for obtaining the information on spatially variable climate indicators. The obtained information can be utilized to assess the relationship of climate indicators with urban built form as well as for urban climate research and studies.

Chapter 3 presents a discussion on the physical, historical, climate, population, built form and locational characteristics of the study area. It also outlines the locational and climate complexities of the study region and also discusses the need to analyze and study in detailing the urban climate characteristics of the study area.

The chapter on characterization of urban canopy parameters (chapter 4) focuses on need of retrieval and characterization of UCPs and use of high resolution (sub-meter) optical stereo data for retrieval of these UCPs in complex and high density urban environment of the study region. It presents novel approaches for the extraction of building height, Building Surface Fraction (BSF) and complete wall surface area which forms the basic inputs for the extraction of other UCPs. The accuracy assessment of basic input parameters (building height, LULC and BSF) revealed reasonable accuracy and therefore recommend the use of optical stereo data of sub-meter resolution for retrieval of UCPs in dense and complex urban environment. The characterization of UCPs in the study region shows highly heterogeneous and complex urban development in the study region.

In chapter 5, LST obtained through Landsat 8 TIRS (30 m) and spatially variable climate indicators at high resolution obtained from WRF model simulations (500m) have been employed to assess the relationship of climate indicators with the UCPs retrieved in chapter 4. The examination of WRF model outputs revealed reasonable accuracy with point observation data of IMD and MODIS LST. The analysis of relationship of UCPs with LST presents strong relationship with 2D UCPs however not relationship with 3D UCPs was not found to be so strong.

The chapter also discusses various methodological and operational concerns for analyzing the relationship between urban built form and urban climate indicators.

Chapter 6 presents the utilization of UCPs for urban climate studies and research through developing applications for ventilation assessment and GIS based LCZ. It also discusses the accuracy of LCZ classification through pixel based classifiers as proposed by WUDAPT and through application of UCPs. The relationship of spatially variable climate indicators with ventilation assessment map and GIS based LCZ map have also been presented that shows higher temperature and lower wind speed in weak ventilation areas. The chapter also discusses future potential applications of UCPs for various urban climate research studies and modeling.

Chapter 7 summarizes key finding and conclusions of the study and also highlights the major contributions of this study, which his followed by key recommendations out of this research work. The discussion ends with the outline of the studies that can be undertaken in near future for utilization of UCPs for urban climate research and modeling to further strengthen the results and observations obtained in this study.

CHAPTER 2

LITERATURE REVIEW

2.1 INTRODUCTION

Systematic review of existing literature is essential for research as it not only provides an insight into the basic concepts and prevalent practices but also assists in identifying the research gaps and formulation of research methodology by reviewing earlier research conducted in the field of study. Accordingly, a systematic review of existing literature has been undertaken starting with impact of urbanization on climate change and vice versa, the need to study urban climate and variations in urban micro climate patterns due to large variability and modification of urban built form characteristics which necessitates obtaining spatially variable information on urban canopy parameters. Recently developed Urban Canopy Models (UCMs) also seek detailed spatial information on Urban Canopy Parameters (UCPs) which is termed as parameters to define urban built form characteristics for improved representation of urban areas for urban climate research and modeling. Accordingly, various urban canopy parameters useful for urban climate studies and modeling have also been discussed. It is followed by a discussion on various methods for obtaining information on UCPs and utilization of geospatial technologies for deriving information on UCPs. To understand the relationship of spatially variable UCPs with climate indicators require spatially variable information on climate variables as well. Hence, further discussion focusses on methods for the retrieval of spatially variable climate indicators through remote sensing and numerical simulations and implications and applications of the spatially variable UCPs for urban climate research and modeling.

Therefore, this chapter discusses various aspects of urbanization, climate change, urban climate, urban built form characteristics, urban canopy parameters, geospatial technologies for retrieval of UCPs, methods for obtaining information on spatially variable climate indicators, relationship of UCPs with spatially variable climate indicators and implications and applications of UCPs for urban climate studies, research and modeling.

2.2 URBANIZATION AND CLIMATE CHANGE

Urban areas are one of the major contributors to global climate change as they are cumulatively responsible for emission of 75% of Green House Gases (GHGs) (IPCC, 2007) contributing for 0.74°C increase in global average surface temperature in past one hundred years. The fifth Assessment report of Intergovernmental Panel on Climate Change (IPCC) predicts that with

higher rates of emissions as of today, the global temperature will exceed 2°C by 2100 and will further rise to 4°C (Stocker et al., 2013). This rise in temperature will be associated with increased frequency and intensity of floods, droughts, famines, heat waves, hurricanes, conflicts and social unrest and will lead to displacement of large section of population (Baklanov et al., 2018). According to World Health Organization (WHO) report, global warming and climate change will be responsible for more than 2,50,000 additional deaths per year between 2030 and 2050 and three million illnesses every year (Wisner & Adams, 2002). Urban areas acts as both perpetrators and victims of climate change. Interestingly, the whole global urban population which is more than 50%, resides in less than 3% of Earth's ice-free land area (Small & Naumann, 2001). Human impacts on environment are much more intense in urban areas as they are hubs of economic activity and centers of population concentration (Tang & Lee, 2016). Urban areas also consume a significant amount of world resources and energy, thereby, contribute immensely to changing climate scenario. On the other hand, the urban population is more vulnerable to impacts of climate change due to their sheer number and density concentration in relatively small land area (~3% of land area) (Grimmond *et al.*, 2010a; Mills *et al.*, 2010). Most of the mega cities of the world are coastal cities and susceptible to climate change impacts severely due to rising sea levels (Blake et al., 2011). Increased intensity of vector-borne diseases (Patz, Diarmid, Holloway, & Foley, 2005) and extreme weather event such as heat waves, flash flooding, cyclones etc. will have substantial impact on loss of lives and properties in urban areas (Revi et al., 2014). Hence, understanding the effects of development in urban areas is fundamental to any efforts made for mitigating climate change impacts and they can play a significant and multidimensional role in global climate and sustainable development (Grimmond *et al.*, 2010a).

Globally, urban population is on rise and it is predicted that by 2030 almost 60% of global population will reside in urban areas (DESA/UN-WUP, 2018). It is predicted that almost 35% of world population growth in next 30 years will be concentrated in urban areas of developing regions especially in Africa, Asia and Latin America (DESA/UN-WUP, 2018). The growing urban population in developing region is continuously exposed to increasing heat loads due to climate change, already high temperatures, and prominent UHI effects. The cities in developing countries not only have high density built-up and large sizes due to intense population pressure but they are also characterized with lack of implementation of planned development which results in the formation of complex urban development with high level of heterogeneity. Coupled with lack of adequate infrastructure facilities, these countries will face numerous challenges in meeting the needs of growing urban populations, including housing, infrastructure,

transportation, energy, employment and basic services such as education and health which is going to place entire population at increasing health and productivity risk (Lundgren & Kjellstorm, 2013). Hence, it is vital to understand how cities in developing regions impact climate and vice versa for ensuring sustainable development, which is discussed further in detail.

2.3 URBAN CLIMATE

Urban Climate can be defined as “*the study of meteorological processes, atmospheric phenomena, and the long term amalgamated expression of these variables in areas that have undergone urban development.*” (Oke et al., 2017). Urban Heat Island (UHI) effect is the most prominent and widely discussed phenomenon in urban climate studies. It is defined as increased air and surface temperatures in the urban atmosphere sometimes several degrees higher (~ upto 12°C) than their surrounding rural counterparts (Rasul et al., 2017; Voogt & Oke, 2003; Vyas, Shastri, & Y, 2014). It has been studied world over and extensive research have been done in the area since the inception of urban climate research. Study of UHI dates back to early nineteenth century, when renowned meteorologist Luke Howard (Howard, 1820) systematically studied differences in temperature between downtown London and surrounding rural areas, which was well before the researchers started linking fossil fuel consumption with global warming (Arrhenius, 1896). It is primarily attributed to changes in surface material, fraction of land surface cover, geometry of urban areas and anthropogenic heat emission which alter the micro scale processes and exchanges, especially below the urban canopy layer (Oke et al., 2017). Trend of increasing temperatures globally as well as in India is further enhancing the UHI which is going to have profound impact on health of urban populace, energy and water supply and consumption, infrastructure and social comfort in urban areas (Chakraborty et al., 2017; Rasul et al., 2017). Higher temperatures in urban areas exacerbates impact of heat waves and effects urban inhabitants negatively. It requires in depth understanding of the phenomenon for devising strategies for mitigating their adverse impacts (D. Li & Bou-Zeid, 2013).

Increased proportion of impervious surfaces, increased run-off and lack of vegetation leads to creation of Dry Island and reduces evaporative cooling in urban areas. It also leads to lower relative humidity levels in urban areas as compared with rural surroundings (XiQuan Wang & Gong, 2010). The high amount of anthropogenic heat emission within small spatial scale in urban areas is primarily due to increased energy consumption by heating and cooling systems, industries and transportation coupled with high population density (Chakraborty, Kant, & Mitra, 2015). Increased emission rates further lead to elevated concentration of aerosols and pollutants

in urban atmosphere creating air pollution island (Maji, Ahmed, & Siddiqui, 2015). Severe to very poor air quality and related respiratory diseases is considered as one of the major issues facing urban areas in present context. The situation is predicted to worsen as warming climates tend to further increase ground level ozone, which will further intensify the air pollution and UHI phenomenon (Taha, Chang, & Akbari, 2000).

Due to its multi-faceted impact on the city environment, wind conditions is a key element in urban studies. It is no surprise that Givoni (1998) states: “*of all the climatic elements the wind conditions are modified to the greatest extent by urbanization*” and more cogently: “*from the viewpoint of modifying the urban climate and urban comfort by urban design, modifying the urban wind conditions offers the greatest potential*”(Givoni, 1998). The natural ventilation in urban areas is much more complex to predict and estimate than the rural areas due to increased surface roughness of the urban areas, which alters the air flow patterns within the urban areas. The increased surface roughness is generally associated with reduced wind speeds, where energy is lost by vertical instability due to height of roughness structures (Oke, 1987). Wind is very important for reducing the thermal stress and influences the health, outdoor/indoor comfort, and the energy consumed by the buildings for cooling/heating (L. Yang & Li, 2011). Wind flow in urban area also helps in dissipating the air pollution levels, which further helps in reducing the impact of UHI (Kato & Huang, 2009). Drop in temperature up to 2 degree Celsius has been observed with an increase in wind speed of 1-1.5 m/s (Erell, Pearlmutter, & Williamson, 2011). Hence, an understanding the relationship between wind flow and urban built form is essential for mitigating the UHI effect.

Urbanization and larger urban areas are known to influence precipitation patterns but still the correlation and exact quantification is unknown (S. J. Burian & Shepherd, 2005). Analysis of historical weather records of eight American cities found significant increases in summer thunder day frequencies (13% to 41%) and hail day frequencies (90% to 450%) (Huff & Changnon, 1973). Similar results were reported in the city of Benin, Nigeria, where a 43% increase was observed in rainfall over the urban area as compared with surrounding rural areas (Efe & Eyefia, 2014). Many researchers state that urbanization has an effect on the intensification of downwind rainfall (S. J. Burian & Shepherd, 2005; Landsberg, 1972; Stout, 1962) also known as “urban rainfall effect”. It is defined as the impact of urban centers on enhancing downwind and peripheral rainfall. The reasons being assigned to the increased surface roughness, enhancement in sensible heat flux, heat island induced convection and changes in amount of aerosols in the urban areas. Intensification of rainfall causes disruption of transport and commerce due to flash

flooding and put enormous pressure on infrastructure and loss of habitats, disrupting settlements and societies (Lankao, 2008). Besides, artificially paved surfaces of urban areas being impervious add more to the runoffs, further aggravating the flood situation. Extent of damages and inconveniences is higher in urban areas that are densely populated areas.

Modification in urban surface roughness and geometry of urban built form is one of the major causes for modified urban climates (Roth, Oke and Emery, 1989; Oke *et al.*, 2017). The continuous growth in urban areas bring a substantial change in its landscape, geometry and configuration. Urban built form differs significantly from surrounding rural areas due to vertical growth of building structures, increase in impermeable surfaces, narrow street canyons and high density of built-up. It is necessary to study the modified characteristics of urban built form to understand its impact on urban environment and surrounding regions.

2.4 URBAN BUILT FORM AND URBAN MICRO CLIMATE

Urban form is defined as the physical characteristics that make up built-up areas, including the shape, size, density and configuration of settlements. It can be considered at different scales viz. at regional, urban, neighbourhood, block and street scales. Urban form of any area evolves constantly in response to social, environmental, economic and technological developments; planning, housing and urban policies; and health, transport and economic policies. Land uses, building structures, plot patterns and street patterns are considered to be the most important elements for the study of urban form and urban layout (Conzen, 2001). Compared to other key elements, land use is the most dynamic and temporary phenomenon. The other key elements such as building structures, plot patterns and street system defines the 3D geometry and inter-building spacing in urban area. The arrangement of these elements defines the porosity and opaqueness of the urban built form. The radiative (geometry, reflectivity, emissivity and transmissivity), thermal (specific heat, heat capacity, thermal conductivity, diffusivity and admittance), moisture (interception and storage capacity, permeability, stomatal characteristics) and aerodynamic properties (roughness, zero-plane displacement height, porosity) of urban surfaces are varied and creates bewildering and complex microclimates. The spatial variability extends from sub meter (walls and facets) to tens of kilometers (whole cities) (Bechtel *et al.*, 2015; Oke *et al.*, 2017). Urban areas with high density of built up and complex morphology exhibits higher temperatures and reduced wind flow (L. Chen & Ng, 2011) (Ng *et al.*, 2011). For example surface roughness, zero plane displacement height, frontal area index are few of the urban roughness parameters (Grimmond and Oke, 2002; Burian, Stetson, Stephen W., Han and Ching, Jason, Byun, 2004;

Wong and Nichol, 2013; Suder and Szymanowski, 2014; Wicht, Wicht and Osińska-Skotak, 2017) which effects wind flow patterns in urban areas. The knowledge of key roughness parameters is important for air flow and pollutant dispersion modeling. The canyon properties such as Height-to-Width(H/W ratio) and Sky View Factor (SVF) has impact on shading, solar gain, heat trapping and wind movement in urban canyons (Bakarman & Chang, 2015; Jhaldiyal, Gupta, Gupta, Thakur, & Kumar, 2018; Middel, Lukasczyk, Maciejewski, Demuzere, & Roth, 2018; Oke, 1987; Shishegar, 2013). Similarly, the fraction of buildings or vegetation in a unit area has impact on evaporative cooling, infiltration and evapotranspiration processes which in turn generates variation in temperature patterns (Surawar, Meenal; Kotharkar, 2017; Weng et al., 2006).

2.5 URBAN CANOPY PARAMETERS

The urban canopy comprises of myriad surfaces and forms arranged in complex 3D configurations. Urban Canopy Parameters (UCPs) or morphological parameters are 2D and 3D urban built form parameters which have direct as well as indirect bearing on urban microclimate (Stewart and Oke, 2012; Middel *et al.*, 2014). They define the heterogeneity of urban built form by characterizing the change in 3D urban configuration, surface cover and materials. 3D configuration or geometry of buildings has significant impact on the temperature and wind flow patterns in urban canyons (Wong, Nichol and Ng, 2011; Berger *et al.*, 2017; Oke *et al.*, 2017). Different UCPs including mean building height, surface roughness characteristics, frontal area index and many other UCPs are necessary to define urban geometry.

The UCPs have been extensively used to characterize the heterogeneity of urban built form and to represent urban effects in meteorological and air quality modeling applications. It has been also applied in meteorological models to account for variations in surface energy budget (Fei Chen et al., 2011; L. Jiang, Lu, Jiang, Qi, & Yang, 2014), drag imposed by urban roughness elements, solar heat gain and turbulent wind flow in urban areas (Brown & Williams, 1998; Martilli, Clappier, & Rotach, 2002; Neophytou, Mouzourides, Kyprianou, Choudhary, & Ching, 2015; Otte, Lacser, Dupont, & Ching, 2004; Salamanca et al., 2011). Recent Urban Canopy Models (UCMs) requires high resolution detailed UCPs to characterize urban areas in mesoscale and micro scale climate models. The simulations in mesoscale numerical models such as MM5 and WRF indicate that accurate and detailed representation of urban areas in numerical models can provide improved results for urban weather forecast, climate change scenarios and pollutant dispersions (Chen *et al.*, 2011; Salamanca *et al.*, 2011; Carter *et al.*, 2012; Bhavana *et al.*, 2018).

Burian and Ching, 2009 presents a detailed approach for derivation of UCPs for integration in Numerical Weather Prediction (NWP) models (Steven Burian & Jason, 2009). National Urban Database and Access Portal Tools (NUDAPT) provide the high resolution gridded urban canopy parameters for 44 cities in USA (Jason Ching et al., 2009). It also provides an extensive list of UCPs for integration in numerical prediction models for urban climate research and modeling (Glotfelty et al., 2013). This data was applied for simulating effect of urbanization in Weather Research and Forecasting (WRF) and mesoscale model (MM5) and for UHI modification studies. This field is still growing and availability of high resolution 3D databases in GIS will enhance the development of gridded UCPs and their ingestion in NWP models. It is expected that the ingestion of these parameters in meso and local scale models will assist in better representation of urban areas, which in turn will help to model the impact of urban areas on global climate scenarios in more realistic manner.

Many researchers over the years have worked on obtaining surface cover properties and morphological (UCPs) parameters over urban areas (Ellefsen, 1991; Brown and Williams, 1998; Burian, Velugubantla and Brown, 2002b; Grimmond and Oke, 2002; Gál and Sümeghy, 2007; Wong, *et al.*, 2010a). Table 2-1 presents a list of various UCPs and computing equations for urban morphological analysis and climate modeling. The list is not comprehensive but it includes most of the UCPs as proposed by Burian and Ching for mesoscale climate modeling (Burian, Han and Brown, 2003a; Ching *et al.*, 2009) such as mean building height, standard deviation of building height, Area averaged building height, Building Surface fraction, Plan area Fraction, Building Plan Area Density, Roof Area Density, Building Area Index, Frontal Area Index, Frontal Area Density, Complete Aspect Ratio, Building Surface Area to Plan Area Ratio, Height-to-Width Ratio, Zero plane Displacement Height and Surface Roughness Length.

Table 2-2 presents the definition of key UCPs and also describes the impact of each UCP on urban micro climate, which are commonly used in climate, air quality and dispersion modeling. The graphical illustration of UCPs is presented in Figure 2-1, Figure 2-2 and Figure 2-3

Table 2-1: Urban Canopy Parameters

S. No.	Parameter Group	Symbol	Parameter	Equation	Description	Source
1	Building height	\bar{h}	Mean Building Height	$\bar{h} = \frac{\sum_{i=1}^N h_i}{N}$	h is Building height at i th location N is number of Buildings A _i is building area at i th location	(Burian and Brown, 2003b; Burian, Han and Brown, 2003a; Oke <i>et al.</i> , 2017; Xu <i>et al.</i> , 2017)
		s_h	Standard Deviation of Building Height	$S_h = \sqrt{\frac{\sum_{i=1}^N (h_i - \bar{h})^2}{N-1}}$		
		\bar{h}_{AW}	Average Building Height weighted by Building Plan Area	$\bar{h}_{AW} = \frac{\sum_{i=1}^N A_i h_i}{\sum_{i=1}^N A_i}$		
2	Plan Area Fraction	λ_p	Building Surface Fraction /Building Plan Area Fraction/ Building Coverage Ratio	$\lambda_p = \frac{A_p}{A_T}$	A _p is Plan Area of Buildings at Ground Level A _T is Total Plan Area A _x is fraction of surface cover type(Building, vegetation and impervious ground(roads, parking etc.) λ _p (z) is Plan Area fraction at Elevation z Δz is height increment	(Stewart and Oke, 2012; Oke <i>et al.</i> , 2017)
		λ_x	Plan Area fraction	$\lambda_x = \frac{A_x}{A_T}$		
3	Plan and Roof Area Density	$a_p(z)$	Building Plan Area Density	$a_p(z) \cong \frac{\lambda_p(z)}{\Delta z}$		
		$a_r(z)$	Roof Area Density	$a_r(z) = \frac{A_p \left[z - \frac{\Delta z}{2} \right] - A_p \left[z - \frac{\Delta z}{2} \right]}{A_T \cdot \Delta z}$		

4	Aspect Ratio	λ_C	Complete Aspect Ratio	$\lambda_C = \frac{A_R + A_G + A_W}{A_T}$	A_R is Roof Area A_G is Area of Exposed Ground A_W is Wall Surface Area A_T is Total Plan Area	(Burian, Han and Brown, 2003a ; Lindberg, Grimmond and Martilli, 2015)
		λ_B	Building Surface Area to Plan Area Ratio	$\lambda_B = \frac{A_R + A_W}{A_T}$		
		λ_S	Height to Width Ratio	$\lambda_S = \frac{H_1+H_2}{2}$ or $\lambda_S = 0.5 * \left\{ \frac{\lambda_w}{(1 - \lambda_p)} \right\}$	H_1 is Height of Upward Building H_2 is Height of Downward Building λ_w is wall area fraction λ_p is Plan Area Fraction	
5	Aerodynamic Roughness parameters	λ_f	Frontal Area Index	$\lambda_f(\theta) = \frac{A(\theta)_{proj}}{A_T}$ or $\lambda_f = \frac{\bar{L}_y \bar{H} \rho_d}{L_y H}$	A_{proj} is Area Projected to Wind θ is Wind Angle \bar{L}_y is Mean Breadth of Roughness Elements \bar{H} is Mean Roughness Element Height ρ_d is Roughness Element Density ($\rho_d = n/A_T$)	(Grimmond <i>et al.</i> , 1998; Grimmond and Oke, 1999; Burian, Han and Brown, 2003a)
		$a_f(z, \theta)$	Frontal Area Density	$a_f(z, \theta) = \frac{A(\theta)_{proj(\Delta z)}}{A_T \Delta z}$	$A(\theta)_{proj(\Delta z)}$ Area Projected to Wind at θ Direction at a Height Increment Z	(Burian, Han and Brown, 2003a)
		z_d	Zero Plane Displacement Height	1. $z_d = f_d \bar{z}_H$ 2. $\frac{z_d}{z_H} = 1 - \left\{ \frac{1 - \exp[-(c_{d1} 2 \lambda_f)^{0.5}]}{(c_{d1} 2 \lambda_f)^{0.5}} \right\}$ 3. $\frac{z_d}{z_H} = 1 + \alpha \lambda_p (\lambda_p - 1)$	f_d & f_0 is Empirical Coefficients: $f_d = 0.5$ & $f_0 = 0.1$, for Urban Areas c_{d1} is Free Parameter ($c_{d1} = 7.5$) ψ_k is Roughness Sub Layer Influence Function	1. (Grimmond & Oke, 1999) 2. (Raupach, 1994) 3. (Macdonald, Griffiths, & Hall, 1998)

				4. $\bar{h}_{vW} * (\lambda_p^{0.6})$	u_* is Frictional Velocity U is Large Scale Wind Speed c_s, c_r is Drag Coefficients; $c_s=0.003, c_r=0.3$ K is Von Karman's Constant ($K=0.4$) α is Empirical Coefficient (4.43 For Staggered Array) β is Correlation Factor for Drag Coefficient (1.0 for Staggered Array) C_D is Drag Coefficient (1.2) C_{dh} is Drag Coefficient Dependent On Obstacle Shape S_{12} Distance Between Building 1 and Building 2	4.(Gal and Sumeghy, 2007; Gál and Unger, 2009)
		z_0	Surface Roughness Length	1. $z_0 = f_0 \bar{z}_H$ 2. $z_0 = (z_{ref} - z_d) \exp\left(-\frac{k}{\sqrt{0.5\lambda_f C_{dh}}}\right)$ 3. $z_0 = (z_{ref} - z_d) \exp\left(-\frac{\sqrt{0.4}}{\lambda_f}\right)$ 4. $\frac{z_0}{z_H} = \left\langle 1 - \frac{z_d}{z_H} \right\rangle \exp\left\langle -k \frac{U}{u_*} + \psi_k \right\rangle$ $\frac{u_*}{U} = \min\left[\left(c_s + c_r \lambda_f\right)^{0.5}, \left(\frac{u_*}{U}\right)_{max}\right]$ 5. $\frac{z_0}{z_H} = \left(1 - \frac{z_d}{z_H}\right) \exp\left\{-\left(0.5\beta \frac{C_D}{k^2} \left(1 - \frac{z_d}{z_H}\right) \lambda_f\right)^{-0.5}\right\}$	K is Von Karman's Constant ($K=0.4$) α is Empirical Coefficient (4.43 For Staggered Array) β is Correlation Factor for Drag Coefficient (1.0 for Staggered Array) C_D is Drag Coefficient (1.2) C_{dh} is Drag Coefficient Dependent On Obstacle Shape S_{12} Distance Between Building 1 and Building 2	1.(Grimmond & Oke, 1999) 2.(Bottema, 1997) 3.(Gal and Sumeghy, 2007; Gál and Unger, 2009) 4.(Raupach, 1994) 5.(Macdonald et al., 1998)
6	Sky View Factor(SVF)	Ψ_{sky}	Sky View Factor(SVF)	$SVF_{maxi} = \frac{\pi}{2} \sin\left\{\frac{\pi \cdot (i-0.5)}{2n}\right\} \cdot \cos\left\{\frac{\pi \cdot (i-0.5)}{2n}\right\}$	n is the count of annular rings, i the number of the actual ring π the mathematical constant Pi.	(Hämmerle, Gál, Unger, & Matzarakis, 2011; Steyn, 1980)

Table 2-2: Definition of key UCPs and their impact on urban micro climate

S. No.	Parameter Group	Definition and Implication for urban micro climate
1	Building Height	<ul style="list-style-type: none"> • Defines the depth at which the urban canopy interacts with the atmosphere (Xu et al., 2017) • Used to derive the surface roughness length by using simple rule-of-thumb approach (Grimmond & Oke, 1999) • important for parameterization of turbulent flow and reduction in wind flow due to urban fabric (Ng et al., 2011) • Indicator of thermal properties which can be used for modeling anthropogenic activities.
2	Plan Area Fraction	<ul style="list-style-type: none"> • Defines the surface cover fractions of an urban systems on a coarser scales • Building Surface Fraction (BSF) (Oke et al., 2017; Stewart & Oke, 2012)(Oke et al., 2017; Stewart & Oke, 2012)/ Building Plan Area Fraction (SJ Burian et al., 2003)/ Building Coverage Ratio (Xu et al., 2017) <ul style="list-style-type: none"> ○ It is the ratio of building area in each grid cell to the grid cell area ○ If building plan area fraction < 0.1 , isolated roughness flow occurs, if it is between 0.1 to 0.6 , then wake interference flow is dominant and if it is > 0.6 then skimming flow prevails (Hussain & Lee, 1980; Oke, 1987) • Pervious Surface Fraction(BSF) or Vegetation Surface Fraction(VSF) <ul style="list-style-type: none"> ○ Ratio of vegetation (λ_v) or pervious surface area (Vegetation, bare soil, water) to the total area (Oke et al., 2017; Stewart & Oke, 2012) ○ Provides cooling effect due to evaporative cooling and high latent heat flux (Naeem et al., 2018; Oke et al., 2017; Perera & Langappuli, 2013) ○ frequently used as urban micro climate regulator ○ Decreasing percentage of PSF – considered one of major reason for increasing UHI effect (Takkanon & Chantarangul, 2019). • Impervious Surface Fraction (ISF) (λ_i) <ul style="list-style-type: none"> ○ is the ratio of all paved grounds such as roads, parking lots, and athletic tracks etc. to the total area (Oke et al., 2017; Stewart & Oke, 2012). ○ Significant increase in ISF in urban areas as compared to surroundings (Yin et al., 2018) ○ considered as one of major modifier of urban climate ○ key parameter in urban flood and climate modeling studies (Wu & Yuan, 2011)

3	Building Plan and Roof Area Density	<ul style="list-style-type: none"> • Building Plan Area Density (Burian, Velugubantla and Brown, 2002a; Burian and Brown, 2003b; Glotfelty <i>et al.</i>, 2013) <ul style="list-style-type: none"> ○ Fraction of building plan area as a function of height ○ depicts that how much air volume is occupied by buildings ○ used to compute Roof Area Density • Roof area Density(RAD) <ul style="list-style-type: none"> ○ Calculated as difference between plan area densities at two different heights ○ Useful for understanding the thermodynamics of urban canopy and used for estimating the urban energy fluxes (Burian, Brown and Linger, 2002b; Burian, Han and Brown, 2003a; Burian, Stetson, Stephen W., Han and Ching, Jason, Byun, 2004) ○ Roofs intercepts solar radiation, gain heat due to reception of radiation and also act as reflectors. It also absorbs short wave radiation and again emit it inside the buildings.
4	Aspect Ratio	<ul style="list-style-type: none"> • Complete Aspect Ratio (CAR) (Burian, Han and Brown, 2003a; Ching <i>et al.</i>, 2009) <ul style="list-style-type: none"> ○ Non-dimensional parameter ○ Computed as the ratio of all three dimensional active surfaces (including walls, roofs and ground) to the total area ○ useful for evaluating urban energy budget ○ Increase in value of CAR signifies increased quantity of active surfaces available for energy exchange ○ effects the potential to absorb, reflect, emit, intercept, retard, store and release energy, water and air pollutants • Building Surface Area to Plan Area Ratio (Burian, Brown and Linger, 2002b; Ching <i>et al.</i>, 2009) <ul style="list-style-type: none"> ○ Sum of building surface area (Roof and walls) divided by the total plan area ○ defines the active 3D building surface area to intercept, store and release the energy in urban area • Height-to-Width Ratio /Aspect Ratio <ul style="list-style-type: none"> ○ Ratio of average building height to the horizontal distance (street width) between the buildings (Oke et al., 2017) ○ effects the quantity of solar access in the urban canyon (Shishegar, 2013) ○ important for defining the flow regimes in urban areas ○ study in Dubai with a hot-arid climate concluded that narrow street canyons could increase the wind speed passing through it (Al-Sallal & Al-Rais, 2012) ○ Ideal value of H/ W ratio each climate zone need to be defined especially in developing regions.
5	Aerodynamic Roughness parameters	<ul style="list-style-type: none"> • Urban areas are the roughest surface out of all earth surface features • important parameter for meteorological, wind engineering and pollutant wind dispersion modelling

		<ul style="list-style-type: none"> • critical for applying logarithmic wind profile or finding the correct coefficient for vertical wind profile in Power Law equation (Oke et al., 2017). • Roughness parameters- Zero-Plane Displacement Height (z_d), Surface Roughness Length (z_0), Plan Area Density (λ_p), Frontal Area Index (λ_f) (Gál and Unger, 2009; Wong, J E Nichol, <i>et al.</i>, 2010a; Wong and Nichol, 2013) Frontal Area Density (Yuan, Ren, & Ng, 2014), Depth of the Roughness Sub-layer (z_r)(Bottema, 1997; Grimmond et al., 1998) and the Effective Height ($heff$)(A Matzarakis & Mayer, 2008; Andreas Matzarakis & Mayer, 1992). • Building Frontal Area Index (λ_f) <ul style="list-style-type: none"> ○ area of vertical wall surface in a particular wind direction which acts as a roughness element and create a drag effect on the wind flow (Burian, Han and Brown, 2003a; Wong, Janet E. Nichol, <i>et al.</i>, 2010b; Wong and Nichol, 2013; Wicht and Wicht, 2018) ○ ratio of frontal area in a particular direction to its unit horizontal surface area ○ defines the barrier imposed by the buildings to the oncoming wind flow and varies with the wind direction, shape of building arrays and their configuration ○ It is a good indicator of surface roughness and can be utilized for ventilation path map generation in urban areas • Frontal Area Density <ul style="list-style-type: none"> ○ Measure of frontal area per unit horizontal area per unit height increment (Burian, Han and Brown, 2003a; Glotfelty <i>et al.</i>, 2013) ○ used to quantify the drag force as a function of height in plant and urban canopy and average wind profiles in the urban canopy. • Zero Plane Displacement Height(z_d) <ul style="list-style-type: none"> ○ One of the Key roughness parameter ○ “the height of a surface formed by distributing the aggregate volume of roughness elements and their wake re-circulation cavities uniformly over the underlying surface”(Macdonald et al., 1998) • Surface Roughness Length (z_0) <ul style="list-style-type: none"> ○ Key roughness parameter ○ defined mathematically as the height above the displacement height plane at which the wind velocity becomes zero (Burian, Han and Brown, 2003a) ○ Both of these parameters(z_0 and z_d) cannot be estimated with certainty by experiment or theory
6	Sky View Factor(SVF)	<ul style="list-style-type: none"> • defined as the “ratio of the radiation received (or emitted) by the ground surface to the radiation received (or emitted) by the entire hemispheric environment”(Johnson & Watson, 1984) • defines the unobstructed view of the sky which effects the solar access in the urban canyons as well as the nocturnal cooling of the urban canyons (Park, Ha, & Lee, 2017)

		<ul style="list-style-type: none"> • value is dependent on the position and orientation of the surface with respect to the obstructed sky. For example, in agricultural fields or on the roof top not obstructed by surrounding roof tops its value is unity, whereas in very narrow and deep canyons its value could be near to zero. • one of the key parameter to define the urban canyon geometry and to study the effect of building geometry and configuration on ambient temperature • an important indicator for urban heat island studies (Tamás Gál, Lindberg, & Unger, 2009; Oke, 1987; Xu et al., 2017) • Estimation of SVF is complex as it requires computation in 3-Dimensional hemispherical sky.
--	--	---

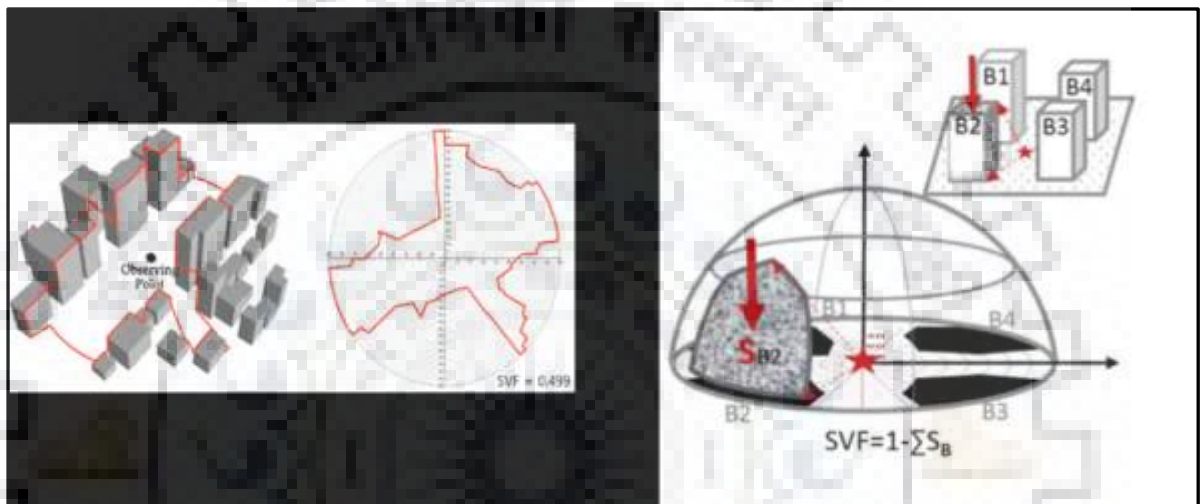


Figure 2-1: Illustrated Calculation of Sky View Factor
(Source: Xu et al., 2017, Park et al., 2017)

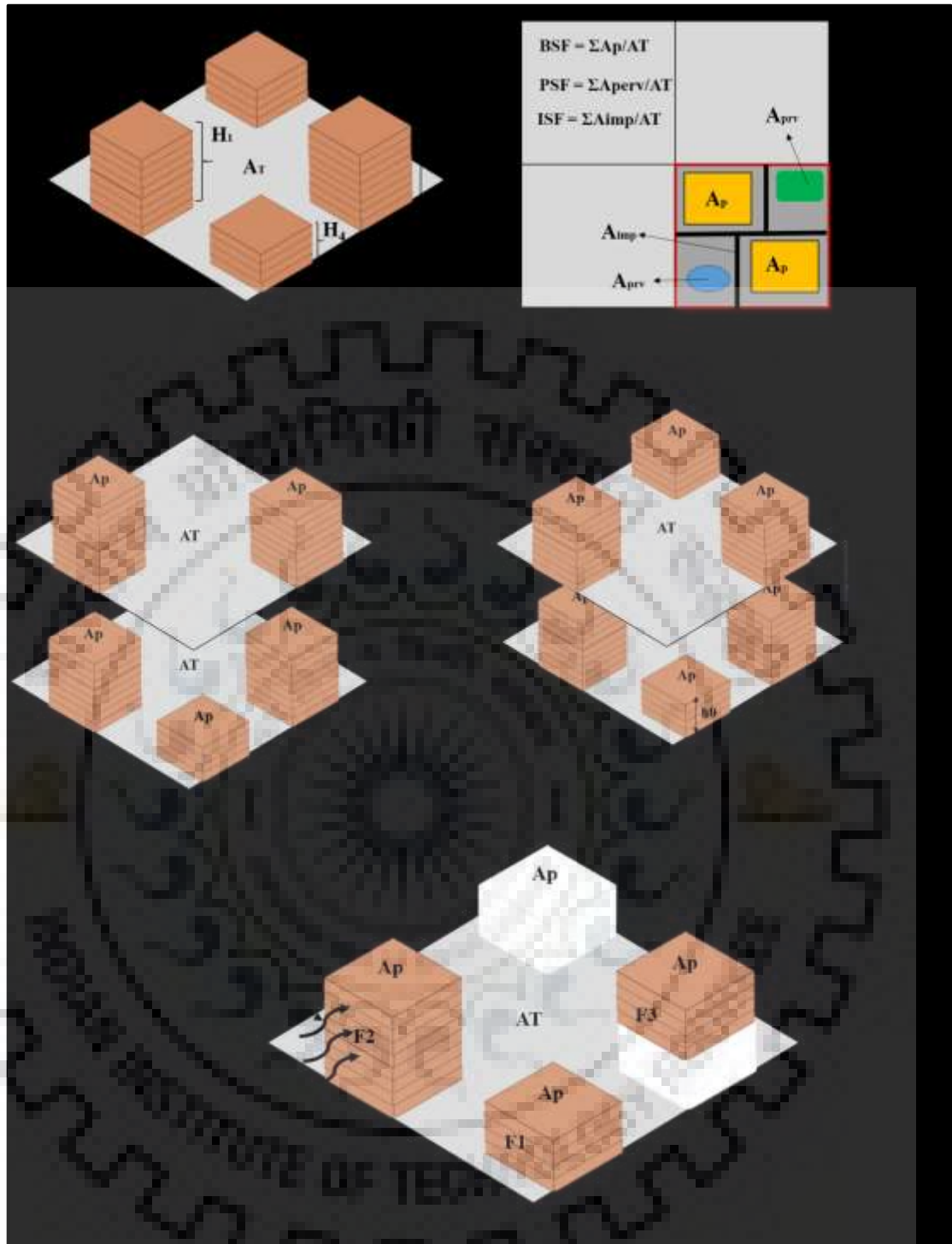


Figure 2-2: Graphical Representation of Urban Canopy Parameters (1) (Source: Author)
 A: Mean Building Height, B: Surface Cover Fractions, C: Building Plan Area Density, D: Roof Area Density, E: Frontal Area Index

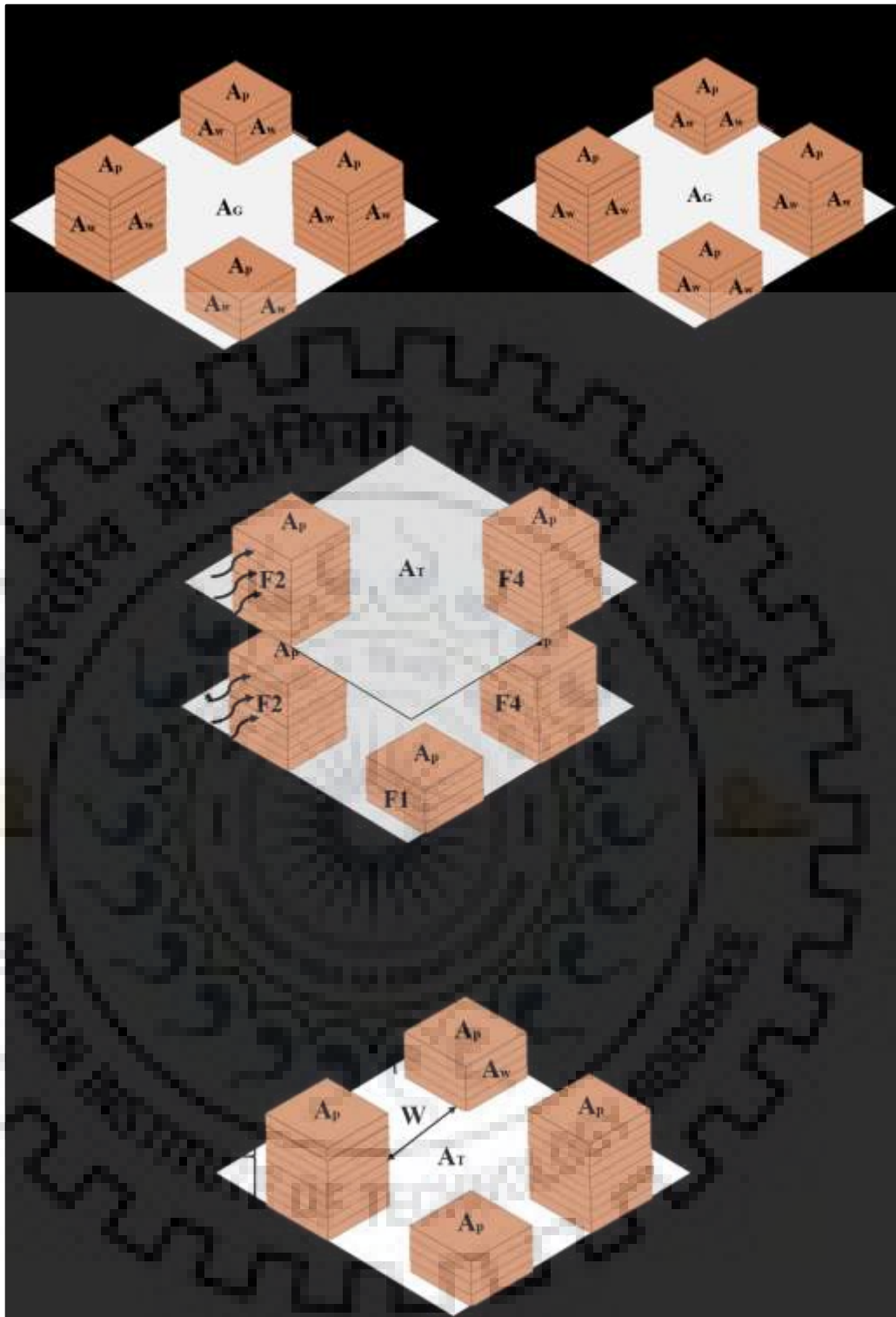


Figure 2-3: Graphical Representation of Urban Canopy Parameters (2) (Source: Author)
F: Building surface Area to Plan Area ratio, G: Complete Aspect Ratio, H: Frontal Area Density, I: Height-to-Width Ratio

2.6 METHODS FOR ESTIMATION OF AERODYNAMIC ROUGHNESS PARAMETERS

Surface roughness of earth's features whether buildings structures, trees, vehicles etc. influences the wind profile in urban areas at micro level. Aerodynamic Roughness parameters in urban areas can be derived using three broad methods such as Reference (classification) based methods, Micrometeorological (anemometric) method and Morphometric methods.

2.6.1 Reference (classification) based methods

This method uses roughness values based on earlier measurements for different land use classes. Davenport, 1960 classified the terrain into eight land use classification and estimated the roughness values for wide range of terrains. Later on, the eight classification scheme was validated and extended by Wieringa, 1992 based on 60 field experiments to ten land use classes (Wieringa, 1992). This method provides an approximate estimation of roughness values and are widely used in global and meso-scale modeling studies.

2.6.2 Micrometeorological method

Micrometeorological methods depends largely on extensive in-situ measurements which includes observations of wind direction and speed at different heights. Later, this field data is used for computations of roughness characteristics using log-law.

$$\text{Log Law: } \frac{u(z)}{u} = \frac{1}{k} \ln \frac{z-z_d}{z_0} \dots \dots \dots \text{Equation 2-1}$$

Where $u(z)$ is averaged wind speed at height z , u is frictional velocity, k is von Karman's constant and z_d and z_0 are zero-plane displacement height and roughness length respectively. This method requires spatially distributed temporal field observations for which a large network of observation towers need to be installed in urban areas (Gal and Sumeghy, 2007) which is time and cost intensive. The observations are sensitive to errors and most of the time fail to adhere to siting specifications for installation in urban areas. Only 9 observations out of 60 observations could pass the defined siting criteria (Grimmond et al., 1998). Besides, most of the studies failed due to non-inclusion of z_d and high values of z_0 .

2.6.3 Morphometric methods

The morphometric approach for computation of urban surface roughness depends on the easily available characteristics of urban morphology/ built form such as shape, size, height, density and configuration (Grimmond & Oke, 1999; Oke et al., 2017). Morphometric methods make use of measures of urban morphology and their relationships with surface roughness parameters derived from wind tunnel or physical models based studies. The less sophisticated method uses height and density of urban structures for computation (Bottema, 1997; Counihan, 1971; Garratt, 1992; Hanna & Chang, 1992; Kondo & Yamazawa, 1986; Raupach, Antonia, & Rajagopalan, 1991), however, more sophisticated methods utilizes other parameters (frontal area index, height, width and density of roughness elements) for estimation (Grimmond *et al.*, 1998; Gál and Unger, 2009; Wong, Janet E. Nichol, *et al.*, 2010a). These method are advantageous as they are able to compute roughness parameters without the use of expensive network of observations towers. The calculations can be performed for any direction of interest with spatial distribution patterns. However, most of the algorithms and equations are derived from wind tunnel studies with idealized arrays (regular, staggered and random arrays) with uniform height and simplified models (Oke et al., 2017). Hence, it does not include the accurate conditions of existing urban areas consisting large variability.

2.6.4 Micrometeorological vs. Morphometric methods

It has been observed that both methods contains significant sources of error in cities (Grimmond et al., 1998). Although most meteorologists consider meteorological observations to be as standards, however, Raupach (Raupach et al., 1991) observed that even on homogeneous terrain, profile based methods are known to be inaccurate. Another limitation is the requirements of the site characteristics for installing the met observation towers. It was observed that very few sites (9 out of 60) could pass the site requirements and strict implementation of these criteria rejects virtually all available observations (Grimmond & Oke, 1999). Besides, Installation of large number of towers in urban area is not at all practically possible to represent the heterogeneity of urban area. It was also noted that the absence of clear trends between roughness density and either z_0 or z_d does not provide a standard against which roughness parameters estimated from morphometric methods could be tested. However, the ease of implementation, applicability across full range of urban morphologies, compatibility with current technologies and availability of input datasets favors application of morphometric methods.

2.7 GEOSPATIAL TECHNOLOGIES FOR SPATIALLY VARIABLE URBAN CANOPY PARAMETERS

Remote Sensing techniques offer unique perspectives to study the urban system and its impact on climate as it provides numerous benefits over conventional methods in terms of synoptic coverage, geographic location, repetitive view and multiple scales. Remote sensing techniques and systems have significantly advanced since the first recorded nadir air photograph acquired from a hot air balloon over the city of Paris in 1858 (Jensen, 2007). Now remote sensing sensors are available in a wide range of spectral, spatial and temporal resolutions and covers a wide range of electromagnetic spectrum (optical, thermal and microwave) for imaging the Earth's surface.

A number of researchers initiated the work for obtaining information on UCPs in urban areas at micro to local scales of study (10^2 to 10^4 m) by utilizing field based measurements (Ellefsen, 1991; Theurer, 1999). Field based methods can provide a high level of detail, however it is time and labor intensive approach and requires skilled manpower. Aerial photography have also been utilized for urban area profiling and subsequent computation of UCPs in Urban areas (Steven Burian & Jason, 2009). This approach is also time and labor intensive exercise and hence, applicable only for small parts of urban areas. Automated and semi-automated approaches are most efficient and have advantage of elimination of subjectivity in interpretation, however, quality of data needs to be ensured for retrieval of UCPs (Steven Burian et al., 2004). GIS based techniques for computation of UCPs by applying morphometric equations have been developed and presented by few of the researchers by applying 3D GIS database (Ellefsen & Cionco, 2002; Grimmond & Souch, 1994; Petersen & Parce, 1994). Grimmond and Oke (1999) presented a review of various morphometric approaches to obtain information on aerodynamic roughness characteristics by reviewing several methods based on building and tree canopy characteristics (Grimmond & Oke, 1999). LiDAR remote sensing data have been utilized to obtain 3D GIS database for the computation of number of UCPs in various US cities (Burian, Brown and Linger, 2002b; Burian, Velugubantla and Brown, 2002a; Burian and Brown, 2003b; Burian, Han and Brown, 2003a) that includes Los Angeles, Phoenix, Salt Lake City, Portland, Albuquerque, Oklahoma City, Seattle, and Houston. Developed approaches also included computation of tree/vegetation canopy characteristics later along with building canopy characteristics using morphometric equations and 3D GIS database (Steven J Burian et al., 2004). The availability of 3D building and tree datasets in many U.S. cities led to development of detailed and gridded UCPs which have been hosted on NUDAPT for integration in numerical models for 44 US cities. However, most of the studies relied on LiDAR derived 3D GIS database for the computation of

UCPs. LiDAR is an active remote sensing data which is considered as the most suitable data for urban surface modeling and rapid auto generation of 3D building models (Tse, Gold and Kidner, n.d.; Mohammad Awrangjeb, mehdi RavanBakhsh, 2010; Bretar, Wagner and Paparoditis, 2011). Tools and algorithms need to be further developed for the processing of the unstructured point clouds for its effective utilization. Besides, higher processing capabilities are also must for processing the large volume of 3D point clouds. The researchers worldwide have used LiDAR data in urban environment for extracting building outlines, as well as, height and structure attributes for parameterizing the urban surface in atmospheric modeling (Carter et al., 2012; Fei Chen et al., 2011). Recently Synthetic Aperture RADAR (SAR) and Interferometric SAR data have also been used for 3D profiling and generation of building volume maps of urban areas (Jeyachandran et al., 2010; Yong et al., 2015). However, as discussed earlier, availability of LiDAR, high resolution InSAR and aerial photographs is limited availability and has high cost in developing regions (Gupta et al., 2017a).

High spatial resolution optical imageries were available from air borne sensors but now with advancement in technology, a range of civilian satellite sensors starting from Ikonos in 1999 (Bhaskaran, Paramananda, & Ramnarayan, 2010) and upcoming satellites are providing sub meter imageries in optical region. These finer resolution imageries contain detailed information about urban areas and can be effectively utilized for characterization of urban areas (Herold & Roberts, 2010). Researchers have used extensively not only the mono satellite imageries, but also high resolution satellite stereo imageries in optical domain (Yom and Oh, 2011; Tack, Buyuksalih and Goossens, 2012b; Rajpriya, Vyas and Sharma, 2014; Gupta *et al.*, 2015; Gupta et al., 2017a) for profiling urban areas in 3rd dimension. Therefore, it is recommended that low cost and widespread availability of sub-meter optical stereo data should be explored for obtaining information on 2D and 3D characteristics of urban areas and subsequent retrieval of UCPs in developing regions. The following sections describes in detail the use of RS data for the retrieval of surface cover characteristics, 3D building database and UCPs in urban areas.

2.7.1 Surface cover characterization

Surface cover fractions (building, pervious and impervious) are the most widely used 2D UCPs for urban climate studies. Optical remote sensing data have been utilized widely for deriving the surface cover fractions in urban areas at varied scales (sub-meter to 1km resolutions) in a faster and economical manner as compared to conventional methods (Xu *et al.*, 2017; Hong-Mei *et al.*, 2006; Wu and Yuan, 2011; Perera and Langappuli, 2013; Kaspersen, Fensholt and Drews, 2015;

Li *et al.*, 2018a). It is also utilized for obtaining information on many biophysical parameters such as vegetation cover (Ridd, 1995; Surawar, Meenal; Kotharkar, 2017), fraction of impervious surfaces (Kaspersen *et al.*, 2015), albedo (Odunuga & Badru, 2015) and emissivity (Srivastava, Majumdar, & Bhattacharya, 2010) at varied scales. Coarse resolution remotely sensed data such as Advanced Very High Resolution Radiometer (AVHRR), Moderate Resolution Imaging Spectro-radiometer (MODIS) and Advanced Wide Field Sensor (AWiFS) have been used extensively to provide LULC information for global and mesoscale climate modeling (Masson *et al.*, 2003). Nowadays, various RS data products of 500 m- 1 km resolution are freely available on web for several Land Surface Parameters (LSPs) such as urban fraction, leaf area index, fractional vegetation cover, Land Use Land Cover (LULC), land surface temperature and so on (Gharai, Rao, & Dutt, 2018; Masson *et al.*, 2003) for ingestion in global and meso scale climate models. With increasing resolutions of climate models, optical medium resolution data have been used to generate the freely downloadable Global Settlement Layer (GSL) by European commission to more accurately represent and analyze the impact of human activities on global climate scenario (“Global Human Settlement - Data overview - European Commission,” 2016). It has improved the representation of urban areas in global climatic models, however, it defines only one urban land use class i.e. urban built-up. Single urban built-up class have been found to be insufficient to represent large variability of urban areas. Hence, Landsat TM data have been utilized to prepare National Land Cover Dataset (NLCD) for US cities with 3 urban classes for ingestion in coupled WRF/Urban Canopy Model (UCM) for representing heterogeneity of urban areas in mesoscale numerical models. It has been found that utilization of this data provided improved results (Bhavana *et al.*, 2018) and found suitable for long-term weather forecasts (F. Chen, Kusaka, Tewari, Bao, & Hirakuchi, 2004). Majority of urban and suburban classification of Urban LULC for urban climate is mainly done by coarse to medium resolution satellites. However, availability of very high (sub-meter to 6 m) resolution RS data enables the development of very high and more detailed classification of urban areas. Further, advancement in computing resources and image processing techniques will allow for development of high resolution information on surface cover fractions, LULC and LSPs for urban scale modeling studies.

2.7.2 3D Building database and urban canopy parameters

Recently developed coupled urban canopy models such as single layer and multi-layer UCMs requires detailed building level 3D UCPs as inputs (Carter *et al.*, 2012; Fei Chen *et al.*, 2011; Hammerberg *et al.*, 2018). Airborne LiDAR systems have been used increasingly to derive the

three dimensional building data sets all around the world (Steven Burian & Jason, 2009; Carter et al., 2012; Sohn & Dowman, 2007; Wicht & Wicht, 2018). It provides the data with very high resolution of the order of 1-5 m. LiDAR provides DSMs and DTMs with sub- meter vertical accuracies, which allow the derivation of building height and size, shape, orientation and relative location with other buildings and urban morphological features. It is considered as the best technology for deriving 3D information of urban areas. However, availability of LiDAR data in some of the countries are limited especially in developing world that limits its use for derivation of 3D building database and subsequently computation of UCPs (K. Gupta et al., 2015).

SAR and InSAR satellite and airborne systems have also been used to map urban building form, distribution, density and roughness elements (Jeyachandran et al., 2010; Xu et al., 2017). The study highlighted the potential of SAR data for deriving urban morphology in tall building area, however, in areas with small building heights the accurate relationship between radar backscatter and UCPs could not be established. Fusion of optical and SAR data for estimating building height in Kowloon peninsula, Hong Kong provided better height estimates in high rise building area. Terra SAR-X system recently launched global urban footprint layer at 12 m resolution and it is expected to provide the world wide data for building volume at 120 meter grid resolution in near future. However, use of SAR technique is still limited due to high data cost and limited availability of very high resolution SAR data.

Knowledge of urban surface roughness plays key role in understanding wind dispersion modelling, detection of urban ventilation paths and heat flux exchange in urban environment. With the advent of higher computation capabilities and availability of 3D urban databases through remote sensing, estimation of roughness values using morphometric methods has become easier and less resource consuming. These recent techniques rely on the algorithms using drag force and force around buildings (Ratti, Di Sabatino, & Britter, 2006). Numerous studies (Burian, Han and Brown, 2003; Gal and Sumeghy, 2007; Wong, Janet E. Nichol, *et al.*, 2010a; Yuan, Ren and Ng, 2014) have used existing 3D building datasets for computation of roughness parameters. GIS based technique have been proposed to investigate urban roughness along the coast of Kowloon peninsula of Honk Kong by using a 3D building database (Wong, J. E. Nichol, *et al.*, 2010b). Remote sensing technologies especially LiDAR have been used widely to generate 3D building and tree GIS database in many of the developed countries. As discussed earlier, use of high resolution satellite optical stereo data needs to be explored for development of 3D GIS database as availability of LiDAR and airborne data is limited in developing regions.

The increased availability of very high resolution stereo datasets, photogrammetric software and computing facilities facilitates the generation of high resolution Digital Terrain Models (DTMs) and Digital Surface Models (DSMs) that allow the extraction of building footprints and height information. Initially aerial photography have been used for manual collection of building footprints and height (Steven J Burian, Velugubantla, et al., 2002a), however, it have been time and resource intensive task. Cartosat-1 data (2.5 m spatial resolution) was applied for semi-automatic extraction of building heights by measurements in 3D environments and digitization of building footprints from the ortho images in Delhi, India (K. Gupta et al., 2015). This method could generate height estimates with reasonable accuracy, however, the digitization of building footprints in large high density urban areas is not feasible. A range of very high resolution satellite stereo such as Pleiades, world view 2, IKONOS, Kompsat-3 etc. with sub-meter resolutions are also available in present context. These datasets have been utilized for extraction of building footprints and 3D information (Yom and Oh, 2011; Tack, Buyuksalih and Goossens, 2012; Gupta et al., 2017a). Most of these satellites acquire stereo in along track or across track mode. But Pleiades satellites has tri-stereo capabilities with imaging in simultaneous mode. The satellite carries three cameras on board for images in nadir, forward and backward direction in a single pass along with high spatial resolution of 0.5 m. Evaluation of the automatic extraction of building heights from Cartosat-2, Pleiades and Kompsat-3 stereo data achieved highest accuracy with RMSE value of 0.31m in building height estimation with Pleiades satellite stereo in compact built environment of Delhi (Gupta et al., 2017a). Hence, satellite stereo data proved to be a good source of information for extracting the 3D information in urban areas. However, the extraction of building footprint in high density built up areas is still challenging. Application of segmentation methods on a part of Delhi provided high accuracy in planned development and isolated building areas however, the method could not yield satisfactory results in very high density (>80%) urban built up of Delhi. The further improvement in segmentation methods or approaches is required for improved results.

2.7.3 Sky View Factor

Various methods such as fish eye photographs(Steyn, 1980), scaled models (Oke, 1981), evaluation of GPS signals (Chapman, Thornes, & Bradley, 2002) and 3D urban database (Tamás Gál et al., 2009; Jhaldiyal et al., 2018) had been applied for computation of SVF. Ratti 2001 developed a method for the computation of SVF using Digital Elevation Model (DEM). Increasing availability of high resolution DEM from LiDAR, satellite photogrammetric and InSAR techniques creates a huge potential for computation of SVF using raster GIS datasets.

Evaluation of SVF computed through vector and raster 3D database in GIS and found a strong correlation with r^2 value of 0.9827. Hence, DEM derived from remote sensing datasets can be utilized effectively for computation of SVF.

Computation of UCPs have evolved in last few decades from detailed inventories using airborne data and extensive field surveys to processing of 2D and 3D GIS database obtained from LiDAR to multi-spectral imagery datasets. The processing is computation resource intensive and requires high end computation facilities. It is required to evaluate available multi-sensor datasets at various resolutions for generation of UCPs. There is also a need to resolve ambiguities and uncertainties in parameter definition and methods and to develop standardized approaches for retrieval of UCPs especially in highly complex and heterogeneous urban environment of developing regions. The advancements in scripting languages, image processing techniques and computation resources have enabled automated extraction of various UCPs. This field is growing and has substantial potential to fill the data gap world over.

2.8 METHODS FOR SPATIALLY VARIABLE URBAN CLIMATE INDICATORS

The methods for urban climate research can be categorized into broad categorization of field observations, physical modelling and numerical modeling. The field observations are further classified into measurements using ground based stations both fixed and mobile measurements, free flow techniques and remote sensing techniques. Physical modelling studies are based on laboratory models and outdoor scale models. The field observations provide the basic understanding of urban effect, while physical models allow researchers to regulate the nature of urban surface as well the properties of overlying atmosphere. The numerical models are important to test and examine how cities effect climate and vice versa as they allow to integrate phenomenon and processes at different scales.

In-situ field observations of climate variables have been widely used for study of urban micro climate (Oke, 1987, 1988; Souch and Grimmond, 2006; Shishegar, 2013; Kotharkar and Surawar, 2016; Oke *et al.*, 2017). It is the oldest method and forms an important input for urban climate studies, research and modeling. It can be obtained through ground based fixed stations, mobile traverses or free flow techniques using balloon, etc. (Oke *et al.*, 2017). However, the high heterogeneity of urban environment calls for an extensive network of observations for obtaining spatially variable information which could be highly expensive, time and resource consuming and most of time practically not feasible in urban areas due to elaborate site requirements (Oke, 2008). Hence, extensive network of ground observation is either not available or if available

through network of portable/automatic weather sensors, poor data quality or insufficient metadata information, limits its use for analysis. Mobile traverses provides limited area and time coverage. Similar limitation is observed with free flowing techniques. Besides, it is difficult to exert control over the measurements due to natural variability of weather and heterogeneous urban surfaces. The data obtained needs to be analyzed carefully by considering the urban environment under study. Measurement errors are always present due to variety of reasons such as definition of source area (turbulent and radiative), appropriate siting, scale of measurement and temporal resolution etc.(Oke et al., 2017).

Physical models whether laboratory models or outdoor scaled models are prototype and simplified versions of real world situations. They have the advantage of having controlled experimentation and observations and can provide spatially variable information on one or more variable at a time. They have been used to simulate turbulent flow, pollutant dispersion and transport, wind energy, wind forcing on bridges and high rise buildings, human comfort and safety and so on. The major limitation is that it requires special sometimes costly facilities and careful design to ensure similitude with real urban environment and generally applied on small area (Oke, 1987; Oke et al., 2017).

2.8.1 Thermal Remote Sensing

Remote sensors deployed on ground based station, aircraft or satellites has huge potential for providing the up-to-date, spatially variable and area-wide information on climate variables which is well suited to study highly variable urban climate patterns. Remotely Sensed Thermal Infrared (TIR) data have been widely used to retrieve Land Surface Temperature (LST) (Rasul et al., 2017; Sismanidis, Keramitsoglou, Bechtel, & Kiranoudis, 2016; Voogt & Oke, 2003; D. Zhou et al., 2019). A series of satellite and airborne sensors have been developed to collect data in thermal region of electromagnetic spectrum such as Heat Capacity Mapping Mission (HCMM), Landsat Thematic Mapper/Enhanced Thematic Mapper (TM/ETM+), AVHRR, MODIS and Advanced Spaceborne Thermal Emission and Reflection Radiometer (ASTER). These datasets have also been used for extracting emissivity data of different surfaces at varied resolutions and accuracies. In urban climate studies, LST and emissivity is mainly used to understand the LST patterns, its relationship with surface characteristics, assessing urban heat island and for relating LST with surface energy fluxes. Landsat TM, ETM+, and TIRS data and ASTER are two sensors, which have been widely used for urban climate studies due to their comparatively finer resolutions (~ 60-120m). This is the highest possible resolution available at the moment, however, the further

finer resolutions data may help to resolve various urban classes. The Landsat data is freely downloadable from Earth Explorer website for a long time now but recently ASTER data is also made freely available in the above website. Both of the sensors provide data at 30 m resolution which still consist of a mixture of urban surfaces. Development of finer spatial resolution TIR sensors in future will be highly useful for urban planning purposes.

TIR Remote sensing have been used increasingly to identify Surface UHI (SUHI) effect and intensity by many researchers. SUHI effect, as mentioned before, displays increased surface and air temperatures in urban areas. Many factors contribute to the formation of UHI such as urban surface permeability, building material thermal properties, population density, anthropogenic heat emission and urban canyon geometry. Previous studies of UHIs using remote sensing data have been conducted by using NOAA AVHRR data (Roth, Oke and Emery, 1989). However, 1km resolution AVHRR data was suitable only for regional level UHI mapping. The Landsat data of 120m resolution have been used extensively to study the UHI effect and derivation of LST (Z.-L. Li et al., 2013; Sobrino, Jiménez-Muñoz, & Paolini, 2004; Srivastava et al., 2010; Surawar, Meenal; Kotharkar, 2017). Many algorithms have been developed for the estimation of LST, which uses different properties and methods such as Split Window Algorithm (Jiménez-Muñoz, J.-C.; Sobrino, 2008), Mono-Window Algorithm (Qin, Karnieli, & Berliner, 2001), Single Channel Algorithm (Jiménez-Muñoz, J.C.; Sobrino, 2010), and Radiative Transfer Equation (Z.-L. Li et al., 2013). There are various COTS software like ArcGIS, Erdas Imagine, ENVI which assist in LST estimation. Recently, open source software QGIS also provides a plugin for the estimation of LST from remote sensed thermal data (Ndossi & Avdan, 2016).

2.8.2 Numerical Modeling

Landsat and ASTER satellites have been utilized for estimation of LST at finer resolution (30-120m) (Z.-L. Li et al., 2013; Rasul et al., 2017; D. Zhou et al., 2019). However, it provides only LST information. Other climate variables such as temperature at 2m, wind speed, humidity, pressure etc. is either not available through remote sensing or available at very coarse resolutions (~4 km). Numerical modeling has huge potential in this area and can be applied effectively to understand the urban climate trends, processes and predictions and to obtain spatially variable climate indicators at high resolution. They are therefore an indispensable tools for understanding the complex interactions of urban built form and climatic exchanges taking place in urban areas. Numerical models simulate real world phenomenon using a set of mathematical equations that link properties to processes (Chen, 2014). Numerical modelling provides opportunities to

examine and test the understanding of how cities effect climate and vice versa. They provide full experimental control and can be employed at all scales of urban climate studies. It can be utilized for forecasting and prediction which can be utilized for practical purposes such as disaster management, climate change prediction and so on.

Numerical models for urban climate studies can be classified into Computational Fluid Dynamics (CFD) Models, urban thermal environment models and mesoscale models (Georgatou & Kolokotsa, 2016). CFD models utilizes fundamentals of fluid dynamics by considering air as compressible fluid to model flow of fluid at each cell (Moonen, Defraeye, Dorer, Blocken, & Carmeliet, 2012). Although, these models are capable of providing very high resolution of nearly 10s of meters, however, due to extensive computational requirements, have been applied only on small areas. Besides, the application of these models requires strong background on fluid dynamics (Georgatou & Kolokotsa, 2016). Ali-Toudert and Mayer has noted that “Most of the CFD microclimate models do not have the capability to assess outdoor thermal comfort since they do not calculate the radiant fluxes reaching the human body within complex urban environment”(Ali-Toudert & Mayer, 2006). The holistic approach of modeling should link building scale to micro scale and mesoscale models. ENVI-MET is a 3Dimensional thermal environment microclimate model to simulate wind flows, turbulence, radiation fluxes, temperature and humidity, however, the model does not consider the heat stored in the walls (Giridharan, 2016).

However, recently developed Urban Canopy Models (UCMs) coupled with mesoscale models integrates various options to model atmospheric processes in urban areas. There have been a significant progress in predictive capacity of numerical models, computational resources and modeling of underlying physics and dynamics and improved resolutions which have created enhanced opportunities to use these models for more realistic understanding of atmospheric phenomenon in holistic manner (Garuma, 2018). In the beginning of 2000s, parameterization of urban surfaces in mesoscale models based on dynamical equations were started. The advancements in computational facilities and modeling of urban physics created prospects to account for heterogeneous urban environment and downscaling of climate variables at higher resolutions in mesoscale models. It also provided opportunities for better prediction of climate and weather processes related to air quality, pollution, and impact of climate change. It has improved representations of finer spatial details and better simulated temporal variabilities. MM5 and Weather Research and Forecasting (WRF) are few of the mesoscale NWP models which integrates urban canopy models to simulate the urban effects. The WRF Model is meso scale

numerical weather prediction system designed for both atmospheric research and operational forecasting applications. The WRF model is a non-hydrostatic, compressible model with a mass coordinate system (Duda, 2007). WRF is designed for numerical weather prediction model and yet it also have been employed widely as regional climate model. WRF is most useful in urban applications to accurately capture influences of cities on wind, temperature, and humidity in the atmospheric boundary layer (Fei Chen et al., 2011; Mohan & Bhati, 2011; A. Sharma et al., 2017). WRF generally provides the capabilities to downscale atmospheric variables to grid spacing of 0.5 to 1 km to reduce the gap between meso scales modeling and micro scale modeling (A. Sharma et al., 2017). It provides spatially variable information on widely used urban climate indicators at comparatively higher resolutions which can be employed to understand the relationship between urban characteristics and urban climate indicators. However, the parameterization and integration of urban characteristics in these models are in initial stages. It needs an interdisciplinary approach by bringing together meteorology, urban planning and design, landscape, architecture and building physics.

2.9 RELATIONSHIP BETWEEN SPATIALLY VARIABLE URBAN CANOPY PARAMETERS AND CLIMATE INDICATORS

The modification in surface cover, building geometry and surface roughness influences radiative fluxes and turbulence flow and results in micro climate variations in urban areas (Souch and Grimmond, 2006). Urban areas differs from rural areas in terms of increased air and surface temperature, low humidity and wind speed and enhanced precipitation. Satellite remote sensing data have been utilized widely to investigate the linkages between urban characteristics and LST majorly due to availability of area wide spatially variable information (Mirzaei, 2015). It is not only capable of providing spatially explicit information of UCPs and biophysical characteristics of urban environment, but also provides information of LST through measurement of upwelling longwave radiation emitted by urban surface features (Z.-L. Li et al., 2013).

Substantial research studies have been conducted to describe LST variations over space and time by utilizing LULC, biophysical descriptors and 2D/3D Urban Site Characteristics (in this study, defined as UCPs). LULC and its spatiotemporal changes is one of the widely studied indicators for assessment of relationship with LST (Roth, Oke and Emery, 1989; Jiang and Tian, 2010; Loridan and Grimmond, 2012). The proportion of built-up, vegetation and water have been utilized as descriptor to explain the spatial variations of LST and SUHI. It was found that buildings and impervious surfaces shows positive correlation with LST (Perera and Langappuli,

2013; Liwen Huang *et al.*, 2015; Li *et al.*, 2018) while vegetation and water shows opposite trend of negative correlation (Hong-Mei *et al.*, 2006; Jiang and Tian, 2010; Babazadeh and Kumar, 2015; Liwen Huang *et al.*, 2015; Berger *et al.*, 2017; Kumar and Panwar, 2017). However, LULC and spatial distribution of land cover features alone are not sufficient to explain the variability of LST in urban areas. Few of the studies applied Land use as a descriptor variable as it considers impact of human activities (Pan, 2015; Yue, Liu, Fan, Ye, & Wu, 2012). For example, Industrial sites exhibits higher temperatures due to high level of anthropogenic heat emissions (Gupta *et al.*, 2017b). Use of LULC as a descriptor explain not only the urban-rural temperature differences but it also elucidate upon intra-urban temperature differences over space and time (Deilami, Kamruzzaman, & Liu, 2018). Biophysical descriptors such as Vegetation Fraction (VF) (Hong-Mei *et al.*, 2006; Liwen Huang *et al.*, 2015; Naeem *et al.*, 2018; Perera & Langappuli, 2013), surface albedo (Bonafoni *et al.*, 2017; Salleh *et al.*, 2014), and impervious surface fraction (Kaspersen *et al.*, 2015; Perera & Langappuli, 2013; Weng *et al.*, 2006) are also commonly used UCPs to describe the spatial variations in SUHI and LST. Use of LULC products also assisted in extraction of various 2D USCs such as fraction of built up, vegetation and impervious surfaces. Various spectral indices such as Impervious Surface Area (ISA) (Li *et al.*, 2018; Wei and Blaschke, 2018), Normalized Difference Built-up Index (NDBI) (Guha, Govil, Dey, & Gill, 2018; Kaplan, Avdan, & Yigit Avdan, 2018; Kikon, Singh, Singh, & Vyas, 2016), and Urbanization Index (UI) etc. have also been employed as descriptors of urban characteristics.

The above discussion highlights that although substantial amount of work has analyzed UCPs-LST relationship, however, the studies of relationship with 2D UCPs have been prominent. On the contrary, although, 3D UCPs such as building volume, height etc has significant impact on urban micro climate variations, very few studies have analyzed relationship of 3D UCPs such as building height, frontal area index, floor area ratio and sky view factor with LST and it remained largely unexplored even for the regions having highly planned urban infrastructure (Chun and Guldman, 2014; Scarano and Sobrino, 2015; Guo *et al.*, 2016; Berger *et al.*, 2017; Yin *et al.*, 2018). The major reason cited is the unavailability of information on 3D UCPs especially in developing regions. A spatial regression analysis by feeding a set of parameters obtained from earth observation data in Columbus, OH revealed that 3D UCPs has strong influence on LST variations (Chun & Guldman, 2014). The similar conclusion was obtained after evaluation of 12 different indicators of configuration of urban cover (2D) and urban geometry (3D) in Bangkok, Thailand (Srivani & Kazunori, 2011). However, a study on linkages of 2D/3D USCs in two German cities pointed out that correlation statistics might be biased towards 2D UCPs as compared with 3D UCPs (Berger *et al.*, 2017). The major reason could be attributed to nadir

viewing sensor geometry of thermal remote sensors. Besides, TIR sensors provides information only on LST but it does not provide spatially variable information on other climate indicators such as temperature at 2m, wind speed, humidity, pressure etc. The information on surface wind speed is either not available through remote sensing or available at very coarse resolutions (~4 km). That limits their use for understanding micro climate characteristics in urban areas.

As discussed earlier, numerical simulations have been employed to obtain spatially variable, high resolution information on urban climate indicators. In recent past, numerical modelling has gained momentum and development of exhaustive Urban Canopy Models (UCMs) facilitates modelling of radiation, heat and energy exchange processes in urban areas. Weather Research and Forecasting (WRF) Model is one of the numerical weather prediction model which have been widely used as mesoscale climate model as well as to downscale urban climate indicators to urban scales (~0.2-0.5 km grid resolutions)(Fei Chen et al., 2011; Hammerberg et al., 2018; Salamanca et al., 2011). It provides spatially variable information on widely used urban climate indicators at comparatively higher resolutions which can be employed to understand the relationship between 2D/3D UCPs and urban climate indicators.

2.10 IMPLICATIONS AND APPLICATIONS OF URBAN CANOPY PARAMETERS FOR URBAN CLIMATE STUDIES

Availability of high quality information on UCPs is imperative to understand impact of urban characteristics on urban climate and vice versa. Lack of availability of up-to-date and spatially variable information on UCPs covering entire urban area results in inadequate understanding of urban climate and limited applications for urban climate research and modeling especially in developing countries (Xu et al., 2017). Since, the countries in developing region are going to witness significant urban growth in near future, they holds the key for climate change mitigation and adaptation strategies (G. Mills et al., 2010). Highly accurate and reliable UCPs information augments the need for urban climate applications, urban planning and climate resilient urban environment. The derived UCPS have been utilized for generation of ventilation path map, GIS based Local Climate Zone map, urban climate map and parameterization in urban canopy models for urban climate research and modeling.

2.10.1 Ventilation assessment

UCPs derived from high resolution optical stereo have great potential for ventilation assessment and identification of ventilation paths in developing world. Unobstructed ventilation path or

corridors enhances natural ventilation in urban areas which assists in mitigation of UHI and dispersion of air pollutants from urban areas. In recent years, Remote Sensing and GIS especially airborne LiDAR or existing 3D building GIS database have been used increasingly for computing aerodynamic roughness parameters and subsequent identification of ventilation path map in urban areas. Ventilation path map in Szeged, Hungary have been generated by using computed zero plane displacement height and surface roughness length in GIS (Gal and Sumeghy, 2007). (Suder & Szymanowski, 2014) used LiDAR data to obtain building height information and 3D database preparation and further to generate ventilation path map in GIS for Wroclaw, Poland. Similarly, LiDAR and satellite derived 3D building database have been utilized for identification and spatio temporal monitoring of identified ventilation paths for three epochs in Warsaw, Poland (Wicht, Wicht and Osińska-Skotak, 2017; Wicht and Wicht, 2018). The study has found that the continuous increase in urban built-up area has blocked many existing ventilation channels. It recommends re-evaluation of existing channels and redesign the paths to ensure citizens' comfort and natural ventilation in urban area. Both the studies have utilized zero plane displacement height, surface roughness length and porosity parameters for ventilation path identification. Few researchers have suggested frontal area index, one of the urban roughness parameter, as a good indicator of urban surface roughness. This parameter have been found to be strongly correlated to flow regimes in urban street canyons for urban dispersion models (Brown & Williams, 1998). Frontal area index have been computed using a customized script in GIS for Hong Kong and least cost path analysis have been applied for the identification of ventilations paths in GIS (Wong, J E Nichol, *et al.*, 2010b). Ventilation path map for Dwarka sub-city, a newly developed planned area of Delhi, have been prepared by developing a satellite based 3D GIS database (Jhaldiyal *et al.*, 2018). Zero Plane displacement height and Surface roughness parameters were computed by using remote sensing derived 3D building database and a customized tool in GIS for frontal area calculation. By combining zero plane displacement height and surface roughness based on the criteria given Matzarakis and Mayer (Matzarakis & Mayer, 1992), the whole area is divided into 3 ventilation classes such as ventilated, partially ventilated and weak or blocked ventilation zones. Availability of remote sensing derived UCPs from high resolution optical data will boost the assessment and identification of ventilation studies in developing countries which is known as one of the major reason for lack of ventilation assessment studies in these regions.

2.10.2 GIS based Local Climate Zone

Urban Heat Island (UHI) studies till recently have focused mostly on the urban–rural temperature gradient (Mohan *et al.*, 2009). However, the mere classification of urban and rural was found to

be insufficient even for UHI studies due to high heterogeneity of urban environment. Hence, a new urban built form classification scheme on the basis of urban structure, urban geometry, urban morphology and anthropogenic heat emission have been proposed (Stewart & Oke, 2012) and is widely known as Local Climate Zone (LCZ) classification scheme. The name is appropriate because the classes are local in scale (10^2 to 10^4 m), climatic in nature, and zonal in representation. LCZ is defined as “regions of uniform surface cover, structure, material, and human activity that span hundreds of meters to several kilometres in horizontal scale”. This scheme defines 10 urban built up and 7 land cover classes as detailed out in Appendix A. It defines geometric and surface cover properties for each LCZ class by defining specific range for a set of the UCPs such as building surface fraction, impervious surface fraction, pervious surface fraction, aspect ratio (height-to-width ratio), sky view factor, height of roughness elements, surface albedo and terrain roughness class (Stewart & Oke, 2012). The availability of information on these UCPs can be utilized for derivation of LCZ maps in GIS.

The LCZ classification scheme have been adopted by World Urban Database and Access Portal Tools (WUDAPT, www.wudapt.org) to collect level 0 worldwide database of urban form and function by utilizing freely available satellite data sources and GIS software (Landsat 8, Google Earth(GE) and SAGA GIS). The method is majorly dependent on pixel based random classifier and have been applied in many countries successfully especially the cities in developed world (Bechtel *et al.*, 2015; Ching *et al.*, n.d.; Bechtel *et al.*, 2019). However, in highly dense and complex urban settings of Hong Kong, the method did not yield reasonable accuracies (Ren *et al.*, 2016). The approach for collection of training data is majorly through crowdsourced approach where interested individuals across various countries collect training samples from GE based on their local knowledge of the area. However, the study by Bechtel (Bechtel *et al.*, 2017) revealed individual capabilities of interpretation and poor understanding of the LCZ scheme were few of the major reasons for large discrepancies in the generated LCZ maps which were mostly ranged from poor to moderate quality. An alternative approach may be needed to prepare good quality LCZ maps especially in developing world with high density developments. UCPs derived either from 3D GIS database or remote sensing data have been utilized to derive high quality GIS based Local Climate Zone(LCZ) map (Geletič & Lehnert, 2016; Mitraka, Del Frate, Chrysoulakis, & Gastellu-Etchegorry, 2015; Unger, Lelovics, & Gál, 2014). A 3D data based approach was employed by utilizing UCPs (Sky View Factor, building density, impervious and pervious surface fraction, building/tree height and surface albedo of urban morphology) to derive the LCZ classification (Mitraka *et al.*, 2015) with high accuracy. The major requirement of this method is the availability of precise GIS data of study area under consideration. Since, in this study, a

detailed database of UCPs have been generated, it can be utilized to generate high quality GIS based LCZ classification map. The developed LCZ maps can provide better understanding and study of the UHI magnitude rather than the conventional urban –rural gradient method. It can also be used by the development authorities and profession like architecture and planners which may use them for master plan and development plan as they can help in analyzing the present climatic condition of an area and also can be utilized for future climatic condition.

2.10.3 Urban climate maps

Urban Climatic Map is a tool which outlines climate sensitive strategies based on the assessment of the climatic characteristics of the region under study (Alcoforado, Lopes, & Andrade, 2015). UC-map generally consist of two parts, first part is climate analysis map which contains analysis of meteorological and urban characteristics of area of interest. Detailed information on UCPs along with meteorological parameters forms an important input for preparation of climate analysis map, Second part outlines the recommendations for climate sensitive planning and design in a language that is understood by planners. The UC-map can assist in integrating climate knowledge in planning for mitigating the effects of climate change and for sustainable development (Alcoforado, Andrade, Lopes, & Vasconcelos, 2009). This tool narrow downs the gap between climatologists and urban planners and provides an effective mechanism for integrating the climate knowledge in the planning process.

The UC-map studies have been pioneered by Germany and more than 30 countries in the world have generated UC-map to support climate oriented urban planning to promote sustainable development (Ng, 2011). Information on UCPs and GIS based methods have been utilized for generation of Urban Climatic (UC- map) map (Chen and Ng, 2011; Xu et al., 2017; Ng, 2011). Extensive use of geospatial technologies and 3D building database for quantitative urban climate mapping in Hong Kong have been carried out to simulate the UHI effect and wind dynamics and subsequent formulation of planning guidelines (Chen & Ng, 2011; Ng, 2011). A customized tool in Arc-GIS was used to simulate Sky –View Factor (SVF) and Frontal Area Density (FAD) to link urban geometry with thermal and wind environment. The simulated results were then synergized and classified to define homogeneous climate units which were further utilized to define climate oriented planning guidelines and recommendations. It can assist planners in identifying the adaptation and mitigation strategies to combat rising temperature and pollution levels, can help in ensuring the proper ventilation in urban areas so as to mitigate the UHI effect.

However, most of the studies on UC-map have been concentrated in developed world (Alcoforado et al., 2015) primarily due to unavailability of detailed UCPs information in complex urban environment of developing regions. However, this study demonstrates that sub-meter optical satellite stereo data can be effectively utilized to obtain UCPs information. Since, the optical stereo data is cost effective and has wider availability, it can be employed in complex urban environment for UC-map studies. The generated UC-maps can be integrated in master plan process for climate resilient urban environment. It can assist planners in identifying the adaptation and mitigation strategies to combat rising temperature and pollution levels and can help in ensuring the proper ventilation in urban areas so as to mitigate the UHI effect. The climate sensitive planning is highly needed to combat ill effects of global warming and to ensure sustainable development. Concerted efforts need to be made to disseminate the state-of-the-art technologies for preparing urban climate maps and their incorporation as an essential part of urban planning process in developing world.

2.10.4 Urban Climate Research and modeling

Parameterization of urban variables or UCPs is a prerequisite “ to understand climate changes, better quantification of the impact of density, land use, thermo-physical characteristics, geometry, local energy consumption, anthropogenic heat release and cool sink is essential “(Chen & Ng, 2011; Georgatou & Kolokotsa, 2016; Giridharan, 2016; Givoni, 1992; Oke, 1988). The configuration and composition of urban variables effects urban micro climate in the form of UHI, air pollution, thermal stress, increased storm water run-off, increased cooling loads and urban rainfall effect. Rapidly growing urban population especially in developing regions necessitates the study of these issues through modeling and simulation. It has been noted that most of the available urban climate models and mesoscale models are inclined towards atmospheric science and on the other hand, urban designers are not exposed to these models for utilization in urban climate research. Besides, mesoscale weather prediction and microscale dispersion models are limited in their ability to perform accurate assessments in urban areas.

Urban morphological characteristics have been employed for simulation of wind and thermal environments (Lindberg, Holmer, & Thorsson, 2008; Raasch & Schröter, 2001) by employing UCPs derived from satellite data and actual 3D buildings GIS database. It was found that simulations by employing remote sensing derived UCP information provides coherent results with the simulations carried out with actual 3D building database. The study paves a way for potential use of detailed UCPs information for urban climate research and simulation of wind

and thermal environment. The availability of UCPs information in developing world has a great potential in this field for generation of alternate scenarios for mitigating the impact of ongoing climate change. Recent development in the field of urban canopy models (UCM) and their coupling with mesoscale models provides opportunities for quantitative assessment of urban climate for improved decision making and urban planning (Fei Chen et al., 2011; Grimmond, Blackett, et al., 2010b). Major constraint faced in the implementation of UCMs is dearth of detailed data on UCPs and local weather network which is imperative for use of these models for urban climate research (Grimmond, Blackett, et al., 2010b; Grimmond, Roth, et al., 2010a) especially in developing regions.

The mesoscale urban-WRF model have been utilized widely for simulation and downscaling of climate indicators at urban scale (0.2-0.5 km). It provides multiple options to represent urban heterogeneity (single urban built-up class, 3-class urban LULC, 10-class LCZ classification and detailed UCPs) in the model. The coupled WRF-urban mesoscale Numerical Weather prediction (NWP) integrates single layer urban canopy model (SLUCM) and multi-layer urban canopy models (MLUCM: Building Energy Parametrization and Building Energy Modeling) with increasing level of complexity and needs detailed UCPs information for accurate simulations. Default Urban-WRF contains only the option of single urban built up and three urban class (commercial, industrial, and high or low residential areas) as an input data for urban areas, which is too coarse to represent urban heterogeneity in the model and do not provide highly accurate simulation results (Salamanca et al., 2011). The use of more precise information on urban characteristics have been investigated by many researchers. The studies have highlighted the need for better parameterization for improved simulations (Burian & Jason, 2009; Hammerberg et al., 2018; Xuemei Wang, Dai, & Dai, 2017). Besides, the gridded UCPs have potential for providing precise and reliable UCPs information for WUDAPT level 1 and level-2 products (Xu et al., 2017). The detailed gridded UCPs also paves the way for direct integration of UCPs in urban-WRF for improved representation of urban heterogeneity and to obtain accurate simulation results. National Urban Database with Access Portal Tool (NUDAPT) outline approaches for ingestion of detailed UCPs information in mesoscale models MM5 and WRF (Chen et al., 2011; Jason Ching et al., 2009; Glotfelty et al., 2013).

Many of the weather prediction agencies including IMD in India have been extensively utilizing the WRF model for short term and long term weather estimations etc. The operational models represent urban areas through bulk parameterization (single urban built-up class) due to less time required for computation. However, the accuracy of this approach over urban areas is

comparatively poor as it takes less parameters into account. However, the GIS based LCZ map as discussed in previous section can also be ingested in WRF-urban for improved simulations of climate variables (Hammerberg et al., 2018; Molnar, Gal, & Gyongyosi, 2018).

2.11 SUMMARY

Review of existing literature, methods and prevalent practices has highlighted that lack of information on UCPs is one of the major constraint for dearth of urban climate research and modeling studies in complex urban environment of developing regions. The study of UCPs to characterize the urban built form is vital and holds the key to the future urban climate research. Airborne LiDAR and aerial data is considered as one of the best technologies for extraction of 3D building database in urban areas, however, limited availability of the data necessitates the use of alternative technologies. The widespread availability of low cost VHRS data especially optical stereo data needs to be evaluated for computation of UCPs in developing regions.

Thermal remote sensing and numerical model simulations are the methods which can be employed in urban areas for obtaining the spatially variable information on climate indicators as large network of observation towers is expensive and not feasible in urban areas due to stringent siting requirements. Research on relationship of UCPs with climate indicators have been carried out extensively by utilizing LST derived from thermal remote sensing data, however the focus was mainly on relationship with 2D UCPs. 3D UCPs effects urban micro climate substantially, however, it is still largely unexplored, hence, there is a need to understand the relationship of 3D UCPs with urban micro climate for better understanding and formulation of climate oriented planning guidelines.

Thus, research has been undertaken in this study for retrieval and characterization of UCPs by employing VHRS optical stereo data and relationship of retrieved UCPs with spatially variable climate indicators in a complex urban environment of a city region in developing country which have been discussed in following chapters.

Availability of UCPs in developing regions can open plethora of applications for urban climate studies, research and modeling such as ventilation assessment, Local Climate Zone, urban climatic map and parameterization for urban climate modeling to name a few. Out of these mentioned applications, two applications ventilation assessment and GIS based LCZ map has been demonstrated in this study.

CHAPTER 3

STUDY AREA CONTEXT

3.1 INTRODUCTION

The Delhi Urban Agglomeration (UA) in India has been selected as the study area due to its sprawled nature, highly heterogeneous and complex development characteristics of urban built form, high air pollution levels, high anthropogenic pressure and challenging climate. It is the third largest UA of the world and largest UA of the India cutting across the boundaries of adjacent states forming an interstate, multi-nucleus urban formation covering approximately 2600 km² area. The composite climate of Delhi consisting of three dominant seasons' summer, monsoon and winter. Summers are very hot with maximum temperature leading to ~ 48°C, monsoons are extremely humid (>85% Relative humidity) and minimum temperature in winters touches ~4-5°C. The extreme weather conditions in the study region necessitates to address the challenges posed by hot-dry, hot humid and cold-dry climate for enhancing thermal comfort. Important characteristics of the selected study area in terms of locational characteristics, historical evolution and urban built form and demographic characteristics and composition of interstate urban area and climatic conditions prevailing in the study area along with air pollution and UHI characteristics in the study area have been discussed in this chapter.

3.2 LOCATIONAL CHARACTERISTICS

Delhi is situated between the latitudes of 28.4° to 28.88° North and longitudes of 76.83° to 77.33° East in northern part of India (Figure 3-1). It is the capital city of India and an interstate urban region. States of Uttar Pradesh and Haryana share the border with Delhi. It is a land locked city (Central Pollution Control Board, 2016) with an area of 1,483 sq. kms and a population of 16.75 million (Anon, 2011). Its maximum length is 51.90 kms and greatest width is 48.48 kms.

The Delhi is known as a relatively flat region and land locked city, consisting of two major geographical features (Figure 3-2). The River Yamuna is the one which splits the city in two parts and traverses north to south. The other feature is the Aravalli Hills mostly situated in the south and south west part of the Delhi UA. The Aravalli hills covered with vegetation (popularly known as Delhi ridges) provides a supply of fresh air to the city (Anon, 2016a). The western and north western boundary is abundant in sand dunes and barren low hills. Its proximity to the great Indian Thar desert (~200km) at the western side brings dust storms and hot air in the summer

months. The Aravalli hills is facing the threat of increasing mining activities which is responsible for spread of desert and has significant impact on the whole region. The increasing pollution in River Yamuna converts the perennial river into a drainage of high turbid and polluted water when it passes through the Delhi UA.

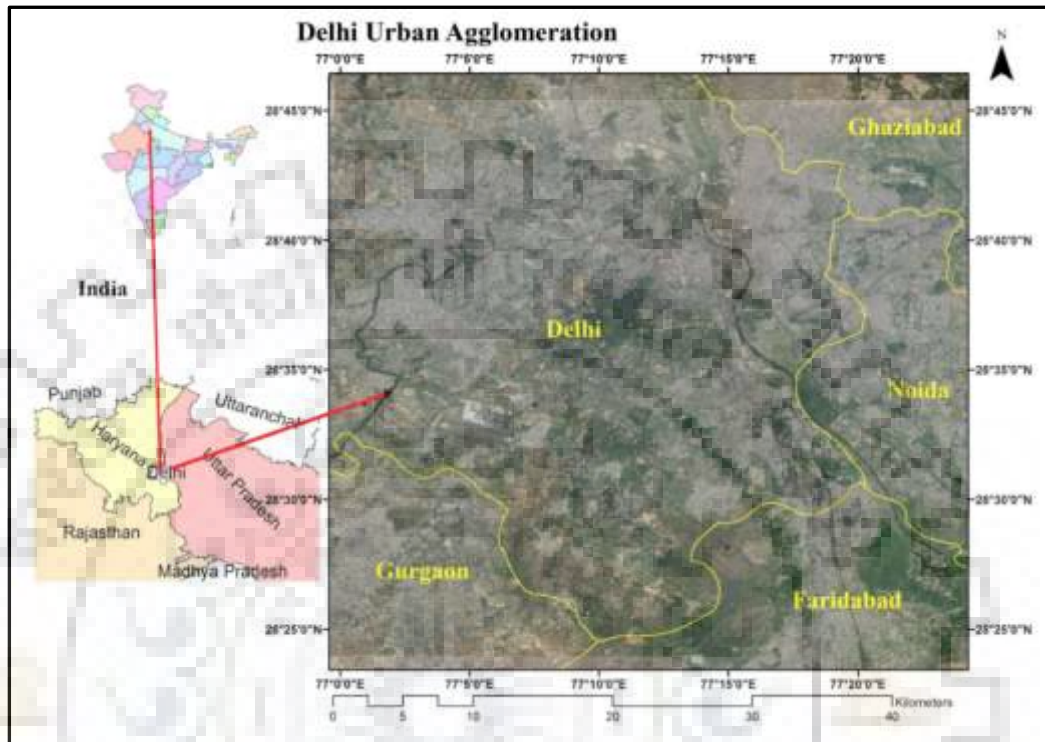


Figure 3-1: Location of Study area

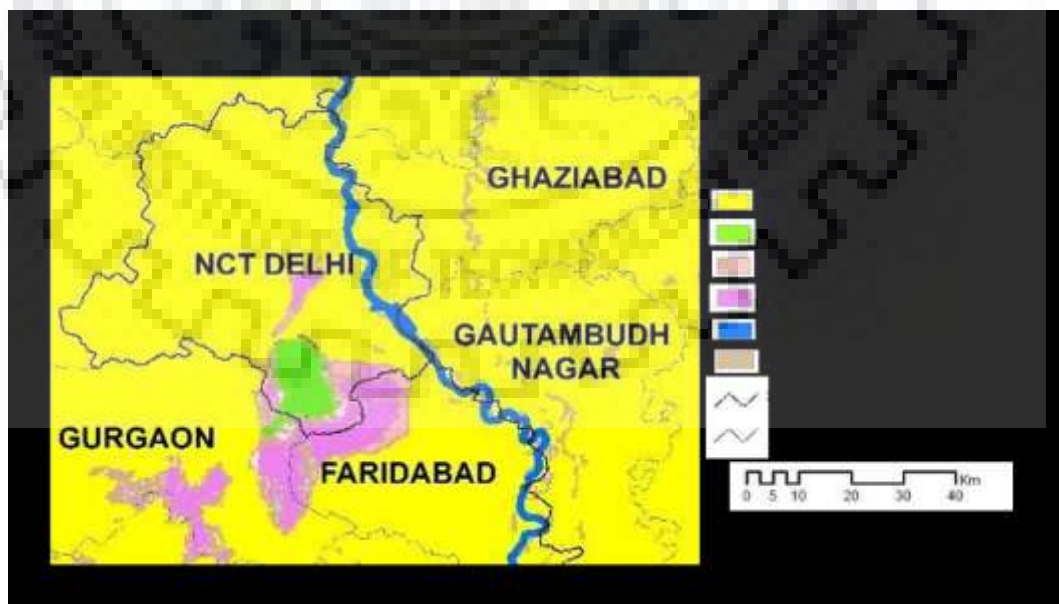


Figure 3-2: Geomorphological Characteristics of Study area
(Source: National Capital region Planning Board, Delhi)

3.3 HISTORICAL EVOLUTION AND URBAN BUILT FORM

The city of Delhi has undergone many transitions and it is said that Delhi has been build and rebuild many times. It has always been a centre of attraction for Indian rulers who considered conquering Delhi important for establishing a rule over entire Indian subcontinent. The history of Delhi has been linked to Indus valley civilization as proved by some recent excavations in the vicinity of Delhi. Mythologically city was also known to exist in Mahabharata(one of the greatest epic of India) era suggested to be around 4th century B.C. when it was called Indraprastha (1450 BC)(Kak, 2013).

The origin of the name Delhi is attributed to Raja Dillu who ruled over Delhi at the beginning of Christian era. The earliest known settlement which exist even today is known as Lalkot whose existence goes back to (700-1000 AD). After that it was shifted to Qila Rai Pithora in 1192 AD during Chauhan dynasty. Later on, Delhi was ruled by Turks and Mughals. During this period Delhi was build and rebuild in different parts by different rulers. While King Balban shifted the capital to Kilokheri(1193 AD), Sultan Ghiyas-ud-din Khilji shifted it to Surajkund(1300 AD), Sultan Mohammad Bin Tughlaq to Tughlaqabad(1330 AD), Sultan Firuz Tughlaq to Firuz Shah Kotla(1354AD) and emperor Sher Shah Suri to Shergarh(1540 AD).

During Mughal Dynasty, Emperor Shahjahan built Shahjahanabad in 16th century AD which exists even today and popularly known as Old city of Delhi. The old city covers an area of 569 ha with a population density of 100 person per hectare (pph) (Chatrath & Pushplata, 2018). The city have been developed in typical Mughal style with dense and compact urban built form and organic street pattern containing predominantly mixed land use. It is a thriving commercial area presently (Anon, 2012). Few of the main features of the old city includes Red fort (the royal palace) on the bank of River Yamuna, the mosque, two main commercial streets (Chandni Chowk and Faiz Bazar), small gardens at different locations and havelis for powerful families(Figure 3-3). A water channel and a tree lined avenue used to run through Chandni chowk which was later replaced by a motorable road. In between these features the old city grew organically with narrow street canyons interspersed with vibrant chowks (common sitting and interaction places). It seems to provide a comparatively comfortable living environment in terms of thermal comfort, a sense of security and traditional lifestyle (Gupta, 1998). After the introduction of railways, construction of a railway station on the north side of Chandni Chowk in 1867 attracted trade and commerce activities in the old city, which spilled over to residential areas as well and it is still a thriving commercial hub of Delhi.

Later on British constructed New Delhi, also known as Lutyens Delhi, in Year 1916 with a low rise low density urban development along with plenty of vegetation. It was planned by Sir Edwin Lutyens on the southern side of the old city with wide tree-lined avenues, large plots and spacious bungalows. This city was built with a density of 25 pph which was in complete contrast to the densely built old city of Delhi (Figure 3-4). It has become the centre of administration and continued to be so even in post-independence era, governed by New Delhi Municipal Corporation (NDMC). It accommodates only a small portion of total population of Delhi. This built form is aesthetically pleasing, provides a significant thermal comfort in summer season but a bit uncomfortable in winter season due to existence of ample vegetation (Gupta, 1998).



Figure 3-3: Old City of Delhi, 1857
(Source: Chatrath Disha, 2018)



Figure 3-4: British Capital of New Delhi
(Source: Chatrath Disha, 2018)

After independence of India in 1947, the country has witnessed huge influx of migrants from Pakistan, which is termed as the greatest mass movement of people in human history. The city of Delhi witnessed an unprecedented surge in population from 7 lakhs in 1941 to 1.4 million in 1951 (Dupont, 2004). The city grown in all directions radially and acquired population density as high as 4400 pph in some areas in 1961 (Chatrath & Pushplata, 2018). The new country and its capital Delhi was struggling to overcome this situation and lot of planned development took place to house migrants and large government work force (Figure 3-5). Northern and western side of the city, many colonies have been developed to permanently settle migrants such as Vijay Nagar,

west of Civil Lines. Model Town, Guru Teg Bahadur Nagar, Rajinder Nagar, West Patel Nagar, Moti Nagar, Rajouri Gardens etc. In the southern side, a number of colonies have been developed to house large government work force, Embassies and migrants such as Chankyapuri, Sarojini Nagar, Defence colony, Lajpat Nagar etc.

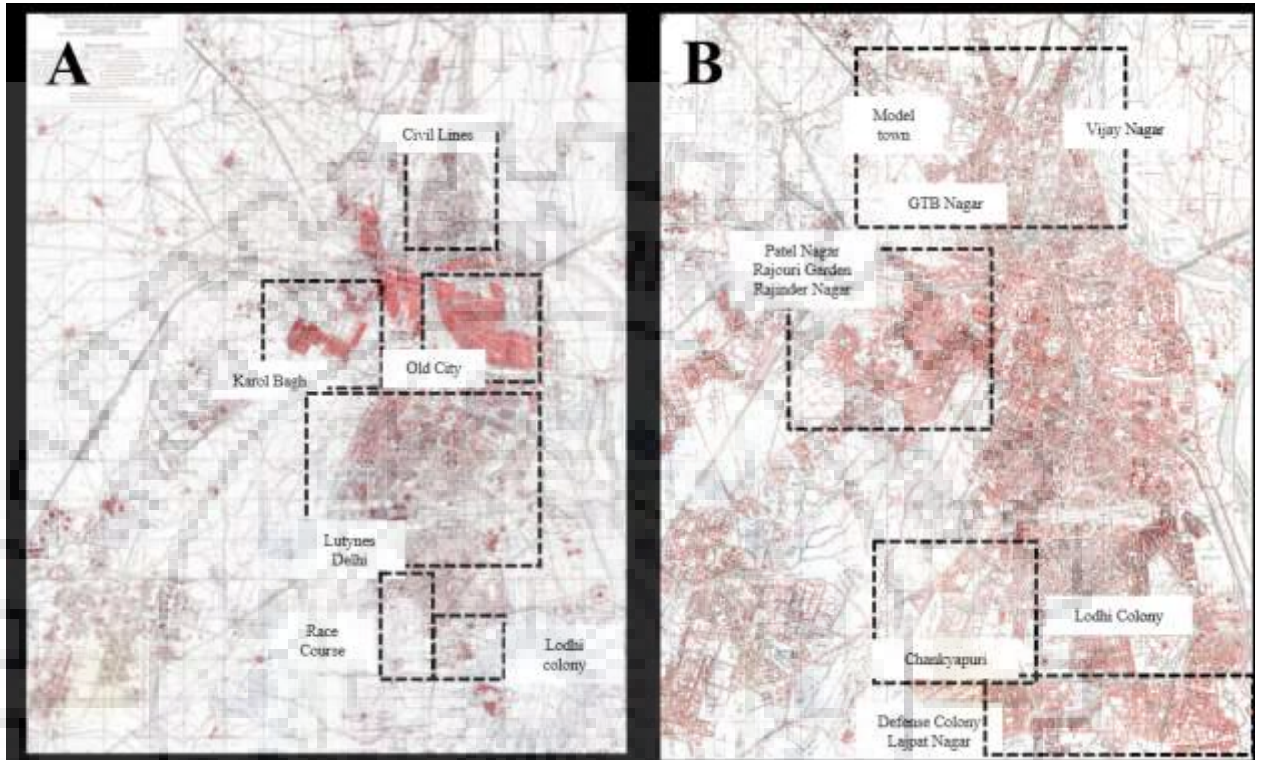


Figure 3-5: (A) Built-up Area of Delhi, 1942 (B): Built-up Area of Delhi, 1952

(Source: Chatrath Disha, 2018 adapted from Hindustan Times)

Rapid haphazard and sub-standard development took place in the study region in the beginning of 1960s, which led to the development of unauthorized colonies and slum areas especially in eastern direction. A high density compact, unplanned, unorganized urban built form could be seen along the stretch of River Yamuna. The development of unauthorized colonies with no planning control led to a development of substandard housing and needed substantial redevelopment to ensure basic civic amenities (Bhagwan Sahay et al., 1962). Some of the pockets developed with very high density of population as high as 650 pph (mainly in old city), while few of them (Lutynes Delhi) has as low as 25pph (Figure 3-6) (Bhagwan Sahay et al., 1962).

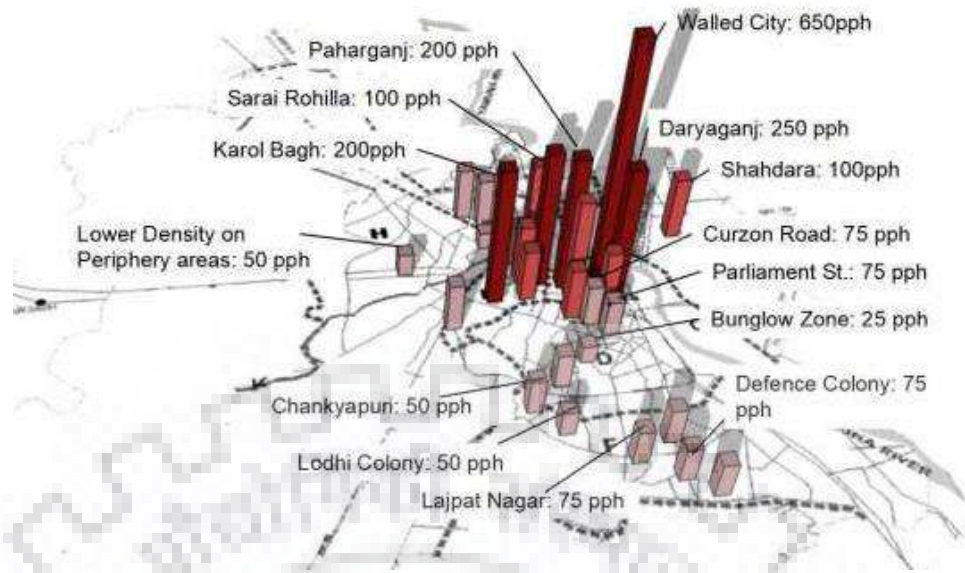


Figure 3-6: Population Density in Delhi, 1962 (Source: Master Plan of Delhi, 1962)

The land use zoning had witnessed significant change from the mixed land use of old city. Independent zones of commercial, institutional and residential have been developed with large distances in between. The segregation of land use zones added transportation cost, time and consumption of energy even for daily commuting. However, industrial zones were developed all over the city mixed with residential areas which led to high level of pollution and chaos in these areas. The mixing of land uses was not planned and often undesirable like residential with shopping and industry; wholesale with retail; business with service industry.

A major planning initiative in the form of development of ring towns (Figure 3-7) also known as satellite towns (NOIDA, Gaziabad, Faridabad, Loni, Gurgaon, Bahadurgarh, Narela) have been adopted to control the haphazard growth of the city as well as to reduce the population pressure on the main city (Dupont, 2004). However, the initiative could not yield results as envisioned and could not dilute the pressure on the main city. The continuous urban growth in Delhi and the peripheral towns received further boost in the post globalization era in year 2001, when large foreign direct investment in the region had resulted in huge spurt for the development of infrastructure in the main city as well as the peripheral towns of NOIDA, Gurgaon and Faridabad. The various planning initiatives taken from 1962 onwards resulted in a centrifugal and multi-nucleated settlement pattern (Dupont, 2004). Despite the continuous efforts to regulate the growth of Delhi UA, it grew exponentially and soon converted into a multi-nucleated large megalopolis with its boundaries extending more than 50 kms in length and breadth. It has grown from a small town in 1901 of 0.4 million population to 16.75 million population in 2011 excluding the population of surrounding satellite town. It has attracted people from all over India due to vibrant

trade and commerce providing excellent employment opportunities. Being the capital city of country, it is also the administrative centre of the nation and hub of modern infrastructure such as health, education and socio-cultural facilities. It also encompasses many beautiful forts, monuments, palaces, gardens, event places and bazaars developed and constructed by many rulers in different time period of history owing to its rich cultural heritage. The multiple amalgamation of facilities, infrastructure, opportunities has attracted a large population (permanent and floating) in the study region (Anon, 2012).

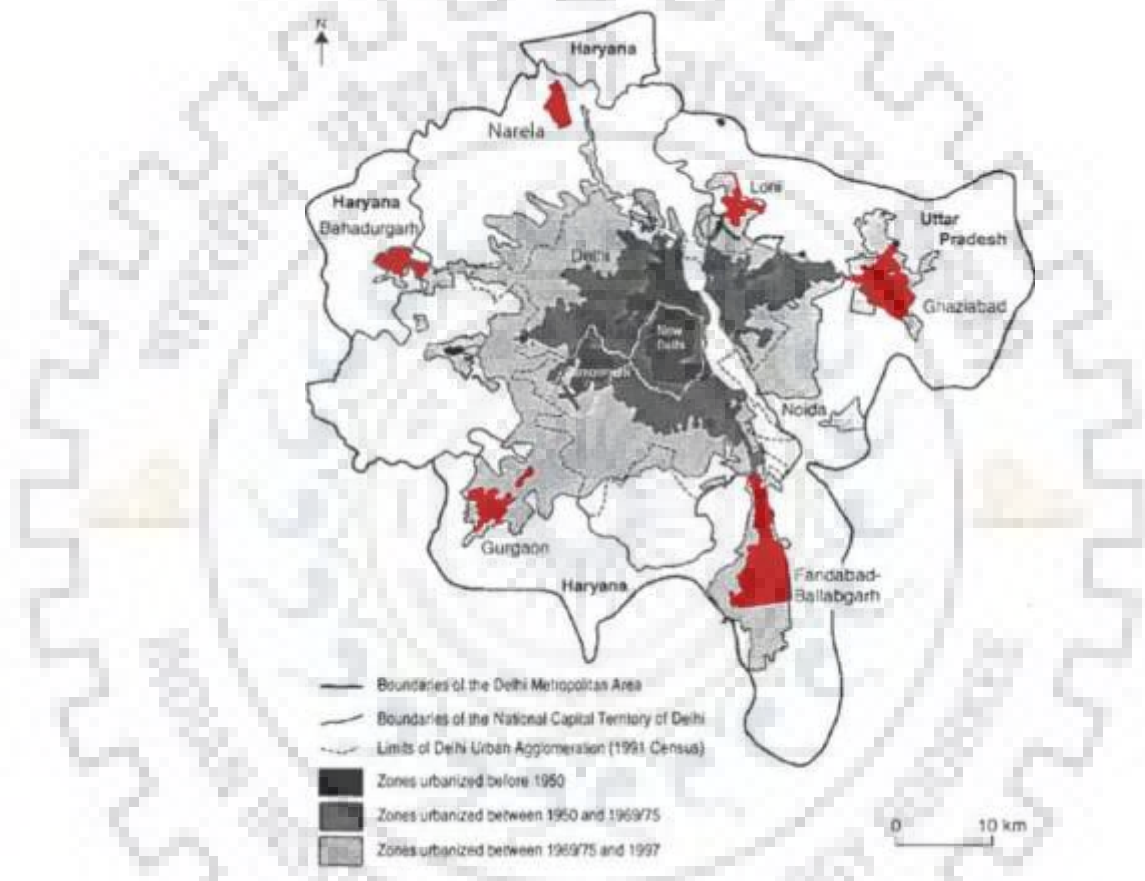


Figure 3-7: Development of Ring Towns (Source: Dupont Veronique, 2004)

Initial Master Plans of Delhi advocated for low rise high density development with restrictions on height and FAR, resulted in sprawled urban built form (Bhagwan Sahay et al., 1962). Hence, most of the inner parts of Delhi is characterized by mid-rise low density urban built form. Later on, to control the growing size of the city in the year 2007, the FAR relaxation were introduced and the city experienced vertical growth upto 8-10 storey structures in the peripheral areas. Recently, a surge in the construction of high rise buildings in the surroundings of Delhi Region can be witnessed. Delhi's urban built form is highly heterogeneous as it has developed in various phases and each phase is characterized by a different kind of urban built form. All these changes

in urban built form or geometry produces a highly heterogeneous urban built form and is responsible for significant microclimatic variations. However, there is no available GIS database which provides the details of 3D geometry and configuration of the urban built form of the Delhi UA. Hence, alternative approaches are required for obtaining the information on 3D configuration of urban built form in the study region and subsequent computation of UCPs.

3.4 DEMOGRAPHIC AND SPATIAL GROWTH OF DELHI URBAN AGGLOMERATION AND COMPOSITION OF INTERSTATE URBAN AREA

The demographic and spatial growth of Delhi is a witness to the urbanization trends in India which is dominated by the concentration of population in large metropolises. Although most of the Indian population is still rural (~69%) as per 2011 census but urban population now tends to concentrate in large cities. The population growth in Delhi is marked by the turbulent history of nation as explained in previous section. After the formation of British capital in 1911, the population of city expanded from 238,000 in 1911 to 696,000 in 1947, while growing four times in spatial dimension (Dupont, 2004). The decade 1941-51 is marked as the maximum population growth in its history owing to the massive transfer of population from Pakistan following the partition of nation in 1947. After Independence, Delhi was declared as the national capital and thus became a center of administration and political power. In the post-independence period also, Delhi witnessed a rapid growth between 4-5 % per annum to reach 16.75 million in 2011 (Table 3-1). Although the growth rate of Delhi has come down in the decade 2001-2011 from 35% to 21.21%, it still holds the position of second largest metropolis of India.

Delhi continues to be the second largest urban area in India as Census of India definition does not allow an urban agglomeration to cross a state or territorial boundary. The population bureau report indicates that Delhi is third in largest world urban agglomerations and largest urban agglomeration of India and continuous urbanization of Delhi encompasses many peripheral towns in the state of Haryana and Uttar Pradesh (Wendall Cox, 2011). Continuous urban area of Delhi has witnessed the quickest growth in last few decades. It consist of urban area of National Capital Territory (NCT) Delhi, as well as NOIDA and Ghaziabad in Uttar Pradesh and Gurgaon and Faridabad in Haryana leading to formation of multi-nucleated complex urban structure (Figure 3-8). The continuous urban area cutting across the boundaries of adjacent states covers approximately 2600 sq km area in which NCT Delhi covers an area of 1483 sq km (Figure 3-1). The outer area of Delhi witnessed the fastest growth from 2.6 million to 5.3 million, an increase

of nearly 105% from 2001 to 2011. Whereas, the population of NCT Delhi increased by 27 % (2001-2011) and the inner area population of NCT grew only by 15 %.

Gurgaon in Haryana, is close to Indira Gandhi International Airport on the southwest side. It has developed as an international information technology center and corporate hub and grew from 250,000 people in 2001 to 900,000 in 2011(Gurgaon, n.d.). Ghaziabad in Uttar Pradesh is adjacent to north east district of Delhi and it is largest among all urban expanses outside NCT Delhi (Anon, 2011a). It has grown from 975,000 people in 2001 to more than 2,350,000 people in 2011. NOIDA again in Uttar Pradesh was developed as special economic zone to reduce the growth burden on NCT Delhi and also houses Software Technology Park other than a number of industries. Its population has also grown twofold from nearly 300,000 in 2001 to 650,000 in 2011(Anon, 2011c). Faridabad in the southern side falls in the state of Haryana and has the slowest growth percentage. It has grown from 1,050,000 people in 2001 to 1,400,000 people in 2011(Anon, 2011b). The similar trend was observed in 1991-2001 census when 26% growth was observed in inner area and 74% growth was observed in outer areas of the National Capital Territory. This vast expanse has high heterogeneity in terms of urban built form which increases the complexity in terms of urban parameterization.

Table 3-1: Urban Growth in Delhi (1951-2001) (Source: Census of India, 2011)

CENSUS YEAR	URBAN POPULATION		URBAN AREA		URBAN POPULATION DENSITY	
	Persons	Decadal Growth (%)	Absolute Area (sq. Km)	Decadal Growth (%)	Persons per sq. km	Decadal Growth (%)
1951	143700	107	201	15	7137	79
1961	2359000	64	327	63	7225	1
1971	3647000	55	446	36	8172	13
1981	5768000	58	592	33	9746	19
1991	8472000	47	685	16	12361	27
2001	12906000	52	925	35	13957	13
2011	16368899	27	1120	21	14584	4

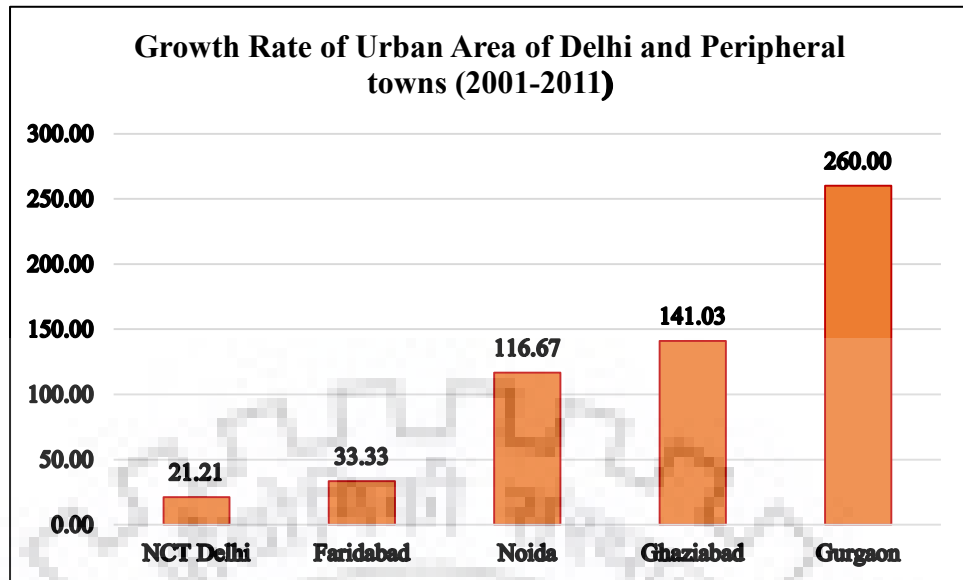


Figure 3-8: Growth Rate of urban area of Delhi and its peripheral towns

3.5 CLIMATE

Delhi comes under the composite climate zone of India which is characterized by variable landscape and seasonal vegetation (Figure 3-9). Since, no climatic condition prevails here for more than six months it is categorized as composite climate (Lall, Pandit, & Appasamy, 1990). The solar radiation intensity is high in summer which ranges from March to June months with less amount of diffuse sunshine. The maximum day time temperature in summer ranges from 32-43° C and even goes sometimes more than 48° C and night time temperature varies from 27 to 32° C. Relative humidity is quite less during summer months ranges from 20-25% (Attri & Tyagi, 2009). However, the monsoon season from July –September are wettest period where it receives more diffused sunlight and relative humidity varies from 55-95%. It also receives strong winds from south-east during this season. Due to high humidity during monsoon season it is desirable that a proper cross ventilation should be maintained during monsoon months. Winters are cold and dry and continues from the month of December to January.

In winters temperature ranges from 7-10° C during night with a diurnal variation of 7-25° C (Figure 3-10). It is desirable to shield cold winds coming from north-east during winter season and hot dusty wind from west in summer season. The February, March, October and November Months are the pleasant months. Besides, it is located in landlocked area of Indo-Gangetic plains and effected by regional weather patterns. Passive strategies for urban built form for climatic comfort in Delhi needs to address the needs of hot-dry, hot humid and cold-dry season. First strategy involves shading and protection from heat and cold (Lall et al., 1990), second strategy is to use of thermal mass in buildings to address to diurnal temperature variation, third is to

control air movement i.e. shielding from hot and cold air and ensuring cross ventilation in hot-humid season. Proper Ventilation can also help to combat high Urban Heat Island Intensity in Delhi which extends up to 6°C. Fourth strategy includes use of vegetation as microclimate modifier.

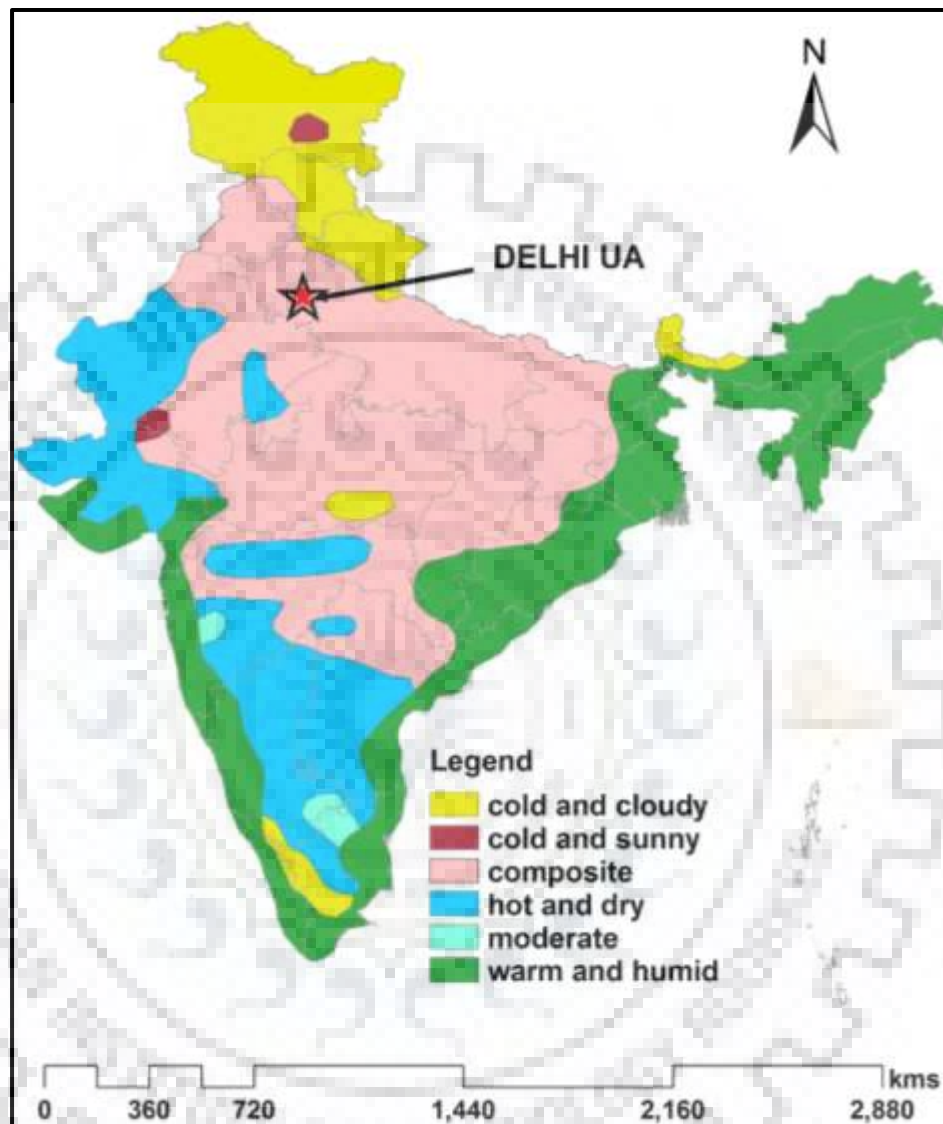


Figure 3-9: Climate zones of India (Source: National Building Code of India, 2005)

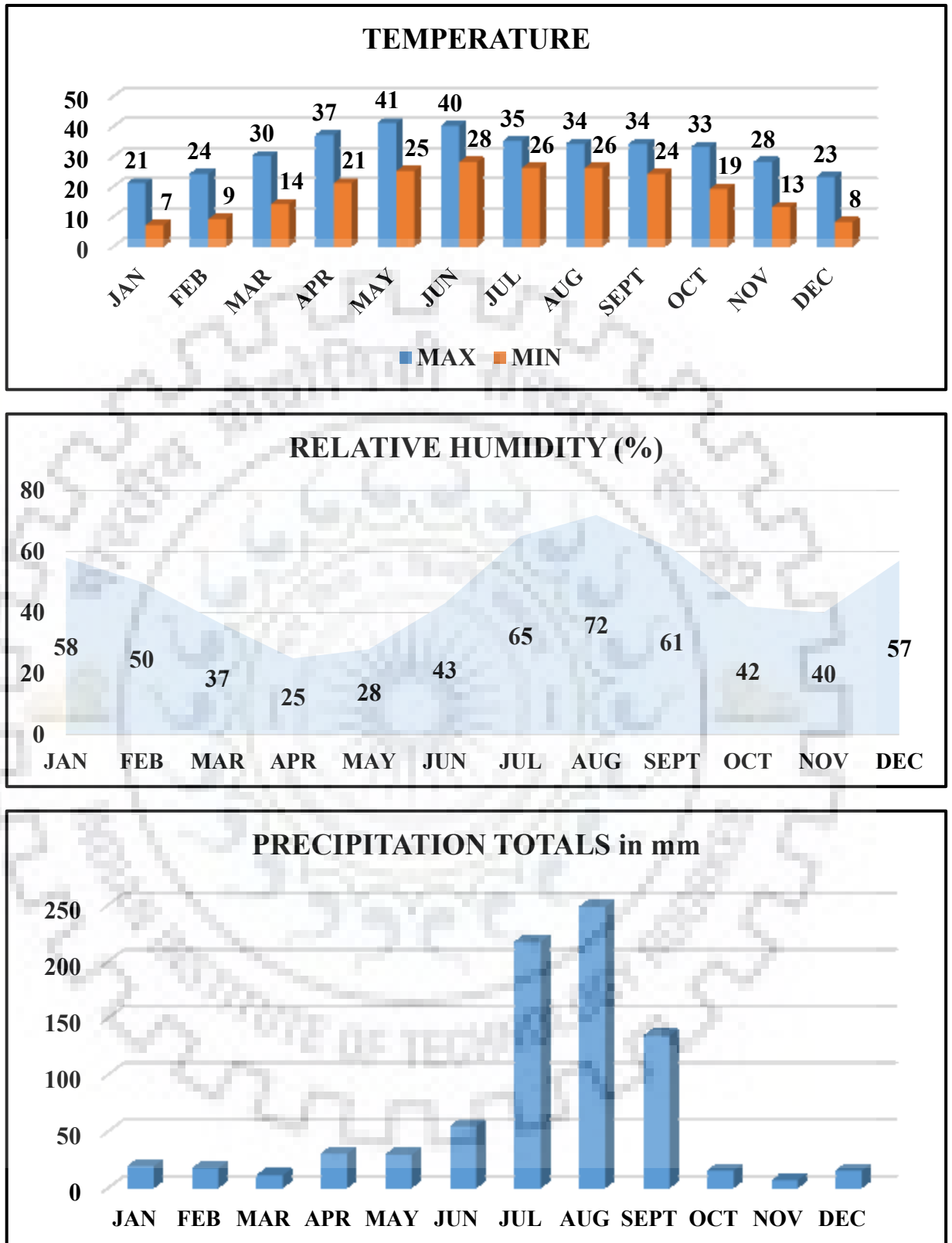


Figure 3-10: Graphical representation of Climate of Delhi (Source: IMD, Delhi)

3.5.1 Air Pollution

Delhi is one of the most polluted megacities of the world with severe air pollution problems especially in winter months (Gurjar et al., 2010). The annual average respirable particulate matter (RSPM) concentration limit has surpassed by more than four times the national annual standards in Delhi (Anon, 2012b). Delhi witnesses severe air pollution conditions especially in winter season almost every year. The increasing level of air pollutants every year in ambient air of Delhi has raised serious concern with respect to human health which is continuously deteriorating at an alarming rate. The major causes attributed to this situation are: increasing industrial exhaust and vehicular emission, agriculture stubble burning in adjacent states of Haryana and Punjab, construction and demolition activities, stagnant wind in winter season, over population and lack of effective public transport which leads to traffic congestion etc. (Sharma, Taneja, Sagar, & Bhatt, 2018). One of the major reason which is not studied well is the land locked status of Delhi urban region and its urban form and geometry which prevents the dissipation of air pollutants from Delhi. The adequate ventilation can be an effective measure to dissipate heat and pollution from the urban regions.

3.5.2 Urban Heat Island

The large interstate continuous urban agglomeration extending beyond state boundaries in Delhi makes it the largest urban agglomeration of India with highest population (“Demographia World Urban Areas: 2019: Population, Land Area & Urban Densities | Newgeography.com,” n.d.). Intensification of urban development, corresponding alteration in surface cover and urban geometry, increased anthropogenic activities in Delhi region aggravates the UHI phenomenon (Grover & Singh, 2015; P. M. et al., 2014; Pandey, A. K. et al., 2014). UHI intensity in Delhi is found to be ~ 2.8°C to 8.3°C depending on the season, surface and synoptic weather conditions (Mohan et al., 2009). The presence of Delhi ridge, river Yamuna and vegetation along the roads moderates the temperature in Delhi and maximum temperatures were witnessed in high density built up areas. A study done by Manju Mohan and group in Delhi region based on field observations reveals that there is an increasing trend in annual minimum mean temperature which is indicative of warming trend in Delhi Region (Mohan, Kandya, & Battiprolu, 2011). Besides, the long term analysis of temperature patterns presents its strong relationship with pace of urbanization. Similar observation of increasing temperature and UHI have been witnessed in NOIDA city, a satellite town of Delhi (Kikon et al., 2016). The increased UHI is also found to be associated with increased concentration of air pollutants that results in decreased air quality

in the region (Babazadeh & Kumar, 2015). India has witnessed increased frequency and intensity of heat waves in last decades with 2019, 2018, 2015, 2014, 2010, 2009, 2007, 2006, 2003, 2002 and 1998 have been recorded as warmest years with increasing intensity each time (Guleria & Gupta, 2016). The health impact of heat waves are more severe in urban areas as urban residents are generally exposed to higher temperatures as compared with surrounding rural areas manifested as UHI phenomenon. It is estimated that over 22,000 heat-related fatalities took place in India since 1992. Growing heat waves in last decades in the study region and UHI results in increased usage of air conditioners which further aggravates the situation. It has been concluded that not only the population densities and changes in surface cover, the change in urban built form such as building density and inter building spacing also effects the UHI phenomenon. Most of the studies concerning UHI in Delhi are either based on the field measurements (Babazadeh & Kumar, 2015; Mohan et al., 2009) or LST derived from thermal remote sensing data linking the land use/land cover, vegetation and built up distribution by applying 2D indices (Grover & Singh, 2015; Singh, 2015). The impact of 3D configuration such as building height and volume, frontal area index, floor area ratio and SVF on LST and UHI is less studied phenomenon due to unavailability of 3D information specially in developing region (Berger et al., 2017). Availability of this information may prove beneficial for understanding the relationship of 3D urban geometry and accumulation of heat in urban structure.

3.5.3 Prevailing Wind Direction

Delhi is located in landlocked region of north India and its climate is generally influenced by monsoons and thunderstorms. The prevailing wind conditions in Delhi is generally observed from westerly or north westerly direction except monsoon and tend to be northerly in the afternoon. During monsoon the prevailing wind direction is observed to be southeasterly (Anon, 2016b). Monsoon is also associated with high humidity levels which requires strengthening of air flow to increase thermal comfort in built up areas. The 30 year long term variation in ventilation coefficient by utilizing radiosonde data has shown considerable decrease in Ventilation Coefficient (VC) over Delhi. The study also shows that there is an increase in mixing depth but significant reduction in wind speed is responsible for decrease in VC (Iyer & Ernest Raj, 2013). However, a global analysis of Natural Ventilation (NV) hours shows high number of (NV) hours in Delhi (~3331 hours) (Chen, Tong, & Malkawi, 2017) which can be exploited to induce natural ventilation to reduce the building energy consumption and to improve indoor environment. The NV hour is employed as an indicator to measure the maximum natural ventilation potentials for each location.

3.6 SUMMARY

The urban built form of Delhi has evolved not only in few years or decades, but over a passage of centuries in a complex, highly dense and multi-nucleated urban structure. Its land locked status along with challenging composite climate and deteriorating climate over a period of last decades poses several challenges for urban climate researchers. Over the years the UA had witnessed severe air pollution conditions especially in winter months, increasing intensity of heat waves and UHI and reduction in natural ventilation hours which may be attributed to its land locked status along with complex and dense urban built form. Hence, there is a need to derive UCPs for scientific understanding and modelling of urban micro climate phenomenon. However, unavailability of 3D GIS database in the study area does not allow for the computation of UCPs. Alternative approaches needs to be explored for the retrieval of UCPs by utilizing widely available datasets. Retrieval and characterization of UCPs for the study area is discussed in Chapter 4. Relationship of UCPS with spatially variable climate indicators are presented in chapter 5 while chapter 6 demonstrates few of the application of UCPs in the study area.



CHAPTER 4

CHARACTERIZATION OF URBAN CANOPY PARAMETERS

4.1 INTRODUCTION

Urban areas are on the frontline of global climate change as they are cumulatively responsible for not just emission of 75% of Green House Gases (GHGs), but also heavily influencing the energy exchange at earth surface, contributing significantly to global warming. Developing regions are expected to house approximately 90% of future urban growth by 2050 and India is one among the three countries where 35% of the future urban growth is likely to be concentrated (DESA/UN-WUP, 2018). Further, the irreversible trend of urbanization in India is characterized with lack of implementation of the planned expansion and large size urban agglomeration which leads to a number of problems and issues faced by Indian cities. Increasing frequency of natural disasters has also been observed in the study region such as urban flooding, heat waves and severe air pollution conditions in the last few decades. The situations is further intensified by the rampant use of artificial energy for cooling and heating, huge share of private transportation, proliferation of slums, high density and complex urban development that has resulted in overall environmental degradation (Grover & Singh, 2015; Gurjar et al., 2010; Lall et al., 1990; Mohan et al., 2009) thereby negatively impacting the urban microclimate.

Recently, significant developments in Urban Canopy Models (UCMs) enable to acquire information on urban micro climate even up to neighborhood scale (200m-500m). The obtained information has huge potential to assist planners and policy makers to define strategies for climate resilient urban environment. However, it requires detailed representation of surface cover and 3D geometry of urban areas i.e. information on Urban Canopy Parameters (UCPs) for improved simulations. UCPs define the geometric, radiation, thermodynamic and surface cover properties of urban areas which have profound impact on urban micro climate. However, the non-availability of precise information on UCPs is one of the major limitations for wide utilization of UCMs for urban climate research (Carter et al., 2012; Chen et al., 2011; Salamanca et al., 2011) especially in the context of developing regions. It has been proven by number of studies that availability of detailed UCPs provide improved simulations which can be further utilized for understanding the Urban Heat Island (UHI), air pollution and climate change scenarios (Bhavana , M., Gupta, Kshama, 2018; Brousse et al., 2016; Chen et al., 2011; Hammerberg et al., 2018; Salamanca et al., 2011). Hence, availability of information on UCPs is critical for application of UCPs for urban climate research. A number of studies have utilized 3D

GIS cadastral databases for the derivation of UCPs, which have extensively used remotely sensed data from various platforms including Aerial Photographs, Airborne LiDAR and high resolution InSAR data (Burian et al., 2003; Carter et al., 2012; Jeyachandran et al., 2010; Wicht & Wicht, 2018; Wicht et al., 2017; Wong, Nichol, et al., 2010; Xu et al., 2017). However, in most of the developing countries like India especially their cities, 3D GIS cadastral database is non-existent and availability of airborne data (stereo and LiDAR) and high resolution InSAR data is expensive and limited. Whereas, VHRS optical stereo data has great potential due to its lower cost and wider area coverage and may prove to be an effective data source for the retrieval, characterization and applications of UCPs for urban climate research. Hence, in this study VHRS optical stereo data has been explored for generation of UCPs in complex urban environment of Delhi UA.

This chapter outlines the need of the retrieval and characterization of UCPs by utilizing the VHRS stereo data, describes various datasets which have been utilized for the generation of UCPs in Delhi UA, their sources and spatial resolution and purpose for which they have been used, explains the detailed methodological steps for extraction of building height, LULC, road network and other key UCPs which have been developed and employed for retrieval of multitude of UCPs, followed by analysis of obtained results, discussion and summarization of the results.

4.2 DATA USED

Table 4-1 describes the various data sources used for development and characterization of UCPs in the study area. Pleiades 1A/1B optical stereo PAN and MX data was utilized for generation of DSM, DTM, nDSM, intermediate outputs and further computation of UCPs.

The Pleiades stereo images have been used for the retrieval of building heights and LULC and subsequent generation of UCPs. The constellation is composed of two very-high-resolution optical Earth-imaging satellites. Pleiades-HR 1A and Pleiades-HR 1B provide the coverage of Earth's surface with a repeat cycle of 26 days (Coeurdevey & Fernandez, 2012). It is designed with a dual purpose of serving as a civil and military system or catering the user needs of very high resolution stereo. The satellite is capable of high resolution tri-stereo acquisition. Since, satellite hosts three cameras on board, it is capable of acquiring stereo in the same pass which enables creation of homogeneous products.

This data is found to be slightly better for obtaining 3 D information as compared with Geo eye-1 and World View -2 data (Poli et al., 2015). It also considered reasonably accurate for defense,

urban and mountainous regions applications. It acquires stereo data in PAN mode with a resolution of 0.5 m and in multi-Spectral (MX) mode with a resolution of 2m. The specification of Pleiades sensor is given in Table 4-2.

Table 4-1: Data used for retrieval of Urban Canopy Parameters

Parameters	Source	Date of Acquisition	Spatial Resolution/Type of data	Purpose
DSM, DTM and nDSM	Pleiades-1A stereo	2013-2017 (14 Stereo pairs)	PAN: 0.5m/ Raster	Retrieval of Urban Canopy Parameters
Land use/ Land Cover			MX: 2m / Raster	
Road Network	OSM website	-	Vector data	
Metro Rail Network	DMRC website	-	Vector data	
Ground Control Points	DGPS Field survey	-	Point data	Photogrammetric Preprocessing of Pleiades stereo
Building Height Measurements	Laser Distance Meter (Field Survey)	-	Height observations at point locations	Validation of Building Height map
Fish Eye Photographs	Hemi View Instrument (Field Survey)	-	Sky View Factor(SVF) computation at point locations	Validation of SVF map
Ground truth	Field Survey	-	Thematic information at different point locations	Accuracy assessment of LULC

14 stereo pairs have been procured to cover the entire study area. Since, archived data have been procured it was available in different dates spanning across few years from 2013-2017. However, the older data sets mostly belonged to earlier development, hence, not much difference have been observed in satellite data and ground during field work. The road network has been obtained from Open Street Map (OSM) website and further modified by overlaying on the HR ortho images to achieve the desired accuracy. Similarly, metro rail network has been obtained from Delhi Metro Rail Corporation (DMRC) website, as most of the metro lines in Delhi has elevated network and further digitized to obtain the metro network in study region.

For photogrammetric preprocessing and registration of satellite stereo pairs, Ground Control Points (GCPs) have been collected covering the entire study area by carrying out the Differential Global Positioning System (DGPS) survey in the study area. Further, to validate the generated building height map and Sky View Factor map, ground observations using Leica Disto meter for Height and Fish Eye photographs for SVF have been collected during field survey. The ground

truth survey have been also carried out in the study area to collect reference data for accuracy assessment of Land Use Land Cover (LULC) map. The entire field work was carried out in different phases from year 2015 to year 2018 (Phase 1 &2: DGPS survey, Phase 3: Building Heights and Fish eye photographs and Phase 4: ground truthing to collect reference data).

Table 4-2: Specification of Pleiades data

Product	50-cm panchromatic (Mono/Stereo/Tristere) 50-cm color (pan sharpened) 2-meter multispectral (Stereo) Bundle: 50-cm panchromatic and 2-meter multispectral (Stereo)
Spectral Bands	P: 480-830 nm Blue: 430-550 nm Green: 490-610 nm Red: 600-720 nm Near Infrared: 750-950 nm
Image Location Accuracy	With ground control points: 1m Without ground control points: 3m (CE90)
Stereo imaging	20 km x 280 km
Imaging Swath	20 km at nadir
Revisit Interval	Daily (Pleiades-1A and 1B)

4.3 METHODOLOGY

This section describes in detail all the methodological steps which were developed and employed for data pre-processing and then generation of UCPs by utilizing high resolution optical stereo data. Data pre-processing outlines the steps for the generation of input layers for extracting the height information, surface cover fractions which were further utilized for computation and characterization of various UCPs. Out of the UCPs listed in Table 2.1, few of the UCPs such as Frontal area index, Frontal Area density, Raupach and Macdonald Surface roughness length and Zero plane displacement height could not be computed as existing tools did not yield satisfactory results as discussed detail in section 4.5.2. Computation of Plan Area Density and roof area density could not be carried out due to high computation requirement.

4.3.1 Data preprocessing

The analytical approaches followed to process and evaluate the datasets for DSM generation, extraction of height information with details of each step is presented in Figure 4-1. Data preprocessing involves DGPS survey for collection of ground control points from the field, photogrammetric processing for generation of Digital Surface Model (DSM), Digital Terrain Model (DTM), Normalised Digital Surface Model (nDSM) and Land Use Land Cover (LULC)

(Figure 4-4) information by utilizing the Pleiades Stereo (PAN and Multi-Spectral Data). A DSM represent the height of all the surface features including terrain, building and vegetation (above ground surface features) on the surface of earth with respect to a reference surface. The DTM is a topographic model of the bare earth (terrain relief) excluding the height of all above ground surface features and can be generated by using morphological filters. nDSM is the surface generated by subtracting the terrain height from DSM and contains the heights of all above ground surface features.

A broad Land Use Land Cover map was generated by classification of Pleiades MX data. Further, number of samples were collected from ground to obtain the information on building heights with the help of Leica Disto Meter and Sky View Fraction with the help of Fish Eye Lens photographs for validation of the results.

4.3.1.1 DGPS survey for collection of ground control points

A Differential Ground Positioning System (DGPS) survey have been carried out in the study area to collect the Ground Control Points (GCPs) for accuracy assessment and accurate registration of Pleiades stereo pairs. More than 38 points have been collected and care was taken to distribute the points evenly in the study area. Minimum 40 minutes observations were obtained at each rover station and base was operated approx. for 106 hours. The collected GCPs have been used for assessing the accuracy of generated DSM with RPC model as well as after processing with GCPs. Care was taken to use different set of GCPs for accuracy assessment and for processing.

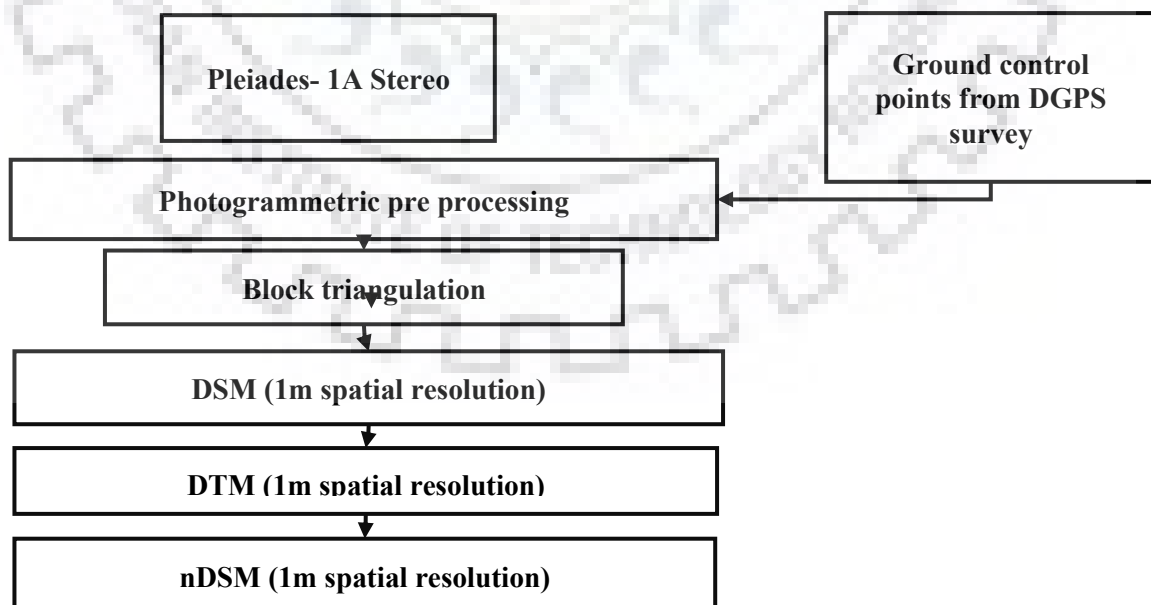


Figure 4-1: Methodology for generation of normalized DSM

4.3.1.2 Photogrammetric pre-processing

Photogrammetric preprocessing involved the reconstruction of the sensor model as it was at the time of image acquisition in photogrammetric software. The Rational Polynomial Coefficients (RPCs) have been utilized to orient the images in the photogrammetry block to process the stereo pairs (Figure 4-2), which defines the geometric model of the sensor. The accuracy of the photogrammetric model has been further improved by ingesting the GCPs obtained through DGPS survey. Further, automatic tie point have been generated in order to measure the corresponding image positions on overlapping images. After the generation of tie points, block triangulation has been carried out to adjust the block in 3D environment to minimize the error in the block and RMSE of less than 1 pixel has been achieved. This process defines the mathematical relationship between images added to the project, the sensor model and the ground. After the definition of relationship, accurate information of Earth's surface have been generated.

4.3.1.3 DSM and ortho-image generation

A digital surface model represents the elevation associated with the surface of the earth including topography and all natural or human-made features located on the surface of the earth. Using multi-image least square matching algorithm, the DSM (1m spatial resolution) for each stereo pair was generated. Since, 14 stereo pairs were used to cover the entire study area, 14 DSMs have been generated and later mosaicked to obtain the single DSM file for the entire 2600 sq km area. The process could not be run on a single desktop as it required intensive computation resources. It could be completed successfully only in High Performance Computing (HPC) environment with 24 core processor and 128 GB RAM. Further, the generated DSM have been utilized to produce 0.5m (PAN) and 2m (MX) spatial resolution ortho image of the entire study area.



Figure 4-2: Photogrammetric preprocessing

4.3.1.4 Digital Terrain Model (DTM) generation

The accuracy of nDSM and subsequent height map is largely dependent on accurate computation of DTM. DTM generation requires removal of all above ground objects whether natural or manmade in order to obtain the underlying terrain. DEM editing of such a large area is a time and resource consuming process (M.,S.; S., M., & Dadhwal, 2015), hence, morphological filters such as minimum filter, bump filter and clump filter have been applied in succession (Figure 4-3). The foremost requirement was the identification of suitable window size for obtaining the reasonable results. This is an iterative process and more than 40 iterations have been carried out with different combinations of parameters to yield the acceptable results. For the study area, a window size of 60 m yielded reasonable results. Again this process was run in HPC environment due to high computation requirements. However, still few of the patches of dense vegetation patches (less than 1% of total area) have been left unresolvable. In those areas, manual editing was carried out and final DTM was obtained.

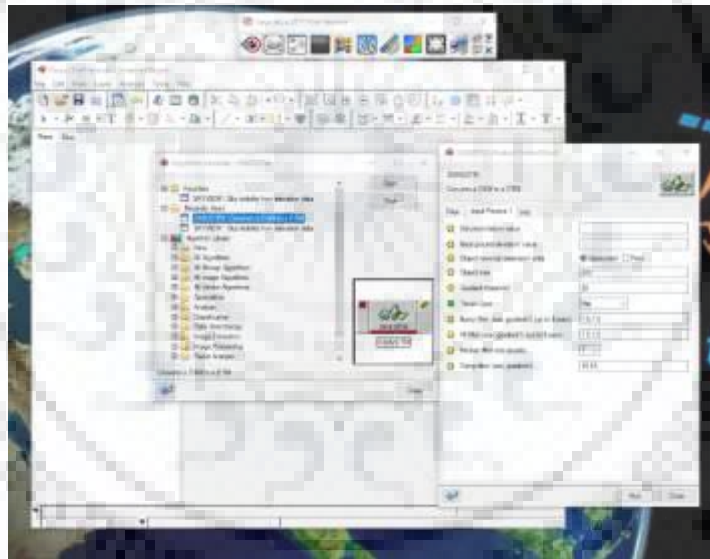


Figure 4-3: Digital Terrain Model generation tool

4.3.1.5 Normalized Digital Surface Model generation

Normalized DSM (nDSM) represents the height of all the objects present on the terrain above ground. It is generated by computing pixel-by-pixel difference between DSM and DTM using a characteristics equation given as $(nDSM = DSM - DTM)$. The final nDSM surface layer consist of above ground objects that includes building, vegetation, flyovers, elevated metro network and any other elevated objects.

4.3.1.6 Validation of Building Heights

The randomly distributed sample heights of the buildings and trees were obtained from ground utilizing the laser distance measurement device. Care was taken to distribute the samples evenly throughout the study area.

4.3.2 Land Use Land Cover Map

The multi spectral 14 ortho images of Pleiades data covering the entire study area was employed for generation of LULC map. The huge variation in the date and year of the images posed significant processing issues as the extent of bare soil and agriculture area is interchangeable depending on season. To overcome the issue, all the images were classified separately with broad level of LULC classes as described in following sections and shown in Figure 4-4.

4.3.2.1 Classification System

Five broad LULC classes' i.e. built up, vegetation, bare Soil, bare rock and water body were identified as target classes. Built-up area are identified on image as areas of cyan color of standard False Color Composite (FCC) with very coarse texture, consisting building structures which display small to large shadows and block like appearance. Vegetation appeared in shades of red and pink on standard FCC consisting natural and cultivated vegetation, whereas area under bare soil display high reflectance and appears bright on imagery as it does not consist any vegetation or building structures. The rocky outcrop of Aravalli hills in south and south west of the study area has been classified as bare rock area. Water body area in general appears on images as dark objects on standard FCC as water absorbs the Near Infrared (NIR) reflectance. These areas have been identified due to their pattern and dark shades from black to dark blue to blue depending on the depth and quality of water.

4.3.2.2 Training Data Sets

The training data for each class have been identified on the image by applying visual analysis of the image. Nearly $30n$ samples were identified for each class as a thumb rule, where n is the number of spectral bands of a satellite data (Mather & Koch, 2011). Care was taken to identify the small size, homogeneous samples in order to avoid mixing of different classes, however, they were large enough to satisfy the various statistical parameters. Since, the Pleiades MX has four bands, minimum 120 pixels were identified for each class. The histogram of the training data sets was found to be unimodal following a normal distribution (Arora M.K., 2010).

4.3.2.3 Land Use/ Land Cover Classification

Supervised parametric classifier (Maximum Likelihood classifier) (Jensen, 2007) was applied for the LULC classification. All the 14 ortho images were classified separately by identifying separate training data sets for each image in defined five classes as described earlier. The extent of bare soil and water body is seasonally dependent hence it has posed a major challenge for classification. Since, the ortho images were of varied season and dates, a careful examination of Google earth images were employed to contextually refine these two classes. Based on the field observations and local knowledge, contextual refinements were carried out in order to improve the accuracy of the final LULC map.

4.3.2.4 Accuracy Assessment

Stratified random sample points were generated for accuracy assessment and further evaluated with reference to ground truth obtained during field surveys and visual analysis of Google earth images.

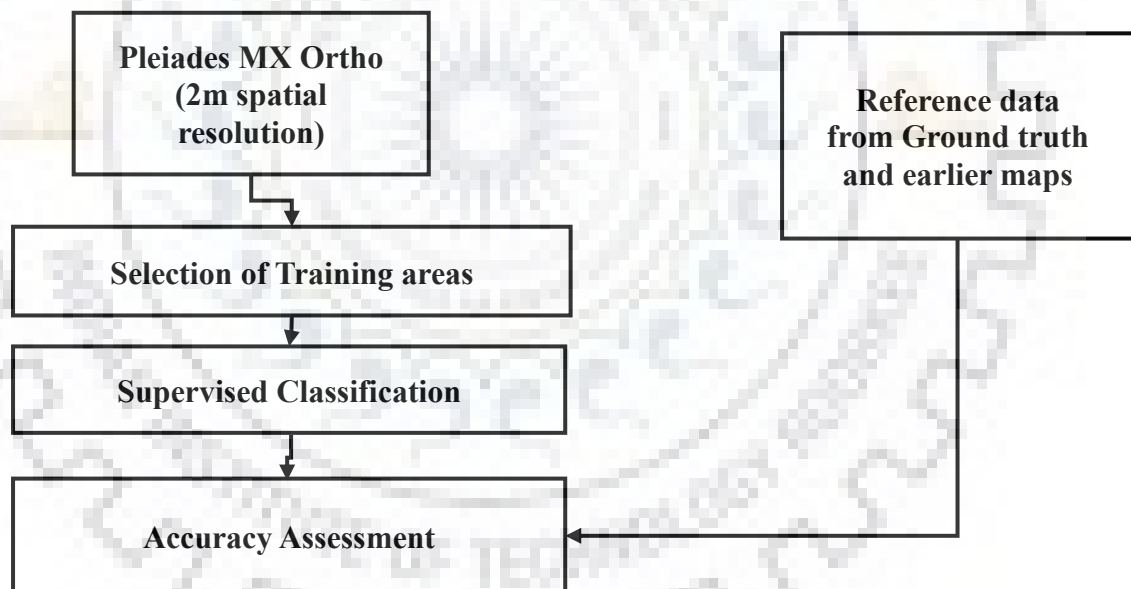


Figure 4-4: Methodology for generation of Land Use Land Cover

4.3.3 Road and Metro Rail network Map

The road network map from Open Street Map for the study area was downloaded and corrected by overlaying it over the ortho image of the study area. It was observed that nearly 20% of the roads needs modification to improve the accuracy. The corrections were carried out after overlaying the road network on ortho images to obtain the final road network map. The metro rail network is the backbone of transportation in the Delhi region, however most of the metro rail

network was elevated on medians of the road to avoid the complexity of underground network and to ensure the speedy implementation. A map of metro rail network was obtained from the DMRC website and a buffer was created to obtain the extent of metro network in the study region.

4.3.4 Sky View Factor (SVF)

The sky view factor (SVF) is the fraction of sky visible from the ground and it is defined by radiations received by entire hemispherical sky. It is a dimensionless parameter that ranges from 0 to 1. The SVF map was computed from the generated DSM using the approach for computation of continuous sky view factor (Gál et al., 2009; Ratti et al., 2006). The available algorithm for computing the SVF (Anon, n.d.-b; Dozier & Frew, 1990) in Geomatica (a COTS software) was utilized to obtain the SVF map (Figure 4-5). Validation of computed SVF map was carried out with the help of Fish Eye photographs (40 photographs) obtained from ground. The fish eye photographs have been processed in Hemi view software (Rich, Wood, Vieglais, Burek, & Webb, 1996) which processes hemispherical photographs to compute the fraction of visible sky. Here, again the care was taken to collect the randomly but evenly distributed samples over the entire study area.

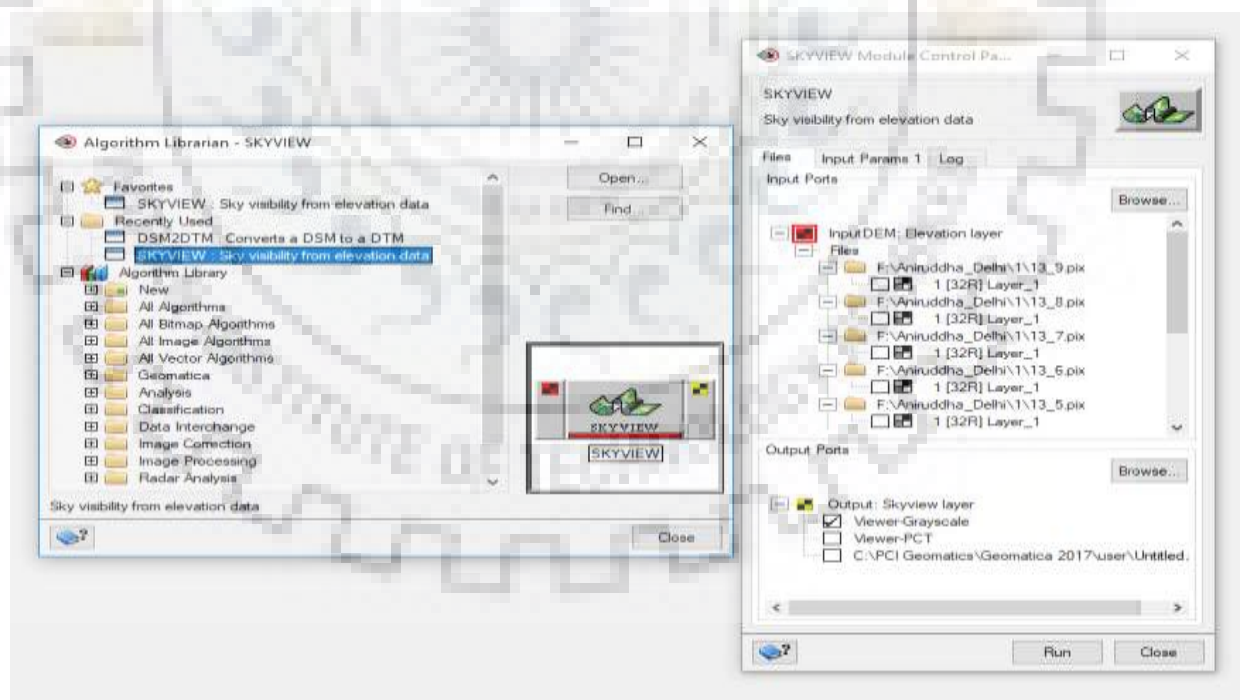


Figure 4-5: Sky View Factor Calculation tool

4.3.5 Building Height, Mean Building Height and Standard Deviation of Height Map

The generated nDSM map was utilized to obtain the Mean Building Height (MBH) map. The nDSM layer contains elevated objects mainly buildings, roads, shrubs, trees and flyovers. Many of the previous studies have utilized the already existing 3D GIS database (Burian et al., 2003a; Hammerberg et al., 2018) or 3D GIS database developed from LiDAR data (Burian & Brown, 2003b; Carter et al., 2012; Wicht & Wicht, 2018) or DSMs obtained from InSAR or fusion of optical stereo and InSAR (Jeyachandran et al., 2010; Xu et al., 2017). A study conducted in Kowloon peninsula, Hong Kong have applied segmentation of ortho images to obtain the building footprints (Xu et al., 2017). However, due to highly dense and complex low rise built-up in the study area, the segmentation of ortho images did not yield accurate results. Even the identification of building groups could not be carried out. To overcome these limitations, a step by step unique filtration method was developed to obtain the final building height layer for the study area that involved filtration of pixels less than 2m in height, vegetation and elevated road and metro rail network, as presented in Figure 4-6.

4.3.5.1 Filtration of Pixels less than 2m in height

First of all, the pixels having elevation value of less than 2m was assigned null value so as to remove small height objects such as shrubs, roads, cars etc. Generally less than 3m or 2.5 m height is recommended for filtering, however, extensive field surveys in the study area brought out that some of the building structures has even 2m height, hence, the criteria for filtration has been modified up to 2m. This step eliminates approximately 90% of the roads and bare rock and bare soil area.

4.3.5.2 Filtration of vegetation

The filtered map obtained after removing the pixels less than 2 m in height does not eliminate the tree vegetation. Hence, the built-up class from LULC map has been utilized to filter tree vegetation from the nDSM. A mask containing the built-up has been created and applied on nDSM to extract the built up area only.

4.3.5.3 Filtration of flyovers and elevated metro network

The obtained filtered map is able to remove roads and tree vegetation, however it still consist of flyovers and elevated metro network. In order to remove these two features, the road and metro rail network map have been buffered and subtracted from the modified nDSM layer in the above

step. Different buffer distances have been applied with respect to different categories of roads. Finally, a map containing only the building surfaces has been obtained.

4.3.5.4 Grid Overlaying

After obtaining the final building surface map by step by step filtration, a grid of 30 m size has been overlaid on the final modified nDSM in order to compute Mean Building Height (MBH) map. Similarly, the standard deviation of building height map has also been obtained.

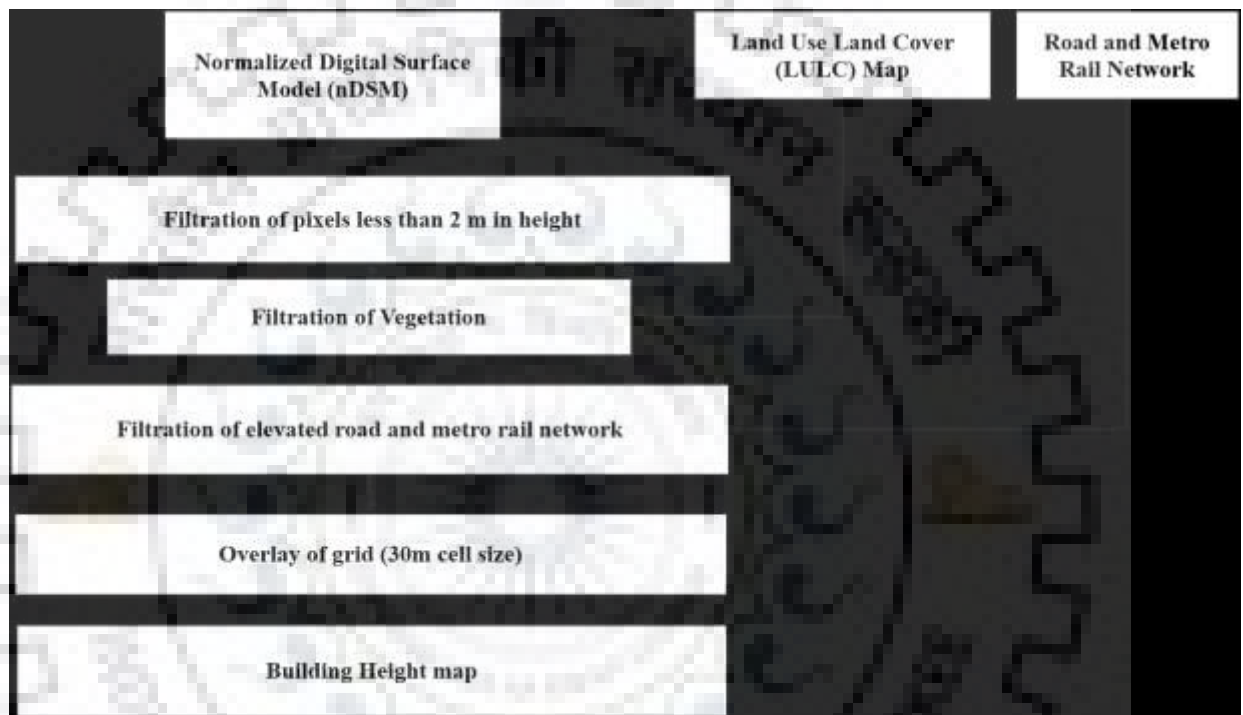


Figure 4-6: Methodology for the retrieval of building heights

4.3.6 Surface Cover Characterization

Characterization of surface cover included the generation of Building Surface Fraction (BSF), Impervious Surface Fraction (ISF) and Pervious Surface Fraction (PSF). The LULC map generated from Pleiades MX data, modified nDSM and road network map have been utilized for obtaining these layers as presented in Figure 4-7.

4.3.6.1 Building Surface Fraction (BSF)

The Building Surface Fraction (BSF) includes only the building roof surface area and its value ranges from 0 to 1. The building height layer created after the filtration of pixels less than 2m in height, vegetation and elevated metro and road network, have been utilized for generation of

building surface map. The whole layer was converted into binary image having two classes building surface area and non-building surface area. A grid of 30 m size was overlaid on the building surface map and BSF in each grid was computed. Most of the studies utilize either cadastral data or 3D GIS database for the computation of BSF and other UCPs. However, due to unavailability of any existing cadastral data or 3D GIS database posed a significant limitation. The very high dense and complex built up of study area also led to unsatisfactory results in the identification of individual footprints with image segmentation and object based classification. Hence, a gridded approach has been employed in this study to characterize the BSF and subsequently for computation of other UCPs as well.

4.3.6.2 Impervious Surface Fraction (ISF)

Impervious Surface Fraction refers to ratio of impervious plan area to total plan area. Impervious surface includes bare rock and paved surfaces. To obtain this layer, bare rock and built-up class from LULC has been extracted and then BSF layers has been subtracted from this map. All these pixels contain only the paved and bare rock area. Further, again a grid of 30 m was overlaid over the impervious surface map and then fraction of impervious surfaces in each 30 m grid has been computed.

4.3.6.3 Pervious Surface Fraction (PSF)

It refers to ratio of pervious plan area to total plan area and its value also ranges from 0 to 1. To identify the PSF the LULC was reclassified into pervious and non-pervious, where pervious surfaces includes the bare soil, water and vegetation class from LULC. All these classes have been classified as 1 and built-up and bare rock class have been classified as 0. A grid of 30 m size has been overlaid to obtain the final PSF map.



Figure 4-7: Methodology for computation of surface cover fraction

4.3.7 Building Volume

Building Volume (BV) is the averaged volume of building in each grid cell. To compute building volume, the BSF map and MBH map have been utilized and building volume has been computed as per the equation 4-1.

$$BV_i = MBH_i * (BSF_i * A_i) \quad \text{Equation 4-1}$$

Where,

BV_i = Building Volume of i^{th} grid cell

MBH_i = Mean Building Height of i^{th} grid cell

BSF_i = Building Surface Fraction of i^{th} grid cell

A_i = Area of i^{th} grid cell

4.3.8 Volumetric Averaged Height

To compute the volumetric averaged height, Equation 4-2 has been utilized. First of all, building volume map was multiplied by the mean building height map and then a moving grid of 60m X60m has been overlaid on the map. Summation of building volume in each 60 m grid which contains four 30m grid have been carried out. In this study a gridded approach have been employed to compute the parameters. The input layers for the computation of volumetric averaged height have been computed at 30m. Since, the parameter needed computation of volume and then averaging of height with respect to volume, 60 m grid encompassing 4 number of 30 m grid have been utilized to compute the volumetric averaged height. Similar process has been applied on BV map and values for the denominator has been obtained. The summation map of building volume multiplied by building height has been divided by the summation of building volume map and final volumetric building height map has been obtained.

$$\bar{h}_{vj} = \frac{\sum_{i=1}^N BV_i * MBH_i}{\sum_{i=1}^N BV_i} \quad \text{Equation 4-2}$$

Where,

\bar{h}_{vj} = Volumetric Averaged Height at i^{th} grid cell

BV_i = Building Volume of i^{th} grid cell

MBH_i = Mean Building Height of i^{th} grid cell

N is number of grid cells

4.3.9 Complete Wall Surface Area

The external wall surfaces receives radiation and also actively participate in modulation and exchange of energy. Hence, it is important to compute information on active wall surfaces in urban canyons. To compute the wall surfaces in each grid cell using raster GIS data, a novel approach has been developed (Figure 4-8). The layer for building surfaces has been first converted into vector polygon data and then intersected with 30 m grid cell. Perimeter of each polygon in the grid has been computed in GIS environment and whole perimeter length in each grid cell has been obtained. This perimeter length was then multiplied by the MBH of each grid cell in order to compute the Wall Surface area in each grid cell (Equation 4-3). The whole computation was quite resource expensive and could be completed only in high performance computation environment. Since, area was quite large (2600Sq km), the whole area has been divided in to four equal parts to finish the computation. Later on, all these four parts have been mosaicked together to obtain the final output.

$$Aw_i = (\text{Sum of perimeter of all polygons in } i^{\text{th}} \text{ grid cell}) * MBH_i \quad \text{Equation 4-3}$$

Where,

Aw_i = Wall area of i^{th} grid cell

MBH_i = Mean Building Height of i^{th} grid cell

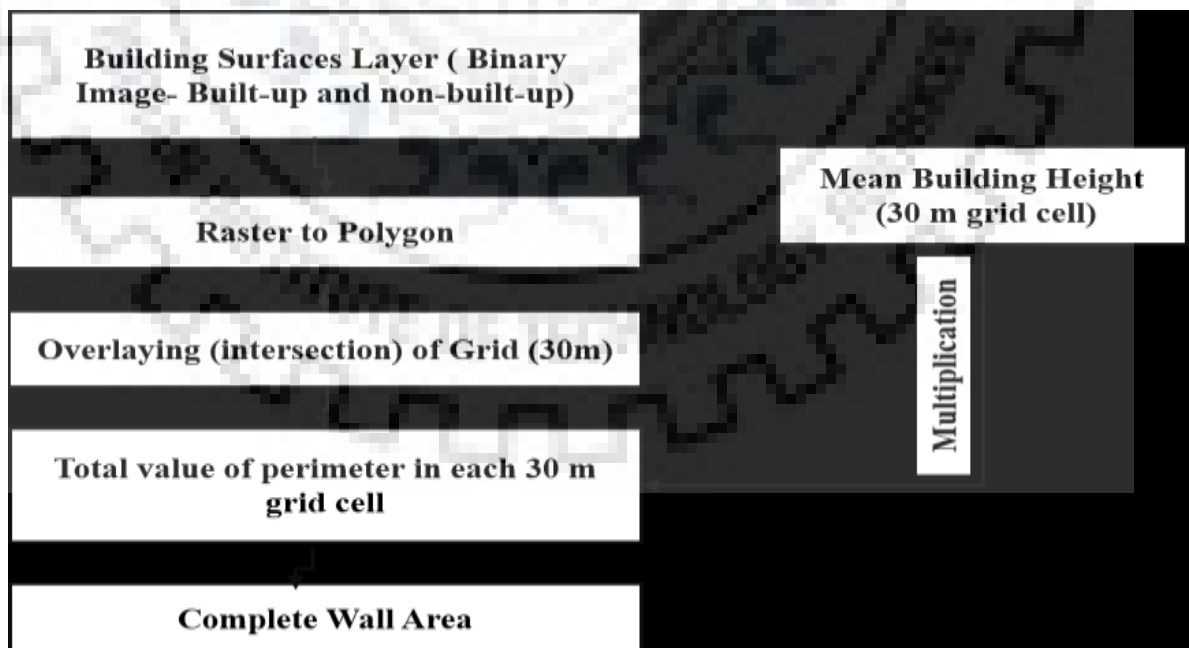


Figure 4-8: Flow chart for the computation of complete wall area

4.3.10 Complete Aspect Ratio

The Complete Aspect Ratio (CAR) as described earlier is the complete surface area which actively takes part in energy exchanges. It includes roof area, wall area and ground area. Since, BSF represents the roof area and remaining area in grid represents the ground area, the equation (Equation 4-4) for computation of CAR has been modified after the equation as given in Table 2-2 .

$$CAR_i = \frac{(BSF_i * A_i) + \{(1 - BSF_i) * A_i\} + Aw_i}{A_i} \quad \text{Equation 4-4}$$

Where,

CAR_i = Complete Aspect Ratio

BSF_i = Building Surface Fraction of i^{th} grid cell

A_i = Area of i^{th} grid cell

Aw_i = Wall area of i^{th} grid cell

The compute the surface roof area the, building surface fraction was utilized. BSF map is nothing but the building roof surface fraction as satellite images the building rooftops. The BSF map has been multiplied by the area of each grid cell. Similarly the ground area in each grid cell has been computed by subtracting the building roof area.

4.3.11 Building Surface area to Plan Area Ratio

Building Surface area to Plan Area Ratio (BSA-PAR) has been computed by following the similar approach as followed for the computation of CAR based on the equation 4-5.

$$BSAPAR_i = \frac{(BSF_i * A_i) + Aw_i}{A_i} \quad \text{Equation 4-5}$$

Where,

$BSAPAR_i$ = Building Surface area to Plan Area Ratio of i^{th} grid cell

BSF_i = Building Surface Fraction of i^{th} grid cell

A_i = Area of i^{th} grid cell

Aw_i = Wall area of i^{th} grid cell

4.3.12 H/ W ratio

The method for computation of H/W ratio is either through ground methods (Gál et al., 2009; Steyn, 1980) or through 3D geodatabase in vector GIS environment (Burian et al., 2003;

Hämmerle et al., 2011). Since, 3D GIS vector database was not available for the study region, the equation given by Lindberg et al (Lindberg et al., 2015) (Table 2-1) have been modified (Equation 4-6) to compute the H/W ratio. A novel method for computation of wall area and subsequently computation of H/W ratio has been developed in GIS environment. First of all, the wall area has been computed as described in 4.3.9. This wall area has been further divided by the total grid area of each cell to obtain the wall area ratio. It has been further divided by the BSF layer as given in equation 4-6.

$$H/W_i = 0.5 * \frac{\frac{Aw_i}{A_i}}{(1-BSF_i)} \quad \text{Equation 4-6}$$

Where,

H/W_i = Height Width Ratio of i^{th} grid cell

Aw_i = Wall area of i^{th} grid cell

A_i = Area of i^{th} grid cell

BSF_i = Building Surface Fraction of i^{th} grid cell

4.3.13 Zero Plane Displacement Height

Zero plane displacement height (z_d) is one of the main aerodynamic roughness parameter which is utilized for the understanding the roughness characteristics of urban area. Zero plane displacement height is defined as “the height of a surface formed by distributing the aggregate volume of roughness elements and their wake re-circulation cavities uniformly over the underlying surface” (Burian et al., 2003). Various equations for the computation of z_d was given by different researchers (Table 2-1), however, in this study, the equation given by (Gál & Unger, 2009) for irregular building arrays have been utilized for the computation of z_d . It was obtained by multiplying the volumetric averaged height and 0.6 power of BSF.

4.3.14 Surface Roughness Length

Surface roughness length (z_o) is another aerodynamic roughness parameters which has significant impact on air flow, permeability and overall drag of surfaces in urban areas. Morphometric methods utilizes either mean height or plan area fraction or frontal area index for computation of z_o (Grimmond & Oke, 1999) by employing different equations. The equation based on plan area fraction applies only if λp is ≤ 0.29 . However, in study area, the range of BSF is high in a large part of the study area, hence, the equation based on λp could not be applied. Other methods proposed the use of frontal area index for the computation of z_o by utilizing the 3D GIS database

and a script in GIS environment. Wong et al., 2010a considered frontal area index as a good indicator of urban roughness for mesoscale and dispersion modeling in urban area (Wong, Nichol, To, et al., 2010a). However, its computation in complex and dense urban area requires automation.

Since, the available tools for computation of frontal area such as Urban Multi-scale Environmental Predictor (UMEP)(Lindberg et al., 2018) and Urban Morphology Extractor (UME)(Jhaldiyal et al., 2018) did not yield satisfactory results in the complex urban environment of Delhi UA, the simple rule-of thumb approach proposed by Grimmond and Oke, 1998 have been utilized for the computation of z_0 (Table 2-1). The coefficients values of 0.1 for buildings, 0.06 for tree vegetation and 0.1 for water body, bare rock and bare soil area (Grimmond & Oke, 1999) was multiplied by the respective mean of heights in each 30m grid cell to obtain the z_0 separately for vegetation and building surface area. Further, both the maps have been combined to derive the final z_0 map.

4.4 RESULTS

This section presents and describes various results of data pre-processing such as DSM, DTM, nDSM and land use land cover. Further the results of retrieved UCPs (Building Height, mean building height, standard deviation of building height, surface cover fractions, building volume, volumetric averaged height, sky view factor, complete aspect ratio, BSAPAR, H/W ratio, zero plane displacement height and surface roughness length) are also presented in this section.

4.4.1 Digital Surface Model Generation

DSM have been generated by utilising all 14 pairs of Stereo images which has been further mosaicked as presented in Figure 4-9. It includes all the surface features whether manmade or natural features as well as the terrain. The height values in DSM varies from 95m to 344m. It can be seen that except rocky area in south and southwest most of the study area has a flat terrain. The eastern side of the study area is traversed by the river Yamuna and its tributaries. The western part also characterized by few major drainage system known as Najafgarh drainage. Other than these natural features most of the area is flat and dominated by built-up and bare soil area.

4.4.2 Digital Terrain Model

DTM of the study area (Figure 4-10) has been obtained after automatic application of various morphological filters with a moving window of 60 m. It can be seen that most of the above

ground objects are removed leaving just the underlying terrain removed (relieved) digitally. The values varies from 89m to 273m. The river system on eastern side and rocky area on the south side could be seen clearly.

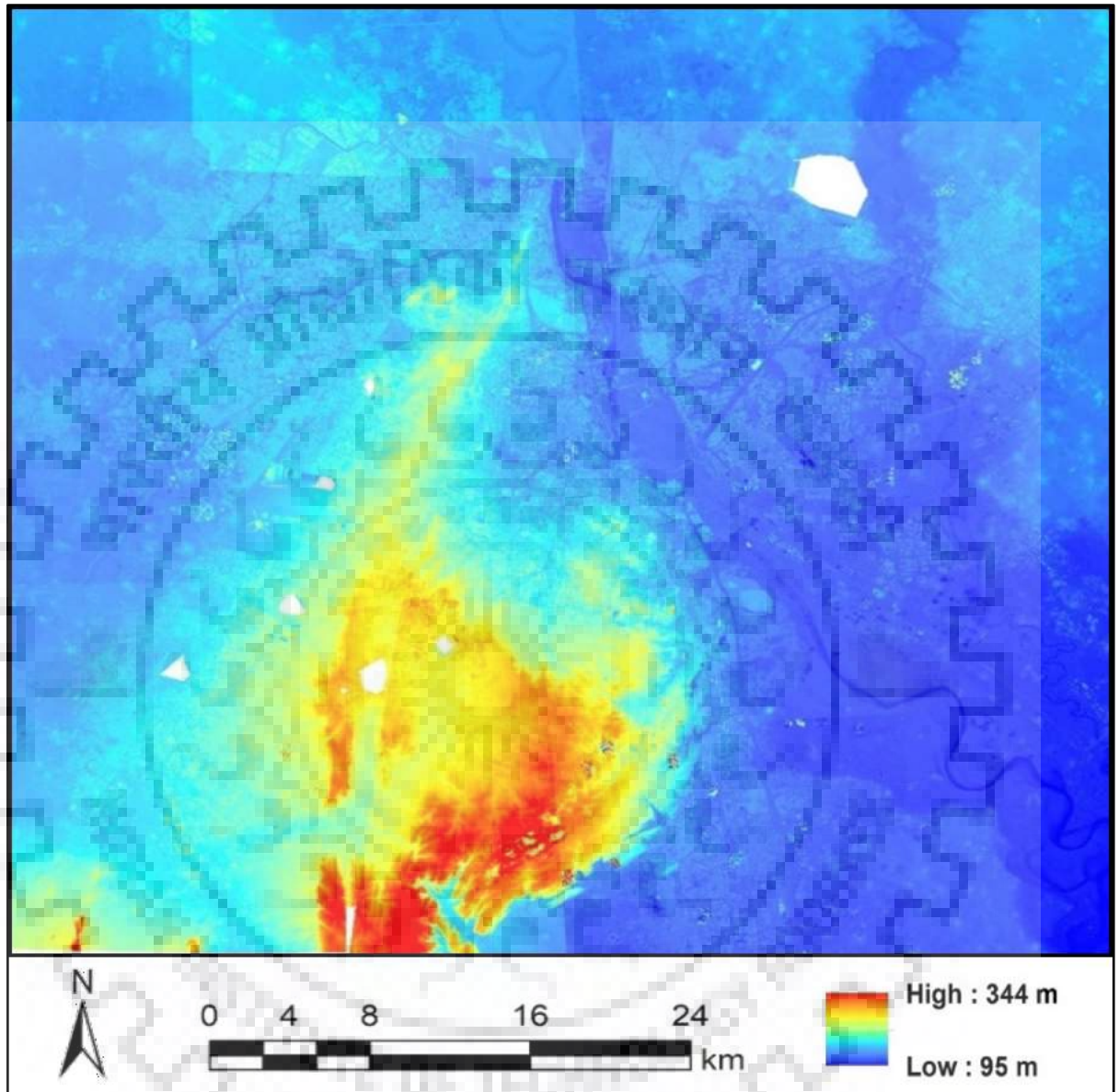


Figure 4-9: Mosaicked Digital Surface Model of the study area

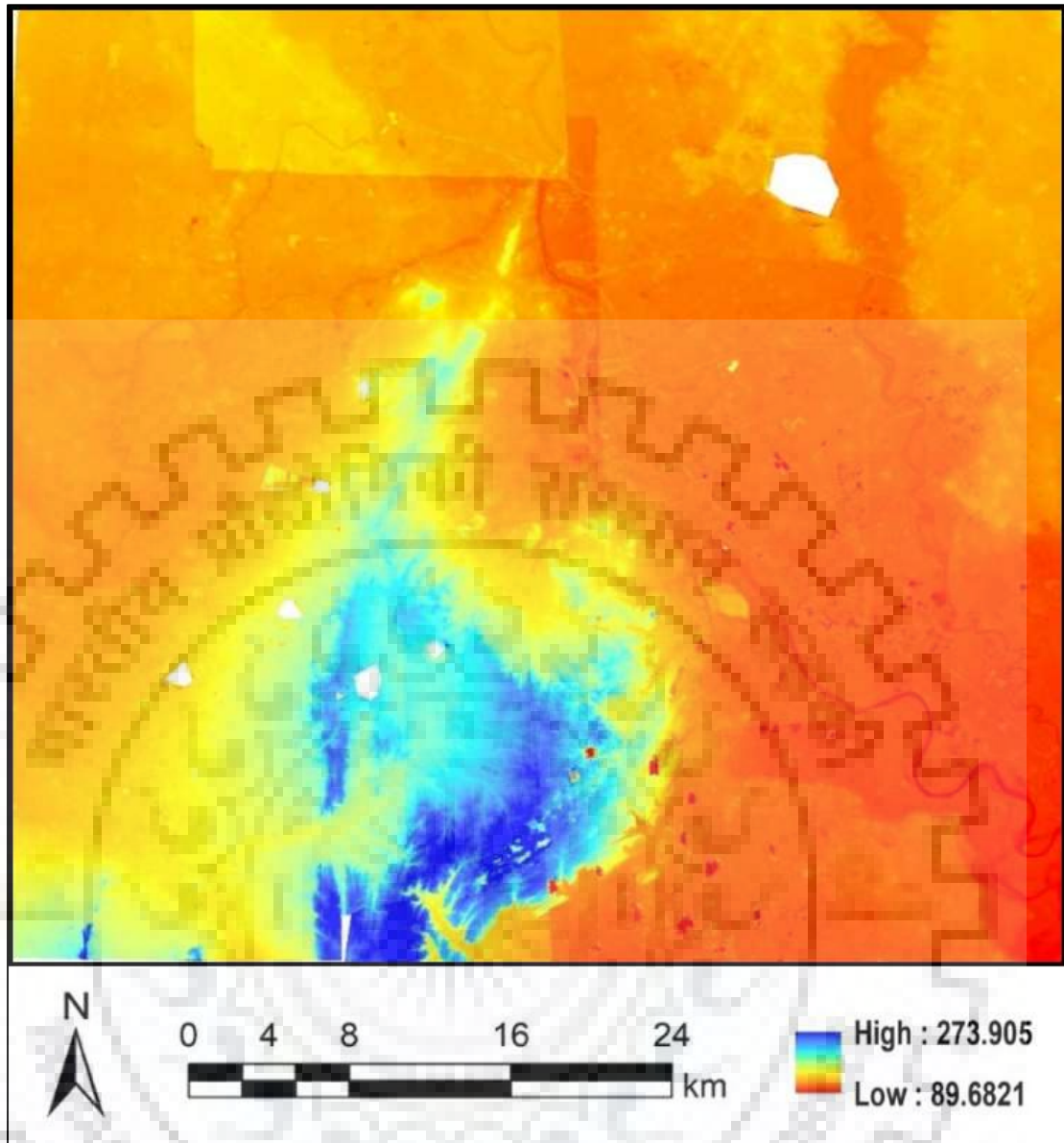


Figure 4-10: Mosaicked Digital Terrain Model of the study area

4.4.3 nDSM (Normalized Digital Surface Model) Generation

After the generation of the DTM, the DTM has been subtracted from the DSM to get the nDSM (Figure 4-11). The values various from 0 m to 206 m. The maximum building height in the study area is 75m. The points more than 75 m in height has been found to be air points due to presence of clouds and has been classified as erroneous points. From nDSM it is clearly visible that most of the built up area does not consist of high rise buildings.

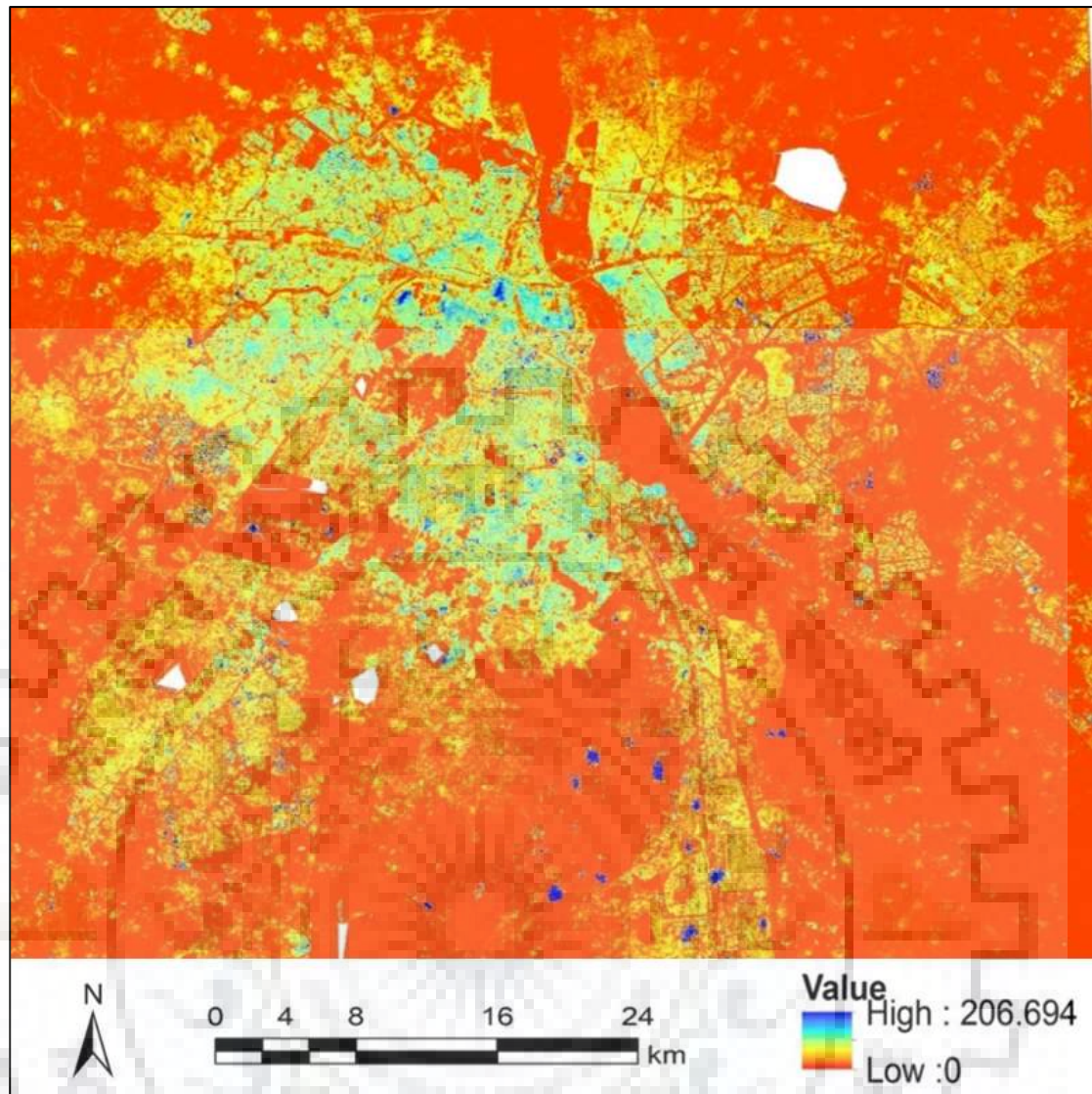


Figure 4-11: Normalized DSM of the study area

4.4.4 Land use/Land Cover map

The ortho images generated from Pleiades MX (2m spatial resolution) satellite data have been utilized for the generation of Land Use Land Cover (LULC) map (Figure 4-12). The LULC map has been classified into five classes' viz., Built-up, Water Bodies, Vegetation, Bare Soil, and Bare Rock. For accuracy assessment, ground samples were collected during field survey. The overall accuracy of the classified image has been found to be 89.60% and the kappa statistics was found to be 0.8455, which is acceptable as it is well within the specified accuracy limit of 85%. It is evident from the Table 4-3 presenting area statistics of LULC, that vegetation, bare soil and built-up are the most dominating classes in the study area. Water body and barren rocky area consist of only a small percentage of total study area.

Table 4-3: Area statistics under different classes for Land Use Land Cover

Classes	Area in sq km	Area in %
Built-up	675.2	24.83
Water Bodies	27	0.99
Vegetation	990	36.41
Bare Soil	968	35.60
Bare Rock	58.5	2.15
Total	2718.7	100

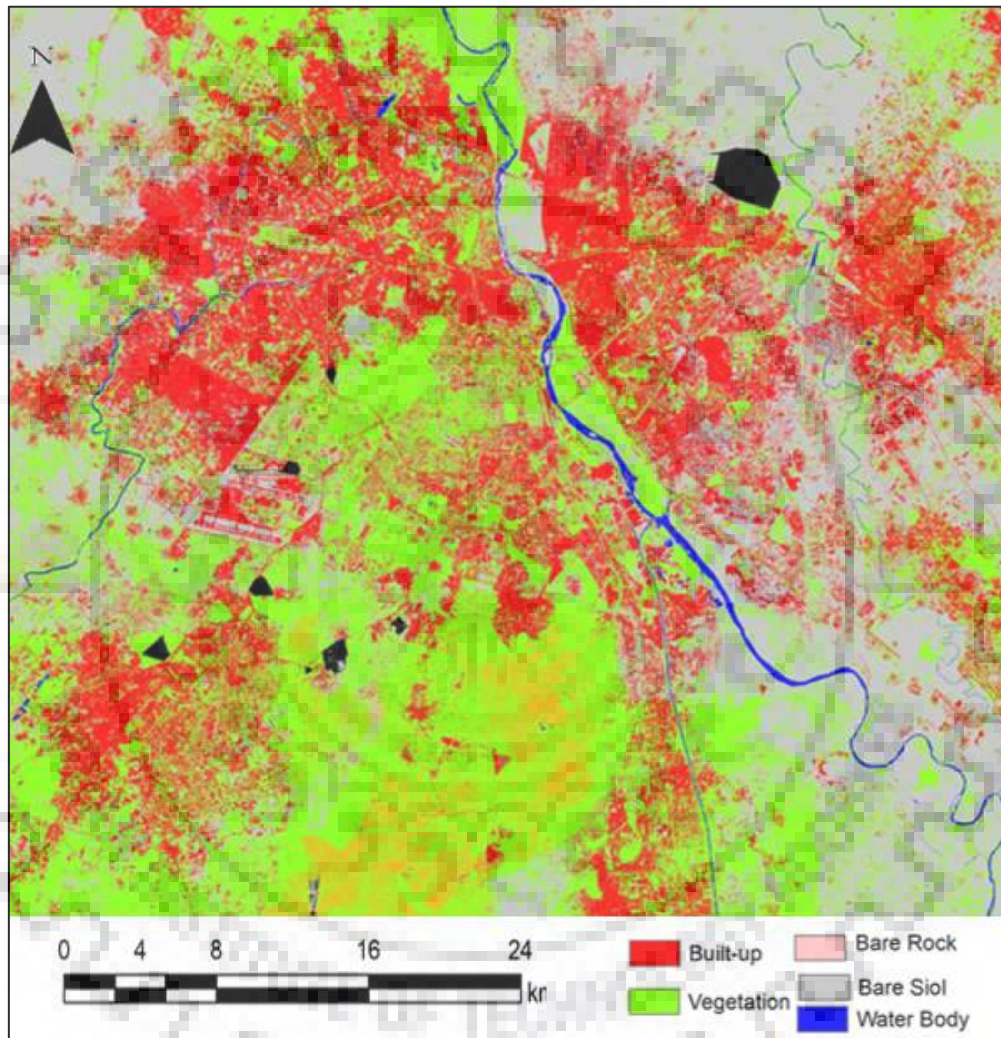


Figure 4-12: Land Use Land Cover map

4.4.5 Building Height Map

The building height map (Figure 4-13) for entire study area has been generated as discussed in section 4.3.5 after the filtration of vegetation, pixels less than 2m in height and elevated road and metro rail network. From Figure 4-13 it could be seen clearly that the patches of building more

than 30 m in height is sparse and few. The maximum inner area is dominated with built-up more than 10 m in height and on the periphery it is mostly dominated by low rise built-up.

Building Height is one of the important characteristics of urban built form. The distribution of building height is an indication of how sprawled or compact city is. As discussed in Chapter 3, Delhi in its initial growth during post-independence era had restriction on FAR that allows a construction of nearly four floor houses only. This has led to a sprawled form of the city.

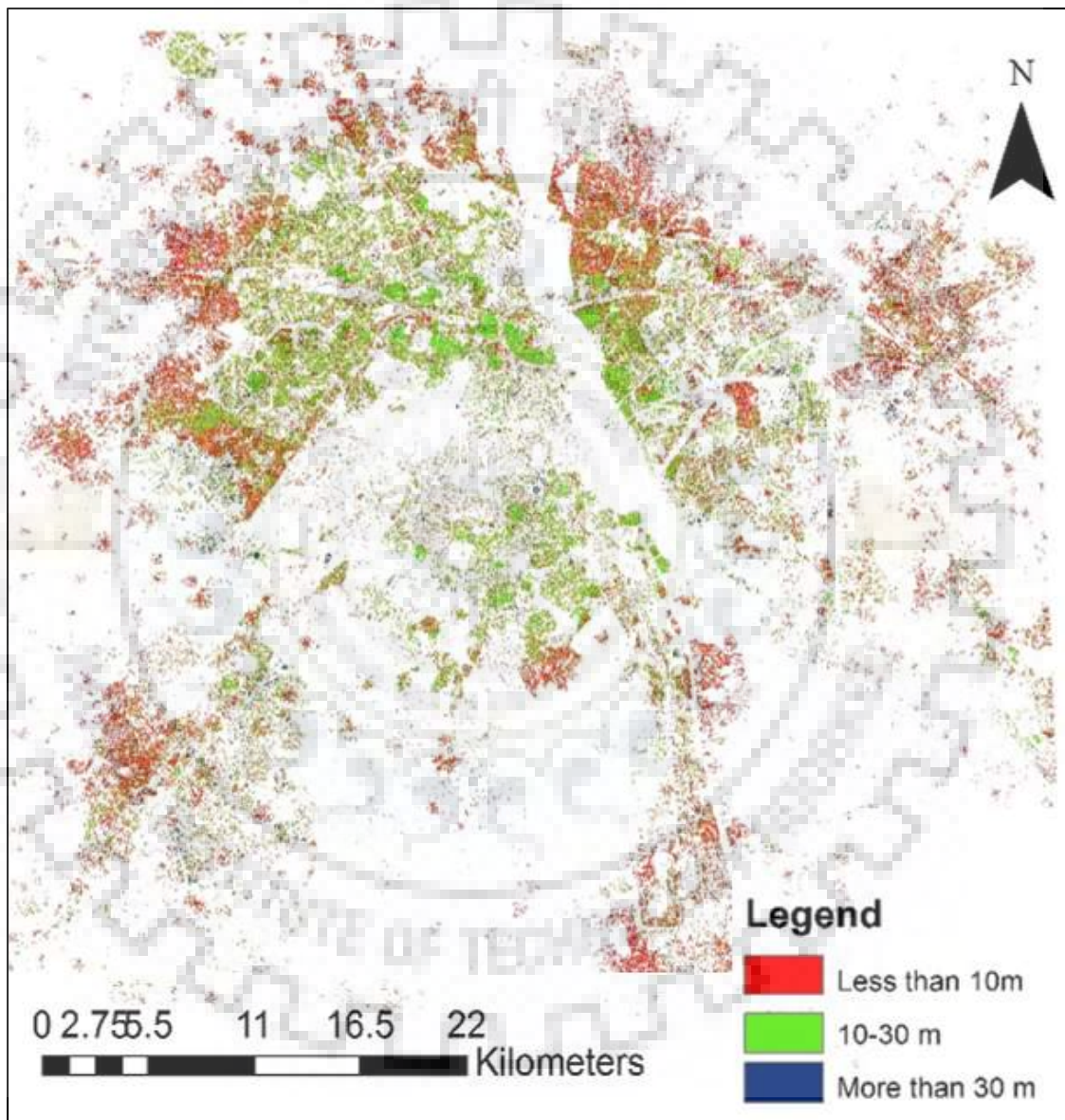


Figure 4-13: Building Height distribution

4.4.5.1 Building Height and Mean Building Height

Figure 4-14, Figure 4-15 and Table 4-4 presents the building height characteristics of Delhi and surrounding towns. From the distribution of building heights in Figure 4-14 it is evident that the study area is characterized mostly by low rise and medium rise development. 58% of built up area lies in height zone of less than 10 m and 41% of built up area lies in medium height zone of less than 30 m. Only 0.62% built-up area has high rise building and that also in small patches and mostly on the periphery of the continuous urban built up area.

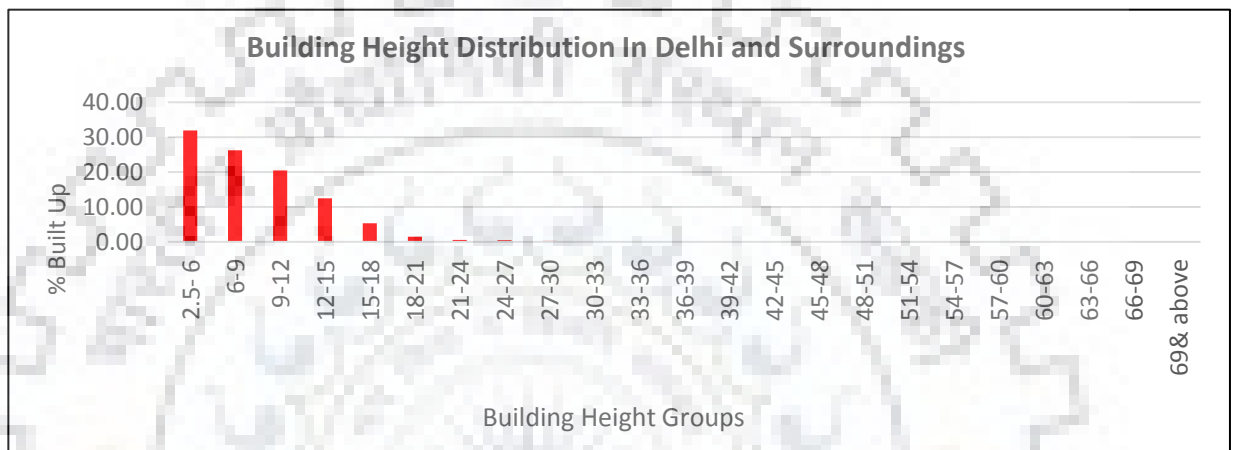


Figure 4-14: Distribution of building heights in Delhi UA

Mean Building height at 30 m grid cell shows a shift towards lower height groups which is due to the high heterogeneity of height in one grid cell. The new development which is coming on the periphery especially in the eastern part is coming up with high rise construction. The continuous built up area has a sprawled character which has strong bearing on travel and energy consumption. Besides, the study area lies in a land locked area which makes it quite difficult for the accumulated heat and energy to disperse and thus creating a highly polluted environment.

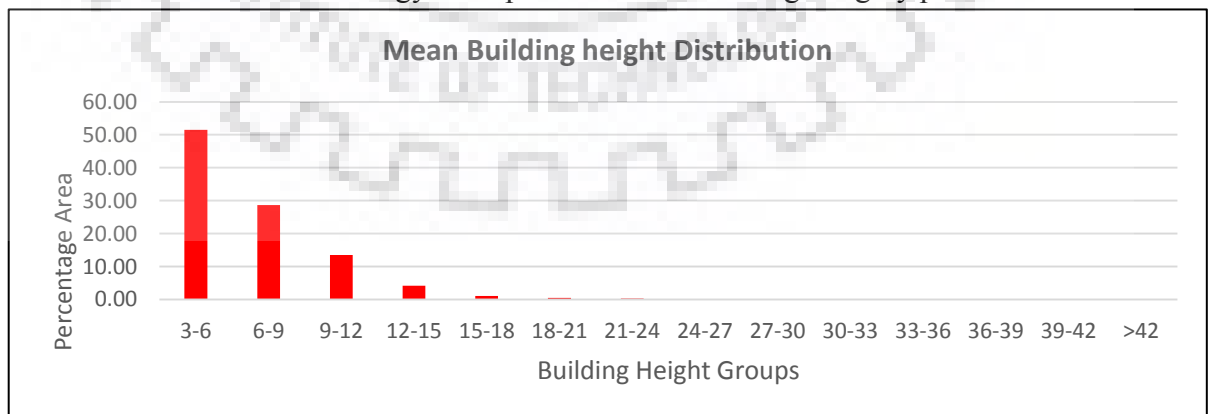


Figure 4-15: Distribution of mean of building height in 30 m grid cell

Table 4-4: Distribution of Building Height and Mean Building Height

Height Group	Percentage Area in each Category	
	Building Height	Building Mean Height at 30 m grid cell
3- 6	31.96	51.48
6-9	26.24	28.68
9-12	20.52	13.54
12-15	12.48	4.17
15-18	5.36	1.08
18-21	1.45	0.43
21-24	0.60	0.24
24-27	0.45	0.14
27-30	0.31	0.08
30-33	0.19	0.05
33-36	0.13	0.04
36-39	0.07	0.03
39-42	0.05	0.02
>42	0.18	0.03

4.4.5.2 Standard Deviation of Building Height

Standard Deviation of Building Height at 30 m grid cell clearly indicates that there is a high heterogeneity of height in Delhi almost 77 % grid cells falls under the standard deviation of more than 1 and less than 10. This indicates non uniform development with respect to height and high heterogeneity of development. Table 4-5 and Figure 4-16 and Figure 4-17 denotes the standard deviation of building height in each grid cell. The grid cell size of 30 m is chosen while considering the minimum loss in height as there was a generalization of height values on higher grid cell size of 50m and 100m due to high heterogeneity.

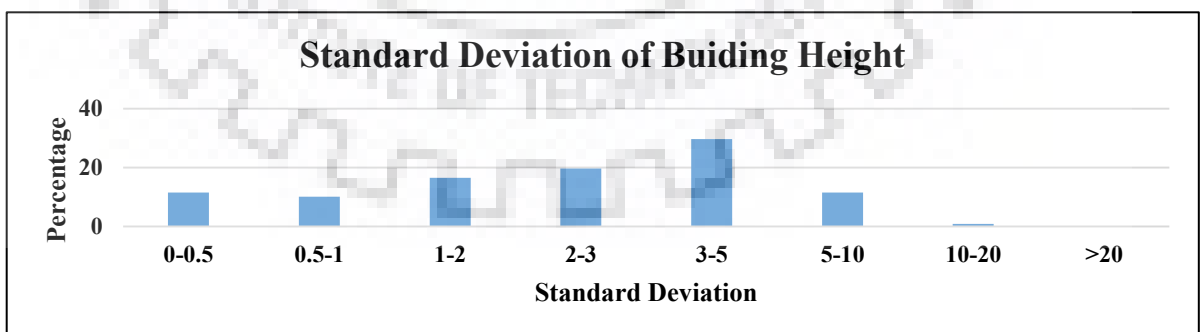


Figure 4-16: Distribution of Standard Deviation of Building Height

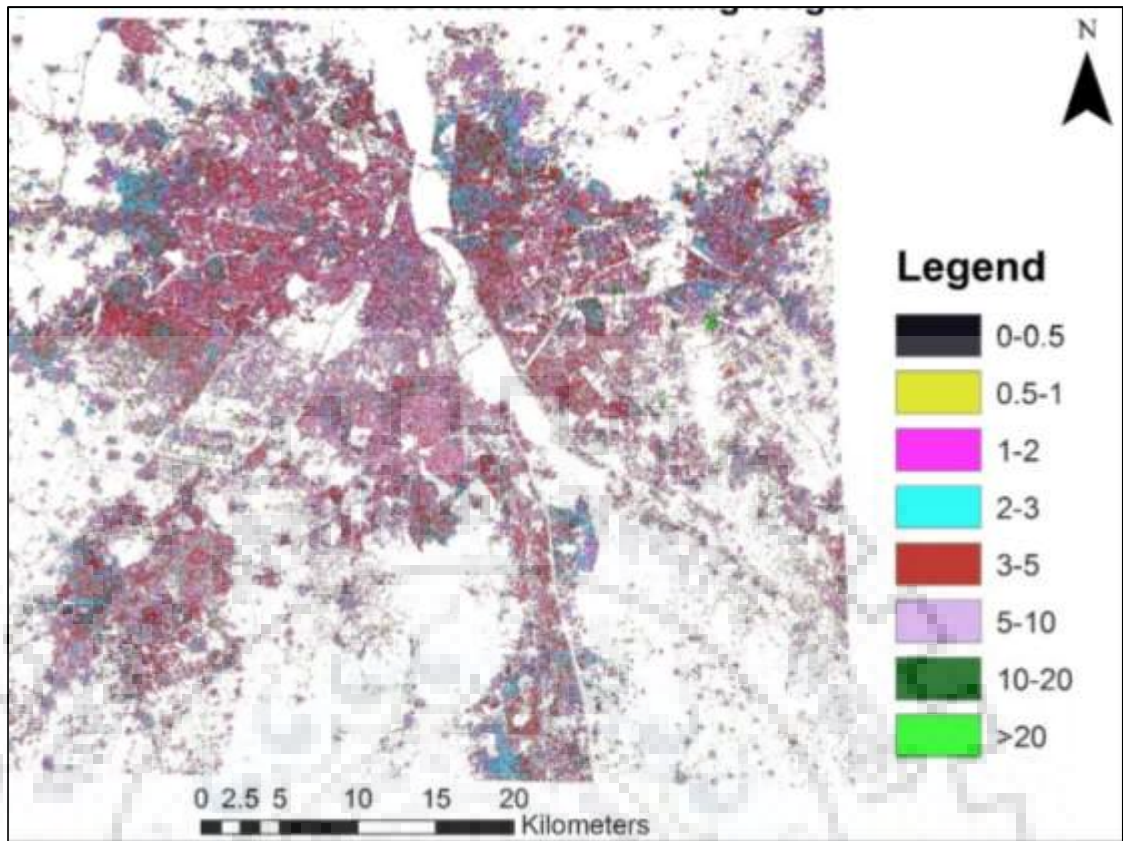


Figure 4-17: Standard Deviation of Building height in each 30 m grid cell

Table 4-5: Standard Deviation of Building height in 30 m Grid cell

Standard Deviation group	Count of Grid Cells	Percentage Grid cells
0-0.5	85770704	11.51
0.5-1	75450209	10.12
1-2	123316130	16.55
2-3	146570155	19.67
3-5	221335903	29.70
5-10	85745561	11.51
10-20	6435517	0.86
>20	504036	0.067
	745128215	100

4.4.6 Building Surface Fraction

Building Surface Fraction (BSF) represents the proportion of ground surface with respect to building cover. BSF affects surface reflectivity, flow, regimes, and heat dispersion above ground. The BSF layer was generated as described in section 4.3.6 by utilizing the MBH layer, since it represents the building surface area. The BSF image (Figure 4-18) shows the building surface

fraction values ranging from 0 to 1, where 1 represents highly building surface area and 0 represents low building surface area. The distribution of BSF in equal range (Figure 4-19) clearly shows that approximately 35% of building surface area fall under 0.6-1 BSF range. It clearly shows the presence of very high density built-up in study area where nearly 9% of building area has more than 90% of built-up.

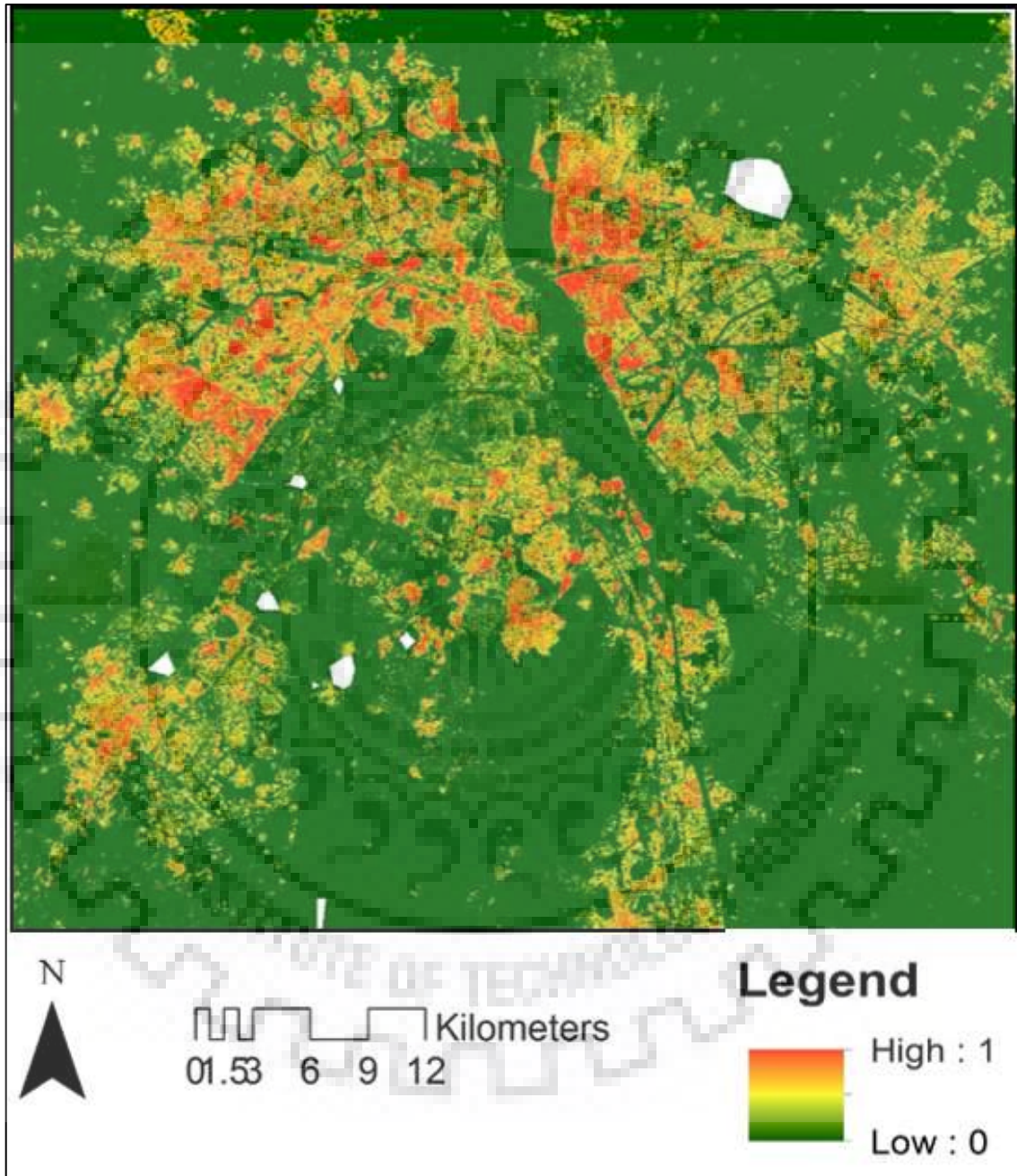


Figure 4-18 : Building Surface Fraction

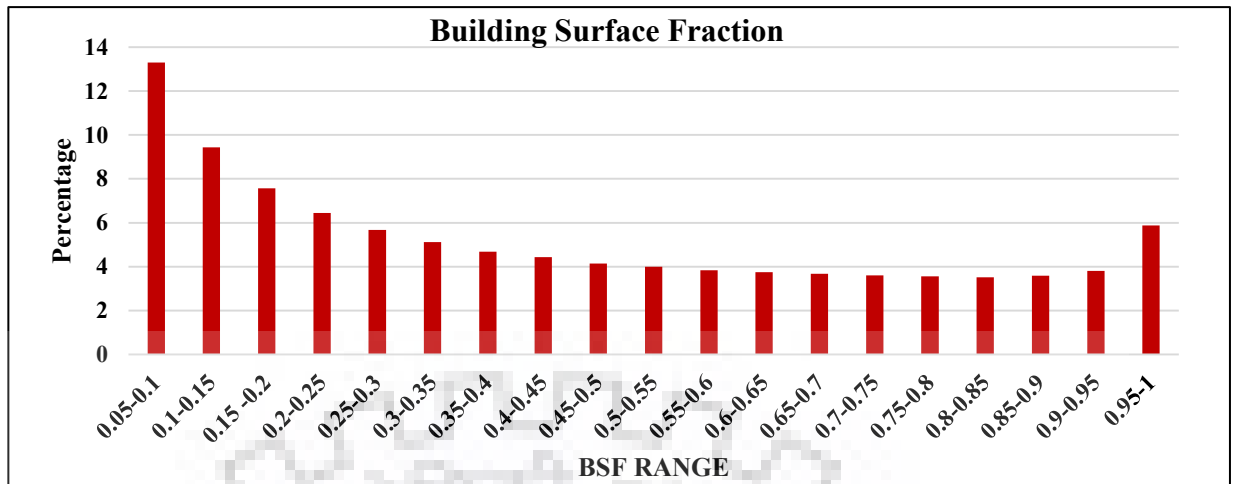


Figure 4-19: Distribution of Building Surface Fraction

4.4.7 Impervious Surface Fraction

The Impervious Surface Fraction (ISF) represents the proportion of ground surface with respect to the impervious cover (paved area, parking areas, footpath and bare rock). The ISF image (Figure 4-21) was continuously stretched from 0 to 1 with 0 representing low impervious areas and 1 representing highly impervious areas. The impervious area consist of 27% of total built-up area which is consistent with the reports which says that road area in Delhi covers approx. 26% of land area (Narain, 2016).. The range wise distribution of ISF in equal ranges shows that nearly 80% of ISF grid cells are within 0-0.5 range. Only 20% of grid cells has ISF more than 50% (Figure 4-20). Bare rock area is found in the south west part of the study area.

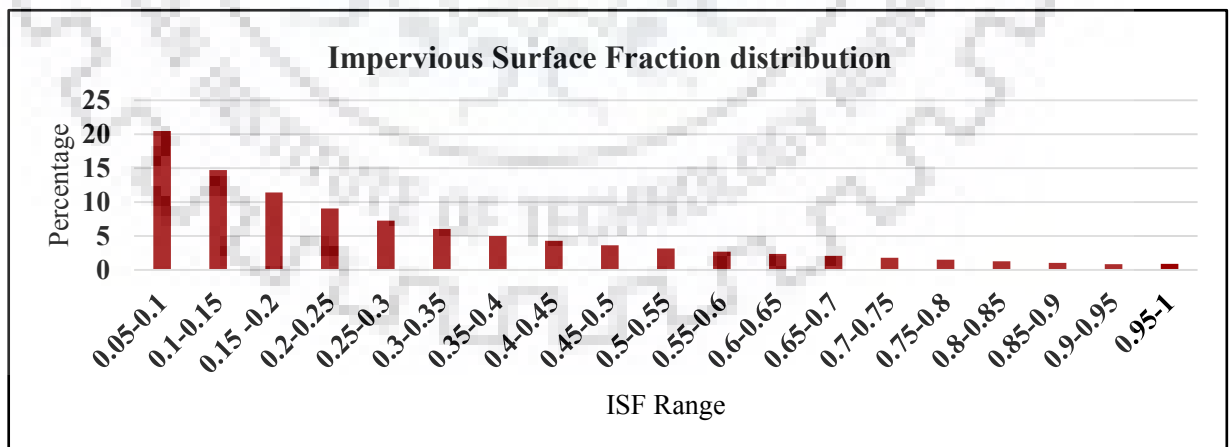


Figure 4-20: Distribution of Impervious Surface Fraction

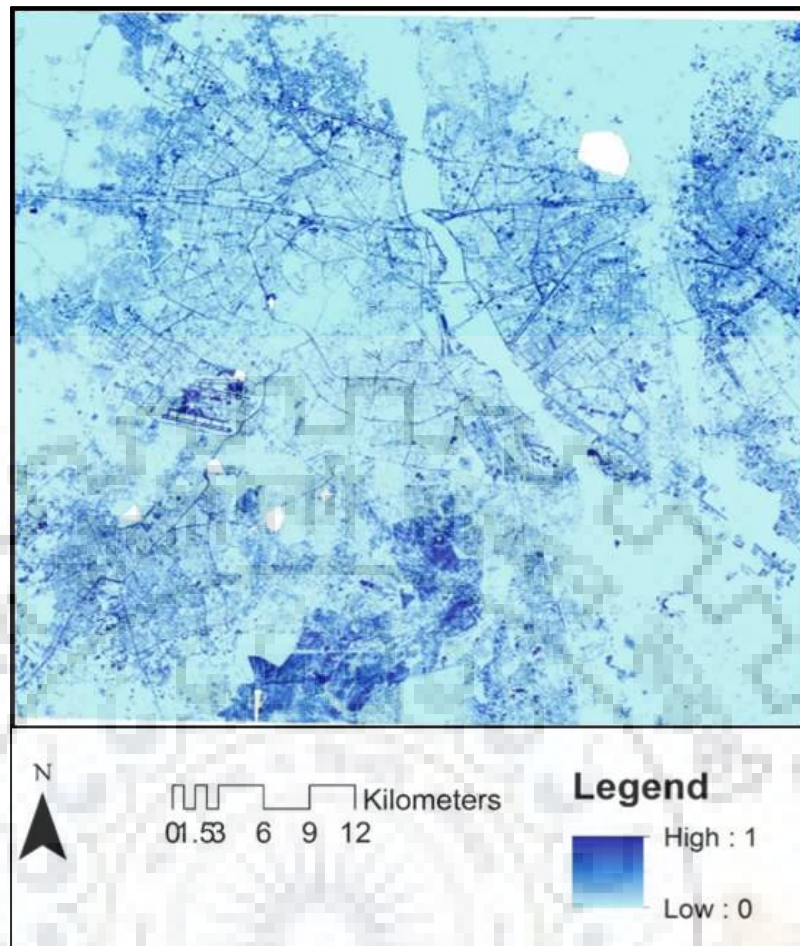


Figure 4-21: Impervious Surface Fraction

4.4.8 Pervious Surface Fraction

The Pervious Surface Fraction (PSF) represents the proportion of ground surface with respect to the pervious cover (bare Soil, vegetation, and water bodies). The pervious map was also stretched from 0 to 1 where 0 signifies low or non-pervious area like paved area and 1 signifies highly pervious area (Figure 4-22). Bare soil, vegetation and water body together occupy highest land area that is approximately 73% of total study area. Nearly 45% of grid cells fall under the range 0.95-1 (Figure 4-23) which denotes more than 95% of grid cell has pervious area, although the pervious area is highly dominated by the bare soil area.

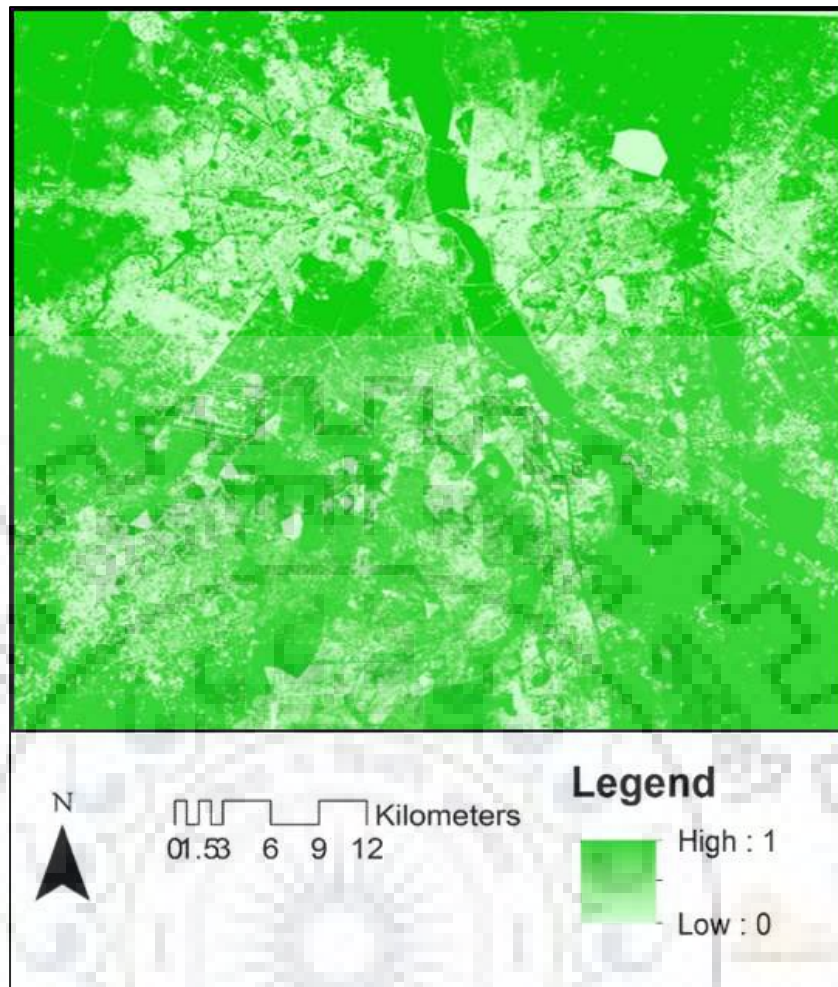


Figure 4-22: Pervious Surface Fraction

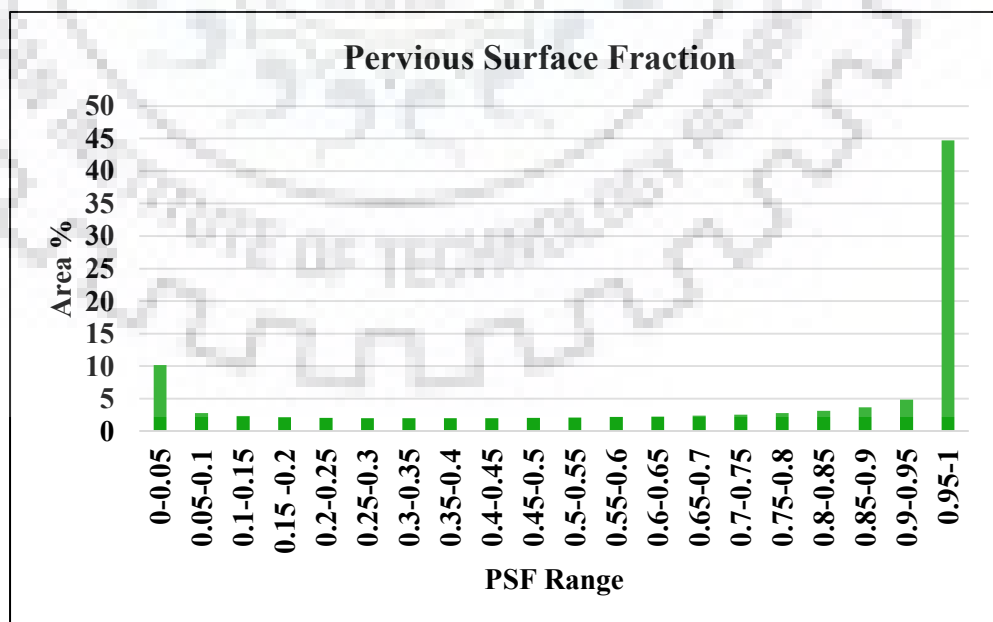


Figure 4-23: Percentage distribution of pervious surface fraction

4.4.9 Building Volume

The generated Building Volume (BV) map and its distribution is presented in Figure 4-24 and Figure 4-25 respectively. It shows that building volume ranges from 500 m³ to nearly 20,000 m³ building volume in 30 m grid cell. Less than 1% grid cells are found to be in the range of 20,000 m³-50,000 m³. Similar pattern was observed in building volume as peripheral areas has lower BV then the inner parts of the study area. The distribution of BV is not homogeneous but higher volume is concentrated in few pockets along the river Yamuna and arterial roads and older settlements with high density of built-up.

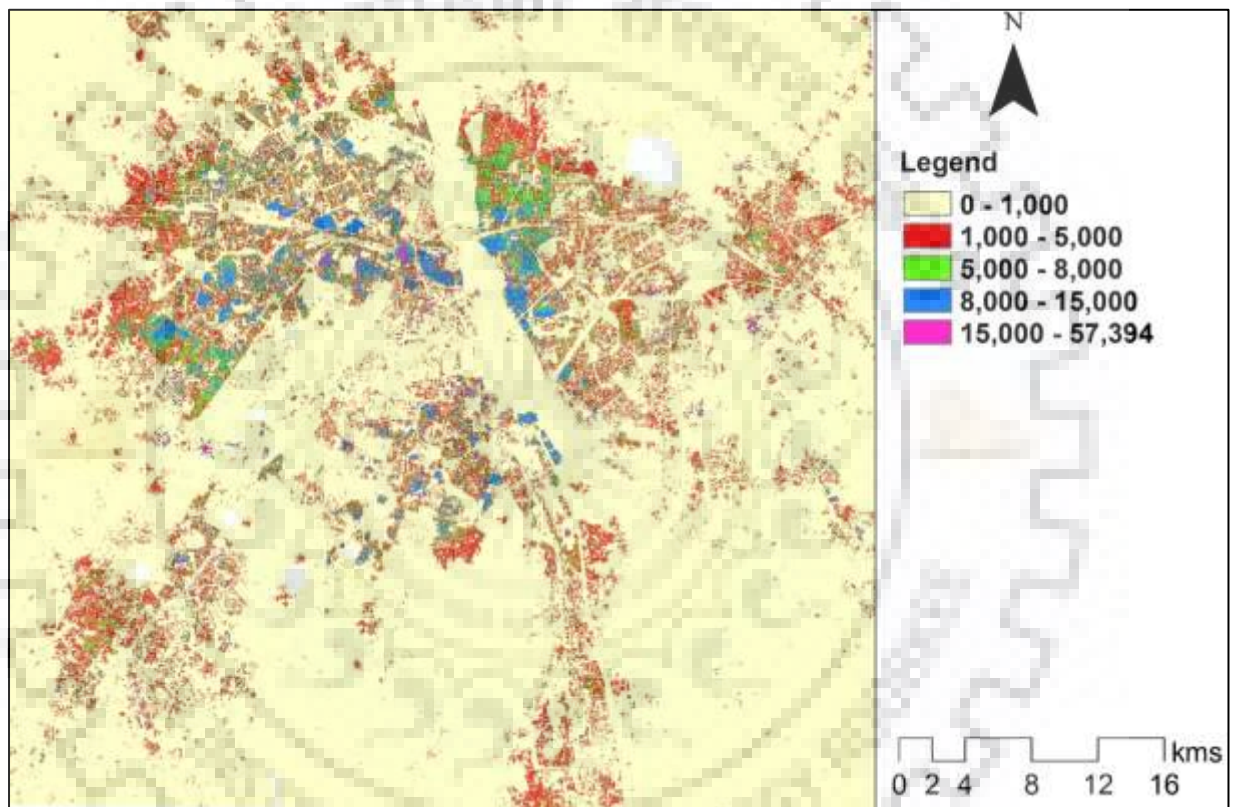


Figure 4-24: Building Volume

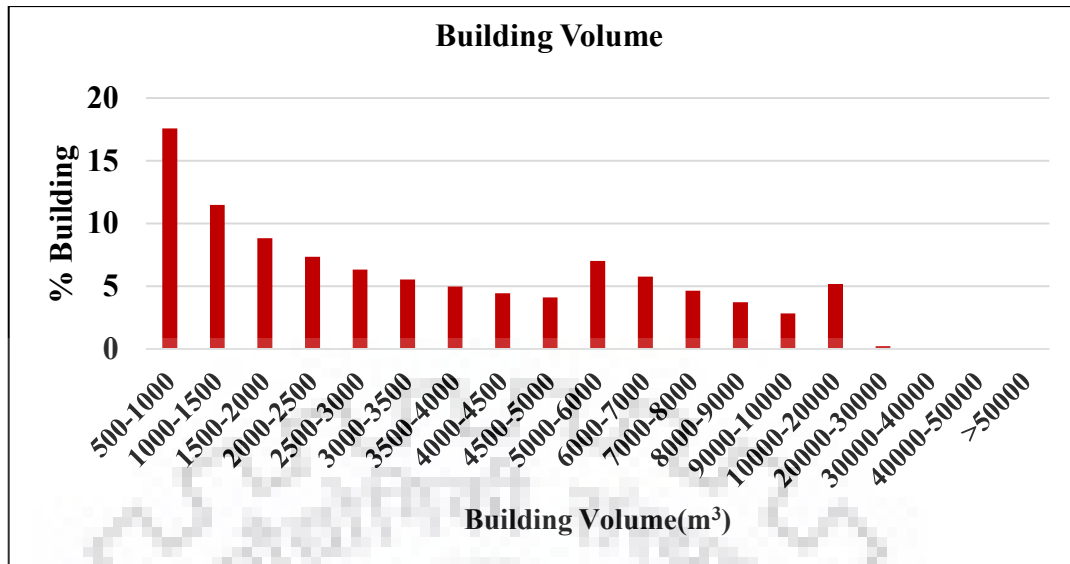


Figure 4-25: Distribution of Building Volume

4.4.10 Height-to-Width Ratio

Height-to-Width (H-W) ratio is a well-known urban canopy parameter which is measured either through ground measurements or by using computation on 3D GIS database. As described in section 4.3.9, a novel approach was applied to compute the wall area ratio which is the major input for the computation of H-W ratio. The computed wall area ratio is presented in Figure 4-26. The computation of H-W ratio have been carried in four parts due to extensive size of study area and computation requirements. The mosaicked H-W ratio is presented in Figure 4-28. It is to be noted that this computation was carried out only in building surface area as wall area information was available only for building area. Approximately 48 % of building area has H-W ratio between 1-2, rest of the 52% area has H-W ratio more than 2, which is quite a high value with respect to earlier studies where the H/W ratio was found to be maximum ~ 2 (Shishegar, 2013; Takkanon & Chantarangul, 2019). Few of the building areas are displaying very high values of H-W ratio due to BSF being quite high and denominator was reaching near to zero (Table 4-6 and Figure 4-27).

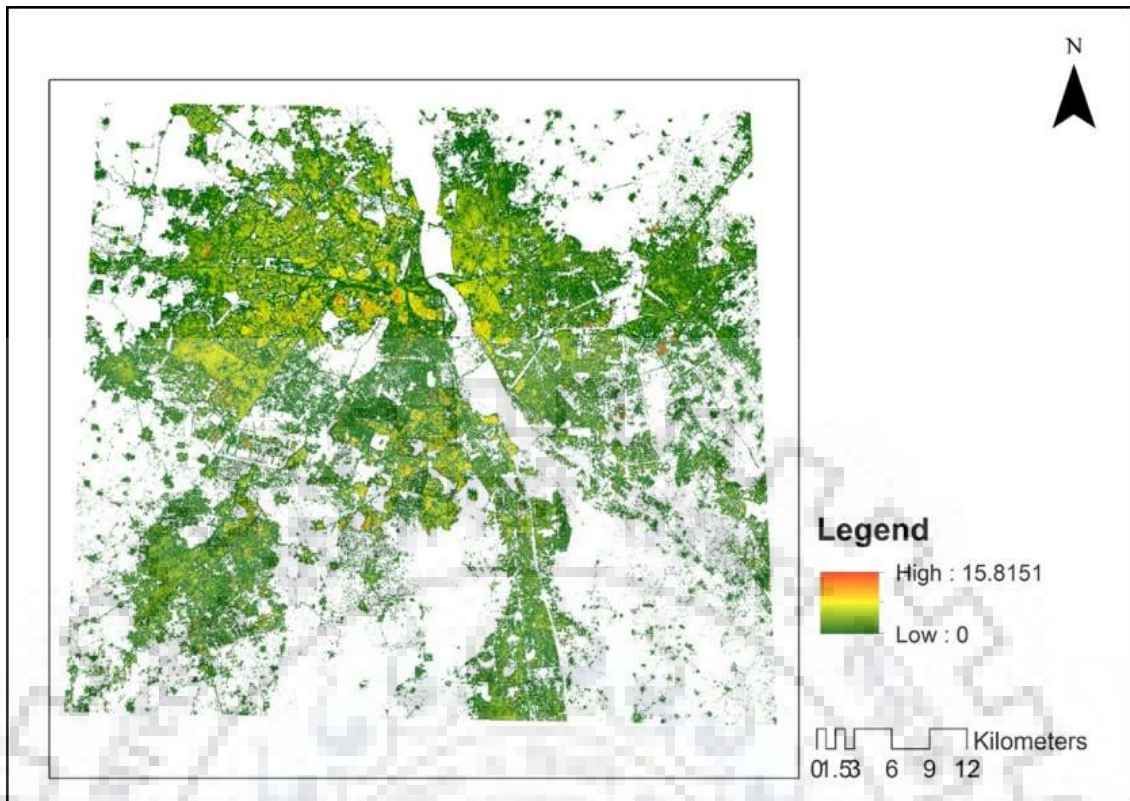


Figure 4-26: Wall Area Ratio (λ_w)

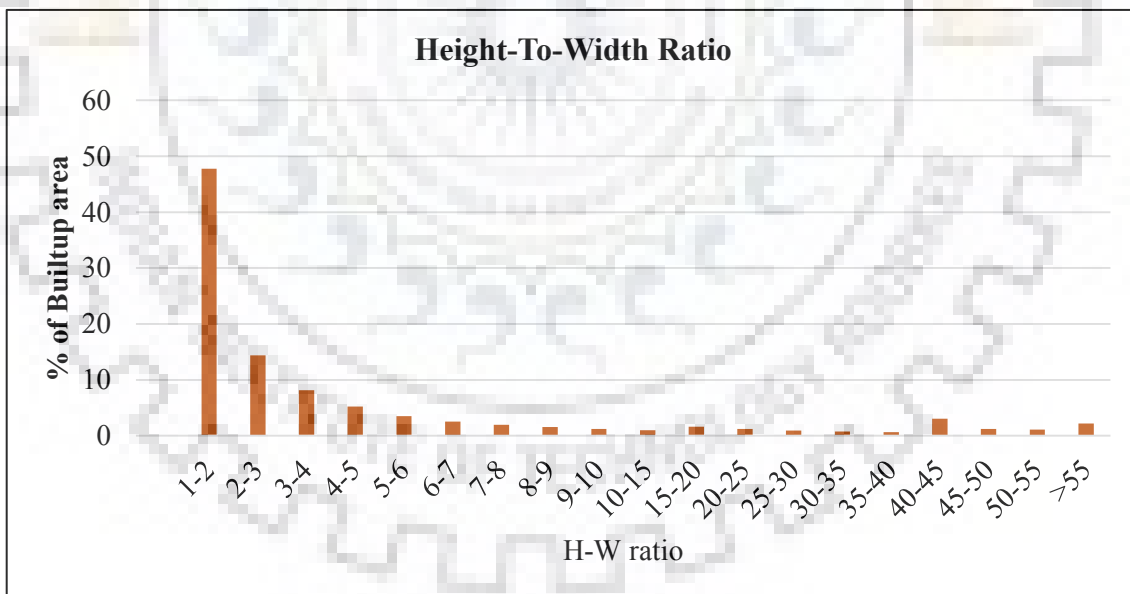


Figure 4-27: Distribution of Height-to-Width Ratio in Delhi UA

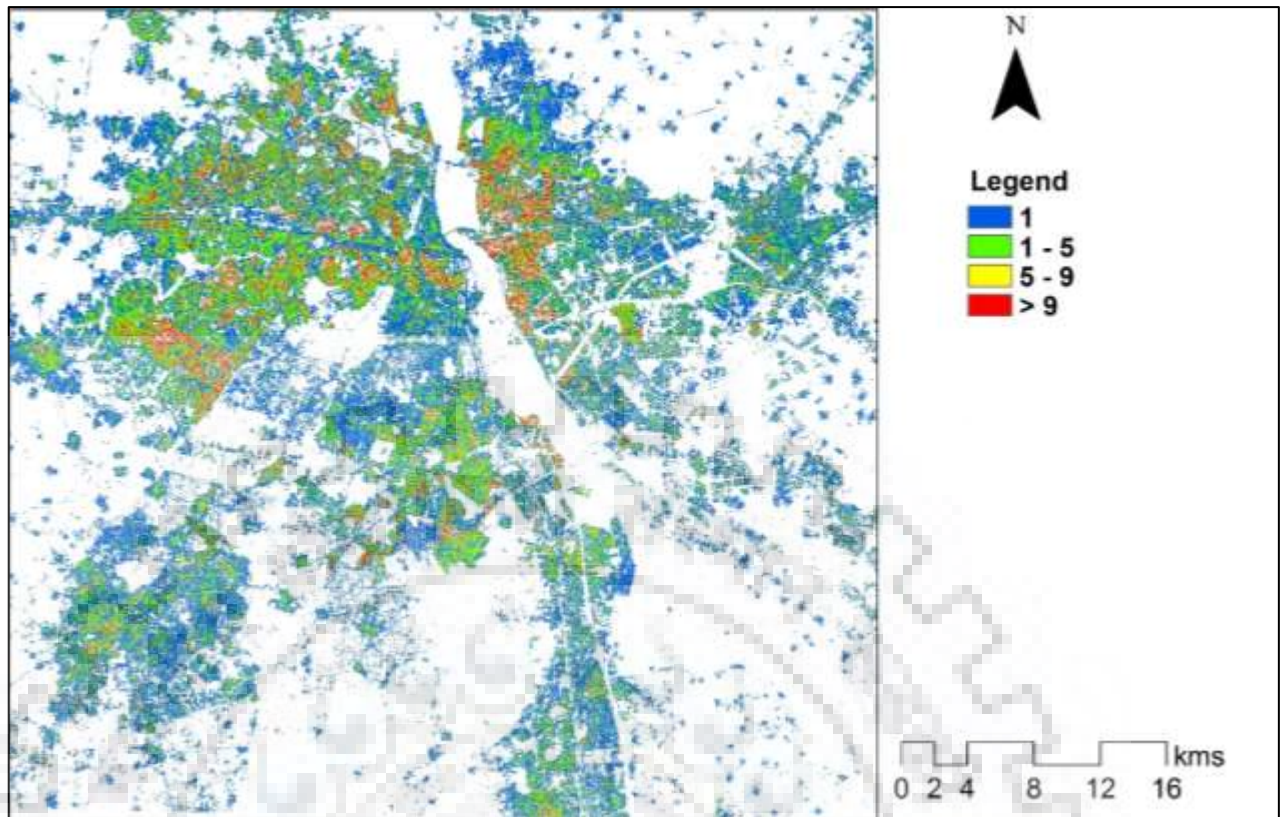


Figure 4-28: Height- to-Width Ratio Map

Table 4-6: Percentage distribution of Height-to-Width Ratio

H-W Ratio	% Built up area	H-W Ratio	% Built up area
1-2	47.75	5-6	3.51
2-3	14.37	6-7	2.54
3-4	8.16	7-8	1.95
4-5	5.20	8-9	1.55
		>9	14.95

4.4.11 Building Surface Area to Plan Area Ratio

The computation of Building Surface Area to Plan Area Ratio is carried out as per the equation 4-5 as presented in 4.3.11. Nearly 88% of the values lies in the range of 0-2.5 (Table 4-7 and Figure 4-29). The inner city area exhibits values in the range of 2-2.5 especially in the eastern part along river Yamuna and some of the peripheral settlements. On the periphery, values are low mostly in the range of 0-1.

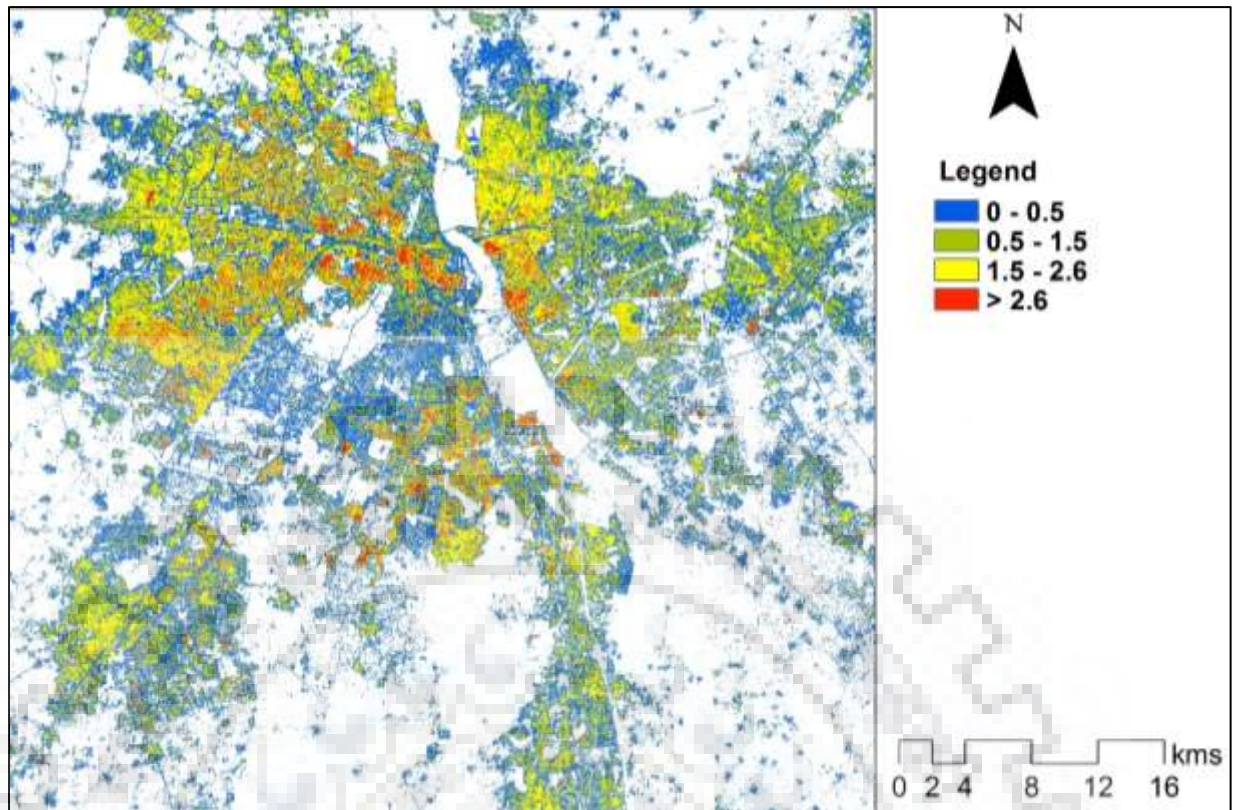


Figure 4-29: Building Surface area to Plan Area Ratio

Table 4-7: Percentage distribution of Building Surface area to Plan Area Ratio

BSA PAR	% of buildings
0-0.5	29.85
0.5-1	17.20
1-1.5	14.41
1.5-2	13.90
2-2.5	12.66
2.5-3	7.22
3-3.5	2.82
3.5-4	1.05
4-4.5	0.41

4.4.12 Complete Aspect Ratio

The Complete Aspect Ratio (CAR) is quite similar to BSAPAR, the only difference being the addition of exposed ground surface area in each cell (Figure 4-30). Hence, there are similarities in BSAPAR and CAR. However, in case of CAR nearly 58% values lies in the range of 1 -1.5 and more than 96 % values lies in the range of 0-3 (Table 4-8).

Table 4-8: Percentage distribution of Complete Aspect Ratio

CAR Class	% Built up Area
0.5-1	6.51
1-1.5	57.29
1.5-2	15.25
2-2.5	11.68
2.5-3	5.96
3-3.5	2.04
3.5-4	0.69
4-5	0.39
>5	0.18

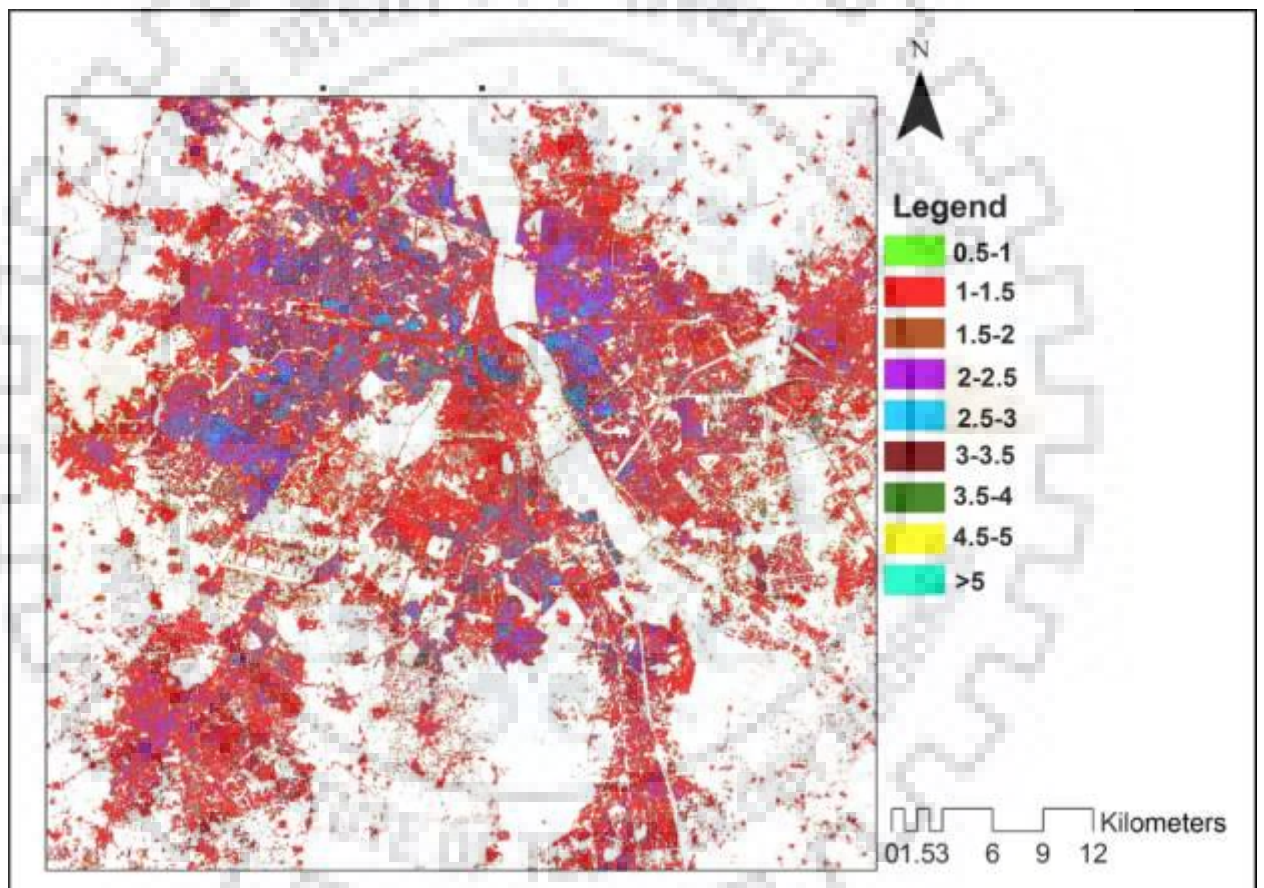


Figure 4-30: Complete Aspect Ratio

4.4.13 Sky View Factor Map

The Sky View Factor (SVF) is a function of sky hemisphere visible from ground level which varies with height and spacing of buildings and trees and affects surface radiational heat/cooling. The SVF image produced was also a continuous image stretching from 0 to 1. 0 value in SVF represents zero sky visibility associated with compact built-up area and 1 represents high sky visibility associated with open land. Ground data from 40 locations was collected with the help

of Fish eye lens and the resultant SVF value was calculated based on Steyn method. The obtained value was used for accuracy assessment of SVF map generated (Figure 4-31) using DSM as shown in Table 4-9. The mean error is 0.019, while RMSE was found to be 0.046 and CRE was approx. 8%. The high correlation value of 0.94 demonstrates good accuracy of the generated SVF map from Pleiades DSM.

The overall SVF including natural and manmade features is mostly within the range of 0.45 - 0.95(Figure 4-32), however, SVF in the built-up area ranges from 0.45-0.75(Figure 4-33). This accumulation of all values in the narrow range makes it extremely difficult to differentiate between various zones based on SVF.

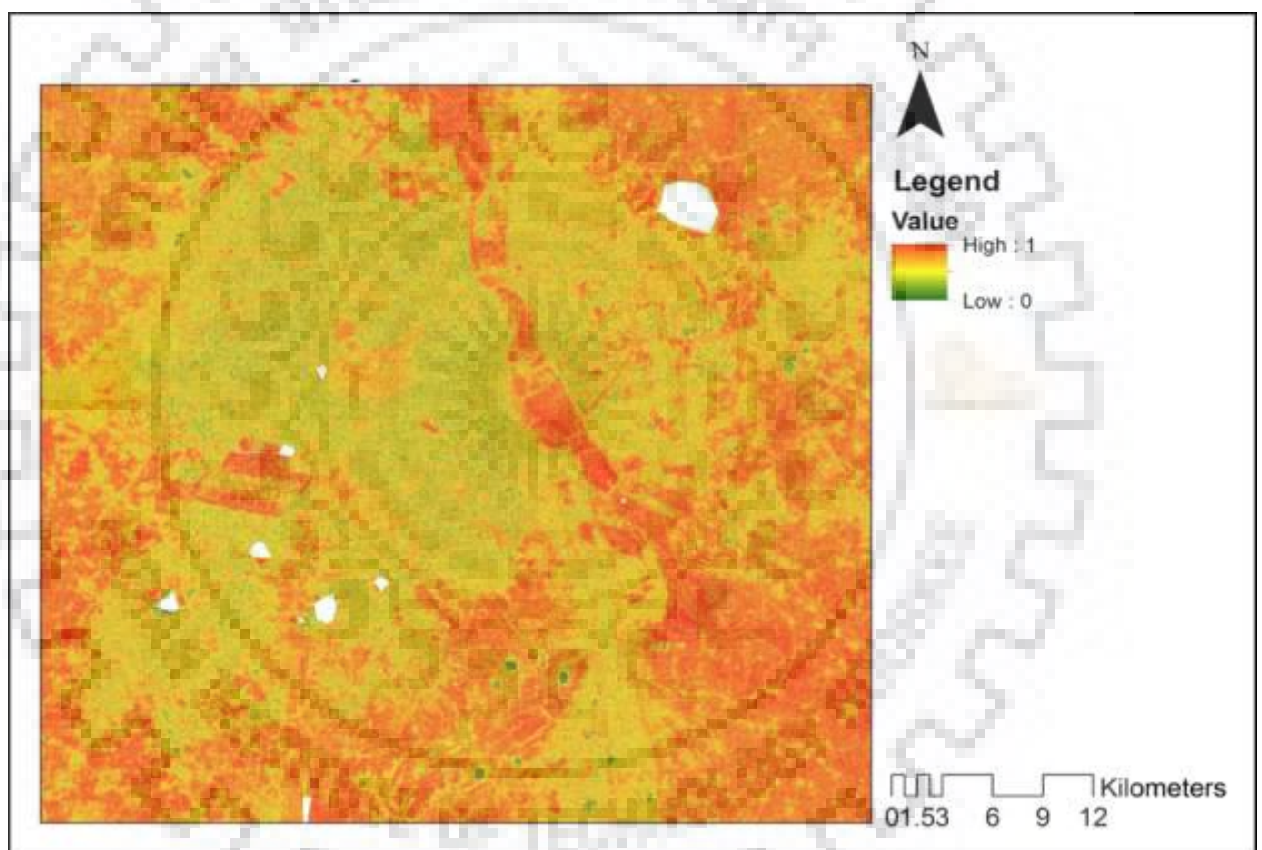


Figure 4-31: Continuous Sky View Factor Map

Table 4-9: SVF Accuracy Assessment statistics

Mean Error	0.019
RMSE	0.046
MAE	0.056
CRE	8.13%
Standard Deviation	0.042
Correlation	0.94

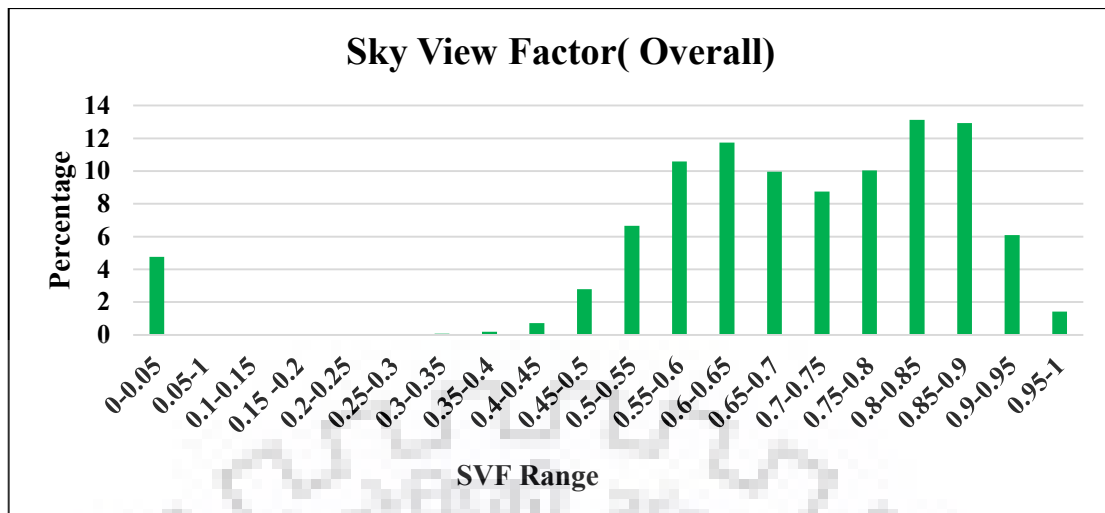


Figure 4-32: Distribution of Sky View Factor (Overall)

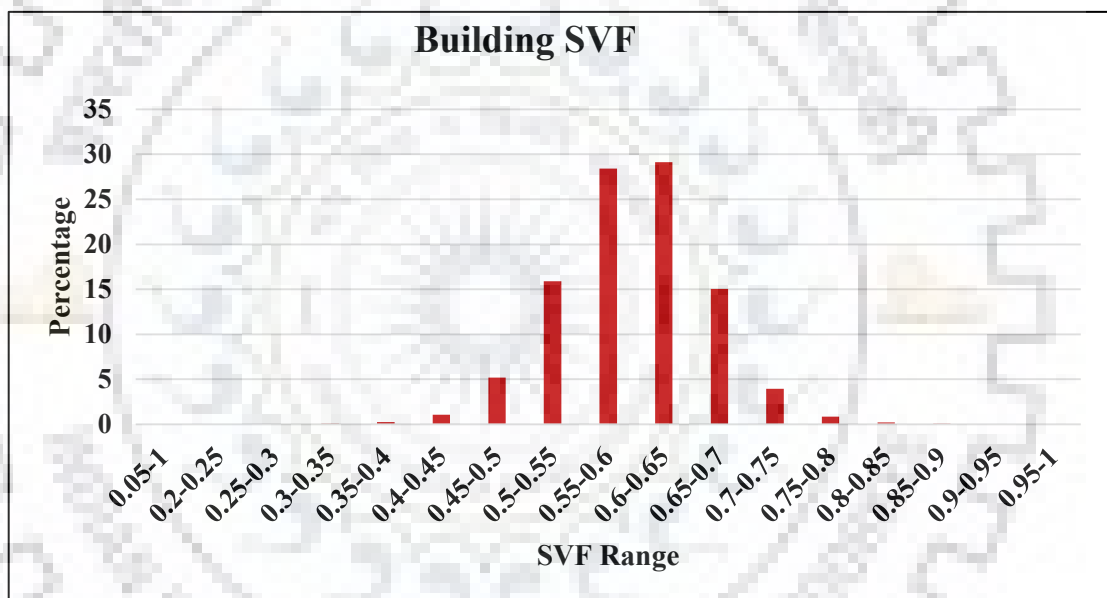


Figure 4-33: Percentage Distribution of Sky View Factor map (Built up area)

4.4.14 Zero Plane Displacement Height

The computation of zero-plane displacement height is carried out as described in section 4.3.13 and the obtained results are presented in Figure 4-34. The generated map is divided into two broad categories that is Less than 3 and more than 3, following the approach given by Matzarakis and Mayer, 1992. Nearly 60% of the building area falls into less than 3 range and 40% area falls into more than 3 range (Table 4-10). It is evident from Figure 4-34 that the inner area of built up has more than 3 value while outer area and New Delhi municipal area (NDMC) in the central part has values less than 3. It shows that outer areas are still under development and built-up density is comparatively less in these areas. NDMC area, the capital district houses all federal

government offices, embassies etc., has lower built-up density. It is designed with ample vegetation during British period and thus exhibits lower values of z_d .

Table 4-10: Distribution of Zero Plane Displacement Height

z_d	% Built up Area
<3	59.55
>3	40.45

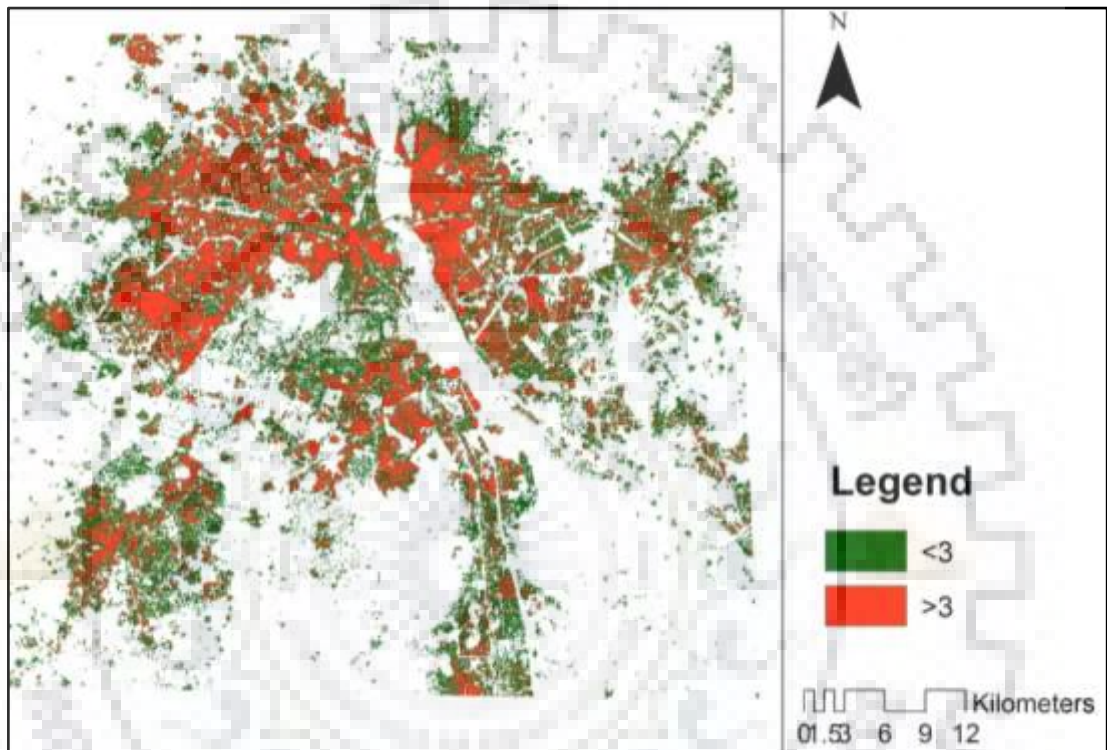


Figure 4-34: Zero Plane Displacement Height

4.4.15 Surface Roughness Length

Surface roughness Length (z_0) as computed by following the simple rule of thumb approach is presented in Figure 4-35. Further, it has been classified by following the classification given by Matzarakis and Mayer 1992 in three categories of <0.5 , $0.5-1$ and >1 . These categories are further utilized for development of ventilation path map for the study area. From statistics, it is noted that approximately 73.71% of the area has less than 0.5 value (Table 4-11). However, this area in mainly comprises non-built up area.

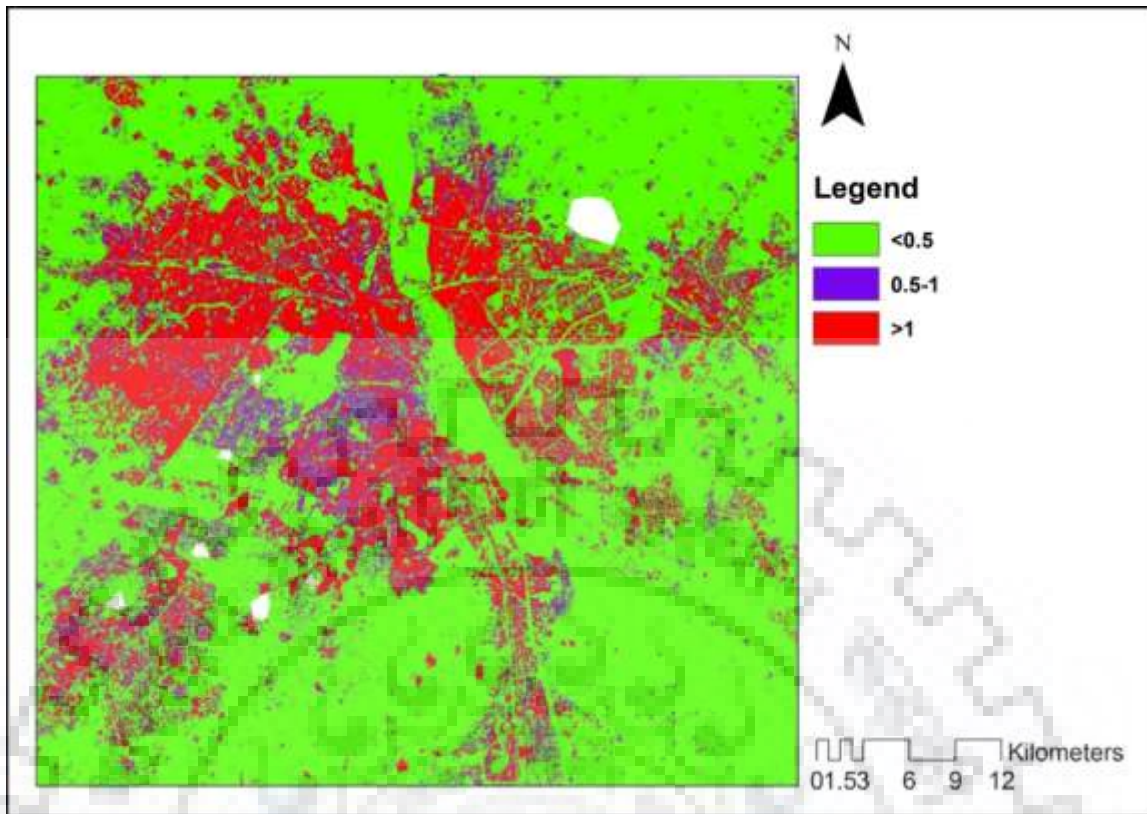


Figure 4-35: Surface Roughness Length

Table 4-11: Percentage Distribution of Surface Roughness Length

Surface Roughness(z_0)	% Area
<0.5	73.71
0.5-1	10.05
>1	16.23

4.5 DISCUSSION

4.5.1 Validation of Digital Terrain Model and Building Heights

Validation of DTM with field observations obtained through DGPS survey displayed low RMSE values of 0.2 m, 0.18 m and 1.33 m in X, Y and Z respectively (Table 4-12). Bias and standard deviation is also found to be very less especially in X and Y direction i.e. 0.04m and 0.31m and 0.12 and 0.08 respectively. In Z-direction, bias was found to be 1.78 m with standard deviation of 0.31. Nearly 1m RMSE in Z-direction shows good accuracy of obtained DTM and found to be reasonable enough for computation of nDSM and subsequent computation of building heights. Building height map obtained from nDSM with ground measurements of DGPS and building heights respectively revealed very high accuracies with sub-meter mean error in all height groups (Table 4-13) and maximum departure or bias is with ± 1 m (Figure 4-36). It is evident from the

validation results that sub-meter accuracies are obtained even in Root Mean Square Error (RMSE) and Mean Absolute Error (MAE) for all height groups. The similar results have been obtained in a study conducted by Poli et al (Poli et al., 2015) in Trento test field. The maximum RMSE was found in low rise buildings and minimum RMSE could be seen in high rise building area. Cumulative Random Error (CRE) was found to be ranging from 2.5% to maximum 10% which is reasonable error. The high value of RMSE, MAE and CRE in low rise (up to 10m) height group may be due to high value of BSF in compact low rise area which may have resulted in poor separation between urban canyon and buildings. It may also be due to shadow caused by buildings and vegetation and presence of trees in open low rise which may have resulted in attenuated signals and resulted in overestimation of building heights. The reasonable level of accuracies recommends the use of sub-meter data for extraction of building heights and further computation of UCPs.

Table 4-12: Validation of Digital Terrain Model with DGPS observations

	X-reference (m)	Y-reference (m)	Z-elevation (m)
Average	0.04	0.31	1.78
RMSE	0.20	0.18	1.33
Std. Dev.	0.12	0.08	0.31

Table 4-13: Validation of Building Heights obtained from nDSM against ground measurements

Height Group	Mean Error (m)	RMSE (m)	Standard Deviation	MAE (m)	CRE %
Low-rise(up to 10 m)	0.22	0.98	0.96	0.85	9.95
Mid-rise(10-25 m)	-0.46	0.83	0.69	0.65	6.27
High-rise(More than 25 m)	0.19	0.80	0.91	0.62	2.48

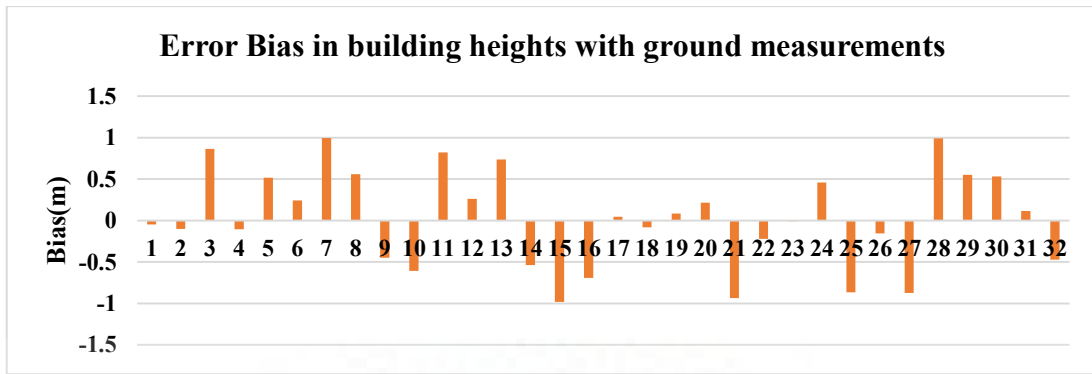


Figure 4-36: Error bias in building heights with ground measurements

4.5.2 Retrieval of Urban Canopy Parameters

The major challenge faced in processing of the UCPs is the huge volume of data (covering more than 2600 sq km), very high density of built-up and multiple scenes (14 Stereo pairs) of different dates. Since, the fresh acquisition of very high resolution data is quite expensive, hence, archived data were procured for this study which consisted of scenes that were varying in dates, season and year. This had posed number of challenges in different stages from DSM processing to LULC classification. All the scenes were processed separately and the post-processed data was then mosaicked to generate the final output. The huge volume of data (~0.5TB) required high end computing resources as even processing of one scene could not be completed on high end regular workstation. Hence, whole DSM and UCPs processing was carried out in High Performance Computing (HPC) system of 24 core processor and 128 GB RAM.

The very high density of built-up as evident from BSF map (~ 17% of built-up having building density of more than 80%) posed challenges in extraction of building footprints and height information in highly dense built-up area. Hence, a novel approach for step-by-step filtration of non-building pixels was developed to obtain the building height. Xu et al, 2017 has utilized fused image of SAR nDSM and optical stereo nDSM to generate the height map in Kowloon Peninsula, Hongkong (Xu et al., 2017) which has the characteristics of dense built up with high rise vertical growth. The study area has the characteristics of horizontal sprawl with limited vertical growth and optical satellite stereo images found to yield reasonable results in low rise and medium rise area (Gupta et al., 2017). The RMSE of less than 1m in all height groups (Table 4-3) corroborates with the existing literature. Hence, nDSM generated from optical stereo was considered optimal to generate the building height information and subsequent generation of UCPs. Besides, the high resolution Interferometric SAR is much more expensive than optical stereo and it would have been costly to procure interferometric SAR data to cover such a large extent of area. Moreover,

the high density of building area might have posed significant challenge as layover effects and volume scattering might have been too high and backscattered signal of individual building might not be obtainable (Jensen, 2007). However, a pilot study may be carried out in future for evaluating the potential of interferometric SAR or fusion of SAR and optical data for obtaining the building height information in such a highly dense and complex urban area with low to medium rise development. In this study, simple stereo images have been utilized to extract the building height as, tri-stereo Pleiades images were not available in archived data. However, availability of tri-stereo with suitable acquisition geometry (one nadir and two off nadir) may have improved the automatic generation of DSM and subsequently extraction of building heights (Poli et al., 2015).

The very high value of BSF (>0.85) may have been due to occlusions (very narrow street canyons) in the optical satellite data. The occlusion due to very narrow street canyons poses limitation in resolving the building from urban canyons. This results in very high density of building surface area. The use of very high resolution satellite data significantly reduces mixed pixels (reflectance of buildings, roads, lawns, trees and water lump together in one pixel). However, new problems such as shadows caused by buildings, trees and topography as well as high spectral variation in same land cover class arise (Dare, 2005; Weng, 2014). Shadows hide the information underneath, which results in loss of information in few pockets. Similarly, Trees overhanging over the building area leads to incomplete extraction of building information. The omission in built up area due to shadows (high rise building area) and complex roof structures (i.e. temple, monuments etc.) also poses limitations in extraction of accurate built up area. However, analysis with ground observations for the extraction of built up area revealed reasonable accuracy ($\sim 84.27\%$). In this study, a gridded approach was adopted for extraction of UCPs rather than the 3D GIS database approach as no cadastral data was available and segmentation of image data did not yield satisfactory results especially in very high density built up areas. In future, availability of improved resolution satellite optical stereo images ($>0.25\text{m}$) or upcoming technology of Unmanned Aerial Vehicles (UAVs) with super resolution (2-4 cm spatial resolution) may assist to overcome this limitation.

As discussed earlier, the rule of thumb coefficients proposed by Grimmond and Oke (Grimmond & Oke, 1999) were considered to compute the z_0 both for vegetation and buildings canopies. Other methods suggest use of plan area fraction (Kutzbach, 1961; Counihan, 1971; Rotach, 1994) or frontal area index (Raupach, 1992; Raupach, 1994; Gál & Unger, 2009; Wong, Nichol, Ng, Guilbert, & Hei, 2010b) for the computation of z_0 . The equation given by Kutzbach

(Kutzbach, 1961) applies only if λ_p is ≤ 0.29 . The study region of Delhi had very high densities of building surface area > 0.8 hence, the equation was not considered for the computation of z_o . Computation of frontal area index in such a highly dense and complex urban environment requires development of an automated tool to cater to such a large area. The existing tools such as UMEP (Lindberg et al., 2018) and UME (Jhaldiyal et al., 2018) were not found to be successful for calculation of λ_f in highly dense, complex large size urban areas such as the study region of Delhi. Further improvement in these tools for automated computation of λ_f may improve computation of z_o . Similarly, in this study, mean of building height was used for the computation of z_o , however, in future, use of maximum building height or frontal area index may be evaluated for improved results.

In this study, for computation of z_o , vegetation was also considered based on mean roughness height. But for computation of z_d was carried out only in building canopies. Most of the morphometric methods to compute the z_d and z_o generally used separate equations for vegetation canopies and buildings. Most of the vegetation in calculations is ignored to avoid complexity (Grimmond, Blackett, et al., 2010b; Grimmond et al., 2011). However a dense tree may exert a similar amount of drag as bluff bodies. Kent et al, 2017 demonstrated that in vegetation canopies leaf-on z_d is 1-4 m larger than leaf-off and leaf-on z_o is smaller than leaf-off (Kent, Grimmond, & Gatey, 2017). Consideration of vegetation canopies in future may result in more accurate results as compared to completely omitting the vegetation (Kent, Christoph w., Grimmond, CSB, Gatey, D., Barlow, J.F.,Kotthaus, S., Lindberg, F., Halios, C., Lee, K., Ward, H.C., Hong, J.W., Hong, J., 2018) especially in areas where large vegetation covers are present and considerably influence the urban micro climatic conditions.

Impact of terrain was considered negligible for the computation of z_o as the terrain of Delhi region is comparatively flat with minor undulations, hence, terrain has limited impact on air flow within the study area. However, in future, the effect of terrain in the computation of aerodynamic roughness parameters (z_o and z_d) may assist in application of developed methodologies for all terrains.

4.5.3 Characterization of Urban Canopy Parameters in study area

The generated building height map presents an interesting finding that in spite of having high growth pressure for urban development in Delhi and surrounding National Capital Region (NCR), most of the growth had spread horizontally. It may have been attributed to easy availability of land in surroundings, may be partly due to the restrictions on Floor Area

Ratio(FAR) in plotted development (Centre For Civil Society, n.d.) and socio-economic preferences. However, recently, a shift can be observed in the peripheral areas of Delhi, Gurgaon, NOIDA and Greater NOIDA area, where increase in FAR and further, demand in land is resulting in new development of high rise nature with 20 storey buildings(~ 60m height)(Wendall Cox, 2011).

The high values of standard deviation (> 75% of grid cells has standard deviation of more than 1) and high fraction of BSF(~ 35% area has more than 60% building surface area) indicates high heterogeneity of heights and built-up density in each 30 m grid cell. It is mainly due to nature of development in Delhi region which is of plotted and heterogeneous nature. On one side there is a properly planned colony and adjacent to it an unplanned colony or urban village exists. Urban villages are habitat areas of earlier rural settlements which have become part of urban development after the acquisition of agriculture land for urban development. Even though they absorb a large amount of development pressure, the zoning rules and regulations which is applicable to planned and approved housing colonies do not apply on urban villages. This system leads to unplanned, unorganized and heterogeneous growth in urban villages. Similarly, large influx of migrant population in Delhi just after the partition of India in 1947 has resulted in a development of many unauthorized colonies where migrants settled without much consideration of planning rules and regulations, which resulted in development of highly dense and heterogeneous urban settlement especially along River Yamuna in eastern and western parts of Delhi. The impact of all these developments has resulted in highly dense, heterogeneous and complex development of Delhi and its surrounding areas.

Nearly 70% of the study region consist of vegetation and bare soil area almost in equal proportions. This proportion is highly varied across seasons and different years depending on the cropping pattern of the season or rainfall in a particular year. Large part of the agriculture area is still rain fed. However, from climate point of view, this proportion has huge significance with respect to evaporative cooling, temperature patterns and energy exchange processes in the surroundings of urban area. As discussed earlier, that due to limitation of fund availability, multiples scenes of varying dates and year were procured. It had posed a significant challenge to classification of LULC especially in vegetation and bare soil class. However, each scene was processed separately and later on with the help of ground truth and Google Earth images, contextual refinements were carried out to obtain reasonable results. However, in future, acquisition of single season data may help to overcome this challenge.

Building volume is found high in either urban villages, western Delhi or settlement stretched along river Yamuna in eastern Delhi as discussed in previous section. Since, there is no ground data or standard that is available, BV could not be validated or discussed. The value of H/W ratio of more than 9 are found to be in 14.95% area. This much high value of H/W ratio is attributed to very high building density almost near to 100% which led to nearly 1 value of BSF in each grid cell and resulted in nearly 0 value of denominator. Approx. 10% area has H/W ratio between 5-9 values which is quite high values of H/W ratio. Again these area have been found to be highly dense building areas where height of the building is in low to mid-rise range of 12-15 m but due to high building density the values of H/W have been found to be high. H/W ratio could only be computed for the built up area. Since, vegetation is an intrinsic part of urban area, in future, development of methodologies for vegetation pockets may help in computation of H/W ratio in vegetation area as well.

The values of BSAPAR and CAR presents a remarkable departure from earlier studies where maximum values of CAR and BSAPAR have been found to be 2.6 and 0.98 for downtown area(SJ Burian et al., 2003). However, in the study area, the value of BSAPAR in the dense built up area have been found to be in the range of 2-2.5 whereas the 96% of CAR values falls within the range of 0-3. The high values of BSF, building volume, BSAPAR and CAR coincides with the higher values of zero plane displacement height and surface roughness length. It clearly indicates that the BSF and building height plays a major role in the distribution of these values. BSAPAR and CAR is quite near to each other as CAR includes the area of roof, ground and wall surfaces whereas BSAPAR includes only the roof and wall surfaces. The distribution of both layers does not vary much except that most of the BSAPAR distribution is in the range of 0-2.5, whereas for CAR, the maximum percentage falls between 1-1.5 values. It is because of very least fraction of ground is visible in many of the compact built-up areas.

The DSM based computation of SVF has the advantage of spatially distributed SVF map which is not obtainable with the 3D Vectors GIS database based approach (Gál & Unger, 2009). The DSM based computation of SVF (Gál et al., 2009) is highly accurate which is evident from the 0.046 value of RMSE, 8% CRE error and 0.94 correlation. However, it should be noted from distribution of SVF for built-up area that most of the SVF value lies within a narrow range of 0.4 to 0.7 in the study area. Further, upscaling of values to 30 m grid cell had the effect of averaging of values. It has resulted in poor distinction between different built-up zones based on SVF.

4.5.4 Effect of grid size

The WUDAPT recommends use of 100 m grid size in order to capture neighborhood characteristics at local scale (Bechtel et al., 2015), however, due to highly heterogeneous development of Delhi, it was found that coarser grid size has strong averaging effect on building heights and most of the high rise building area was converted into mid-rise buildings area. On the other hand, small grid sizes depicts larger objects in more number of pixels. For example, a large size industrial building or shopping mall is covered in more than one pixel. It leads to BSF values of 1 in few of the grids. Although it constitutes a very small fraction of total built up area. The study on the scale effect in Hong Kong revealed that accuracy of urban morphological characteristics increases with the coarser spatial scale (Xu et al., 2017). The study achieved better fitting accuracy with 500m grid size. However, further investigation is needed in the study area for better understanding of the effect of scale/grid size for the retrieval of UCPs.

4.6 SUMMARY

Novel methods have been developed and presented in this chapter for the extraction of building height, building surface fraction and computation of wall area by utilizing sub-meter resolution optical stereo satellite data in a very dense and complex urban environment of Delhi. The widely used data sources for the computation of UCPs in urban environment includes 3D GIS database computed either through field surveys or through remotely sensed data sources such as air borne LiDAR, aerial photography and high resolution InSAR data. However, neither 3D GIS database is available for the study region nor the remote sensing datasets of air borne LiDAR, aerial photography and high resolution InSAR data. Since, optical stereo data has wider and easier availability as compared to other data sources, the study demonstrates its utilization for retrieval of UCPs in complex urban environment of developing regions. Validation of basic input layers (building heights, LULC and Sky view factor) against field measurements revealed high accuracy, hence, it is recommended to use very high resolution optical stereo images for the computation of UCPs in developing region with complex urban development.

The characterization of UCPs revealed highly dense, complex and sprawled character of Delhi UA. It has posed number of challenges for the retrieval of UCPs. The retrieved UCPs therefore needs to be widely utilized for urban climate research so as to assist planners and policy makers for formulating appropriate strategies to mitigate the challenges of climate change faced by the study region. The relationship of UCPs with spatially variable climate indicators has been discussed in the Chapter 5.



CHAPTER 5

URBAN CANOPY PARAMETERS AND THEIR RELATIONSHIP WITH URBAN CLIMATE INDICATORS

5.1 INTRODUCTION

Urban climate is the study of atmospheric and meteorological processes in an urban settlement which undergoes a distinct modification due to development of built-up in that region (Oke, 1987; Oke et al., 2017). The urban climate differs from rural areas in terms of energy exchange processes, alteration in temperature, humidity, wind flow and precipitation patterns. Urban Heat Island (UHI) is one of the phenomenon which have been widely researched and discussed globally. It is identified in the form of increased surface and air temperatures of urban areas as compared to rural surroundings. Surface Temperature, air temperature, humidity, wind speed, pressure and precipitation are few of the climate indicators which have been used widely to define climate characteristics and differences of a specific geographic region. Information on urban climate indicators are generally obtained through field observations, physical modelling and numerical modelling. The field observations can be classified into in-situ measurements using ground based (fixed or mobile) stations, free flow techniques using balloon etc., and remote sensing techniques.

Numerous studies have employed in-situ measurements to obtain the information on climate indicators as well as to understand the relationship between climate indicators and UCPs (Kotharkar & Surawar, 2016; Oke et al., 2017). Spatial distribution of ground observation stations in urban areas is largely constrained due to siting requirements for meteorological observations and thus has limited availability. Besides, it requires vast network of observation stations to address the high heterogeneity of urban environment. The data of few of the stations are not valid due to insufficient metadata information or poor quality of data which restricts their use for a detailed and comprehensive analysis and research on urban climate. Hence, satellite remote sensing data have been widely used for obtaining information on spatially variable climate indicators. It have been also extensively employed to investigate the linkages between urban characteristics and spatially variable Land Surface Temperature (LST). Most frequently used UCP is the vegetation surface fraction (Hong-Mei et al., 2006; Liwen Huang et al., 2015; Naeem et al., 2018; Perera & Langappuli, 2013), surface albedo (Bonafoni et al., 2017; Salleh et al., 2014) and impervious surface area (Kaspersen et al., 2015; Perera & Langappuli, 2013; Weng et al., 2006). Although, the impact of 3D UCPs on urban climate is significant and it is considered

as one of the main contributor to UHI phenomenon. However, a very few studies have analyzed relationship of 3D UCPs such as building height, frontal area index, floor area ratio and sky view factor with LST. It has remained largely an unexplored area even for the regions that have highly planned urban infrastructure let alone the developing region (Berger et al., 2017; Chun & Guldmann, 2014; Guo et al., 2016; Scarano & Sobrino, 2015; Yin et al., 2018). Hence, there is a need to explore the relationship of 2D/3D UCPs with spatially variable climate indicators.

LST obtained from thermal remote sensing provide surface temperature at varying resolutions from 1 km to 30 m (highest resolution available). Thermal remote sensing data of Landsat and ASTER satellites (30 m spatial resolution) have been widely used in urban climate research (Li et al., 2013; Rasul et al., 2017; D. Zhou et al., 2019). However, information on other climate indicators such as temperature at 2m, wind speed, humidity, pressure etc. is either not available through remote sensing or available at very coarse resolutions (~4 km or 12.5 km). That limits the use of these datasets for understanding micro climate characteristics in urban areas. Physical modelling and numerical modelling are the methods which could be employed to obtain spatially variable, high resolution information on urban climate indicators. However, application of physical models becomes limited as it require special facilities, which are expensive and needs careful design (Oke et al., 2017). In recent past, numerical modelling has gained momentum and development of exhaustive Urban Canopy Models (UCMs) facilitates modelling of radiation, heat and energy exchange processes in urban areas. Weather Research and Forecasting (WRF) Model is one of the numerical weather prediction model which have been widely used as mesoscale climate model as well as to downscale urban climate indicators to urban scales (~0.2-0.5 km grid resolutions) (Chen et al., 2011; Hammerberg et al., 2018; Salamanca et al., 2011). It provides spatially variable information on widely used urban climate indicators at comparatively higher resolutions which can be employed to understand the relationship between urban characteristics and urban climate indicators.

The detailed methodology for the retrieval of Land Surface Temperature and WRF model simulations, data used and their characteristics, obtained LST maps for different seasons, WRF outputs and their validation with in-situ point observation and MODIS LST, relationship of UCPs with LST, spatial and diurnal variability of Surface Urban Heat Island Intensities (SUHII) and Urban Canopy Layer Heat Island Intensities (UCLHII), methodological and operational concerns pertaining to retrieval of LST, grid size of WRF simulations have been discussed in this chapter.

5.2 MATERIALS AND METHODS

This section describes in detail the methodology adopted for derivation of Land Surface Temperature (LST) and WRF model simulations, simulation period and WRF model setups for deriving the information on climate indicators. Derivation of LST involves preprocessing of satellite data, computation of TOA radiance, Land surface emissivity and inversion of Plank's equation to obtain the LST. Methodology for WRF simulation includes preparation of multi-class Urban LULC, WRF model setup, domain configuration, simulation periods and WRF model work flow. The generated LST and WRF outputs were further utilized to assess the relationship with urban canopy parameters. The overall methodology is presented in Figure 5-1.

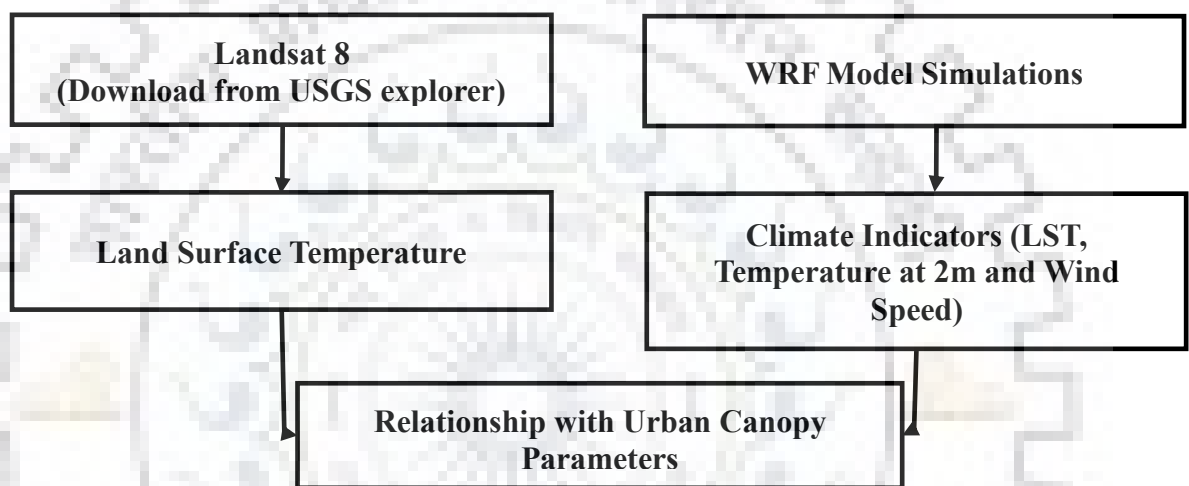


Figure 5-1: Broad Methodology for derivation of urban climate indicators

5.2.1 Land Surface temperature

Estimation of LST have been performed on Landsat 8 data set of 30 m spatial resolution. Landsat is the longest series Earth Observation Satellite (EOS) in use today. The overall process for calculation of LST have been performed in QGIS, which is an open source software. The procedure for calculation of LST using Radiative Transfer Equation (RTE) is presented in Figure 5-2 and described in following sections.

5.2.1.1 Procurement of Landsat data

Landsat is a longest series of Earth observation satellites available from 1972 onwards. In 1972, Landsat 1 was launched and afterwards total Landsat satellites were launched to maintain the data continuity. The series has provide large volume of temporal data which have been used in many studies. It provides highest spatial resolution thermal infrared data since 1984 after the launch of Landsat 4 Thematic Mapper. The thermal band data provided by Landsat mission had

been extensively used for urban climate studies since launch (Li et al., 2018; Li et al., 2013; Rasul et al., 2017). The latest in the series is Landsat 8 which has been launched in 2013 and consist of 11 bands (Table 5-1) consisting two sensors Operational Land Imager (OLI) in optical region and Thermal Infrared Sensor (TIRS) in Thermal region. The orbit of Landsat 8 is such that it covers the same area on the earth every 16 days.

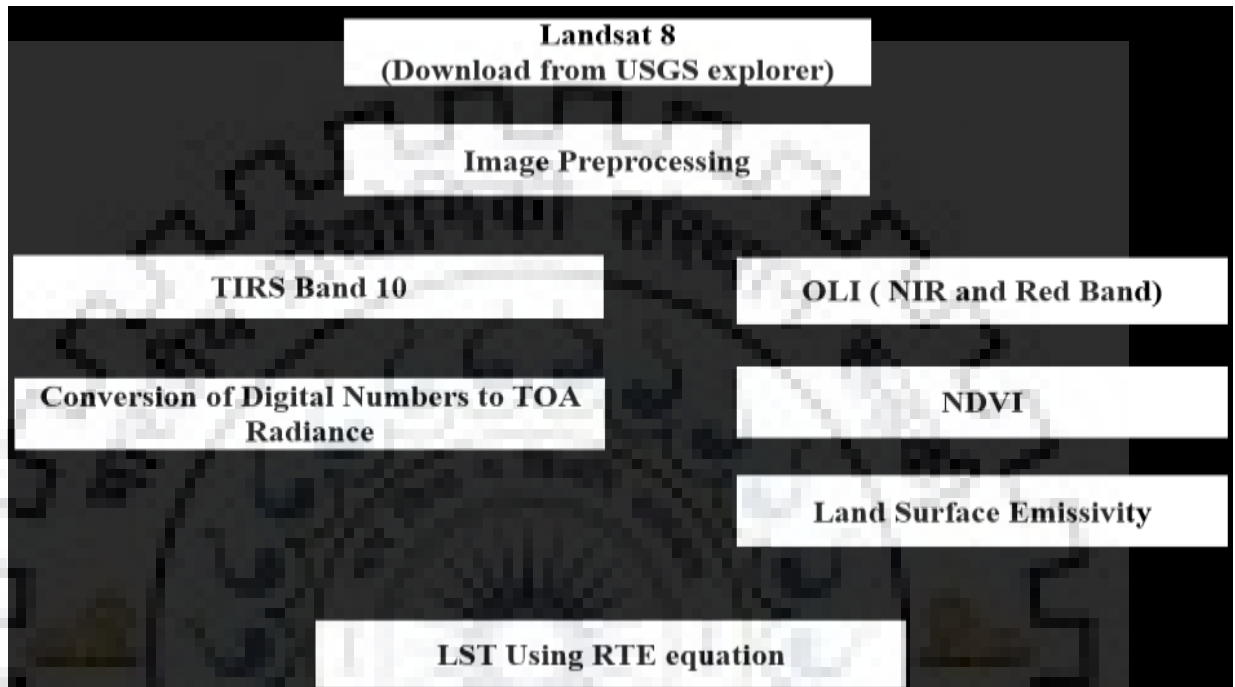


Figure 5-2: Methodology for Estimation of Land Surface Temperature

Table 5-1: Specification of Landsat 8 Operational Land Imager (OLI) and Thermal Infrared Sensor (TIRS) (Source: Barsi, Lee, Kvaran, Markham, & Pedelty, 2014)

Bands	Wavelength (micrometers)	Resolution (meters)
Band 1 - Ultra Blue (coastal/aerosol)	0.435 - 0.451	30
Band 2 - Blue	0.452 - 0.512	30
Band 3 - Green	0.533 - 0.590	30
Band 4 - Red	0.636 - 0.673	30
Band 5 - NIR	0.851 - 0.879	30
Band 6 - SWIR 1	1.566 - 1.651	30
Band 7 - SWIR 2	2.107 - 2.294	30
Band 8 - Panchromatic	0.503 - 0.676	15
Band 9 - Cirrus	1.363 - 1.384	30
Band 10 - Thermal 1	10.60 - 11.19	100* (30)
Band 11 - Thermal 2	11.50 - 12.51	100* (30)

Out of these two bands band 10 and band 11 records emitted radiation by earth surface features in thermal region at 100m spatial resolution but after resampling is provided to users at 30 m spatial resolution. Due to some issues with band 11 data, mostly band 10 data is utilized for the LST calculation. The Landsat 8 images were downloaded freely from United States Geological Survey (USGS) explorer web site for the year 2016 corresponding to the four predominant seasons prevailing in the study region (winter, summer, monsoon and post-monsoon). The details of downloaded Landsat data are given in Table 5-2. It is to be noted that availability of cloud and haze free scenes in monsoon and winter season was limited due to prevalent cloud conditions in monsoon and fog conditions in winter season.

5.2.1.2 Image preprocessing

For temporal or seasonal study, multi-temporal images must be co-registered in the same coordinate system (e.g., UTM/WGS84). Since, Landsat images are already georeferenced in UTM/WGS 84, their co-registration with Pleiades ortho images were checked. 1-2 pixel deviation was found which was corrected with a RMSE of 0.5 pixel. Further, the atmospheric correction was carried out using the FLASH algorithm in ENVI software to reduce the effect of atmosphere on derived surface temperature.

Table 5-2: Details of downloaded Landsat data

Satellite	Date of Acquisition	Season	Time (IST)	Path/Row
Landsat 8(OLI and TIRS)	2016/05/21	Summer	10:48	146/40
	2016/08/16	Monsoon	10:55	147/40
	2016/10/12	Post-monsoon	10:49	146/40
	2016/02/13	Winter	10:48	146/40

5.2.1.3 Conversion of Digital Numbers to Top of Atmospheric (TOA) Radiance

The satellite image data is stored in a form of Digital Number (DN), so after the downloading of Landsat 8 images, the first step is to convert the image DN values to spectral radiance. The values of constants (M_L , A_L and O_i) for the computation of TOA (Equation 5-1) were extracted from the metadata file available with each downloaded image (USGS, 2018).

$$L_\lambda = M_L Q_{cal} + A_L - O_i \quad \text{Equation 5-1}$$

Where,

L_λ : Top-of-Atmosphere (TOA) spectral radiance ($W / (M^2 * sr * \mu m)$)

M_L : band specific multiplicative rescaling factor.

A_L : band-specific additive rescaling factor

Q_{cal} : quantized and calibrated standard product pixel values (DN).

O_i : offset calibration

5.2.1.4 Determination of Normalized Difference Vegetation Index

Normalized Difference Vegetation Index (NDVI) based emissivity method is applied in this study for calculation of surface emissivity. NDVI is the ratio of Near Infrared (NIR) and Red band and it is been widely applied for vegetation studies. Computation of NDVI is carried out by utilizing the Equation 5-2 (Griend, Owe, Chang, & Vugts, 1992; Srivastava et al., 2010).

$$NDVI_i = \frac{(NIR_i - RED_i)}{(NIR_i + RED_i)} \quad \text{Equation 5-2}$$

Where,

$NDVI_i$ = Normalized Difference Vegetation Index of i^{th} pixel

NIR_i = DN value of NIR band at i^{th} pixel

RED_i = DN value of Red band at i^{th} pixel

For, Landsat 8 NIR = Band 5 & RED = Band 4

5.2.1.5 Determination of Proportional Vegetation Cover

Proportional vegetation cover (PVC) depicts the amount and nature of vegetation cover, and modulates the proportions of vegetation and non-vegetated ground (e.g., bare soil) visible to a sensor (Yu, Guo, & Wu, 2014). It normalizes the NDVI value. PVC is a variable on which Land Surface Emissivity (LSE) is dependent. It is calculated as per the equation 5-3.

$$P_{vi} = \left\{ \frac{(NDVI_i - NDVI_{min})}{(NDVI_{max} - NDVI_{min})} \right\}^2 \quad \text{Equation 5-3}$$

Where,

P_{vi} = Proportional Vegetation Cover at i^{th} pixel

$NDVI_i$ = Normalized Difference Vegetation Index of i^{th} pixel

$NDVI_{min}$ = Minimum value of Normalized Difference Vegetation Index

$NDVI_{max}$ = Maximum value of Normalized Difference Vegetation Index

Where, $NDVI_{max}$ and $NDVI_{min}$ are the maximum and minimum value of NDVI image. P_v varies from 0 to 1 where 0 represents areas with lowest vegetation and 1 represents areas with maximum vegetation.

5.2.1.6 Determination of Land surface emissivity

It's a threshold method in which the emissivity estimation is done by distinguishing the pixels between the soil pixels ($NDVI < NDVI_S$) and vegetation pixel ($NDVI > NDVI_S$), globally the NDVI values for soil and vegetation has been described as 0.2 and 0.5 (Ndossi & Avdan, 2016; Sobrino et al., 2004), the classes were defined on the basis of,

1. ($NDVI < NDVI_S$) in this all the pixel are considered under bare soil or rock.
2. ($NDVI > NDVI_S$) in this all the pixel are of vegetation cover and none of them consist of bare soil or rock.
3. ($NDVI_S < NDVI < NDVI_V$) it consist of mixture of pixel of the vegetation and soil. On the basis of it the equation has been defined through which the emissivity is calculated by using the above derived proportional vegetation cover and the surface geometry is also put under consideration.

The equation for emissivity is,

$$\epsilon_{\lambda} = \epsilon_{v\lambda} P_v + \epsilon_{s\lambda} (1 - P_v) + C_{\lambda} \quad \text{Equation 5-4}$$

Where,

ϵ_{λ} : Land surface emissivity,

$\epsilon_{s\lambda}$: emissivity of soil,

$\epsilon_{v\lambda}$: emissivity of vegetation,

P_v : Proportion vegetation cover

C_{λ} : Geometry of surface, ($C=0$ when surface is flat), it takes into consideration is the cavity effect due to surface roughness.

The geometry of surface is calculated through,

$$C_{\lambda} = (1 - \epsilon_{s\lambda}) \epsilon_{v\lambda} F'(1 - P_v) \quad \text{Equation 5-5}$$

Where,

$\epsilon_{s\lambda}$: emissivity of soil,

$\epsilon_{v\lambda}$: emissivity of vegetation,

P_v : Proportion vegetation cover

Here F' is the geometrical factor whose range is 0 to 1. Its mean value (0.55) is considered when it's applied to urban area. The emissivity values for soil, built-up, vegetation and water were used as 0.966, 0.962, 0.973 and 0.991 respectively (Srivastava et al., 2010; Yu et al., 2014).

5.2.1.7 Estimation of the atmospheric parameters

The estimation of atmospheric transmittance, upwelling and down-welling radiance for the sensor Landsat 8 have been calculated from the NASA atmospheric parameter calculator (Table 5-3). It uses National Centre for Environmental Prediction (NCEP) modeled atmospheric global profiles for estimation with respect to latitude and longitude of particular place in accordance to the satellite data acquisition time. The tool provides atmospheric profile from January, 2000 to till date.

Table 5-3: Details of atmospheric parameters

Date	Time	Atmospheric Transmittance	Up-welling Radiance (W/m ² /sr/um)	Down-welling Radiance (W/m ² /sr/um)
2016/05/21	10:48	0.63	3.53	5.62
2016/08/16	10:55	0.50	4.50	6.73
2016/10/12	10:49	0.90	0.88	1.51
2016/02/13	10:48	0.93	0.50	0.86

5.2.1.8 Land Surface Temperature using Radiative Transfer Equation

For determination of LST, Radiative Transfer Equation (RTE) method have been utilized. It uses the single band or single channel of thermal sensor for land surface temperature calculation. For computation of RTE, the equation 5-6 have been utilized (Yu et al., 2014).

$$L_{\lambda RTE} = [\epsilon_{\lambda} L_{\lambda} (T_s) + (1 - \epsilon_{\lambda}) L_{\lambda down}] \tau + L_{\lambda up} \quad \text{Equation 5-6}$$

$L_{\lambda RTE}$: Thermal Infrared Radiance by RTE,

ϵ_λ : Surface emissivity for the Thermal Band 10,

$L_\lambda(T_s)$: Blackbody radiance target of kinetic temperature(T_s),

$L_{\lambda up}$: up-welling Radiance or atmospheric path radiance,

$L_{\lambda down}$: Down-welling Radiance or sky-radiance

τ = Atmospheric Transmittance For a particular day and location

The blackbody radiance for Land surface $L_\lambda(T_s)$ is calculated using Equation 5-7,

$$L_\lambda (T_s) = \frac{L_\lambda - L_{\lambda up}}{\tau \epsilon_\lambda} - \frac{1 - \epsilon_\lambda}{\epsilon_\lambda} L_{\lambda down} \quad \text{Equation 5-7}$$

Here,

L_λ = Top-of-Atmosphere (TOA) spectral radiance

5.2.1.9 Derivation of Land Surface Temperature

After the computation of radiance equation 5-8 has been used for the computation of LST by using two prelaunch calibration constant K_1 and K_2 provided in the metadata file of the imagery.

$$T_s = \frac{K_2}{\ln\left(\frac{K_1}{L_\lambda(T_s)} + 1\right)} \quad \text{Equation 5-8}$$

T_s : LST in Kelvin.

K_1, K_2 = pre-launch calibration constants from metadata

5.2.2 Weather Research and Forecasting Model Simulations

WRF-urban is an integrated coupled modelling system with downscaling capabilities upto urban scale (~ 500 m). It also integrates three UCMs with different degree of freedom to parameterize urban surfaces as well as provides multiple ways to ingest urban Land cover information in the model. This section describes the methodological steps for the preparation of inputs for ingestion in WRF model, domain configuration, model parameterization, setup and validation of modeled outputs.

5.2.2.1 Broad Methodology

The broad methodology adopted for WRF Simulations is shown in Figure 5-3. Multi-class urban LULC (3-class) has been generated by using Level 1 broad LULC classification using neighborhood function and region merge algorithms. Further, the generated High resolution 3-class urban LULC has been recoded in accordance with USGS classification. The high resolution 3-class urban LULC and Land Surface Parameters (LSPs) have been integrated in WRF model and simulations have been carried out subsequently. The outputs generated by WRF model are different meteorological parameters like temperature, wind speed, relative humidity, wind direction, rainfall etc. WRF outputs generated were then validated and analyzed with ground observation data from IMD and MODIS LST data.

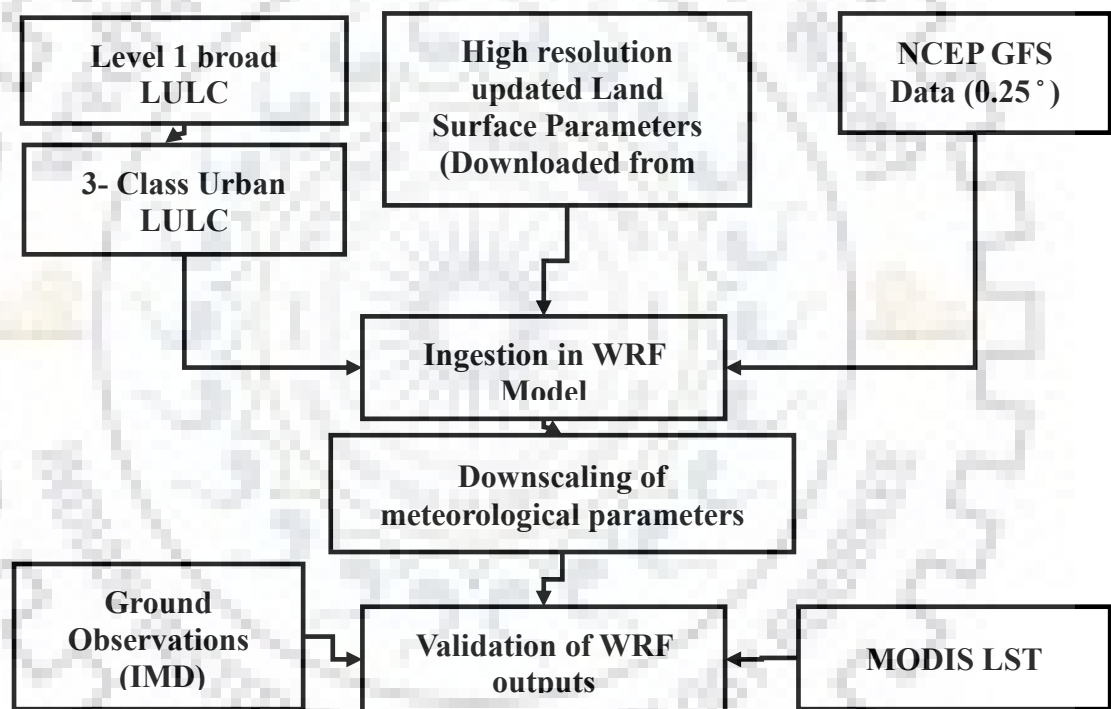


Figure 5-3: Methodology for WRF Simulations

5.2.2.2 Domain Configuration

WRF allows the users to create a multiple domains within a parent domain with increasing inner domain resolution with minimum of 1 domain and maximum of n number of domains. This process is called nesting. The domain with coarser resolution is called as parent domain and the domain with the finer resolution within the parent domain is called as child domain. The parent and child domain resolutions are generally kept with a ratio of 3:1. The time step for the WRF model is defined as the 6*parent domain resolution. Time step indicates the model restart period.

It is always measured in seconds. In WRF, two nesting options are available that is One way nesting and two-way nesting. In one-way nesting, the lateral boundaries information from parent domain is feed into inner or child domain. The interaction is only in one direction which is from parent to child. The region climate conditions are fed to inner domain whereas the inner domain local climatic conditions are not taken into consideration.

In two way nesting, the parent domain values are fed into child domain whereas the child domain values are averaged and fed back into parent domain. The regional climate conditions are fed into child domain and therefore local climatic conditions are also preserved. In this way, two way interaction between domains is made possible. In this study, two way nesting option was selected to maintain two-way interaction between regional and local conditions. Hence, two domains (parent domain, child domain) for the study region have been created with grid resolutions of 1.5km and 0.5km respectively. Figure 5-4 shows the domain configurations of the study area. The inner domain has been created by covering the continuous built up urban area whereas outer or parent domain has been created by covering the inner domain as well the surroundings which is required to integrate the impact of regional climate. The two –way nesting between these two domains ensure interaction of regional and local climate. An uncertainty analysis of 0.5 km and 1 km grid resolution with respect to ground observations revealed stable results, however 0.5 km domain displayed comparatively less mean error and similar RMSE values for temperature as compared to 1km grid resolution (Lalitha, Gupta, & Rao, 2018).

5.2.2.3 Data Used

For WRF simulations, various data sets including RS datasets and outputs have been used from different sources. The data used are meteorological data, satellite data, and ground observation data. The description of data is described in subsequent sections and the details are presented in Table 5-4.

Meteorological data for initialization of model

Global forecasting System (GFS) data is a meteorological data freely available for entire globe with a horizontal resolution of 0.25degrees for every 3 hours. It is the high resolution data available at present for defining initial and boundary conditions in WRF model. In this study, GFS meteorological data is used which is downloaded from National Center for Atmospheric Research (NCAR) website (<https://rda.ucar.edu/datasets/ds084.1/>) for providing the initial and boundary conditions for the model simulations

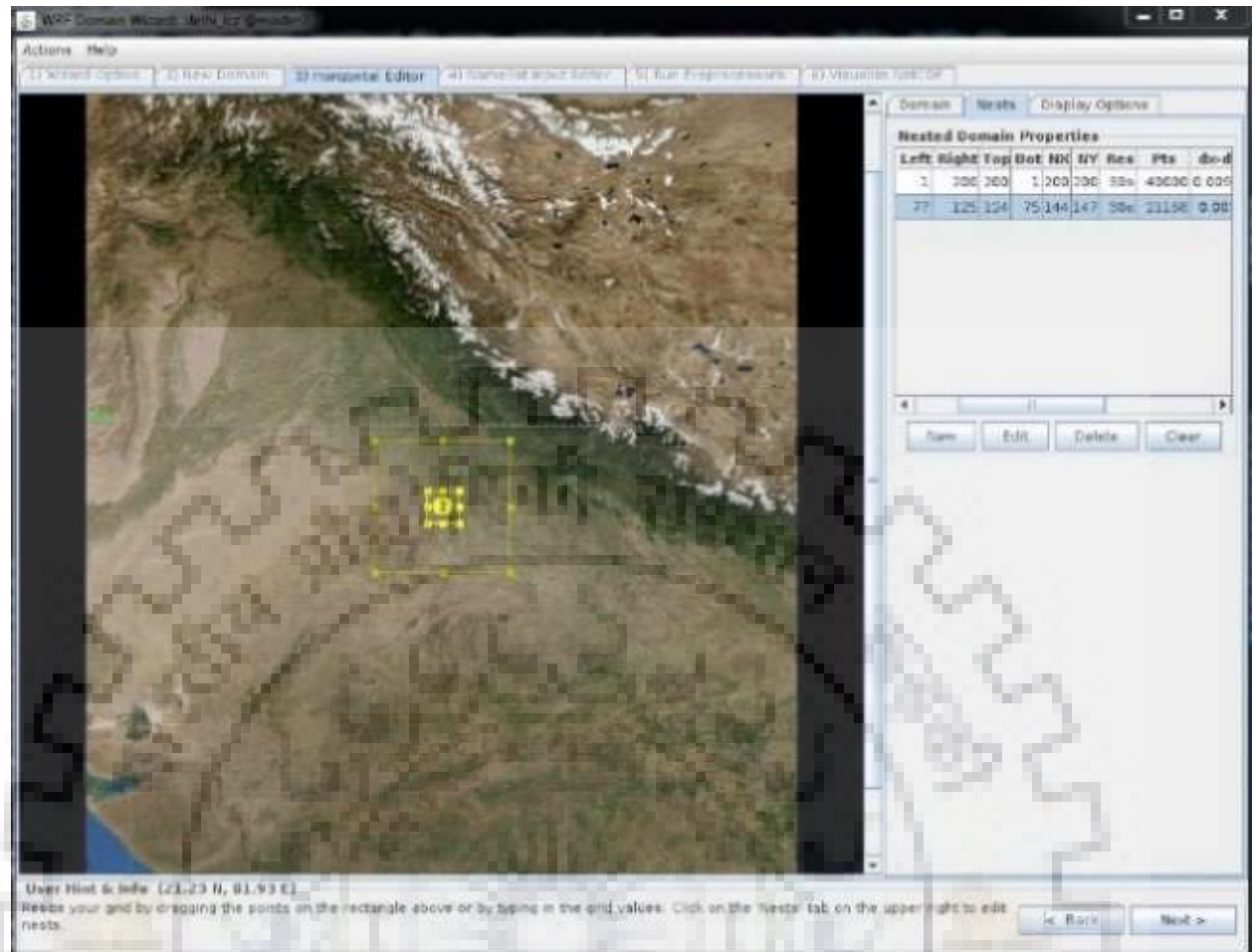


Figure 5-4: Domain configurations of the study area

Land Use Land Cover

IRS P6 LISS IV data of 5.8 m resolution is found extremely suitable for identification of urban features and delineation of accurate urban LULC classification (Gupta & Jain, 2005). Hence, in this study, Resourcesat-2 Linear Imaging Self Scanner (LISS) IV (an extension of IRS P6 LISS IV sensor) was utilized for generating the high-resolution 3- class urban LULC to parameterize urban heterogeneity in the model inputs covering the entire area of Domain 2. The earlier developed LULC in chapter 4 has not been utilized as it covers area smaller than domain 2 area. Resourcesat-2 LISS-IV is a sensor having high spatial resolution of 5.8m and multi-spectral camera operating in three spectral bands (Green, Red and Infrared). The data for Delhi region has been procured with date of acquisition of February 21, 2017 and coordinate system of UTM 43 N.

The high resolution urban LULC prepared by using LISS-IV covers only the area of domain 2 i.e. child domain. Hence, WRF compatible AWiFS Land Use Land cover (1 km spatial resolution), which is freely available, has been downloaded from Bhuvan (Mediseti Bhavana, Gupta, Kshama, Kumar, & Gummapu, 2018) to provide updated LULC information for parent domain covering the rural area of parent domain. The above LULC map have been prepared by NRSC using AWiFS (Advanced Wide Field Sensor) sensor of Resourcesat-2 with a resolution of 56m. The generated LULC has been reclassified according to USGS classification in a format compatible with WRF meso scale modelling. This data is freely available for every year for the entire Indian region. It has been used as the default LULC in WRF modelling to cover the parent domain of the study area.

Meteorological data for Model Validation

IMD (Indian Meteorological Department) is responsible for collection of ground observations of meteorological parameters in India. It maintains a vast network of surface observation network across entire Indian region and also provides weather forecast at coarser resolutions. Generally, it provides the observations data for a number of met parameters and 7 days future prediction for the major cities (<http://www.imd.gov.in/Welcome%20To%20IMD/Welcome.php>). The hourly interval data of ground observations (temperature, wind speed, relative humidity and rainfall) have been obtained from IMD for validation of model outputs. However, the ground observation data could be obtained only for one met station from IMD in the study region. One station data is not enough for assessing the impact of spatial heterogeneity by integrating the multi-class urban LULC and parameterization. Hence, Moderate resolution Image Spectrometer (MODIS) LST data have been also utilized to validate the LST outputs obtained from WRF model. MODIS data is freely downloaded from USGS earth explorer. MODIS data used is of Aqua satellite for the surface temperature and emissivity having 1km spatial resolution and available every day for both day and night if cloud cover is not present.

Land Surface Parameters

Land Surface Parameters (LSPs) has a major impact on outputs generated by WRF especially for high resolution simulations. WRF model consist of default static geographic data which is quite outdated and of coarse resolution. Because of this, the simulations carried out with old geographic data lead to erroneous results. LSPs displays high variability across seasons as well as annually which have profound impact on WRF model outputs (Kirthiga & Patel, 2018). Besides, the coarse resolution of default LSPs in WRF model is not optimal for high resolution

simulations. Hence, updation of LSPs such as albedo, vegetation fraction, Leaf Area Index (LAI), Fraction of Absorbed Photosynthetically Active Radiation (fAPAR), Fractional cover (Fcover) have been carried out to obtain improved climatic indicators. Albedo and vegetation fraction, which have been downloaded from Bhuvan website (<http://bhuvan.nrsc.gov.in/data/download>) is available two times for every month with 15 days average and 1 km resolution. LAI, fAPAR, Fcover have been downloaded from Copernicus website, (<http://land.copernicus.eu/global/products>) which is available at 500m resolution for every 6 months (Table 5-4).

5.2.2.4 Multi-class urban Land Use Land Cover

For integration in WRF, a 3 – Class urban LULC has been prepared by using Resourcesat-2 LISS-IV image of spatial resolution 5.8m which is further up scaled to 50m (Figure 5-5). Generally, there is a loss of information while upscaling the LULC through majority class or dominant class approach. Hence, in this study, for identification of 3- urban classes as well as upscaling of classified outputs, a novel approach through coding in MATLAB has been developed by applying the neighborhood functions and region merge algorithm to minimize the loss of information (Figure 5-5). The algorithm applied upscales 2 times of original resolution in each step. First of all, the satellite images were classified by applying the Maximum Likelihood Classifier (MLC) which is a pixel based supervised classification method in broad level-1 classes. The classes which were identified includes forest, agriculture, vegetation, built-up, water, dry river body, fallow lands, vacant lands and bare rock. Further, the classified outputs were resampled to 6.25m by using nearest neighbor resampling method. Then it was up scaled to 12.5 m by applying the region merge algorithm. The built-up class was then reclassified into two urban land use classes of Low Intensity Residential and High Intensity Residential by applying the neighborhood function. The commercial/transportation/industrial layers were obtained from Master Plan of Delhi and road network as described in 4.3.3. These layers were superimposed over the classified outputs and further, upscaled to 25m and subsequently to 50 m by applying region merge algorithm. The accuracy assessment of the obtained final map was carried out with respect to reference data from ground truth. The final map thus obtained were recoded to adhere to the USGS classification and then integrated in WRF model (Table 5-5).

Table 5-4: Details of updated Land Surface Parameters

Data/Parameters	Resolution	Source
Multi- class Urban Land use/ Land cover	5.8m	Resourcesat-2 LISS IV
WRF Compatible AWiFS LULC	1 km (30 Seconds)	https://bhuvan-app3.nrsc.gov.in/data/download/index.php?c=p&s=NI&p=wrf&g=TS
Topography	30m	http://earthexplorer.usgs.gov/
Bhuvan Albedo	1 km	http://bhuvan.nrs.c.gov.in/data/download/index.php?c=t&s=TR&p=albedo
Vegetation Fraction	1 km	http://bhuvan.nrs.c.gov.in/data/download/index.php?c=p&s=NI&p=vf&g=TS Sensor: OCM II
fAPAR	500m	http://land.copernicus.eu/global/products/fapar Sensor: SPOT-VGT, PROBA-V
LAI	500m	http://land.copernicus.eu/global/products/lai Sensor: SPOT-VGT, PROBA-V Temporal resolution:30 days
FCover	500m	http://land.copernicus.eu/global/products/fcover Sensor: SPOT-VGT, PROBA-V Temporal resolution:30 days
NCEP GFS data (Every 3 hrs.)	0.25°	https://rda.ucar.edu/datasets/ds084.1/
Met data - Ground observations	Point data	IMD , India (28° 34.998'N, 77° 12.000'E)
MODIS LST	1 km	https://modis.gsfc.nasa.gov/data/dataproduct11.php , Product ID: MYD11A2

5.2.2.5 Weather Research and Forecasting model setup

Before the commencement of model simulations, various physics options including microphysics and urban physics options, cumulus parameterization, planetary boundary layer, land surface model etc. have been defined. A summary of the different physics options used in this study has been listed below in Table 5-6. Since, urban physics scheme of BEP+BEM is compatible with

Unified Noah Land Surface model, hence it have been selected as LSM. Other physics options have been identified based on previous experiences in the study region (Mohan & Bhati, 2011).



Figure 5-5: Flowchart for the preparation of upscaled 3-class urban LULC

Table 5-5: Modified LULC codes for USGS classification

LULC	USGS original class names	USGS classification
Agriculture	Irrigated Cropland and Pasture	3
Fallow lands	Cropland/Grassland Mosaic	5
Scrubs	Shrub land	8
Vegetation	Mixed Shrub land/Grassland	9
Forest	Mixed Forest	12
Water body	Water Bodies	16
Vacant lands	Barren or Sparsely Vegetated	19
Low intensity residential	Low Intensity Residential	31
High intensity residential	High Intensity Residential	32
Industrial/Commercial/Transportation	Industrial or Commercial	33

Table 5-6: Physics schemes used for WRF simulations

Physics	Domain 1&2
Micro Physics	WSM6
Long wave radiation scheme	RRTM
Short wave radiation scheme	Dudhia
Surface layer(sf_sfclay_physics)	Monin-Obukhov(Janjic Eta) scheme
Land Surface Physics(sf_surface_physics)	Unified Noah land surface model
PBL scheme(bl_pbl_physics)	Mellor-Yamada-Janjic scheme
Urban surface physics (sf_urban_physics)	BEP+BEM
Cumulus scheme	Kain-Fritsch(new Eta)scheme, New Grell Scheme(G3)

5.2.2.6 Simulation Periods

To identify the seasonal variation of weather present with in an urban area, three seasons namely Summer, Monsoon, and winter of Delhi, 2017 have been selected and simulation have been carried out for three days (Table 5-7). The first 24 hour simulation have been considered as spin-off period and hence, have not been used for analysis. The 3-days of simulation period was selected based on representative dates of the season and the availability of point observation data for validation.

Table 5-7: Simulation Dates for WRF simulations

Season	Date of simulation	LULC	Land surface parameters	Urban physics	Urban parameter table
Summer	June 04-06, 2017	Modified 3-class Urban LULC using Region and merge algorithm	Updated parameters	BEP+BEM	Updated parameters
Monsoon	August 08-10, 2017				
Winter	December 15-17, 2017				

5.2.2.7 Integration of urban LULC and Land Surface Parameters in WRF

After the creation of domains, high resolution 3-class urban LULC has been ingested in WRF model along with the downloaded LSPs of corresponding duration for model simulations. First of all, all above mentioned datasets have been converted into binary format and their paths have been defined in GEOGRID.TBL, which stores characteristics of all geographic data used for model simulations.

5.2.2.8 WRF Simulations and validation

In the first step Geogrid.exe has been executed which interpolates all the geographic data including LULC, LSPs, topography to the domain resolutions and extents. Further, GFS meteorological data (0.25°) have been ungridded to extract the meteorological parameters from grib2 format of GFS data of the corresponding dates (Table 5-7). This step is followed by execution of metgrid.exe to interpolate the GFS data to the domain extents. After the modification of parameters, real.exe is executed to interpolate the meteorological data in the vertical direction along by taking consideration of parameters like surface physics options, cumulus parameterization etc. URBPARAM.TBL table has also been updated to define urban parameters for 3-class urban LULC based on the available literature. Finally, wrf.exe has been executed to generate the outputs at the desired resolution of 0.5km. The outputs generated by WRF model are in NetCDF format, which have been converted in tiff format in GIS environment. These outputs were further validated by using point observation data of IMD and MODIS LST.

5.2.3 Relationship between Urban Canopy Parameters and urban climate Indicators

In the final stage of work flow, relationship between UCPS and climate indicators have been assessed by performing the correlation analysis. The spearman's rank correlation coefficient has been computed as it is better estimator of correlation when input data do not follow Gaussian distribution. To perform the analysis, sample points by applying stratified random sampling have been generated corresponding to LULC map. The UCPs layers have also been also resampled at the resolution of 30m corresponding to the resolution of LST map. The LULC map have been employed to distinguish intra-urban dependencies and only those Landsat pixels have been considered that fall within a single LU block.

Further analysis of Surface Urban Heat Island Intensities (SUHII) have been carried out for those UCPs which have exhibited strong relationship with LST. Generally, UHI is defined as urban-rural difference, however, this definition holds a large uncertainty regarding selection of urban

–rural reference frame. To overcome this uncertainty (Stewart & Oke, 2012) defined UHI as a difference between compact high rise and low plants area of LCZ classification. Based on this recommendation, in this study, SUHI intensity have been computed as a difference in mean temperature of high intensity residential and agriculture area. Further, WRF model outputs of LST and Temperature at 2m have been utilized to assess the diurnal variation of SUHII and Urban Canopy Layer Heat Island Intensities (UCLHII) in the study region.

5.3 RESULTS

The obtained results at each step are presented in this section. First of all, generated LST maps are presented which is followed by WRF outputs and then their validation with respect to ground observations and MODIS LST.

5.3.1 Land Surface Temperature

The LST maps of different seasons have been produced by applying RTE method on Landsat 8 TIRS band 10 data. Figure 5-6 shows the LST maps produced for 21 May 2016, 16 August 2016, 12 Oct 2016 and 13 Feb 2016 corresponding to summer, monsoon, post-monsoon and winter season respectively. It could be seen from the LST maps that maximum variation in temperature among land surface features could be seen in summer and winter months. In summer maximum temperature reaches more than 45 degrees while in monsoon max temp observed was 31.50 degrees. In Post monsoon season maximum temperature reaches upto 39 degrees and in winter also the maximum temp observed is near to 35 degrees. Urban Built-up shows moderate temperature as compared to surroundings in all seasons except monsoon season. This may be due to time of pass is near to 11 AM in the morning. The data for monsoon season was available only for half of the study area owing to clouds in the study area.

5.3.2 WRF Model Simulations

5.3.2.1 Multi- class Urban Land Use/Land cover

3-class urban LULC for study area has been generated by applying supervised classification and then by employing region merge algorithm and neighbourhood function at the grid resolution of 50 m. Figure 5-7 presents the 3-class urban LULC map prepared by region merge algorithm. The

kappa coefficient for LULC generated by employing region and merge algorithm is 0.93. The area statistics (Table 5-8) of the area shows that agriculture is the most dominant class followed by fallow land, high intensity built-up, and low intensity built-up. Vegetation and water body has very small percentage of total area.

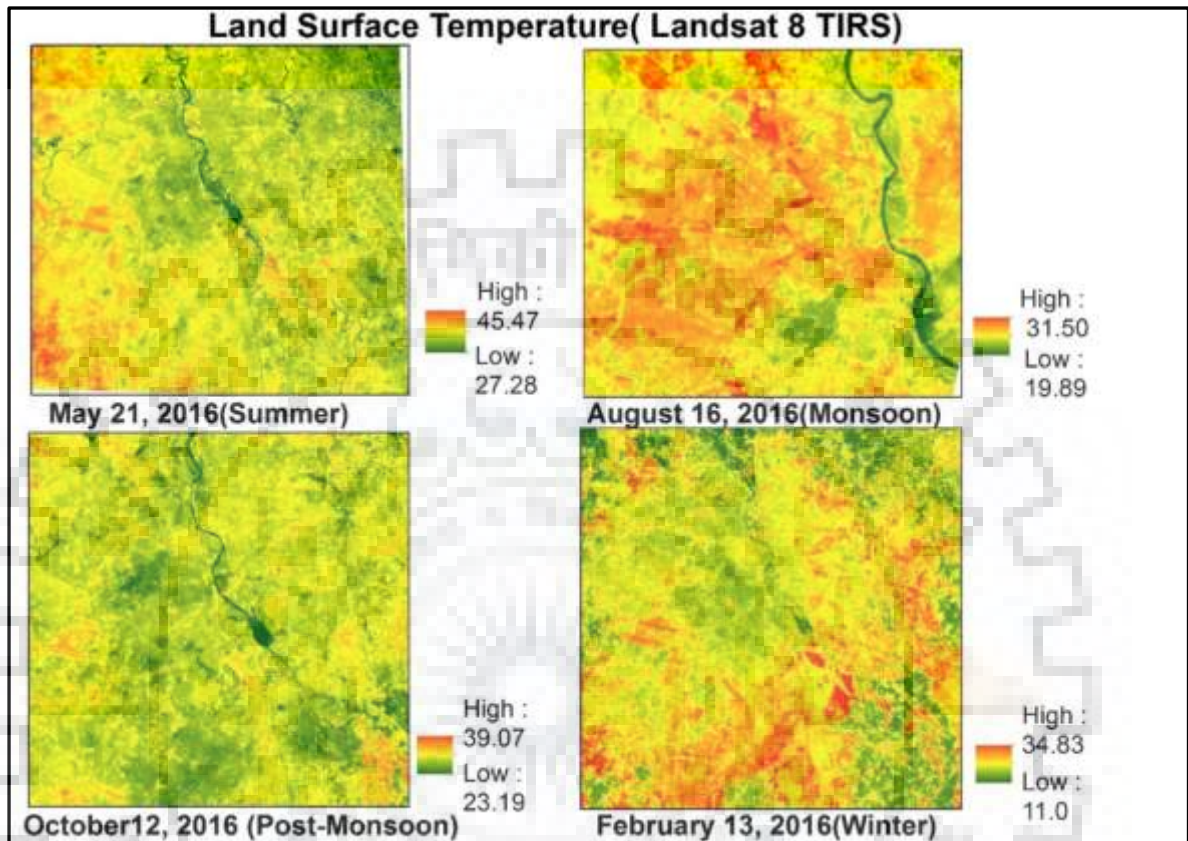


Figure 5-6: Land Surface Temperature maps of the study region

Table 5-8: Area statistics of 3-class Urban LULC at 50 m grid resolution

Class Name	Area (sq km)	% of Area
Agriculture	1579.9	29.35
Vegetation	112.42	2.09
Scrubs	370	6.87
Water body	10.19	0.19
Fallow land	1031.14	19.15
Vacant lands	257.76	4.79
Low intensity residential	838.69	15.58
High intensity residential	851.38	15.81
Transportation/ Industrial/ Commercial	332.26	6.17
Total Area	5383.74	100.00

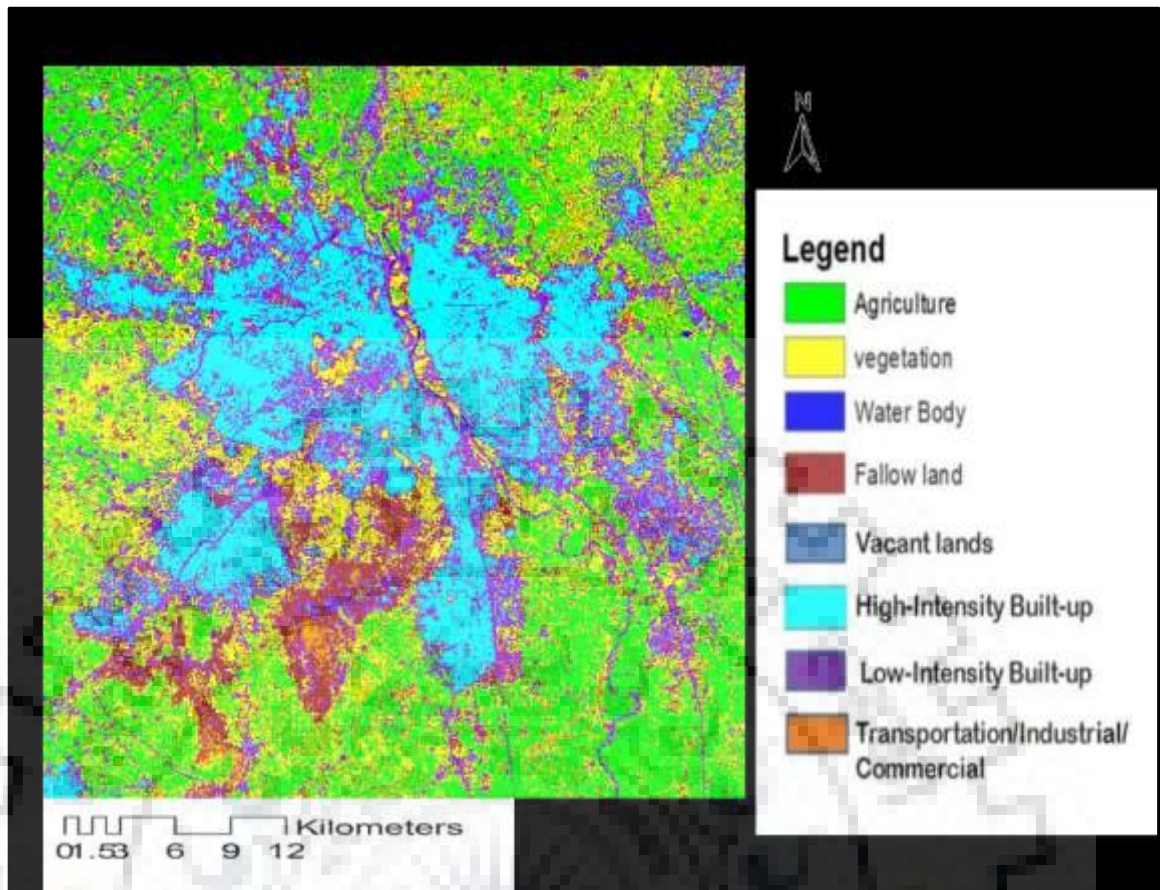


Figure 5-7: Multi class (3- class) Urban Land Use Land Cover at 50 m grid resolution

5.3.2.2 Weather Research and Forecasting Outputs

The simulation for three seasons of Delhi have been carried out. Since, Delhi has no dominant season, it is known to have composite climate. Figure 5-8 presents the spatial distribution of the three meteorological parameters for two domains of urban LULC model outputs of Delhi for the month of June, 2017. Meteorological parameters derived from Domain 2 of 0.5km spatial resolution shows better spatial variation as compared to Domain 1 of 1.5 km spatial resolution. The temperatures in the city is less compared to the surrounding because the output presented here corresponds to 11:30 IST. By this time, the surrounding fallow land /bare soil heats up more than the urban area. However, built-up area takes time to warm up and emit the radiation due to shading effect (3D geometry of buildings) and material time lag (depending on thermal properties of materials). Relative humidity is less in the city whereas wind speed is moderate owing to the high roughness characteristics of building surface area. These differences are clearly visible in case of domain 2 as compared to domain1.

Figure 5-9 shows the spatial distribution of the four meteorological parameters for two domains of model outputs of Delhi for August, 2017. For August, the meteorological parameters shown

in the figure are of 20:30 IST. Relative humidity is high in the city because of the monsoon season whereas wind speed is less to moderate. Figure 5-10 shows the spatial distribution of the three meteorological parameters for two domains of Delhi for December, 2017. The temperatures in the city is high because it is of day time at 14:30 IST. Relative humidity is less in the city because of the winter season whereas wind speed is moderate within the city.

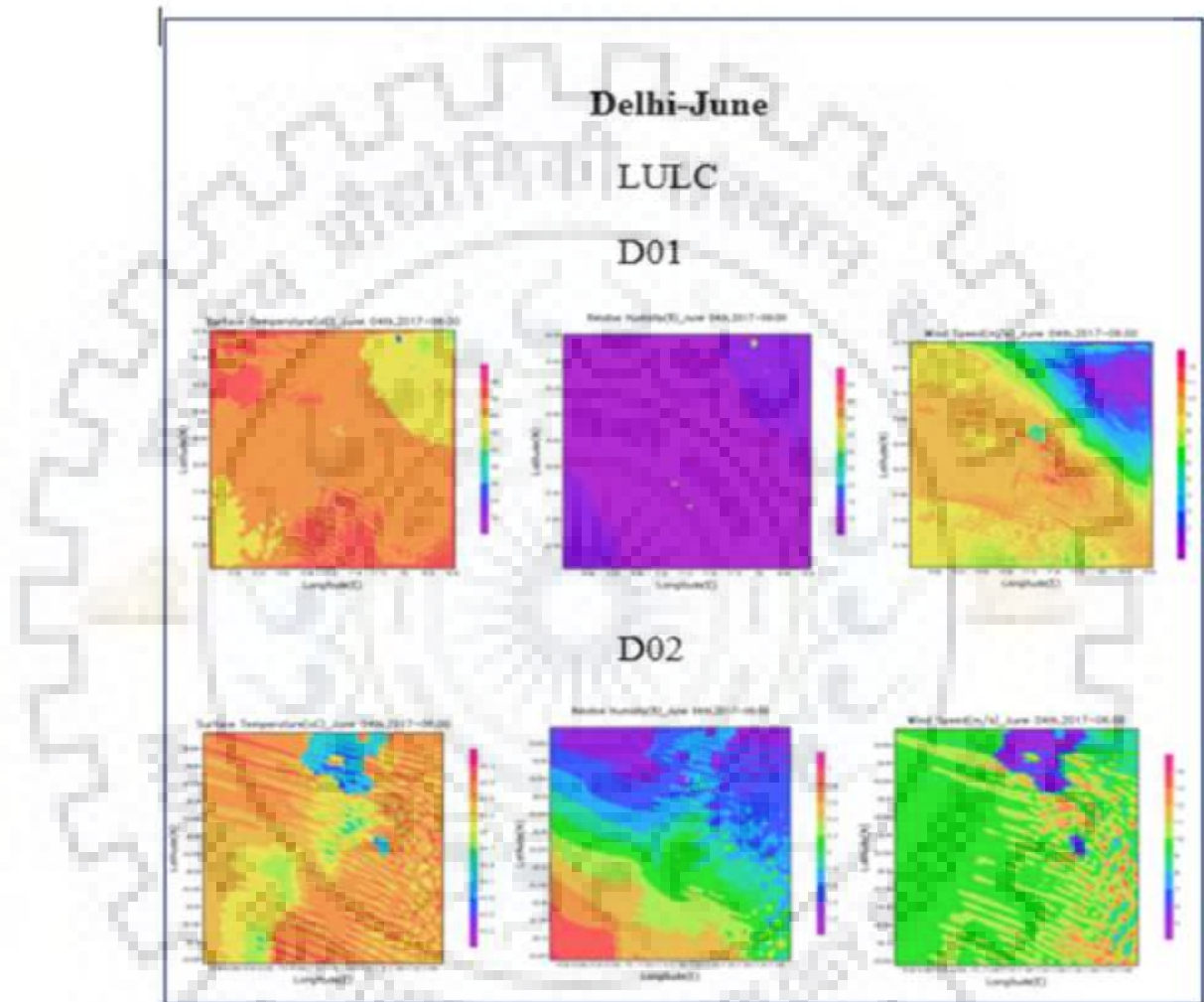


Figure 5-8: Spatial Distribution of Temperature, Relative Humidity and Wind Speed in Domain 1 and Domain 2 of the study region (June 2017)

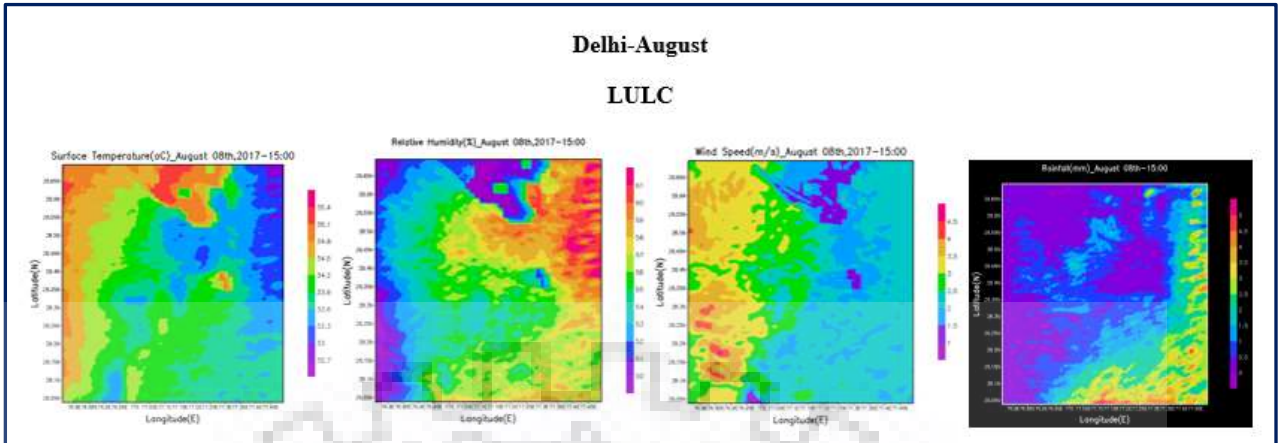


Figure 5-9: Spatial Distribution of Temperature, Relative Humidity and Wind Speed in the study region (August 2017)

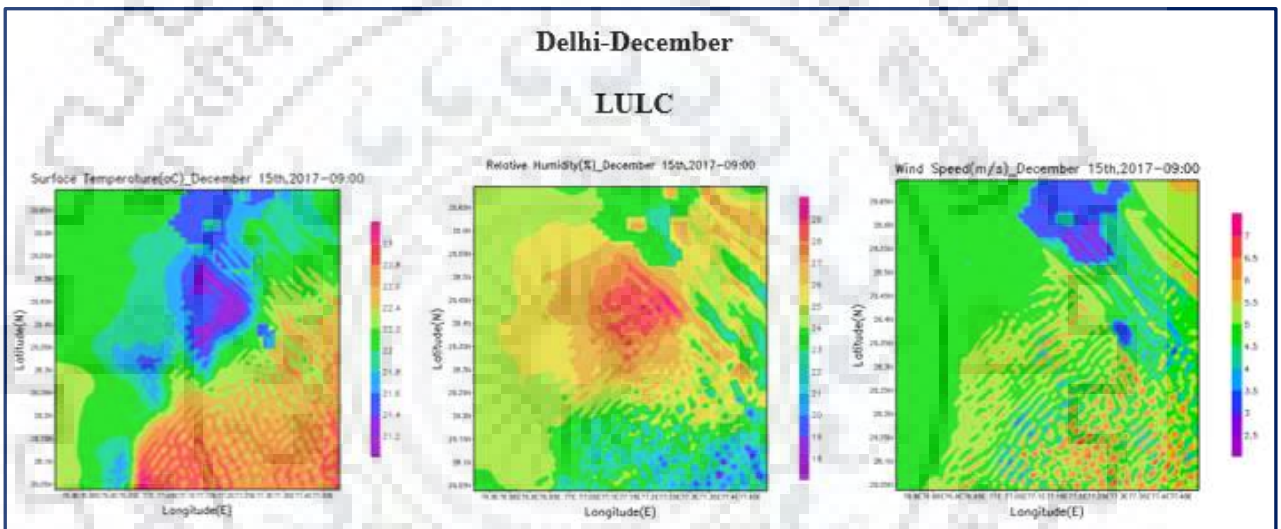


Figure 5-10: Spatial Distribution of Surface Temperature, Relative Humidity and Wind Speed in the study region (December 2017)

5.3.2.3 Validation of WRF Model Simulations

Delhi is a complex city with composite climate. It experiences hot summers and cold winters along with high humidity during monsoon season. The simulations have been carried out for three days in each predominant season and have been validated against point observation data provided by Indian Meteorological Department (IMD), Delhi. Only one station data could be utilized for validation as data available from other stations were either of poor quality or metadata was insufficient.

Figure 5-11 presents the correspondence of the Temperature at 2m for all three simulation periods. The maximum correspondence is seen in June simulation (summer season), whereas model overestimates the temperature at 2m in the monsoon season (August). In winter season

(December), model overestimates some time and sometime underestimates. There is no pattern in seasonal variation which could be attributed to bias or could be added or subtracted from the model outputs.

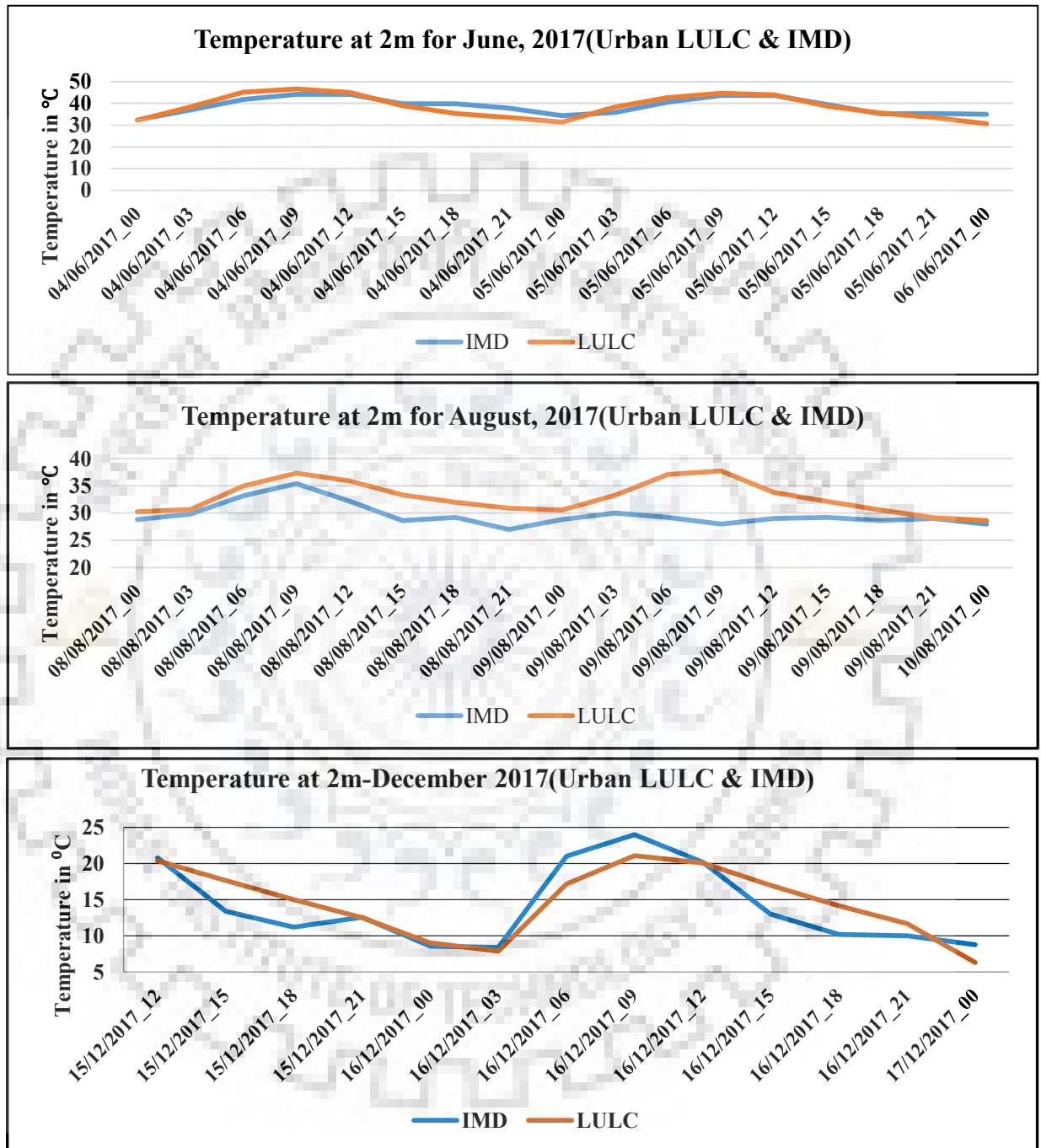


Figure 5-11: Validation of Temperature at 2m with point observation data of IMD, Delhi

Figure 5-12 shows the correlation graphs for Temperature at 2m with point observation data that shows strong correlation in the month of June but moderate correlation in the month of August and December.

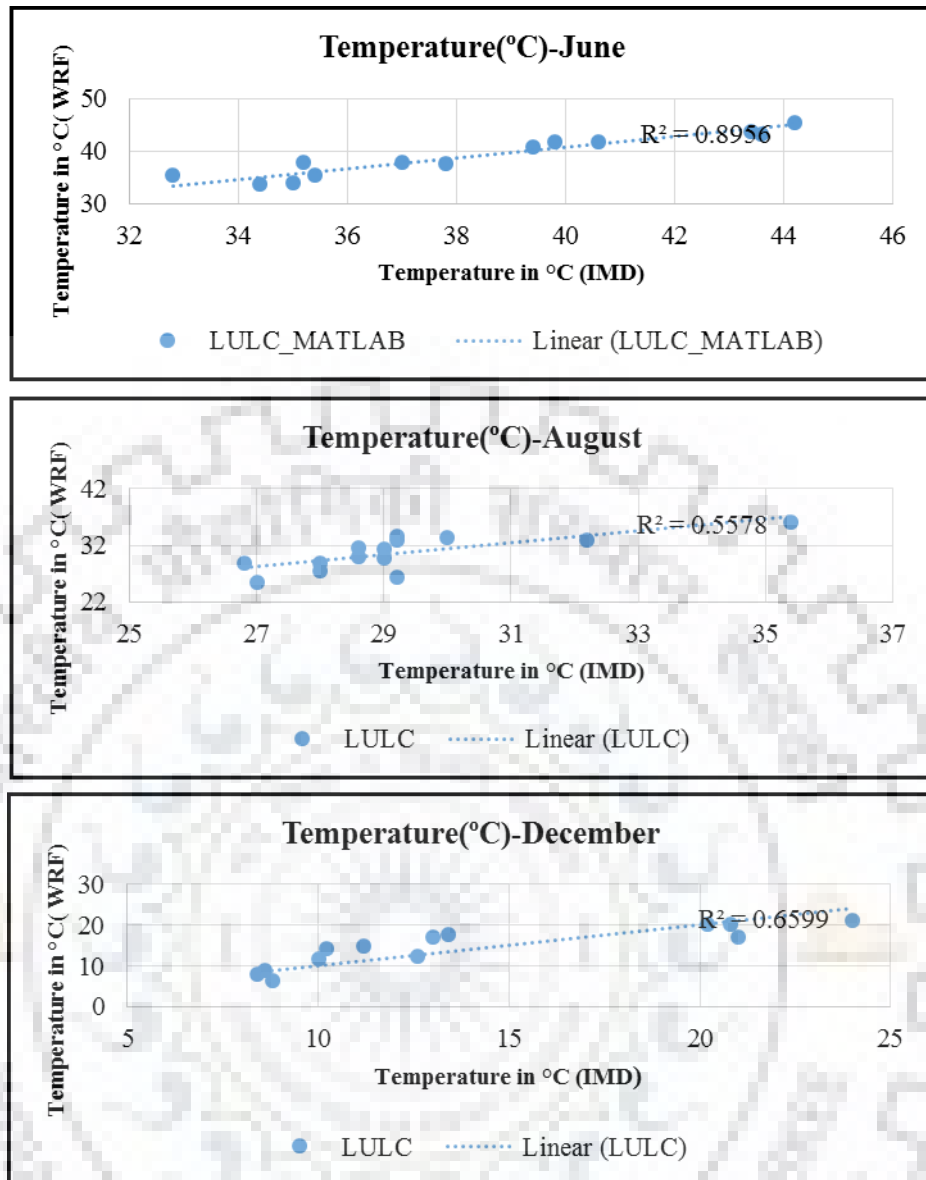


Figure 5-12: Correlation graphs for the Temperature at 2m with IMD, Delhi

The model tends to underestimate relative humidity in all seasons (Figure 5-14) however, it shows strong correlation (~ 0.9) and lower RMSE values ($\sim 3\%$) in all seasons with point observation data. The RH is high in monsoon ($\sim 88\%$) and winter season ($\sim 74\%$) while in summer season, RH is very low ($\sim 30\%$). Wind speed shows a poor correlation in summer and monsoon season but shows a good correlation in winter season (Figure 5-15 and Table 5-10). The mean wind speed is high in summer season ($> 3\text{m/s}$) while in monsoon and winter season, the speed is $\sim 1\text{ m/s}$. Generally, the wind speed is higher in afternoon hours and lower in morning hours. The model has overestimated wind speed in some of the instances and underestimated in few of the instances. It does not show any specific pattern in any of the season.

5.3.2.4 Validation with MODIS Land Surface Temperature

Point data provided by IMD, Delhi provides observations at single point only and do not provide spatially variable LST to account for heterogeneous urban environment. It is understood that this data is clearly non- representative of spatial heterogeneity. However, in the absence of availability of any other data source, only one station data have been utilized for validation of model output. To overcome this limitation, MODIS LST images of corresponding dates downloaded from USGS Earth explorer website have been utilized to validate the spatial variation of LST obtained through WRF model simulations. Figure 5-13 shows the difference images of the Delhi by subtracting the WRF model outputs of LST from MODIS image for June, August, and December and results of validation are presented in Table 5-9. It clearly shows that nearly 70% pixels of WRF LST are within the range of $\pm 1^\circ\text{C}$ in Winter and monsoon season images whereas in summer season more than 85% pixels are in the range of $\pm 1^\circ\text{C}$. More than 80% of the pixels exhibit temperature within $\pm 2^\circ\text{C}$ in all the seasons. It shows a high correlation of WRF LST with MODIS LST.

Table 5-9 Percentage of pixels in difference image with MODIS LST

Range in $^\circ\text{C}$	June 2017		August 2017		December 2017	
	No. of pixels	% of Pixels	No. of pixels	% of Pixels	No. of pixels	% of Pixels
-1 to 1	1316	85.51	1053	68.43	1043	67.77
$<\pm 2$ to ± 1	27	1.75	291	18.91	291	18.91
$>\pm 2$	196	12.74	195	12.67	205	13.3
Sum	1539		1539		1539	

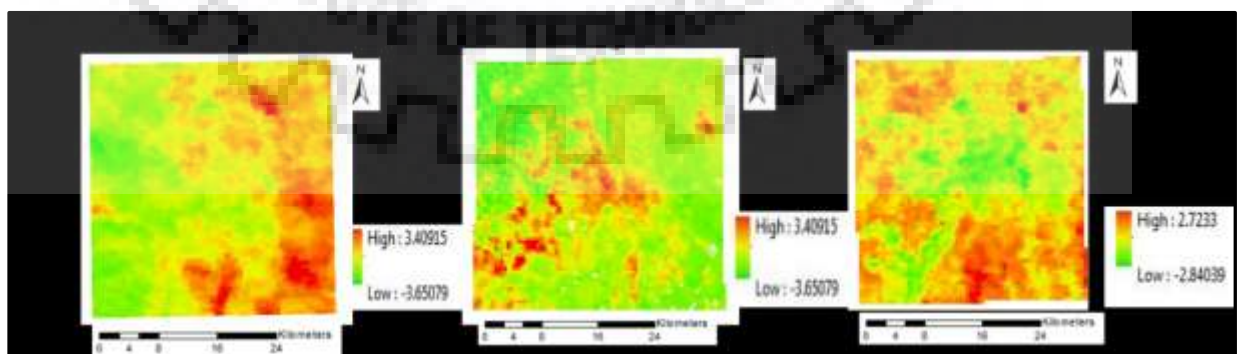


Figure 5-13 Validation of WRF model results with MODIS LST for three seasons of Delhi

Table 5-10: Statistical parameters derived from the observed (IMD) and simulated WRF outputs for three seasons of Delhi, 2017

Month	Temperature at 2m						Relative Humidity at 2m					Wind speed at 2m				
	Mean °C	RMSE °C	MAE °C	STDV	Correlation	Mean %	RMS E %	MAE %	STDV	Correlation	Mean (m/s)	RMSE (m/s)	MAE (m/s)	STDV	Correlation	
June (Summer)	IMD	38.35			3.81		32.31		10.25		3.76			2.49		
	LULC	38.58	1.44	0.19	3.89	0.95	30.81	3.25	1.5	10.07	0.96	3.08	2.35	0.68	0.82	0.43
August (Monsoon)	IMD	28.83			1.36		89.54		7.64		1.28			1.81		
	LULC	30.24	2.45	1.41	2.68	0.64	88.07	3.56	1.46	13.6	0.9	1.99	1.99	0.71	0.98	0.33
December (Winter)	IMD	14.02			5.5		74		22.84		1.01			1.58		
	LULC	14.62	2.73	0.61	4.87	0.86	73.84	2.88	0.16	21.27	0.99	1.71	1.3	0.7	0.62	0.81

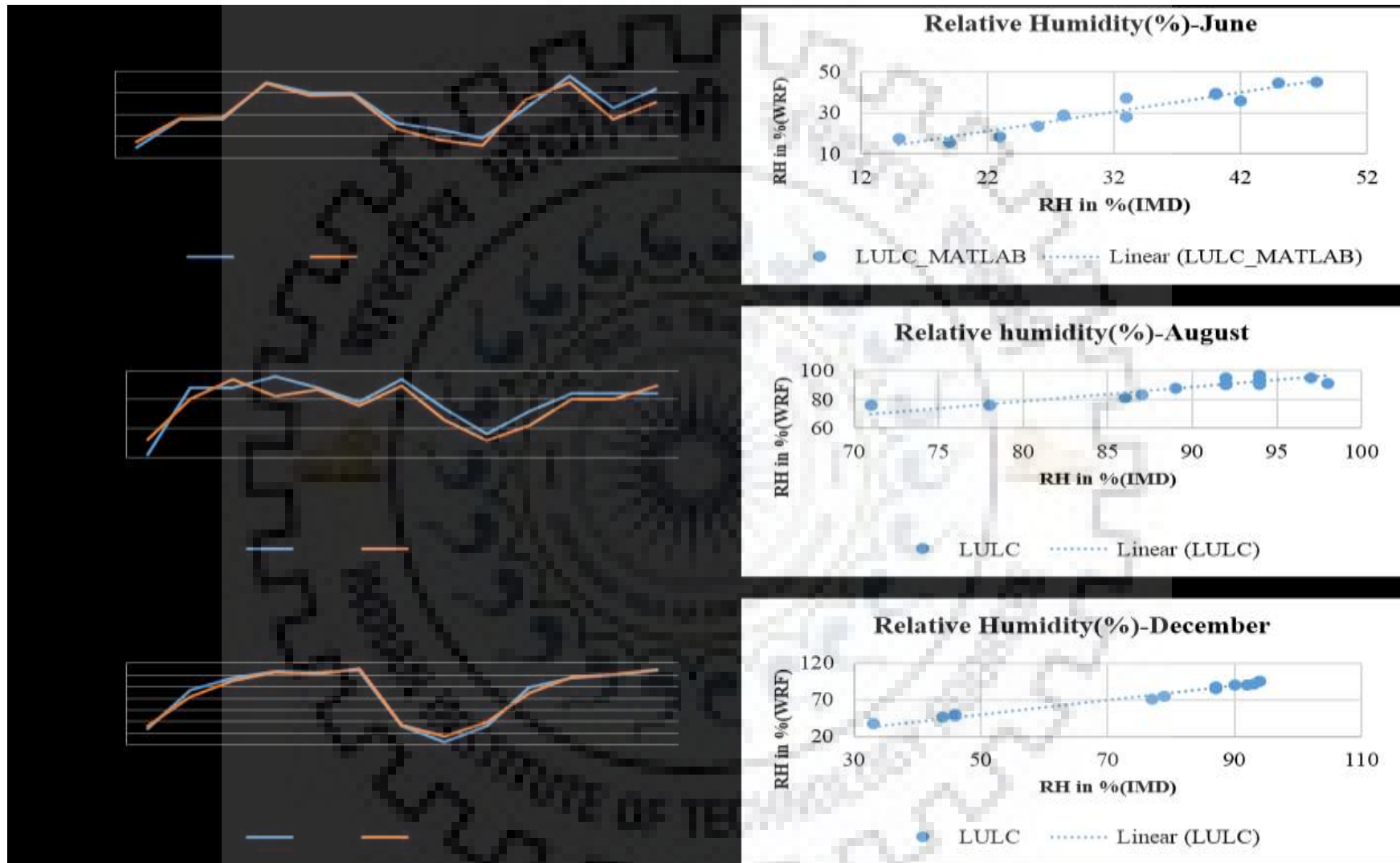


Figure 5-14: Validation and Correlation graphs for Relative Humidity at 2m with point observation data of IMD, Delhi

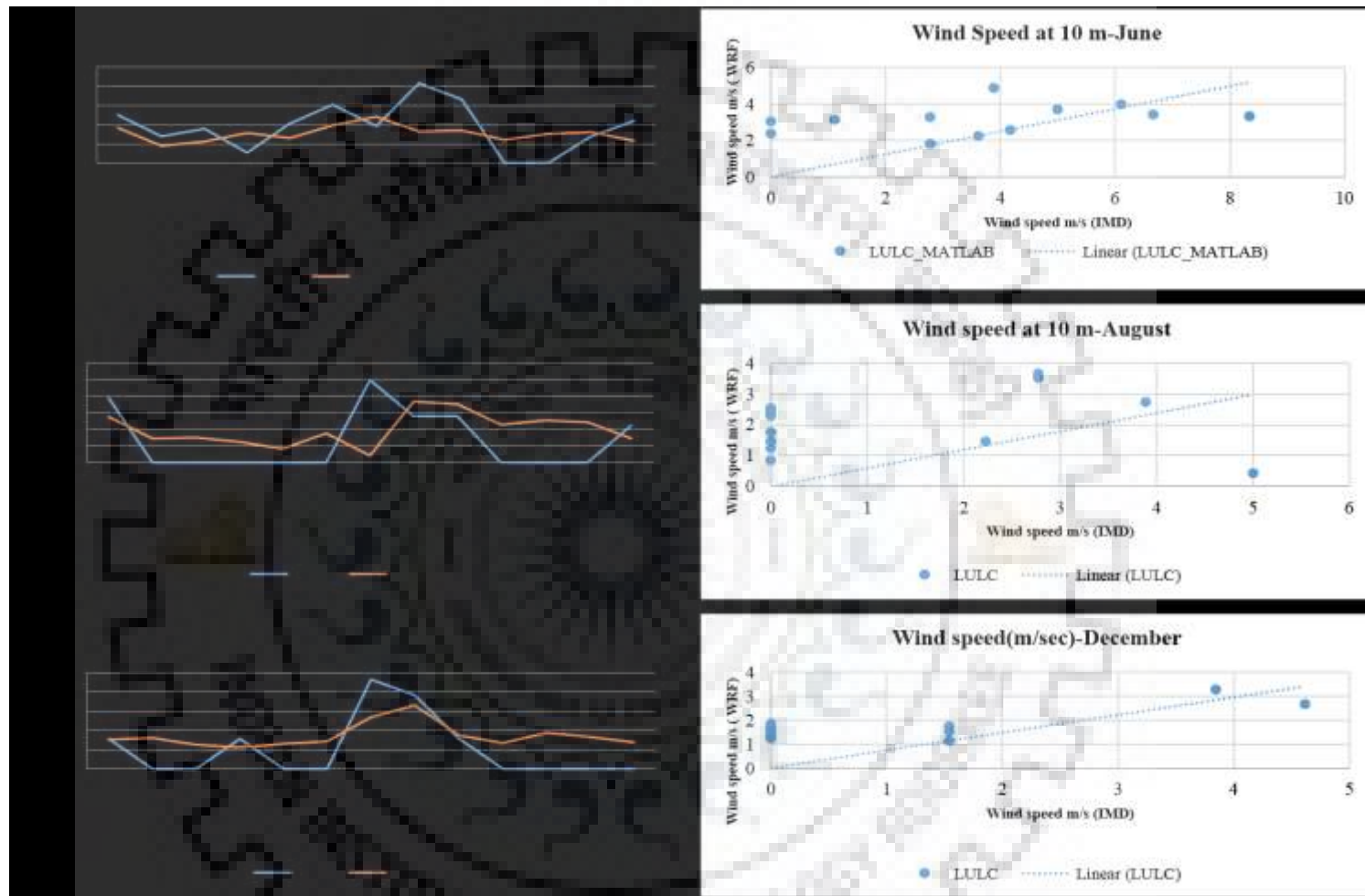


Figure 5-15: Validation and Correlation graphs for Wind Speed at 10m with point observation data of IMD, Delhi

5.4 DISCUSSIONS

This section discusses the obtained results, the relationship of UCPs with LST, spatial variability of seasonal SUHI intensities with UCPs and diurnal SUHI and UCLHI intensities. It also dwells into methodological and operational concerns in the retrieval of LST and WRF simulations respectively and future directions for research.

5.4.1 UCPs-LST relationship and seasonal variability

The primary results of UCPs-LST relationship is presented in Table 5-11. It quantifies the correlation between UCPs and LST for different seasons. All correlation values were significant at 0.05 level. The columns present the correlation values for different seasons whereas rows present the correlation values for each UCPs.

It is to be noted that PSF, BSF and ISF yields the highest correlation and outperform all UCPs, however the correlation varies in different seasons. For example, ISF shows ~ 0.7 correlation except in monsoon season which may be due to increased moisture content and presence of grassy vegetation in impervious area. Similarly BSF exhibits lower correlation values in Post Monsoon and winter season which may be attributed to slant sun rays and shading effect. Since, Landsat satellite pass is at ~ 11 AM, the impact of shading in building surface area is more dominant which further increases due to low sun elevation angle. The variation in correlation across season may be dependent on shading effect and direction of wind flow. PSF also shows strong correlation in all season except winter season which is possible due to effect of bare soil and fields that leads to increased temperature in bare soil area. Since, the LULC was extracted only for one season, the seasonal effect cannot be entirely comprehended. For better understanding of relationship, temporal surface cover fractions covering different seasons may provide improved correlation for all seasons.

It is evident from Table 5-11 that most of the 3D UCPs exhibit poor correlation with LST except building height. Building height exhibits very strong negative correlation which again may be attributed to shading effect which is quite dominant near to 10:30-11 AM satellite pass. Most of the 3D UCPs such as SVF, Zo, CAR, Building Volume, BSAPAR exhibits moderate to weak negative correlation with LST. Some UCPs had displayed varying correlation with respect to season such as Zo, CAR and SVF.

The underperformance of 3D UCPs can be explained in terms of determination of LST from Landsat data. The TIRS sensor onboard Landsat satellite has nadir viewing geometry due to

which it is more focused on horizontal surfaces. Hence, horizontal surfaces such as roads, building roof tops are excessively sampled while vertical surfaces such as wall surface areas are under sampled in Landsat LST. It explains the strong relationship of 2D UCPs (surface cover fractions) as compared to most of the 3D UCPs.

The improved and independent assessment of 2D and 3D UCPs would only be possible if temperature of all 3D surfaces which actively take part in exchange of radiation and heat (roof, ground and walls) is considered. The availability of complete temperature data cube at different vertical levels or complete surface area temperature may assist in drawing better correlation statistics (Roth et al., 1989; Voogt, Oke, Voogt, & Oke, 1997). Alternative approaches needs to be developed to obtain information on complete 3D temperature data cube and its integration with LST and subsequent analysis of UCPs (both 2D and 3D) with temperature data. It is anticipated that 2D UCPs may have stronger relationship with LST while 3D UCPs may have strong relation with air temperature or temperatures at different vertical levels (Oke, 1988; Voogt et al., 1997).

Table 5-11: Correlation of Urban Canopy Parameters with Landsat LST

Parameter	Post Monsoon	Monsoon	Summer	Winter
BSF	0.61	0.82	0.87	0.65
ISF	0.77	0.54	0.71	0.66
PSF	-0.90	-0.92	-0.93	-0.48
VSF	-0.58	-0.84	-0.51	-0.66
Zd	0.21	0.24	0.40	0.24
SVF	-0.40	-0.81	-0.55	-0.58
Zo	-0.59	-0.45	-0.67	-0.82
CAR	-0.46	-0.35	-0.55	-0.82
Bldg Vol	-0.38	-0.38	-0.41	-0.35
H/W Ratio	0.65	0.62	0.47	0.61
BSAPAR	-0.51	-0.52	-0.69	-0.70
Bldg Height	-0.85	-0.88	-0.79	-0.88

Here,

BSF: Building Surface Fraction, ISF: Impervious Surface Fraction, PSF: Pervious Surface Fraction, VSF: Vegetation Surface Fraction, zd: Zero Plane Displacement Height, SVF: Sky view Factor, zo: Surface Roughness Length, CAR: Complete Aspect Ratio, Bldg Vol: Building Volume, H/W Ratio: Height to Width Ratio, BSAPAR: Building Surface Area to Plan Area Ratio, Bldg Height: Building Height

5.4.2 Spatio- seasonal variability of SUHI intensities

The spatio-seasonal variability of SUHII with UCPs displays interesting results. SUHII intensities were found to be maximum during winter season while lowest during post-monsoon season across all UCPs. This is generally attributed to synoptic weather conditions prevailing in the region. Summer season is known for frequent dust storms and higher wind speed in the study region which creates strong mixing and assist in dissipation of the heat in surrounding environment. While lower wind speed and cold conditions in winter season is responsible for the trapping of pollutants and heat in the urban fabric and leads to the higher SUHI intensities. However, it could be debated whether more SUHI intensities in winter is a welcome phenomenon or not. Increased temperature of urban fabric may provide thermal comfort but on the other hand trapping of pollutants in urban atmosphere is known to have severe pollution conditions and increased frequency of respiratory diseases in Delhi region (Anon., 2012a; Sharma et al., 2018). The monsoon season also displayed higher SUHI intensity in the study region, which adds to thermal stress as relative humidity levels are also high (>80%) during this period. Over the years, the increased humidity levels coupled with higher SUHI intensities have been considered as one of the major driving factor for enhanced use of air conditioners in the study region (Campbell, Kalanki, & Sachar, 2018).

BSF (Figure 5-16) shows increasing SUHII magnitude with increasing value of BSF. It shows a strong positive correlation except in winter season where BSF more than 60% displays less temperature as compared to LST for 40-60% BSF. This may be attributed majorly to shading effect and time lag of building material in case of highly dense built up areas. PSF and ISF shows consistent results across all seasons as with increasing value of ISF, SUHII magnitude is also increasing (Figure 5-18), while SUHII magnitude decreases with increasing values of PSF (Figure 5-17). Building height and surface roughness also displayed general trend of decreasing SUHII values across all seasons, however, the trend is not strictly linear (Figure 5-19 and Figure 5-20). SVF had displayed varying trend as during summer and post –monsoon season it shows positive trend whereas in monsoon and winter season it displays the negative trend (Figure 5-21) with no consistent pattern across season. The direction and speed of wind flow in urban canyons may have an impact on varying patterns, however, further investigation of SUHI intensities along with wind speed and wind direction across season and years may assist in improved understanding.

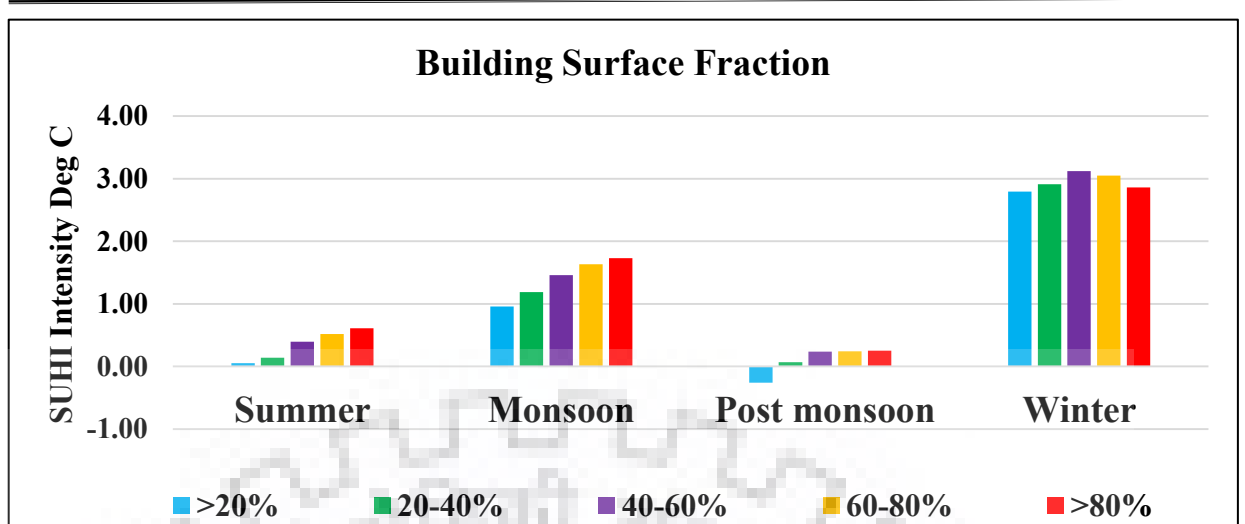


Figure 5-16: Building Surface fraction and SUHI Intensity

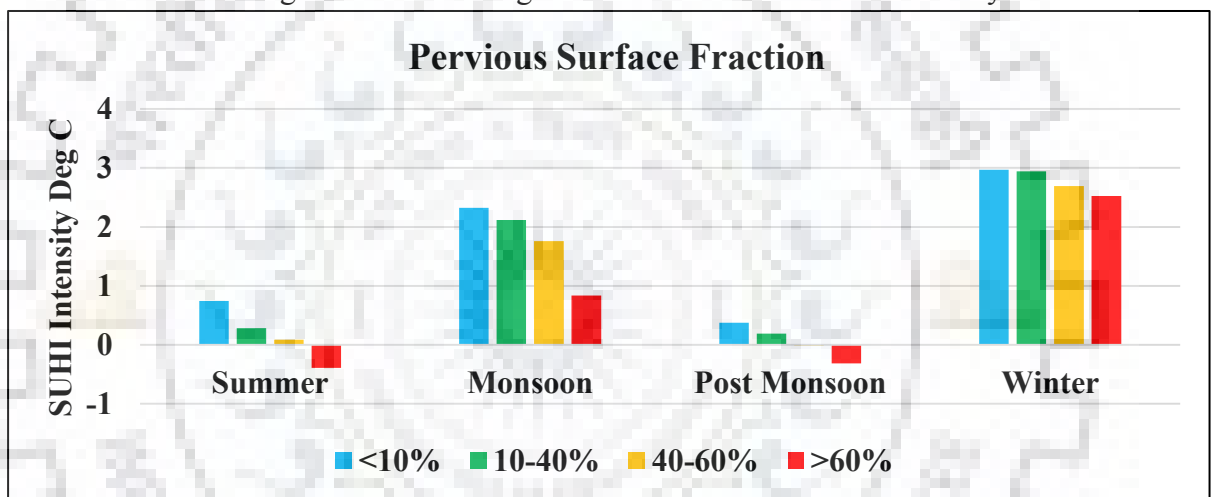


Figure 5-17: Pervious Surface fraction and SUHI Intensity

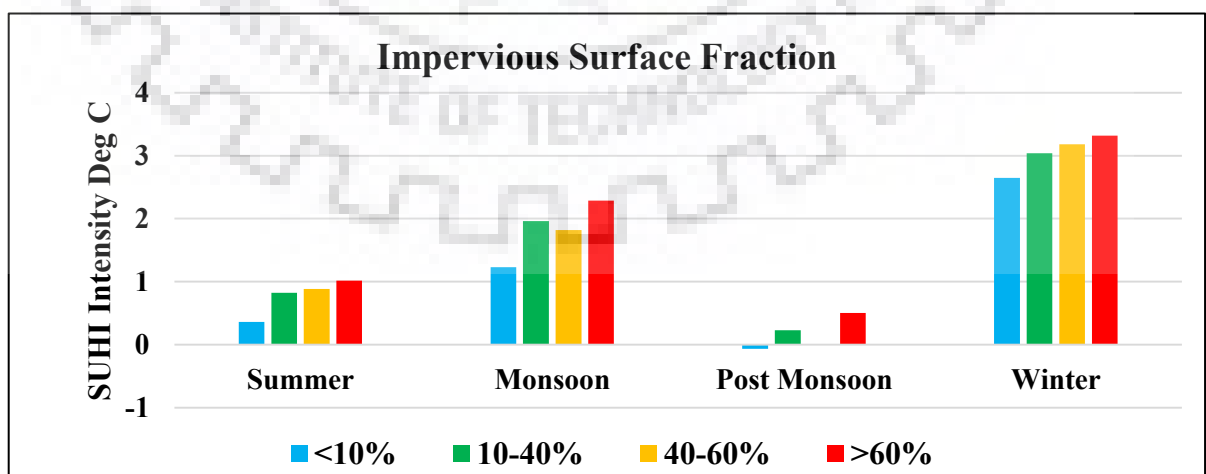


Figure 5-18: Impervious Surface fraction and SUHI Intensity

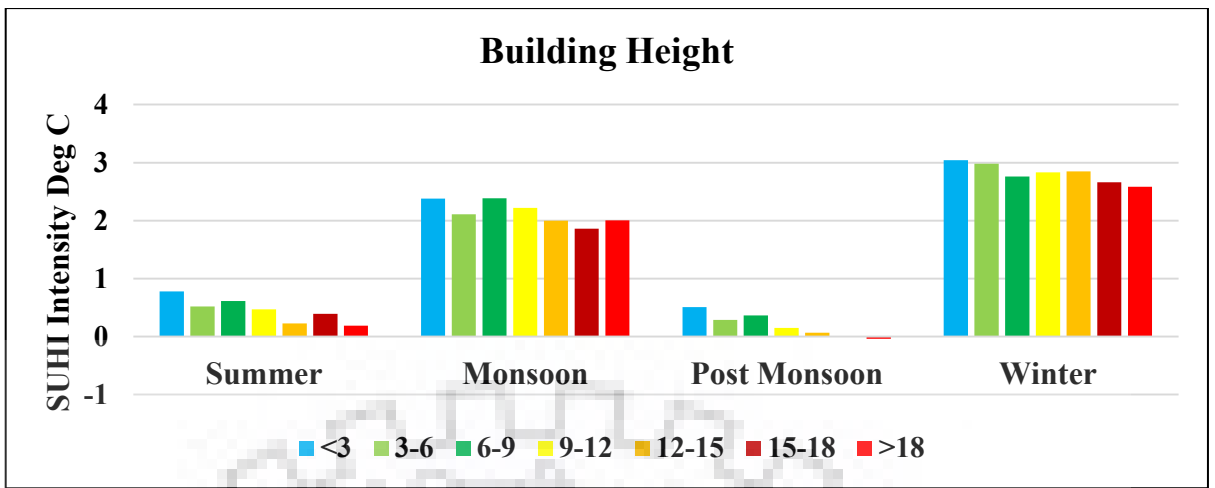


Figure 5-19: Building Height and SUHI Intensity

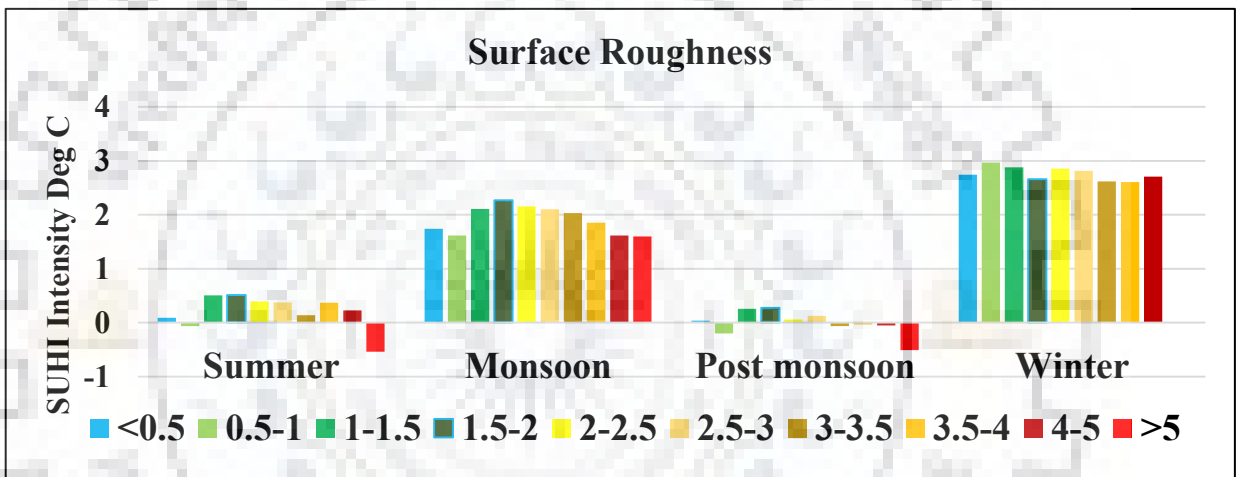


Figure 5-20: Surface Roughness and SUHI Intensity

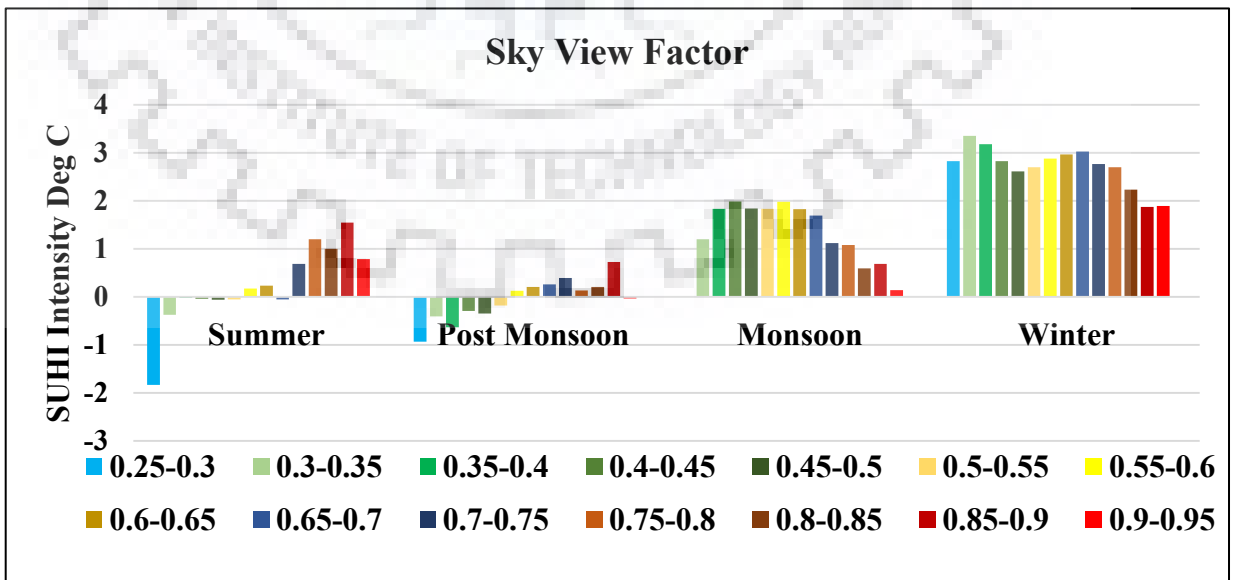


Figure 5-21 : Sky View Factor and SUHI Intensity

5.4.3 Diurnal- seasonal variability of Urban Heat Island Intensity

The diurnal variability of UHI intensities was computed by utilizing the WRF model outputs. The SUHI intensity was computed using Land Surface temperature while UCLHI was computed from temperature at 2m. The difference between urban and rural LST pixels were computed to obtain the spatial distribution of SUHII magnitude. The diurnal variability of SUHII for summer season (Figure 5-22) revealed that maximum SUHII was observed at 5:30 IST whereas minimum SUHII value were observed during daytime at 11:30 IST and 14:30 IST. As a matter of fact, urban area displayed cool island effect at 11:30 IST and 14:30 IST. It clearly shows that the study area experiences more intensity of SUHI during night time as compared to day time in summer season. Since, urban areas displayed lower temperature as compared to its surrounding at 11:30 AM time, the time of Landsat TIRS (pass time ~ 11AM) raises concern for SUHI studies. This requires special attention in arid and semi-arid regions where the urban areas are generally surrounded by sand or bare soil and heats up faster than urban built up. Similar observations were noted while studying the pattern of winter SUHII (Figure 5-24). However, significant differences were observed between summer and winter SUHII in magnitude and duration.

In summer season maximum magnitude observed is less than 0.8 degree while in winter season the difference is more than 1 degree. In summer season, prominent difference in SUHII is observed during night 2330 IST to 530 IST whereas in winter season difference of nearly 1 degree was observed throughout the nighttime from 1730 IST to 530 IST. In monsoon season (Figure 5-24), the pattern of SUHII varies during first day with almost nil value of SUHII. However, on second day, urban area displays more SUHII during evening time from 1430 hrs to 2330 hrs.

Diurnal variability in Canopy Layer Urban Heat Island Intensity (CLUHII) which is computed from model outputs of Temperature at 2m also displays similar pattern of UHI during winter (Figure 5-25) and summer (Figure 5-26) season as displayed by SUHII. However, in winter UCLHI displayed comparatively more magnitude as compared with winter SUHII. Monsoon season UCLHI displays cool Island on first day of simulation (Figure 5-27) while similar pattern as summer and winter season was observed on the second day of simulation. 1730 IST to 2030

IST displayed higher magnitude of UCLHI (Nearly 1 degree) while till morning time the magnitude is much smaller.

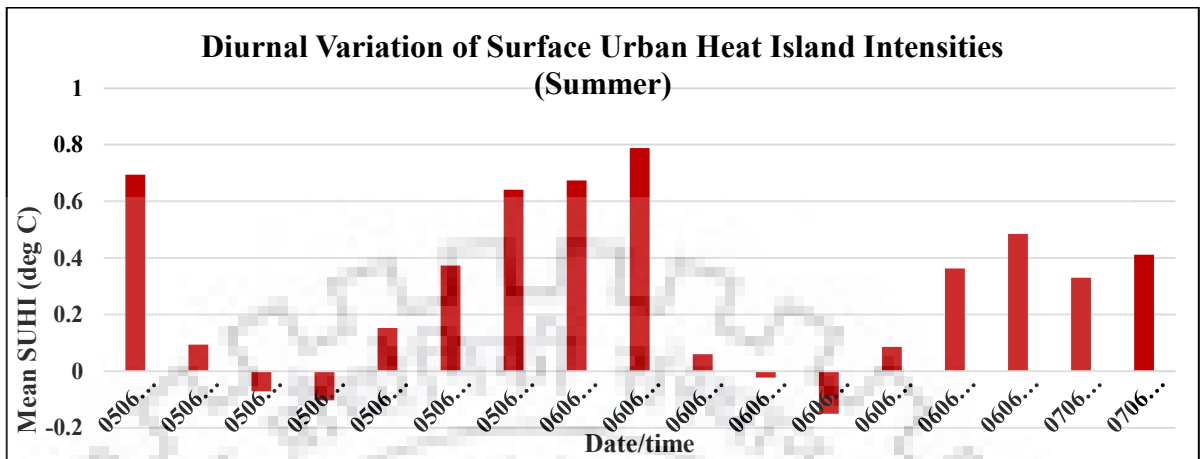


Figure 5-22: Diurnal variability of Surface Urban Heat Island Intensity in Summer Season

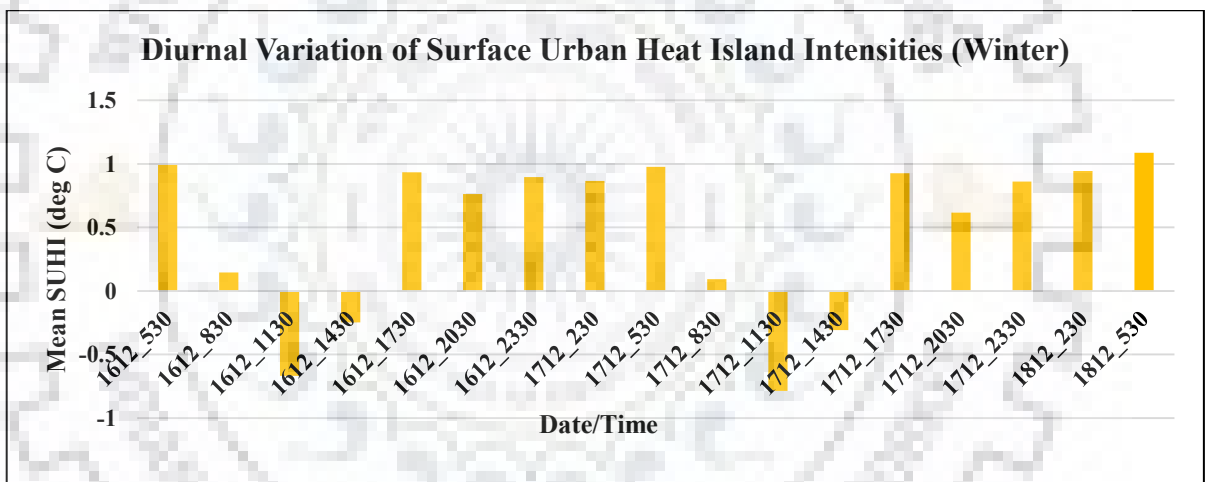


Figure 5-23: Diurnal variability of Surface Urban Heat Island Intensity in Winter Season

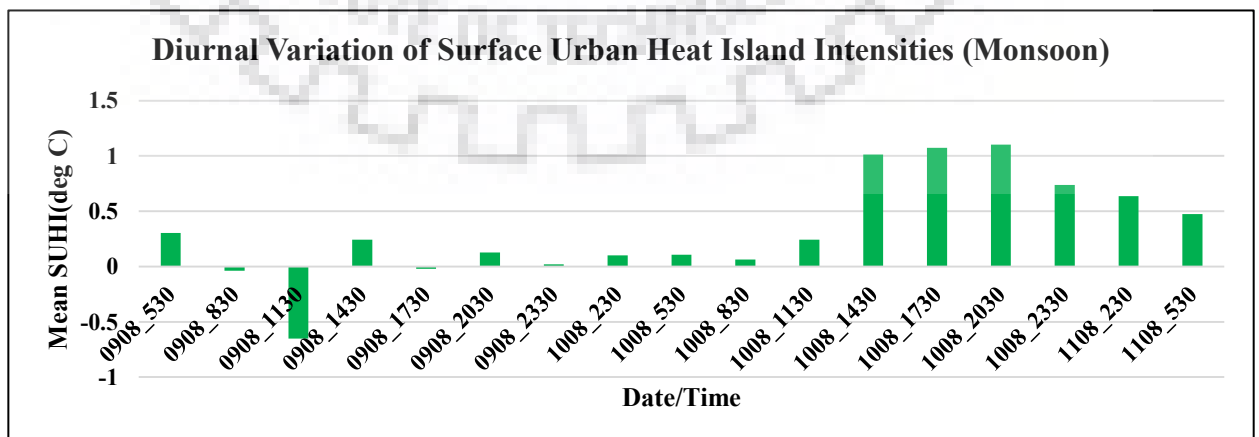


Figure 5-24 : Diurnal variability of Surface Urban Heat Island Intensity in Monsoon Season

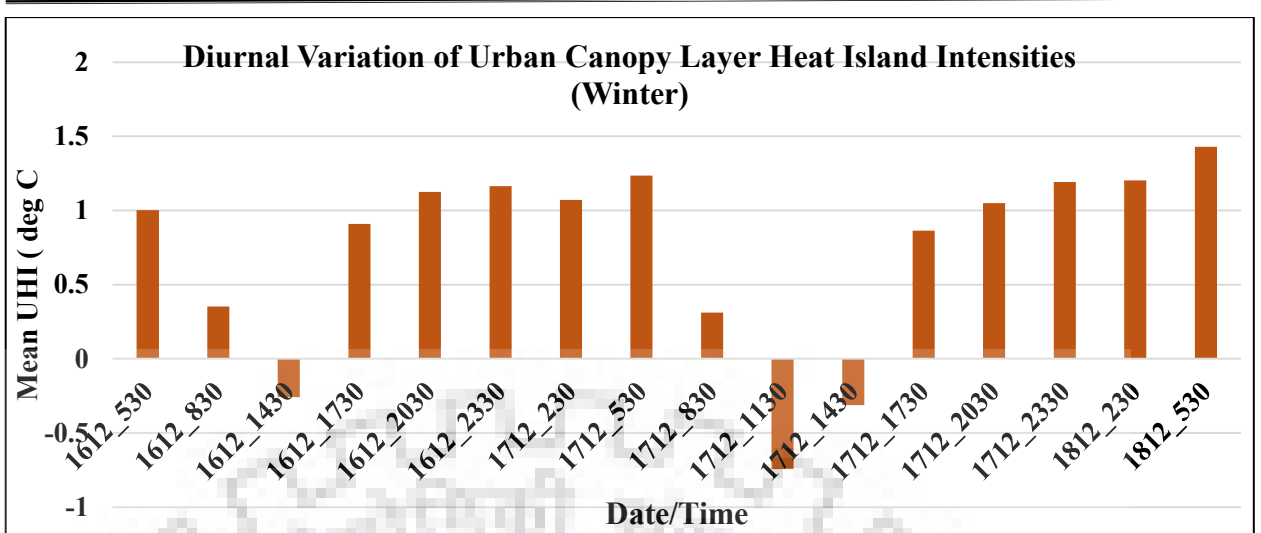


Figure 5-25: Diurnal variability of Canopy Layer Urban Heat Island Intensity in Winter Season

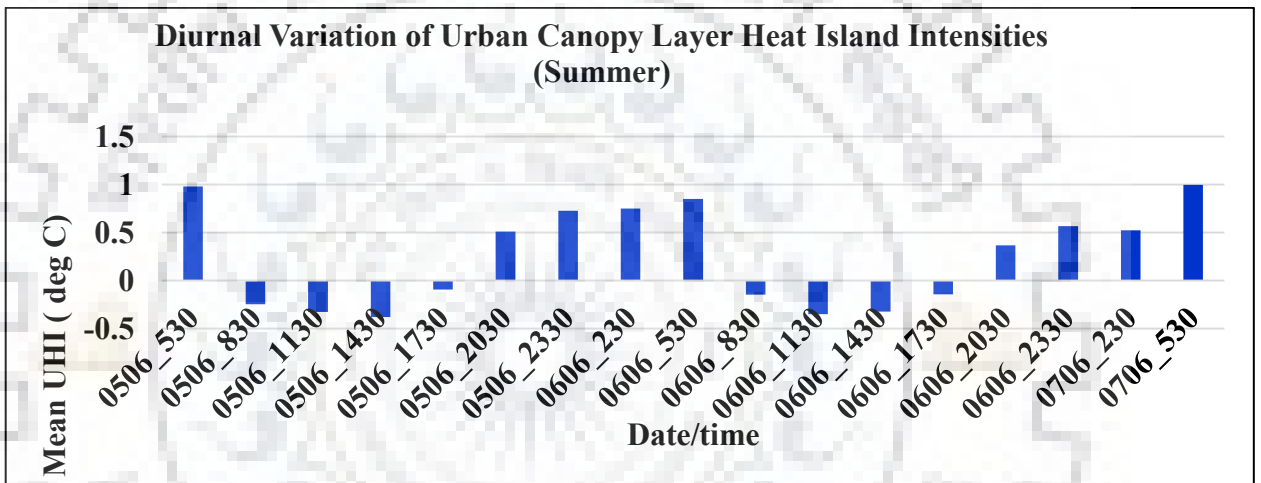


Figure 5-26: Diurnal variability of Canopy Layer Urban Heat Island Intensity in Summer Season

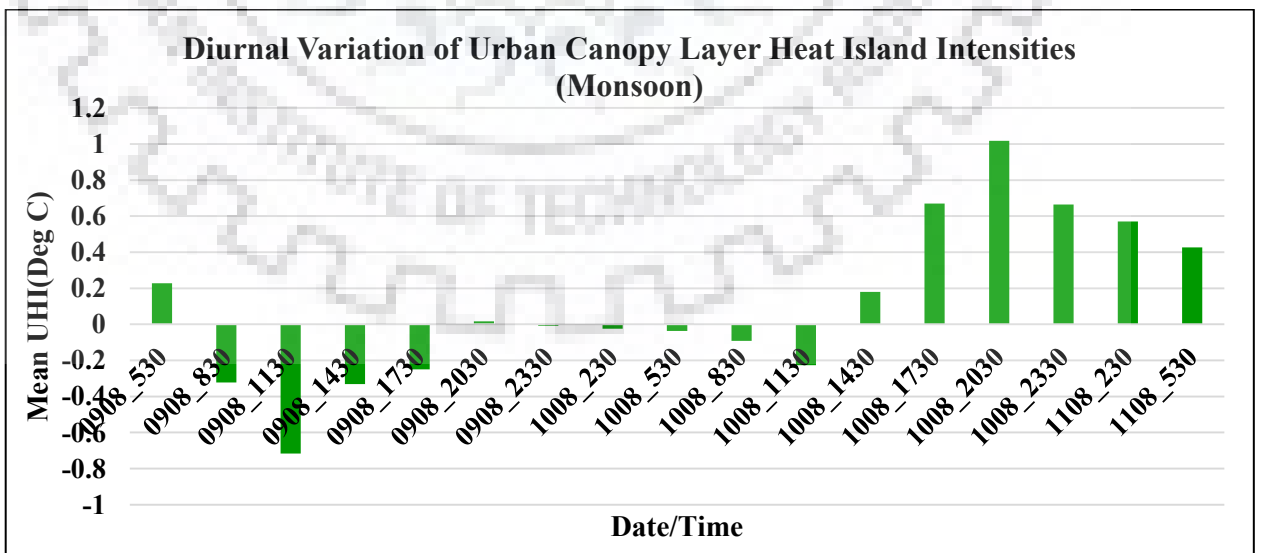


Figure 5-27 : Diurnal variability of Canopy Layer Urban Heat Island Intensity in Monsoon Season

5.4.4 Methodological and operational concerns

5.4.4.1 Land Surface Temperature from Landsat TIRS

The data of Landsat TIRS is acquired at 100m spatial resolution, however, the data product is provided at already oversampled resolution of 30 m using cubic convolution interpolation method (USGS, 2018). The oversampling creates redundant information and consist of mixed pixels, it introduces biasness in the studied correlations.

It is assumed that derived LST maps has consistent observation across all LULC units and uncertainties in extraction of LST values are not more than 1-2 K. However, this value is a rough estimate based on literature (Sobrino et al., 2004) and may have inter and intra scene variations. Thermal sensors measure LST indirectly by sensing upward longwave radiation from the Earth with a narrow angle of view. It is modulated by the atmospheric interaction, surface moisture and emissivity, near surface atmospheric conditions, turbulent transfer and sensor viewing angle. Therefore, atmospheric corrections and accurate estimation of surface emissivity plays a major role in precise estimation of LST. The estimation of these two parameters with strong precision is quite difficult considering the large coverage of satellite sensor. The estimation of surface emissivity assumes a large area to be homogeneous while urban regions are highly heterogeneous and do not display isothermal properties. This creates a substantial gap between LST and air temperature which is highly influenced by the turbulence and wind flow in the surroundings. Hence, the validation of LST is challenging with ground measurements as the relationship between air temperature and LST is still not fully known (Zhou et al., 2019).

Besides, the nadir viewing geometry of TIRS sensor oversamples the horizontal urban surfaces but 3D vertical surfaces are not well represented in these datasets. Hence, a large section of active urban surfaces is not discerned and it creates biasness in correlation statistics. It is evident from the discussion that LST from thermal sensors is not optimal for analyzing the relationships with UCPs, however in the absence of alternative datasets, this is the only data which provides the spatially variable information on LST. Alternative approaches needs to be developed for the integration of LST and air temperature as well as to obtain 3D temperature data cube in urban areas for improved understanding of temperature variation due to heterogeneous urban areas (Voogt et al., 1997).

UHI is a relative phenomenon and it is generally defined as urban–rural temperature difference, its identification is majorly governed by surrounding land cover and their thermal properties.

However, urban area takes time to accumulate heat due to shading of buildings on other buildings and narrow street canyons which restricts the access of solar radiation. Besides, the thermal mass as well as the time lag required to heat the built mass also slows down the heating of urban built areas as compared with the surrounding bare soil and bare rock areas especially in arid and semi-arid regions. Hence, at the time of pass of Landsat satellite especially in arid and semi-arid regions, urban area exhibits lower temperature as compared to its surroundings. The SUHI phenomenon calls for more research in order to achieve detailed understanding in these regions.

5.4.4.2 Validation of WRF model Outputs

Validation of WRF model outputs with point observation data of IMD revealed strong correlation in summer and winter season but moderate correlation in monsoon season for temperature at 2m. The moderate correlation in monsoon season needs further investigation as it may be due to absence of convective rainfall mechanism prevalent in tropical and semi-tropical regions. Relative humidity has provided strong correlation in all the seasons but wind speed displayed poor correlation in summer and monsoon and strong correlation in winter season. The lower values of correlation in wind speed may be due to broad class approach which have adopted. Here, a broad 3-class urban LULC have been ingested in the model with single roughness value for each class. Since, wind is a dynamic phenomenon and highly modifiable due to roughness characteristics of terrain, inclusion of detailed roughness UCPs such as gridded surface roughness, zero plane displacement height and frontal area index may provide improved wind speed.

The validation of MODIS LST with WRF LST revealed that a large percentage of pixels falls under $\pm 1^{\circ}\text{C}$ (~86% in summer, ~68% in monsoon and winter). More than 80% of the pixels exhibit temperature within $\pm 2^{\circ}\text{C}$ in all the seasons. It shows a high correlation of WRF LST with MODIS LST and is indicative of reasonable accuracy of WRF model simulation. In future, further downscaling of climate indicators ~ 100-200 m grid resolution may also be attempted. However, the simulation run time also needs a serious consideration for operationalization of high resolution simulations for weather forecast and predictions in urban environments.

5.4.4.3 Grid size of WRF model outputs

WRF model is a mesoscale model which provides capabilities for downscaling of met variables at urban scale. Although grid sizes of 200 m has also been tested, most of the studies have downscaled upto 500 m grid size. In this study also, downscaled outputs at grid size of 500 m

have been utilized for assessment of diurnal variability of SUHI intensities. Although, it is considered as quite a high resolution, it is still coarse with respect to the scale of the UCPs. The assessment of relationship of UCPs with model outputs required upscaling of UCPs to 500 m grid size which may have resulted in significant loss of heterogeneity and information. However, in future, further downscaling of WRF model outputs up to 10s of meter scale through coupling with high resolution urban scale climate models (for example large eddy simulation models etc.) may be attempted. The spatially variable outputs thus obtained may be utilized for understanding the relationship with UCPs. However, use of these models for operational purpose for downscaling of climate variables to high resolution micro scale require number of days for completion of one simulation. Hence, optimization of models or increase in computing resources is required for downscaling at high resolution grid size.

5.5 SUMMARY

The spatially variable climate indicators for the assessment of relationship with UCPs were obtained from Landsat 8 TIRS and WRF simulations. LST from thermal remote sensing have been employed extensively for assessment of relationship with 2D urban characteristics mainly impervious surface area, vegetation fraction and LULC. However, the relationship with 3D urban characteristics is largely unexplored all over the world especially no such kind of study exists for the study region Hence, in this study, the relationship of 3D UCPs with LST such as building height, Sky view factor, height-to –width ratio, complete aspect ratio etc. have been also carried out in complex urban environment of Delhi, a city in the developing world.

The primary results of UCPs-LST relationship revealed strong correlation with 2D UCPS while 3D UCPs other than building height and surface roughness length did not show strong correlation. This finding is consistent with the findings of Berger et al (Berger et al., 2017a) and it may be attributed to the nadir viewing geometry of Landsat 8 TIRS sensor and oversampling of thermal measurements from 100m to 30m. For assessment of relationship with 3D UCPs, complete 3D temperature data cube in horizontal as well as vertical direction may help in analyzing the relationship.

New approaches need to be developed for derivation/simulation of complete 3D temperature data cube by integration of in-situ field observations, thermal remote sensing and numerical modelling. The key UCPs which exhibited strong relationship with LST were utilized to analyze the variability of SUHI intensities across all four seasons in a year. SUHI intensities were found to be maximum during winter season while lowest during post-monsoon season across all UCPs.

Diurnal variability of SUHI and UCLHI intensities in the study region revealed more UHI during nighttime to morning time, however during daytime urban area exhibited lower temperature from mean temperature mostly at 0830 and 1130 AM. The downscaling of met variables at urban scale by WRF model simulations have been carried out at 500m grid resolution which is still a coarse resolution considering the scale at which UCPs have been generated. In future, further downscaling of climate indicators by coupling the WRF model with high resolution urban climate models may help in obtaining high resolution climate variables.

Chapter 6 presents few applications of UCPs in complex urban environment of the study region and their relationship with spatially variable climate indicators.





CHAPTER 6

APPLICATION OF URBAN CANOPY PARAMETERS FOR URBAN CLIMATE STUDIES

6.1 INTRODUCTION

Urban morphology influences the local urban climate through morphological characteristics. Numerous studies have proven that quantification of urban morphological characteristics or urban canopy parameters could be utilized for simulation of wind and thermal environment in urban area (Ng, 2011; Ng et al., 2011). Urban Canopy Parameters (UCPs) derived from remote sensing have the advantage of wider coverage and easy availability, the potential that can be harnessed to derive the urban morphological characteristics even in the developing world. UCPs have been employed for various applications in the field of urban climate research and modeling. For example, they have been utilized to simulate the wind environment to assess the pedestrian level wind velocity ratio (Raasch & Schröter, 2001) while (Lindberg et al., 2008) developed SOLWEIG model to simulate the thermal environment.

The aerodynamic UCPs such as surface roughness length, zero plane displacement height, frontal area index estimated through morphometric methods and 3D GIS database have been utilized widely for derivation of potential corridors for ventilation in urban areas (Gal & Sumeghy, 2007; Gál & Unger, 2009; Suder & Szymanowski, 2014; Wicht et al., 2017; Wong, Nichol, To, et al., 2010b.; Yuan et al., 2014). Adequate natural ventilation in urban area is known to mitigate UHI effect and also impacts the dispersion of air pollutants from urban areas (Grimmond & Oke, 1999; Shishegar, 2013). Similarly, UCPs and ventilation path map have been employed for developing the urban climatic map (Chen & Ng, 2011; Ren et al., 2011; Xu et al., 2017). The urban climatic map is based on assessment of thermal and ventilation environment in urban areas, which is further utilized to identify climate responsive urban planning strategies for climate resilient urban environs (Alcoforado et al., 2015; Ren, Ng, & Kaztschner, 2009; Xu et al., 2017). More than 30 countries have developed urban climatic map, however, these effort were mainly concentrated in developed world (Ng, 2011).

To overcome the limitation of standard urban classification system for urban climate research, a Local Climate Zone (LCZ) scheme was developed on the basis of urban structure, urban geometry, urban morphology and anthropogenic heat emission (Stewart & Oke, 2012). Although this scheme is defined primarily for UHI studies, it has been widely used for urban climate

research worldwide. The scheme consist of 10 urban built form classes and 7 land cover classes. The details of this classification system is given in section 2.6.4. It defines geometric and surface cover properties for each LCZ class by defining specific range for a few of the UCPs such as building surface fraction, impervious surface fraction, pervious surface fraction, aspect ratio (height-to-width ratio), sky view factor, height of roughness elements, surface albedo and terrain roughness class(Stewart & Oke, 2012). UCPs derived either from 3D GIS database or remote sensing data have been utilized to derive LCZ map (Geletič & Lehnert, 2016; Mitraka et al., 2015; Unger et al., 2014). World Urban Database and Access Portal Tools (WUDAPT, www.wudapt.org) also adopts LCZ classification system to generate the worldwide level 0 database of urban form and function by employing freely available data sources and software (Bechtel et al., 2015; Gerald Mills et al., 2015). However, applicability of method in complex urban environment needs investigation as the method have been reported to deliver lower accuracy in as study conducted in dense urban environment of Hong Kong (Ren et al., 2016) . The generated LCZ maps have been utilized for mesoscale climate modeling in Weather Research and Forecasting (WRF) model for improved simulations (Brousse, Martilli, Foley, Mills, & Bechtel, 2016; Jason Ching et al., 2009; Hammerberg et al., 2018). Detailed and gridded UCPs have also been ingested directly for mesoscale modeling of urban climate in WRF model (Chen et al., 2011; Jason Ching et al., 2009). However, no such study exists in the developing world especially in Indian context primarily due to unavailability of up-to- date and spatially variable UCPs information.

This study has retrieved number of UCPs from optical stereo satellite data for complex urban environment of Delhi, the results of which have been presented in Chapter 4. The retrieved UCPs can be applied for number of urban climate applications as discussed above. However, in this study, the retrieved UCPs have been employed to demonstrate few applications such as ventilation path assessment and GIS based Local Climate Zone. In near future, derived ventilation path map may be employed for preparation of urban climate map and GIS based LCZ map may be ingested in WRF model for improved urban scale climate modeling.

This chapter describes the brief introduction to the few of the major applications of UCPs, methodology for the derivation of ventilation assessment map and GIS based LCZ classification map, derived ventilation assessment map, its relationship with spatially variable climate indicators, derivation and accuracy assessment of LCZ maps derived by employing WUDAPT methodology and GIS based methods and relationship of LCZ map with Land Surface

Temperature(LST), discussion on inherent issues faced in application of UCPs and various aspects of the utilization of UCPs for climate applications.

6.2 METHODOLOGY

As discussed above, numerous applications have been carried out by employing remote sensing derived UCPs for urban climate studies and research. Out of these applications, two applications i.e. Ventilation path and GIS based LCZ classification have been demonstrated in this study. This section describes in detail the methodology adopted for ventilation assessment and GIS based LCZ classification in study area. The generated ventilation path map and LCZ map was further analyzed to assess their relationships with climate indicators available through processing of Landsat 8 TIRS and WRF simulations as described in Chapter 5.

6.2.1 Ventilation assessment map

Urban built-up is perceived as the roughest surface (Suder & Szymanowski, 2014) and their aerodynamic roughness properties affects the wind flow patterns at micro scale. The altered wind flow pattern has an impact on micro scale temperatures patterns and air flow within the urban canopy (Al-Sallal & Al-Rais, 2012; Oke, 1988; Shishegar, 2013). It also has significant impact on thermal comfort and stress in urban areas. The decreased wind flow in urban built-up is also considered as one of the major factor for the formation of UHI and increased levels of air pollution in urban areas (Oke, 1987; Oke et al., 2017). Since, more than 50% of world population lives in urban areas, hence, proper management of the development in urban areas to ensure effective ventilation can help in mitigating the UHI and air pollution in urban built-up.

The recent studies on urbanization reveals that developing world especially Asian, African and Latin American countries are going through the phase of rapid urbanization and are likely to witness more and more urbanization in near future (DESA/UN-WUP, 2018). However, most of the urban climate studies and research is still focused on developed world leave alone ventilation assessment studies. Most of the developing world cities are situated in tropical and sub-tropical climate region where wind flow management along with management of solar access can greatly improve the thermal comfort for urban inhabitants (Emmanuel, 2016). The studies on ventilation assessment in developing world can pave way for better management of urban climate besides it may assist in mitigating the impact of global climate change (Ng et al., 2011).

The identification of natural ventilation requires large scale aerodynamic modeling (Wicht & Wicht, 2018; Wong, Nichol, Y Ng, et al., 2010). Physical modeling through wind tunnel studies

and numerical modeling through CFD models provide data for airflow in urban canopy layer (Chang, Jiang, & Zhao, 2018; Moonen et al., 2012; Oke et al., 2017). However, they are expensive, time consuming and most of the studies are limited to small area coverage due to requirement of high end facilities or computational resources. Similarly, micrometeorological methods for the wind and air quality studies require vast network of ground observations in urban area to characterize the heterogeneous urban environment (Jhaldiyal et al., 2018). The installation of vast network of met towers and their maintenance is resource consuming. Besides, the acquisition of data over large urban regions therefore is a major challenge and not practically feasible. Further, the rapid changes in urban area requires continuous monitoring and quick evaluation. It was stated that for planners a rough understanding of urban morphological characteristics impacting the wind environment can be a useful method for rapid assessment of wind environment (Yuan et al., 2014). Hence, morphometric methods have been widely utilized for identification of potential ventilation path and ventilation assessment.

6.2.1.1 Identification of Input parameters

For determination of ventilation profile, morphometric methods are applied widely (Gal & Sumeghy, 2007; Gál & Unger, 2009; Ng et al., 2011; Wicht et al., 2017; Wong, Nichol, To, et al., 2010; Wong, Nichol, Y Ng, et al., 2010). Numerous methods were developed in last few decades and each one has its own limitations and assumptions. A number of indicators have been proposed for analysis of natural ventilation in urban area: density, rugosity, porosity, sinuosity, occlusivity, compactness, continuity, solar admittance and mineralization (Adolphe, 2001). The building height and width depending on the wind direction was considered to estimate rugosity, however, this study was limited to small neighborhood. Surface roughness length derived from logarithmic wind profile have been considered as one of the indicator for assessment of natural ventilation in urban areas. However, the basic assumption in the morphometric methods as stated by Macdonald (Macdonald et al., 1998) is *“It is assumed that there is negligible wake interference between surface obstacles and that the mean velocity profile approaching each obstacle is logarithmic”*. These models are valid only when frontal area density is low (0.3-0.5). Recirculating flow is promoted among obstacles with increased roughness interference. Hence, it is argued (Macdonald et al., 1998; Yuan et al., 2014) that displacement height should also be included for ventilation assessment in densely built urban areas. Therefore, zero plane displacement height and surface roughness length as derived in Chapter 4 have been utilized for the ventilation assessment in study area. For computation of z_d the approach proposed by Gal and Unger (Gál & Unger, 2009) have been applied on a gridded data set. The simple thumb of

rule approach (Grimmond & Oke, 1999) have been applied for the computation of surface roughness (z_0) as discussed in 4.3.14.

6.2.1.2 Ventilation assessment map

Following criteria have been defined for mapping ventilation paths based on Verein Deutscher Ingenieure (VDI), 1988 and 1989 (standards by Association of German Engineers) for Munich, Germany (Matzarakis & Mayer, 1992):

- a. Aerodynamic surface roughness length lower than 0.5 m
- b. Negligible zero plane displacement height which is considered as less than 3
- c. Sufficient great length in one direction , at least 1000m
- d. Sufficient great width, minimum width is double to four times the height of the lateral obstacles, but at least 50 m
- e. The edges of ventilation paths should be comparatively smooth
- f. The width of obstacles, such as single buildings or tall trees, in a ventilation path should not be greater than 10% of the width of the ventilation path.
- g. The height of an obstacle in a ventilation path should not be greater than 10 m.
- h. An obstacle in a ventilation path should be oriented in such a way that its greatest width is parallel to the axis of ventilation path.
- i. Any single obstacle within a ventilation path should have a ratio of height to obstacle to horizontal distance between two successive obstacle of 0.1 for building and 0.2 for trees.

These guidelines have been adopted by many researchers for the identification of ventilation corridors in their respective study areas (Gál & Unger, 2009; Jhaldiyal et al., 2018; Wicht et al., 2017). Since, no other guidelines are available in literature, these guidelines were adopted in this study for ventilation assessment. Based on the above guidelines, both z_0 and z_d maps were resampled to 50 m to adhere to the minimum width criteria of 50m. Further they have been reclassified (Table 6-1) based on the criteria described by (Matzarakis & Mayer, 1992).

For integration of z_0 and z_d map, the raster based additive method were employed on reclassified maps in defined ranges. Since, the entire data of UCPs was in raster, regular mesh of 50 m was applied to ease the additive process in raster. Further, the additive combinations (11- ventilated area, 12, 21, 22 and 31- Partial ventilation and 32- Weak Ventilation) were reclassified in three ventilation classes as described in Table 6-1.

Table 6-1: z_0 and z_d classification for Ventilation assessment (Source: Matzarakis and Mayer, 1992)

Value Range	Reclassified Value	Value Range	Reclassified Value	Class Name
$z_0 \leq 0.5$	10	$Z_d \leq 3$	1	Ventilated
$0.5 < z_0 \leq 1$	20			Partially Ventilation
$z_0 > 1$	30	$Z_d > 3$	2	Weak Ventilation

6.2.1.3 Ventilation –UCPs and Ventilation- climate indicators relationship

To analyze the relationship between ventilation assessment map, UCPs and climate indicators, stratified random sampling was carried out and more than 600 random points were generated. Only those UCPs which is found to have strong relationship with LST were utilized to understand the relationship with ventilation classes. The climate indicators generated from Landsat 8 TIRS data (Land Surface Temperature) and WRF simulations (Land Surface Temperature, Temperature at 2m and Wind speed) have also been utilized for analyzing the relationship between climate indicators and ventilation assessment map.

6.2.2 Local Climate Zone map

The WUDAPT method for Local Climate Zone (LCZ) have been adopted worldwide by utilizing freely available datasets and software. The method proposed collection of training samples for each LCZ class through crowdsourcing where interested individuals across various countries collect training samples from Google Earth based on their local knowledge of the area (Bechtel, et al., 2017). It was found that experience and interpretation capabilities of individuals and poor understanding of LCZ scheme were few of the reasons responsible for large discrepancies and poor to moderate quality of LCZ maps (Bechtel, et al., 2017). In highly dense and complex urban settings of Hong Kong, this method did not yield reasonable accuracies (Ren et al., 2016). An alternative approach may be needed to prepare good quality LCZ maps especially in developing world with high density urban developments. A 3D data based approach employed by utilizing UCPs (Sky View Factor, building density, impervious and pervious surface fraction, building/tree height and surface albedo of urban morphology) to derive the LCZ classification (Geletič & Lehnert, 2016; Mitraka et al., 2015; Unger et al., 2014) displayed high accuracy. The major requirement of this method is the availability of precise GIS data of study area under consideration. Hence, in this study LCZ maps have been derived both from WUDAPT

methodology and GIS based LCZ mapping method and an accuracy assessment have been carried out to evaluate the accuracy of both the methods.

This section describes the methodological steps for development of WUDAPT LCZ and GIS based LCZ map. It includes collection of training samples from Google Earth and classification in SAGA GIS for LCZ classification. The steps for derivation of GIS based LCZ classification includes derivation of input layers, modification of criteria ranges and classification output, which is followed by accuracy assessment of WUDAPT and GIS based LCZ.

6.2.2.1 WUDAPT Local Climate Zone map

The methodology as provided by WUDAPT portal is presented in Figure 6-1. It includes preprocessing of downloaded Landsat data, collection of training samples in Google Earth (GE) and classification in SAGA GIS.

Image Pre-Processing

Image pre-processing forms an integral and vital component of data processing workflow for image classification. The downloaded data of Landsat 8 from Earth Explorer website (Date of Acquisition: February 11, 2013) have been rectified to a common UTM (Universal Transverse Mercator) projection and WGS 84 datum and resampled using the nearest neighborhood algorithm and converted into format compatible with SAGA GIS.

Defining Region of Interest (ROI)

Region of Interest (ROI) is the area for which the classification needs to be carried out. ROI is defined in G by drawing a polygon around the study area of interest (Delhi UA) and further saving it as KMZ file for collection of training samples. The ROI file thus defined is then imported into SAGA GIS, which is an open source GIS software, where the file is projected in UTM WGS 84 coordinate system as shape file.

Digitizing the training areas

ROI file saved in SAGA GIS is again opened in GE to collect training samples for each LCZ class based on visual interpretation of Google Earth satellite data. For each class, 10-15 training samples needs to be collected by using polygon tool in GE. The minimum size of training samples is recommended to be a homogeneous neighborhood of 1 km x 1km (Bechtel et al., 2015). However, due to high heterogeneity of urban development and building configuration in the

study area, 1kmx 1km size of samples have not been found to be feasible for some of the LCZ classes such as compact high rise (LCZ 1), Open high rise (LCZ 4) and Large low rise classes, water(LCZ G) etc. It was difficult to find substantial tracts (nearly 1 sq km in size) of areas with homogeneous characteristics. Hence, training samples of 250x250m size have been collected wherever large size was not feasible. All digitized training samples have been saved in kmz file as per LCZ classification scheme guidelines.

Generation of LCZ classification using SAGA GIS

In SAGA GIS , a direct tool have been provided by WUDAPT for LCZ classification based on random forest classifier at a pixel resolution of 50 m. After providing the path of satellite data and training samples, the tool performs the LCZ classification. The classification output is saved as KMZ file in order to validate its accuracy in GE. A post classification majority filter of 200m radius have been applied to remove the salt and pepper effect from the LCZ classified output which is commonly seen in pixel based classifiers. This step assist in removing the fragmented effect and provides a smoothed output.

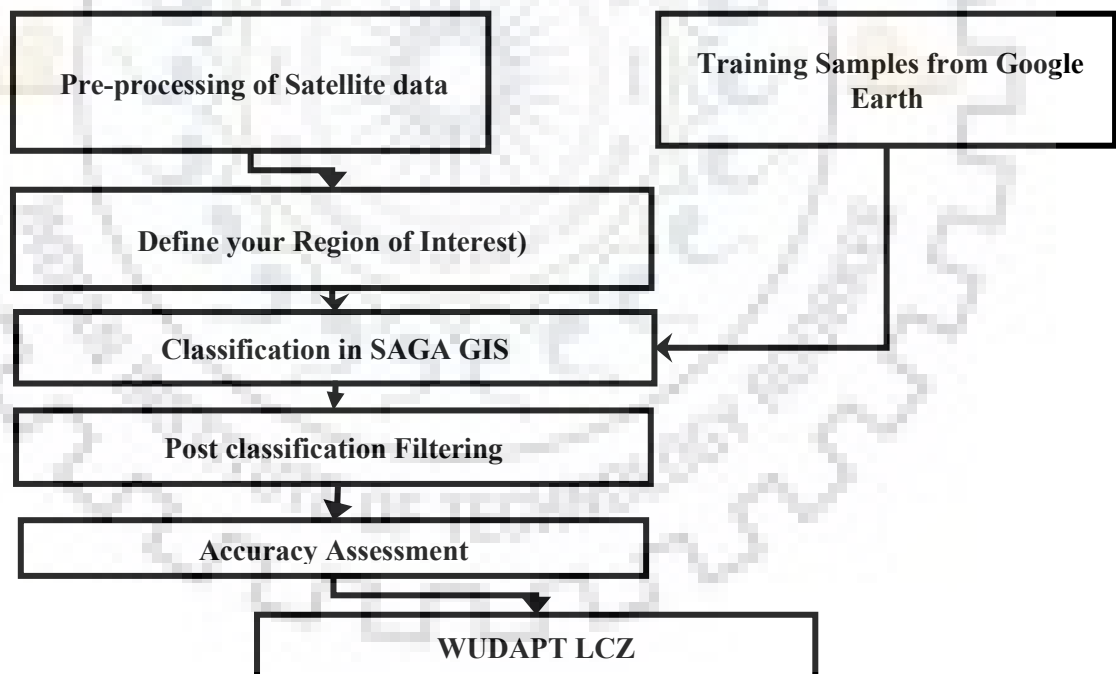


Figure 6-1: WUDAPT methodology for Local Climate Zonation Classification (adapted from www.wudapt.org)

6.2.2.2 GIS based Local Climate Zone map

This section describes the methodological steps for the derivation of GIS based LCZ classification. This method is also known as (Lelovics-gal) method. The methodology flow chart

is presented in Figure 6-2. The method utilizes number of UCPs such as Mean Building Height (MBH), Pervious Surface Fraction (PSF), Building Surface Fraction (BSF), Impervious Surface Fraction (ISF) and SKY View Factor (SVF). The other parameters such terrain roughness class, aspect ratio, and surface albedo could not be utilized as at the grid size of 50 m , averaging effect was too high and unique values for each LCZ class could not be obtained.

Derivation of input layers

All the input UCPs such as BFS, ISF, PSF, MBH and SVF have been retrieved as discussed in chapter 4 section 4.3 step by step. Further , all parameters thus identified have been brought to single resolution by applying different functions in GIS at 50 m spatial resolution grid in order to bring uniformity for step-by- step addition.

Modification of criteria ranges

Further, based on training samples collected from ground, the modification in ranges of each parameter from Stewart and Oke, 2012 have been carried out for each LCZ class to define the study area specific criteria ranges.

Derivation of GIS based Local Climate Zone classification

After modification of criteria ranges based on training samples from ground, all the layers have been reclassified according to the ranges defined. Since, there was an overlap in criteria ranges among some of the classes, a novel step-by-step methodology have been developed to obtain the final classification (Figure 6-2). In the first step, first six classes of urban built form (CHR, CMR, CLR, OHR, OMR, and OLR) have been derived using conditional tool in GIS by combining all input parameters. In the second step, the next two classes of urban built form (Large Low medium rise and sparsely built) have been derived based on criteria ranges from the above six classes of urban built form. Since, there was a significant overlap in the criteria ranges, the heavy industries class have been superimposed separately based on the visual interpretation of ortho image and information obtained from Master Plan of Delhi. Then, first four classes of land cover A-D (Dense Trees, Scattered Trees, Bush/Scrub and Low Plants) have been integrated based on differences in SVF and height ranges. The bare rock, bare soil and water land cover classes have been directly integrated from the LULC map. A majority filter have been applied on the classified output to remove the fragmented effect and to obtain the smooth product.



Figure 6-2: Methodology Flow Chart for GIS based Local Climate Zone

6.2.2.3 Accuracy Assessment

Accuracy assessment of both WUDAPT and GIS based LCZ map have been carried out with reference to the ground truth collected from the field. The care was taken to obtain uniformly distributed and homogeneous samples.

6.2.2.4 LCZ-LST spatio-seasonal relationship

Spatio- seasonal relationship between GIS based LCZ map and LST derived from Landsat 8 TIRS data have been analyzed to understand the LST-LCZ relationship. Stratified random sampling approach have been adopted to obtain random points for the analysis of relationship. Care was taken to represent each LCZ class by distributing the random points evenly across LCZ classes. Bias from Mean value of LST was computed to understand the spatial distribution of LST among LCZ classes.

6.3 RESULTS

This section presents the derived maps of ventilation assessment and WUDAPT and GIS local climate Zone map and their accuracy assessment.

6.3.1 Ventilation Assessment

Aerodynamic roughness parameters such as Surface Roughness length (z_0) and zero plane displacement height (z_d) have been utilized for deriving the ventilation assessment map (Figure 6-3). It is divided in three classes based on the criteria as discussed in section 6.2.1.2. The three classes are: ventilated, partially ventilated and blocked/weak ventilation. The area statistics of the classes (Table 6-2) revealed that ~76% of whole study region is ventilated whereas partially ventilated area covers 16.43% and weak or blocked ventilation covers merely 7.84% area. However, the distribution of ventilation classes in built-up area revealed a dismal picture as merely 17% of built-up area is classified as ventilated area. More than 45% area falls under blocked ventilation and nearly 38% area is partially ventilated. The lower percentage of ventilation in built-up area has significant consequences on thermal comfort as well as air pollutant dispersion in urban canopy layer.

Table 6-2: Area Statistics of Ventilation Assessment Map

Ventilation Class	Whole Area (%)	Built Up area (%)
Ventilated	75.73	16.81
Partially Ventilated	16.43	37.67
Blocked/ Weak Ventilation	7.84	45.52

The visual analysis of ventilation assessment map indicates that, there is no unobstructed and sufficiently long major breezeways which can provide adequate ventilation in the core areas of the city except river Yamuna. Even River Yamuna ventilation corridor is also not completely clear. Some small obstructions could be seen in the map in the form of connecting bridges. Most of the blocked could be seen in the northern and eastern part of the city. The East Delhi along river Yamuna is highly dense and closely packed built up with very narrow canyons and very high density. Few of the minor corridors could be seen in eastern part of development. It is to be noted that in the study region rather than building height, density of built-up has more impact on ventilation as high rise structures are just a small percentage of study area. Southern Delhi is less compact as compared to other parts, however, it is also partially ventilated. It may be due to narrow range of parameter range ($z_0 < 0.5$ and $z_d < 3$ for ventilated areas). Orientation of streets with respect to prevailing wind direction also has significant impact on mitigation of UHI and dispersion of air pollution, an aspect which needs to be thoroughly investigated in the study region. In this study z_0 was calculated based on height of roughness elements, however, in future,

development of automated tools for direction specific frontal area index may assist to analyze ventilation potential with respect to wind direction.

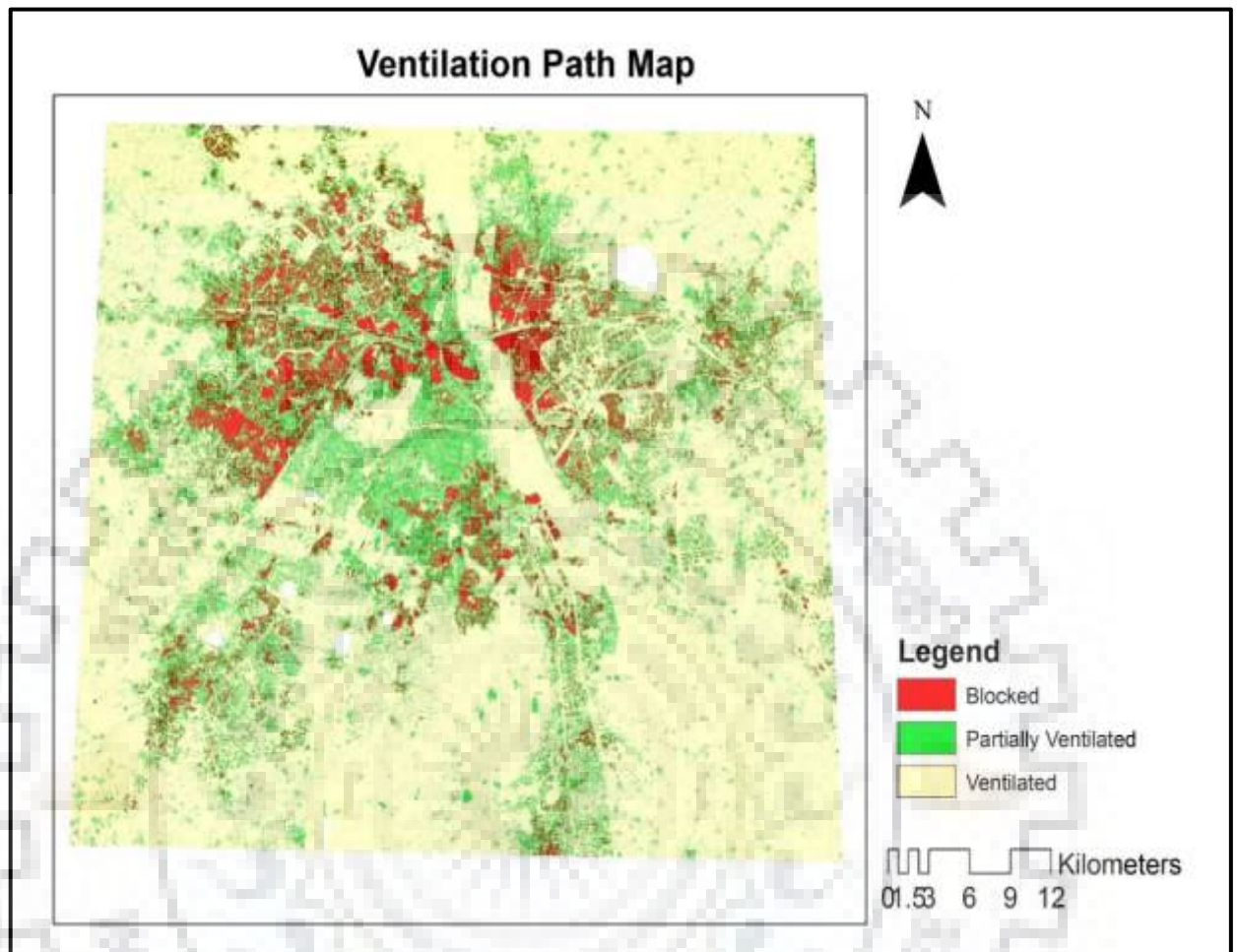


Figure 6-3: Ventilation Assessment Map

6.3.2 WUDAPT Local Climate Zone

The LCZ classification obtained through the application of WUDAPT methodology is presented in (Figure 6-4) and its area statistics is presented in Table 6-3. The low plants (LCZ D) consisting of agriculture and urban parks is the most dominant class in the study region comprising 55% of the area. The next dominant class is open low rise (LCZ 3- 9.42%) followed by compact low rise (LCZ6- 8.4%) and bare soil (LCZ F- 7.68%). However, at the time of ground truthing it was observed that compact low rise is the most dominant urban LCZ in the study region. The WUDAPT LCZ map also highlights that high rise structures are very few in the study area and the Delhi urban agglomeration in general has sprawled character. It has been observed that at the time of identification of training samples from Google Earth, the season of Landsat 8 image needs

to be taken care. Otherwise the seasonal variation in image characteristics and training samples may lead to highly poor classification of LCZ.

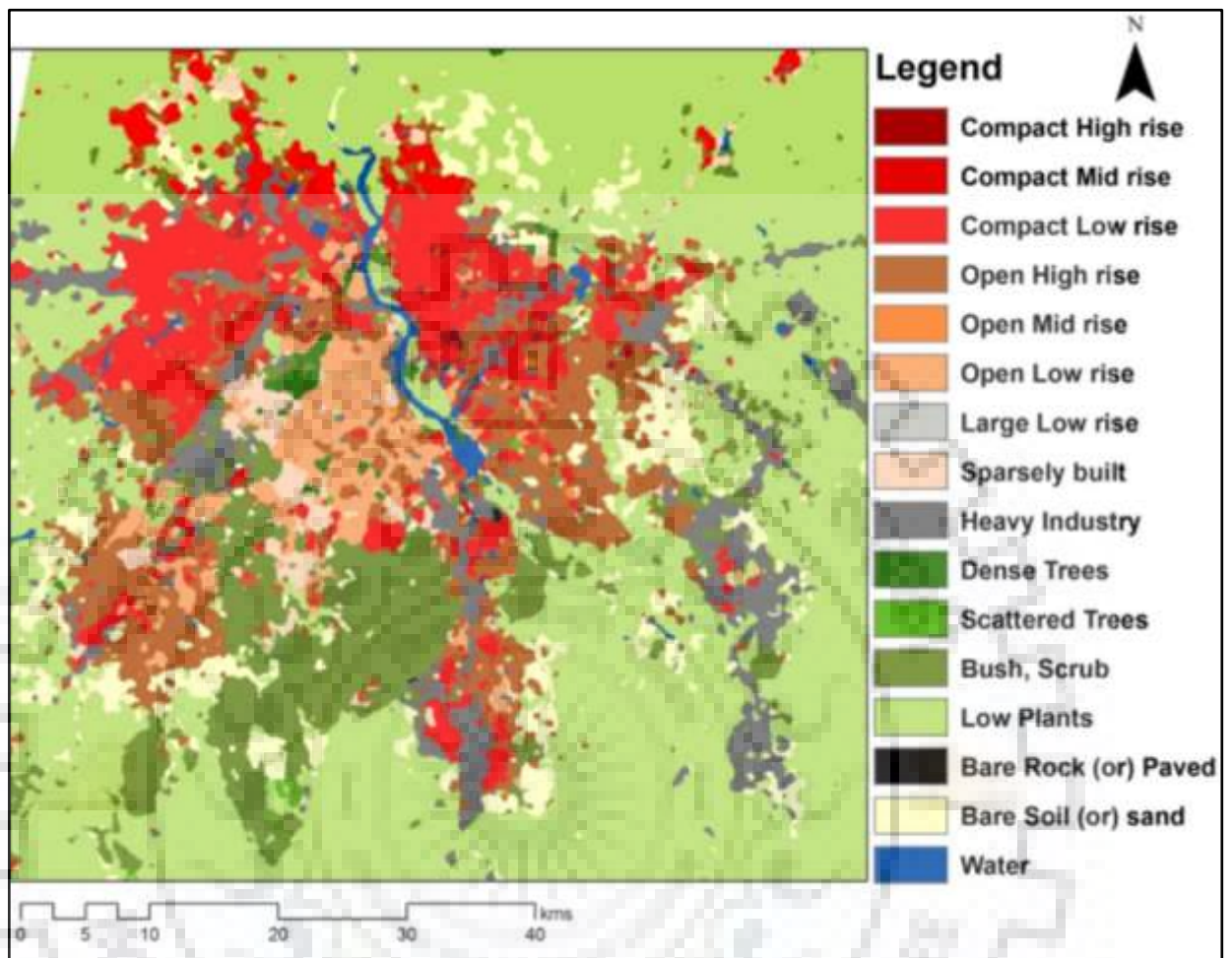


Figure 6-4: WUDAPT Local Climate Zone Classification

6.3.3 GIS based Local Climate Zone

GIS based LCZ map has been derived by combining various UCPs as discussed. In the first step, criteria ranges for each geometric and surface cover properties have been modified to obtain study area specific ranges based on training samples collected from ground. The UCPs layers reclassified according to modified ranges have been combined through raster additive process to obtain GIS based LCZ map.

Table 6-3: Percentage area of WUDAPT and GIS based LCZ classification

Class	Percentage Area	
	WUDAPT LCZ	GIS based LCZ
Compact high Rise (LCZ1)	0.21	0.09
Compact Midrise (LCZ 2)	0.46	1.80
Compact Low rise (LCZ3)	7.82	5.76
Open High Rise (LCZ4)	8.16	0.06
Open Midrise (LCZ5)	0.06	0.77
Open Low rise (LCZ 6)	2.83	4.36
Large Low rise (LCZ 8)	0.01	0.08
Sparsely Built (LCZ 9)	1.64	0.28
Heavy Industry (LCZ10)	5.41	1.00
Dense trees (LCZA)	0.85	1.85
Scattered Trees (LCZ B)	0.12	3.51
Shrubs (LCZ C)	7.64	3.73
Low Plants (LCZ D)	58.60	27.26
Bare Rock or Paved (LCZ E)	0.02	13.09
Bare Soil ((LCZ F)	5.44	35.31
Water (LCZ G)	0.76	1.0

6.3.3.1 Modified Criterion range for GIS based Local Climate Zone (LCZ)

Stewart and Oke, 2012 proposed specific ranges of different parameters (BSF, PSF, ISF, SVF, H/W ratio, height of roughness elements(HRE), albedo, thermal admittance and anthropogenic heat flux) for each LCZ classes. After a thorough examination of UCPs generated in the study region with respect to training samples collected from ground, it was deemed necessary to modify the ranges proposed by Stewart and Oke, 2012 to suit to the study region characteristics. The modified ranges along with original ranges is presented in Table 6-4. The upper portion in bold letters represents ranges as proposed by Stewart and Oke, 2012 and lower part in normal font represents the modified ranges. Few of the major changes which could be noticed are in the ranges of BSF and HRE or MBH. Compact low rise is comprised of significant part of study region and its density is very high ranging from 0.85- 1. The height of building in CLR and OLR also found to be nearly 12 m for 3 storey buildings. Hence, the range of BSF for CLR is modified to 0.85-1 and HRE is modified to 12m. The range of BSF for CMR and CHR is also modified as per the ground scenarios. It is to be noted that there is very less variation and high overlap in SVF among built-up LCZ classes due to averaging effect at 50 m. Similar averaging effect was observed in building height at 50 m grid cell due to very high heterogeneity and complex development in study region. The large low rise, sparsely built LCZ classes in the study region exhibited height in midrise height range of ~10-20m. Whereas Heavy industry class also

displayed higher height range than the range proposed by Stewart and Oke, 2012. Other notable differences could be observed in the value ranges of BSF, ISF and PSF for LCZ 8, 9 and 10. Since, LCZ 7 i.e Lightweight low rise was not present in the study region, it has been omitted from the classification.

Table 6-4: Modified Criteria ranges for Local Climate Zone*

Local Climate Zone (LCZ)	SVF	BSF	ISF	PSF	HRE/ (m)	MBH
LCZ1 Compact high-rise	0.2–0.4 0.2-0.65	40–60 50-90	40–60 50-80	<10 <20	>25 >25	
LCZ 2 Compact mid-rise	0.3–0.6 0.3-0.7	40–70 70-95	30–50 70-90	< 20 <30	10-25 12-25	
LCZ 3 Compact low-rise	0.2–0.6 <0.6	40–70 80-100	20–50 20-50	< 30 <20	3-10 2.5-12	
LCZ 4 Open high-rise	0.5–0.7 0.3-0.6	20–40 10-50	30–40 20-60	30–40 >20	>25 >25	
LCZ 5 Open mid-rise	0.5–0.8 0.5-0.8	20–40 10-40	30–50 20-60	20–40 >70	10-25 12-25	
LCZ 6 Open low-rise	0.6–0.9 0.4-0.6	20–40 <20	20–50 <30	30–60 >80	3-10 2.5-12	
LCZ 8 Large Low-Medium rise	>0.7 0.4-0.6	30–50 >80	40–50 >70	<20 <20	3-10 10-20	
LCZ 9 Sparsely Built	> 0.8 0.3-0.4	10–20 10-20	< 20 <20	60–80 >80	3-10 10-18	
LCZ 10 Heavy Industry	0.6–0.9 0.6-0.8	20–30 >70	20–40 >80	40–50 <20	5-15 10-35	
LCZ A (101) Dense Trees	<0.4 <0.65	<10 <10	<10 <10	>90 >90	3-30 >3	
LCZ B (102) Scattered Trees	0.5–0.8 >0.65	<10 <10	<10 <10	>90 >90	3-15 >3	
LCZ 103 Bush or scrub	0.7–0.9 >0.7	<10 <10	<10 <10	>90 >90	<2 <2	
LCZ 104 Low plants	>0.9 >0.9	<10 <10	<10 <10	>90 >90	<1 <1	
LCZ 105 Bare rock or paved	>0.9 >0.9	<10 <10	>90 >90	<10 <10	<0.25 <0.25	
LCZ 106 Bare soil or sand	>0.9 >0.9	<10 <10	<10 <10	>90 >90	<0.25 <0.25	
LCZ 107 water	>0.9 >0.9 <10	<10 <10 >90	<10	>90	-	

* Values in bold letters given by Stewart and Oke, 2012 and normal font represents modified ranges for each LCZ.

6.3.3.2 GIS based Local Climate Zone Classification

The modified ranges as described in Table 6-4 have been utilized to derive various LCZ classes by using a step-by step methodology as discussed in section 6.2.2. The final LCZ map thus prepared, is presented in Figure 6-5. The visual analysis of map highlights the dominance of bare soil and low plants LCZ classes.

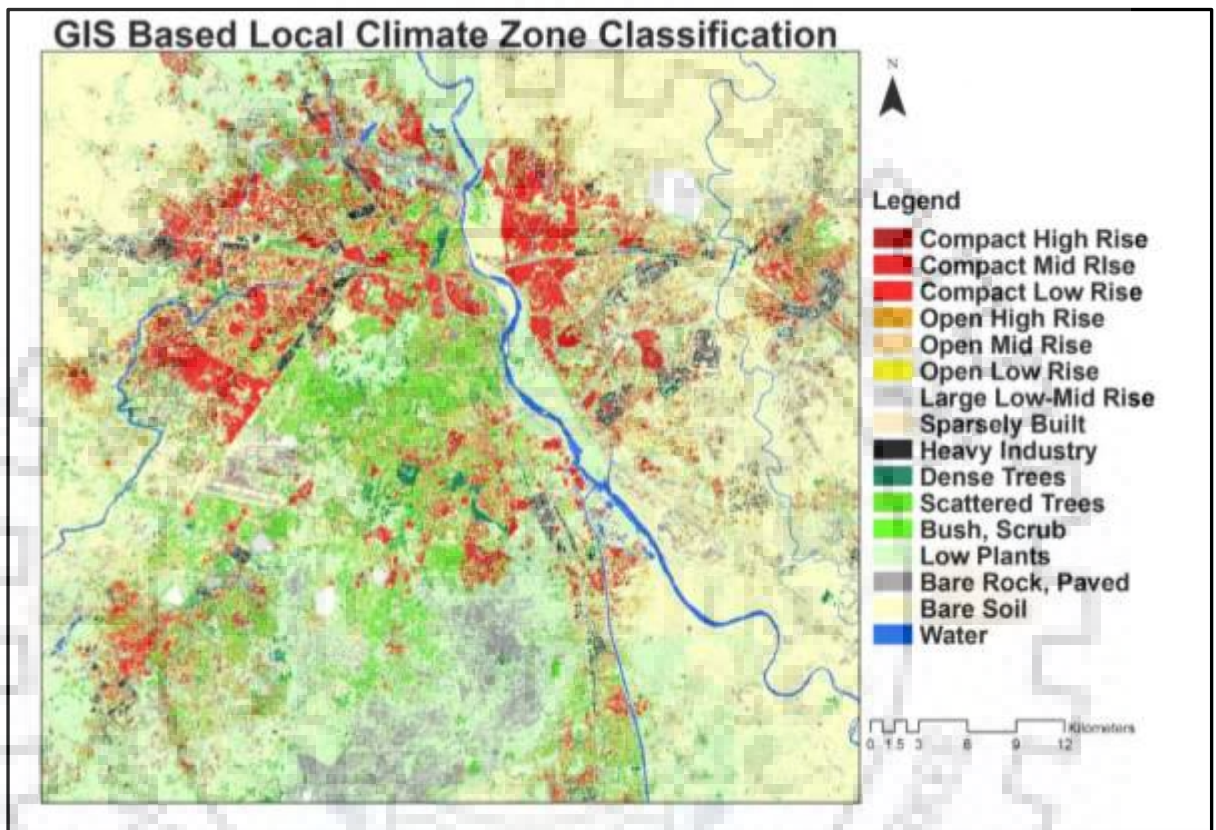


Figure 6-5: GIS based Local Climate Zone Classification

The area statistics of LCZ classes (Table 6-3) also ratifies the observation as bare soil and low plants covers approx. 63% of total study area. It is followed by the bare rock or paved class (~13%) which is further followed by compact low rise (~6%) and open low rise (~4%) LCZ classes. The area statistics of built-up LCZ classes (Table 6-5) from LCZ 1-10 reveals that compact low rise (LCZ3) and open low rise (LCZ 6) are the dominant built-up LCZ classes encompassing approx. 71% of built-up area. Next dominant class is compact midrise (LCZ 2) which covers approx. 13% of total built-up area. Heavy industries cover only 7% of total built-up area whereas large-low-midrise covers approx. 0.54% of built-up area. Large low-midrise class is mainly found in the form of upcoming shopping malls with large structures and high percentage of paved area. Compact high rise and Open high rise together forms only 1% of total study area which also is an indicative of sprawled urban built form of Delhi region.

Table 6-5: Area statistics of built-up GIS based Local Climate Zone

Class	Area (Sq Km)	Percentage Area	Class	Area (Sq Km)	Percentage Area
Compact high Rise	2.49	0.66	Open Low rise	115.18	30.65
Compact Mid rise	47.64	12.68	Large Low mid-rise	2.05	0.54
Compact Low rise	152.23	40.51	Sparsely Built	7.52	2.00
Open High Rise	1.65	0.44	Heavy Industry	26.51	7.06
Open Mid rise	20.47	5.45			

6.3.4 Accuracy Assessment

Application of WUDAPT methodology in a complex and highly dense built up of Delhi region had resulted in overall poor accuracy (49.43%) and kappa (0.46) statistics primarily due to poor accuracy of urban LCZ classes. It is mainly due to high heterogeneity and complex development in study region. However, it should be noted that accuracies of land cover classes from LCZ A-G found to be good enough with WUDAPT method (>70% except Bush, Scrub class).

Accuracy assessment of GIS based LCZ classification (Table 6-6) revealed reasonable accuracy (overall Accuracy >85% and kappa ~0.86). GIS based method delivered high accuracies of built-up LCZ classes (70-95%) as well due to utilization of high resolution and unique UCPs information of the study area. Even the land cover classes also exhibited high accuracies except bare rock class.

6.4 DISCUSSIONS

6.4.1 Criteria for Ventilation path assessment

Most of the studies for identification of ventilation path or assessment utilizes the criteria given by Matzarakis and Mayer, 1992 which is based on VDI, 1988 and 1989 defined by federal government of Germany (Andreas Matzarakis & Mayer, 1992). Since, there are no other available guidelines, this study also utilized the same guidelines for ventilation assessment in the study area. However, there is substantial differences in characteristics of climate region, urban development patterns and socio-economic status of Germany and the study region in developing world. The application of same guidelines may result in underestimation of ventilation potential in the study region. Hence, in future, studies needs to be undertaken to define unique ventilation assessment guidelines for different climate regions with varying development characteristics.

Table 6-6: Accuracy Assessment of WUDAPT and GIS based Local Climate Zone

LCZ Class	Accuracy (%)	
	WUDAPT LCZ Classification	GIS Based LCZ Classification
CHR (LCZ 1)	20.13	71.9
CMR (LCZ 2)	33.3	86.36
CLR(LCZ 3)	77.27	90.9
OHR(LCZ 4)	38.52	81.8
OMR(LCZ 5)	53.25	81.9
OLR(LCZ 6)	22.72	69.1
LLMR(LCZ 8)	48.29	99
Sparsely Built(LCZ 9)	45.45	74.5
Heavy Industry (LCZ 10)	65.26	95.4
Dense trees(LCZ A)	75.7	91.67
Scattered Trees(LCZ B)	65.38	84.62
Bush,scrub(LCZ C)	45.83	90.37
Low plants(LCZ D)	96.4	85
Bare rock(LCZ E)	50.7	40.9
Bare soil(LCZ F)	72.2	93.01
Water(LCZ G)	81.8	100
Overall Accuracy	69.43	87.15
Kappa Statistics	0.61	0.86

6.4.2 Relationship of Ventilation assessment map with spatially variable climate indicators

6.4.2.1 Relationship of Ventilation assessment map with LST

The analysis of relationship of ventilation path map with LST (derived in Section 5.2.1) of four different seasons reveals that in general the ventilated areas displayed lower average temperature and weak/blocked ventilation area displayed higher average temperature (Figure 6-6). Bias from Mean LST in every season demonstrates intra seasonal variations. The maximum difference of ~5.7 Celsius degrees in average temperature of ventilated and weak ventilation was observed in

monsoon season. In post-monsoon season the difference is minimum and it ranges from -0.020 to +0.126 degree Celsius i.e. early 0.15 degree Celsius. In winter and summer season also difference of nearly 0.5 degree Celsius to 1 degree Celsius was observed (Table 6-7).

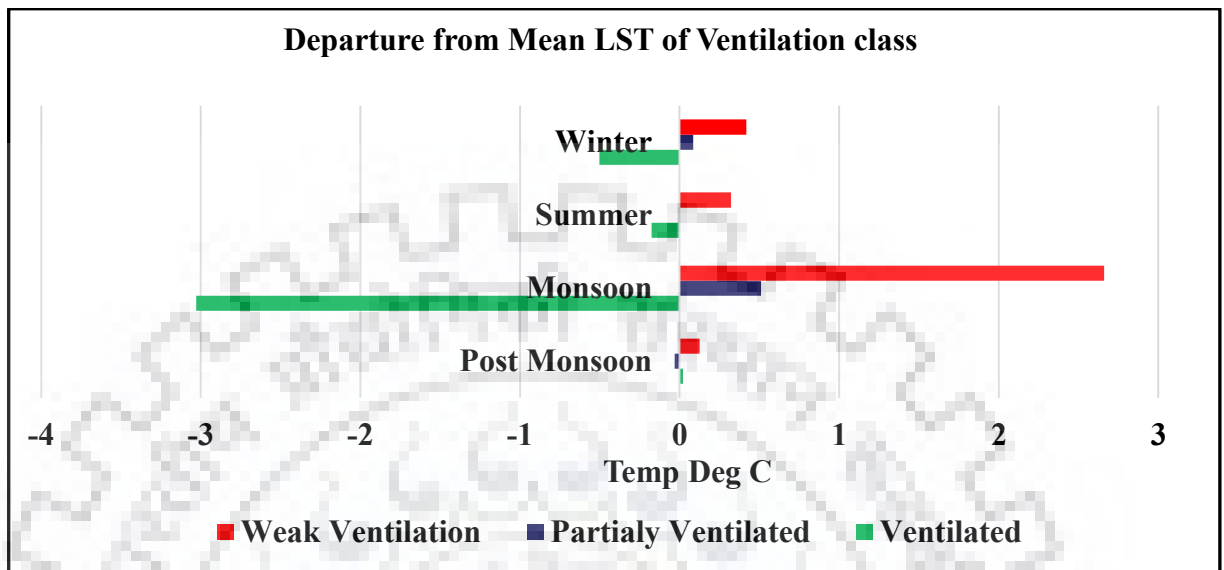


Figure 6-6: Class wise departure from Mean LST for each ventilation class

The large difference in mean LST of ventilated and blocked ventilation class especially in monsoon season has significant impact on thermal comfort in urban canopy layer. Relative humidity levels are generally very high in monsoon season (>80%), hence, natural ventilation is important for increasing the thermal comfort. Based on outdoor thermal comfort study in Hong Kong it is stated that “An easy to understand rule-of-thumb could be that providing urban air ventilation of 1 m/s can mitigate a 2°C rise in air temperature”(Ng, 2016). The difference of ~6°C in mean LST requires almost three time of existing wind speed to mitigate the thermal stress. A study of natural ventilation hours in the study region shows availability of more than 3000 hours of natural ventilation which can be effectively exploited to provide air ventilation to increase thermal comfort (Chen et al., 2017). However, highly dense and closely packed buildings with more than 60% of building surface area in different pockets increases roughness of the land surface with high zero plane displacement height. It slows down the wind speed in the urban fabric which is corroborated with the studies that shows a significant reduction in ventilation coefficient in the study region during last 30 years (Iyer & Ernest Raj, 2013).

Table 6-7: Departure in Degree Celsius from Mean LST of each ventilation class

Season	Ventilated	Partially Ventilated	Weak Ventilation
Post Monsoon	0.020	-0.031	0.126
Monsoon	-3.028	0.51	2.66
Summer	-0.175	-0.0056	0.32
Winter	-0.502	0.085	0.42

6.4.2.2 Relationship of Ventilation assessment map with UCPs

The UCPs which had shown strong relationship with LST, were analyzed to assess their relationship with ventilation assessment map (Table 6-8). BSF shows negative relationship with ventilation as higher BSF range falls under weak ventilation zone. PSF and VSF displayed positive relationship as with increasing PSF and VSF values moves towards the ventilated zones. Out of 3D UCPs analysed building height and H/ W ratio exhibited negative relationship while SVF demonstrated the positive relationship. Increase in SVF values i.e. amount of visible sky assist in more ventilation. In case of building height upto 9m building heights showed ventilated to partial ventilated zones whereas with increasing building height, it retards the wind speed and leads to the weak ventilation zones.

The assessment of relationship with UCPs displayed interesting findings. The areas with high building density (high BSF) impedes the flow of the air. The situation worsens if high density building areas are allowed to have more FAR which will further result in medium rise development in high density built-up. FAR should be defined in such manner so that areas which has more than 60% of built-up density should not be allowed to have building height more than 9 m. Similarly, for maintaining the flow of air in these areas, H/W ratio and SVF should also be maintained below 4 and more than 0.55 respectively. The findings may assist planners to define the zoning regulations, FAR relaxations and building regulations. Rather than defining the same zoning regulations for entire city, the city can be divided into different density zones and separate guidelines and regulations may be defined for each density zone. However, findings of this study need further investigation in other high density cities of India for conclusive recommendations.

Table 6-8: Relationship of UCPs with ventilation assessment

Parameter	Ventilated	Partially Ventilated	Weak Ventilation/Blocked
BSF	0- 0.4	0.4-0.6	0.6-1
PSF	0.6-1	0.3-0.6	0-0.3
VSF	0.25-1	0.1-0.25	0-0.1
Building Height(m)	0-6	6-9	>9
H/W Ratio	< 2	2-4	>4
SVF	0.65-1	0.55-0.65	<0.55

6.4.2.3 Relationship of Ventilation assessment map with climate indicators from WRF simulations

WRF model have been utilized to downscale the climate variables at 500m grid to bring them to urban micro scale. This grid resolution is still coarse, hence, the ventilation assessment map of the entire region was upscaled to 500m. Further random stratified points corresponding to all ventilation classes were utilised to assess the relationship with WRF outputs. Mainly three parameters i.e. LST, temperature at 2m and wind speed in m/s were analysed. The bias from mean LST for summer, winter and monsoon season is presented in (Figure 6-7). For all the seasons, ventilated zones displayed lower temperatures as compared to weak ventilation zones. In monsoon season, on August 9, 2017, difference between ventilated and weak ventilation zone is barely noticeable. It is primarily due to rainfall which happened on the same day. While on second day, difference between ventilated and weak ventilation zone is clearly visible (~ 7 to 13 degree) which corroborates the findings presented in 6.4.2.1. In summer and winter season the difference range varies from 3 degrees to maximum 8 degrees. It is also interesting to note that more difference was noticed in afternoon and evening hours as compared to morning hours. Similar pattern could be seen in winter season where throughout the day ventilated zones displayed lower temperatures as compared to weak ventilated areas. Temperature at 2m (screen height temperature) has strong connection with thermal comfort levels of human beings in urban canopies.

The association of ventilation classes with temperature at 2m is presented in Figure 6-8 for all the three seasons monsoon, summer and winter. Bias from mean temperature in all the seasons reveals the similar pattern as LST. The average temperature of weak ventilation zones are higher

as compared to ventilated zones. However, few dissimilarities could also be observed. During the 2-days simulation in monsoon period, relationship with LST showed negligible difference in temperature on first day of simulation, however, Temperature at 2m presented significant difference in temperature of the range of ~ 3 degrees even on the first day. The maximum difference was visible during morning which is different from LST (more difference is displayed in afternoon and evening hours). Summer and winter season assessment of T2 with ventilation map revealed the similar pattern where ventilated zones showed lower temperatures as compared to weak ventilation zone. Partially ventilated zones shows nearly similar temperatures or comparatively high temperatures as shown by weak ventilation zones in all outputs.

Figure 6-9 shows the relationship of wind speed at 10 m with ventilation classes. It is observed that irrespective of time, day and season, most of the time, ventilated area exhibited higher wind speed than the weak ventilation zones. The difference in wind speed ranges from 0.1 m/s to 2m/s. In winter season the difference is quite consistent and followed a pattern where weak ventilation zone has lowest wind speed while partially ventilated zone had higher speed and ventilated zone has the highest wind speed. No specific pattern was found for maximum and minimum difference. In general, morning hours displayed comparatively calm conditions whereas afternoon and evening hours displayed larger variability in wind speed across ventilation classes.

As discussed earlier that although approximately 76% of area falls under ventilation class, only 17% of built-up area comes under ventilated zone and more than 45% displayed weak ventilation area. The ventilation in built-up area has direct impact on alleviating the thermal stress in built-up area. Hence, an assessment of ventilation classes with climate indicators in only built-up area was also attempted. Figure 6-10 shows relationship of ventilation classes in built up area with LST and Figure 6-11 presented relationship with temperature at 2m. In built-up area also ventilated zones has lower temperatures as compared to weak ventilation zones, however, the difference in temperature between ventilated and weak ventilation is much more pronounced in built up area. The magnitude of difference in LST is prominent and stretching maximum upto 9 degree celsius, 19 degrees and 22 degrees in monsoon, winter and summer season respectively. When analysed with respect to temperature at 2m, the general observation of higher temperature in weak ventilated area and lower temperature in ventilated area proved to be same. The difference lies in magnitude which is quite varying with time, day and season. In monsoon season, the difference in temperature is least ranging maximum up to 1 degree. Whereas in winter season the difference in temperature is much more pronounced and reaching maximum upto 15-17 degrees. One more interesting fact is to be noted that in winter season most of the time even

ventilated zone in built up area showed temperature more than mean temperature, the pattern which is not seen in other seasons. The summer season exhibits greatest difference in urban canopy level temperature (T₂) which peaks upto 20 degrees difference. In general also, ~10 degree temperature difference between weak ventilation and ventilated zones was observed during summer season. As discussed earlier, the difference in temperature and wind speed in ventilated and weak ventilation zones has a significant impact on thermal comfort. Weak ventilated zones with higher temperature and lower wind speed induces substantial thermal stress and therefore, necessitates the use of mechanical controls to achieve the desired thermal comfort. With the increasing buying capacity of consumers and current global warming scenarios, the use of air conditioners is increasing day by day in these areas for achieving the desired thermal comfort. Use of mechanical controls works as feedback mechanism to global warming cycles with the increased emission of Green House Gases (GHGs) which again will feed to enhanced use of mechanical devices.

In winter season, study area generally experiences severe air pollution conditions with significant increase in respiratory diseases. The situation worsens with synoptic calm conditions, when lower wind speed that prevails in winter season as cold wind, tends to settle down. Since, the available air pollution data is mostly available mostly on traffic junctions, the impact of weak ventilation and high ventilation zones on air pollution could not be established. However, in future studies needs to be undertaken to assess the impact of urban canyon geometry on mitigation of air pollution in the study area. The analysis of mean wind speed with ventilation classes in built-up area revealed that wind speed is comparatively higher in ventilated zone as compared to weak ventilation zone (Figure 6-12). However, the difference in magnitude is not very high as was the case with ventilation in entire area. In monsoon season the minimum difference observed was 0.1 m/s and maximum was 1.1 m/s on 11/08/2017 5:30 AM. Here, also no definite pattern of maxima and minima could be observed. In summer season maximum difference of 2 m/s was also observed, whereas minimum difference was even less than 0.1 m/s. In summer season, minimum difference was observed during morning hours generally at 5:30 AM and 11:30 AM, whereas maximum difference was observed around 8:30 AM. During winter season minimum difference in mean wind speed of ventilated and weak ventilation zones was observed which could be attributed to general calm conditions prevailing in winter season. The major result which emerged from the above discussion is that, in general, ventilated area exhibited lower temperatures and higher wind speed as compared with weak ventilation zones. Partially ventilated zones presented no specific pattern. Few of the times their temperatures were

at par with weak ventilation zone and most of the time, it exhibited temperatures lower than weak ventilation zone.

6.4.3 Effect of Scale in LCZ classification

The characteristics of urban areas in most of the part are dependent on scale. The patterns and amount of information significantly varies with scale in urban areas(Weng, 2014). By definition LCZ is defined as the area which is local in scale and zonal in characteristics. Hence they have been defined as “hundreds of meters to several kilometers in horizontal scale”(Stewart & Oke, 2012). The grid size of 100-150m was found to be a good compromise and recommended for WUDAPT LCZ (Bechtel et al., 2015). However, in this study, grid size of 50 m have been utilized for LCZ classification due to high heterogeneity and complex urban structure in the study area. It was noticed that at the grid size of 100 m, averaging effect is too high which results in poor separability between LCZ classes. Use of smaller grid sizes such as 20 m or 25m resulted in large number of grid cells falling in very high values of BSF, which may lead to erroneous classification. Hence, grid size of 50 m have been considered as a good trade-off after few iterations and have been utilized for LCZ classification. However, it is noticed that few of the LCZ classes such as buildings in heavy industry (LCZ 10) and large low rise (LCZ 8) had fallen in more than one grid cell. It has resulted in difficulty in the classification of these LCZ classes. In future, more investigation may be carried out on the effect of grid size on LCZ classification.

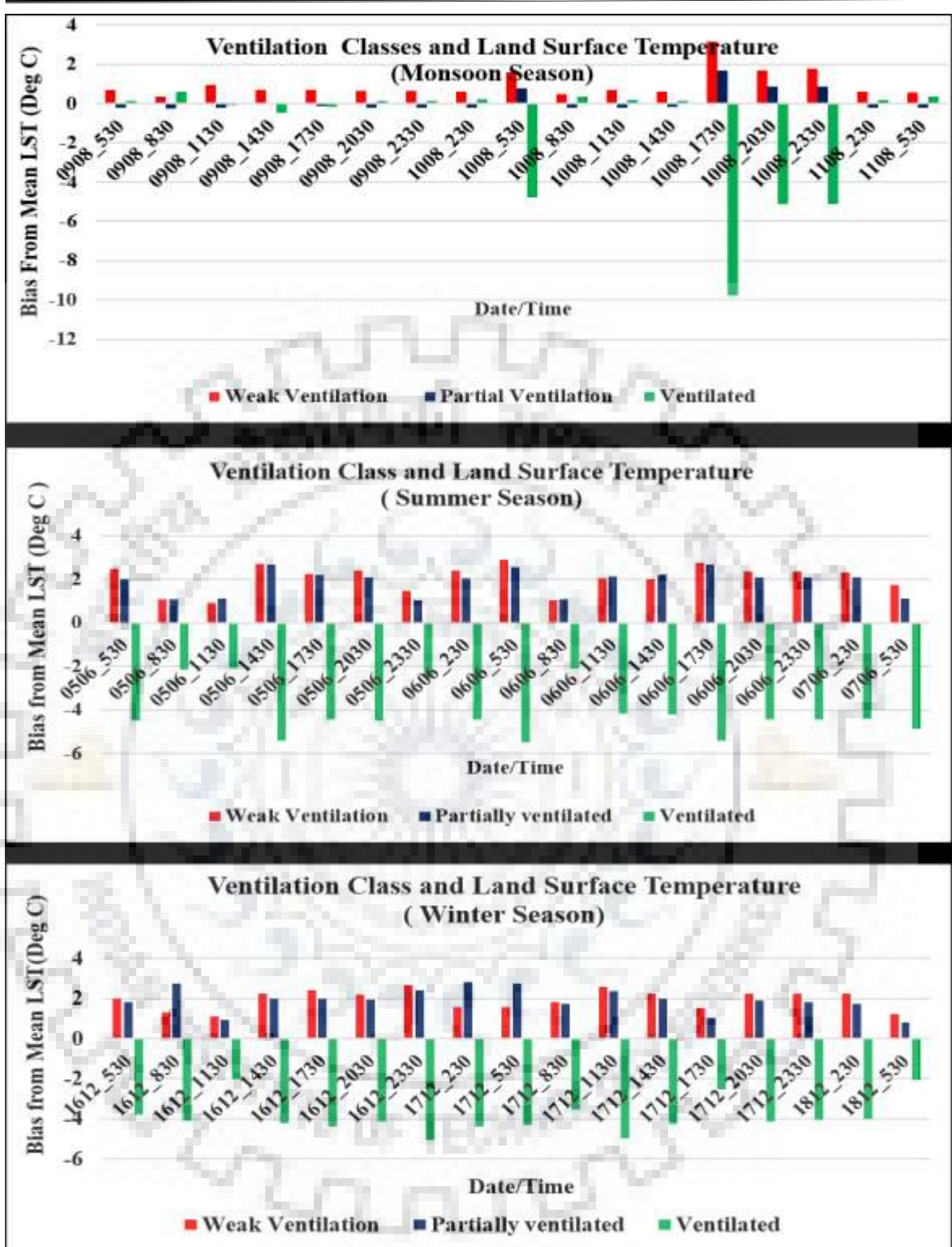


Figure 6-7: Diurnal variability from Mean LST of Ventilation class

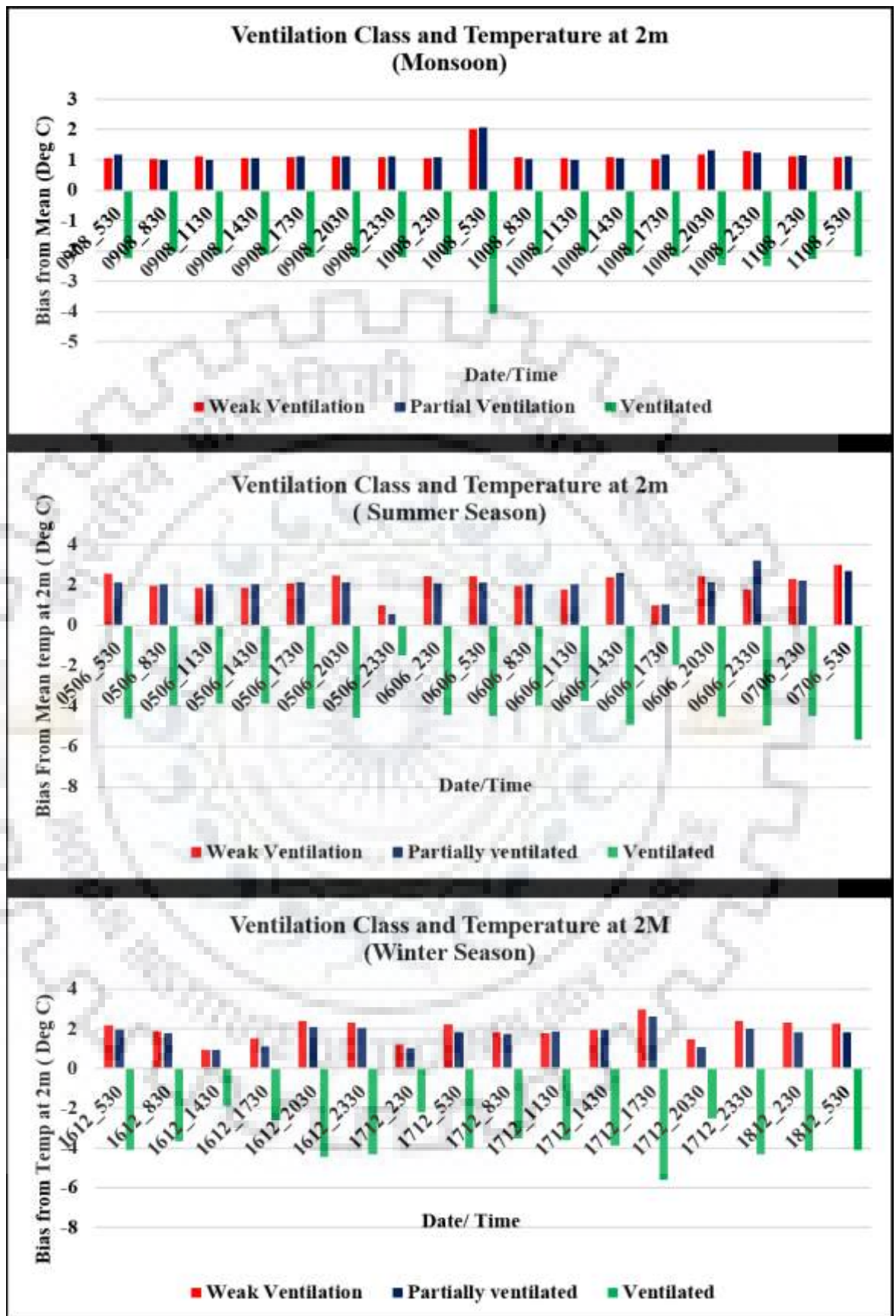


Figure 6-8: Diurnal variability in bias from Mean temperature at 2m of Ventilation class

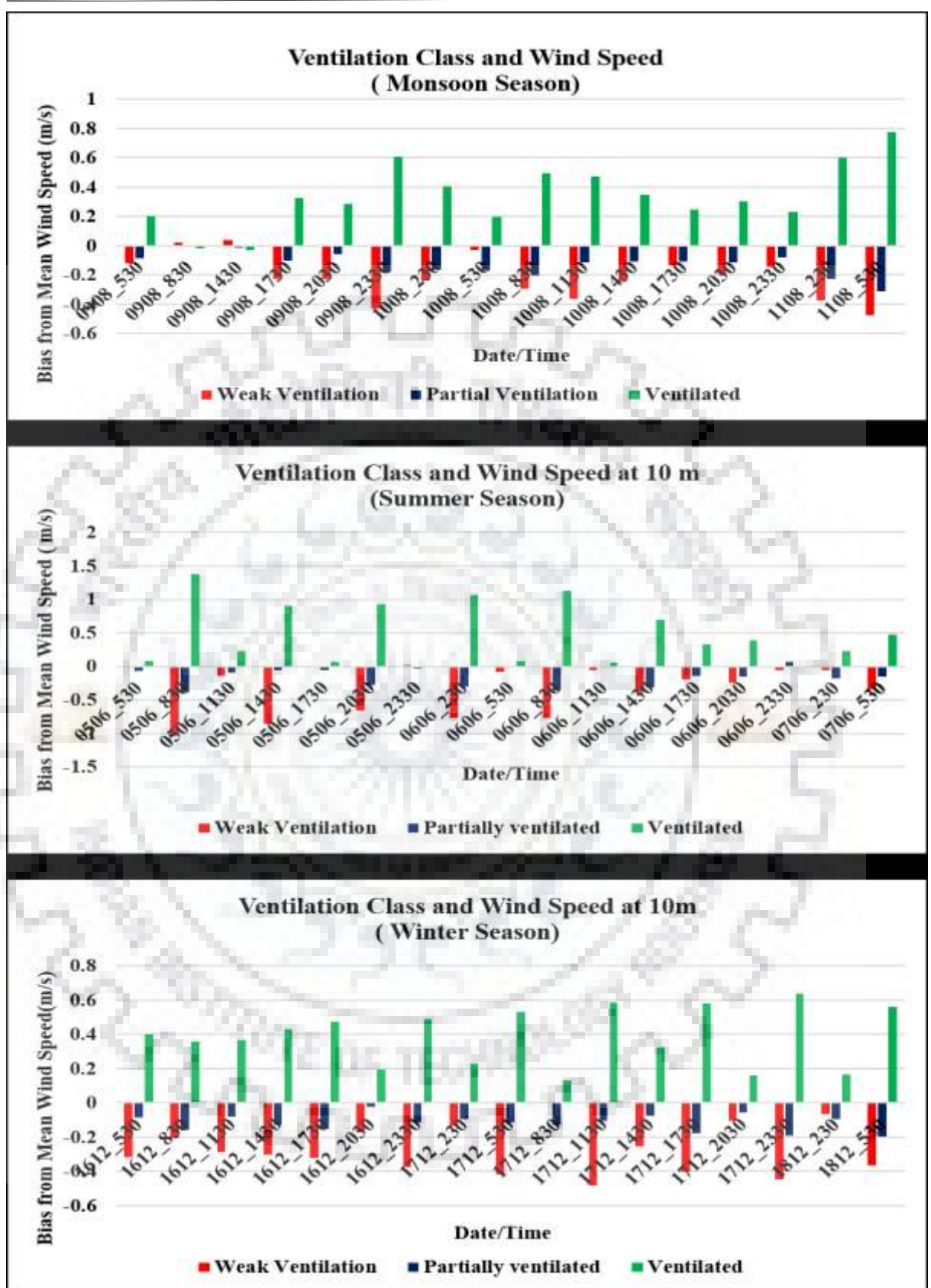


Figure 6-9: Diurnal variability in bias from Mean Wind Speed at 10 m of Ventilation class

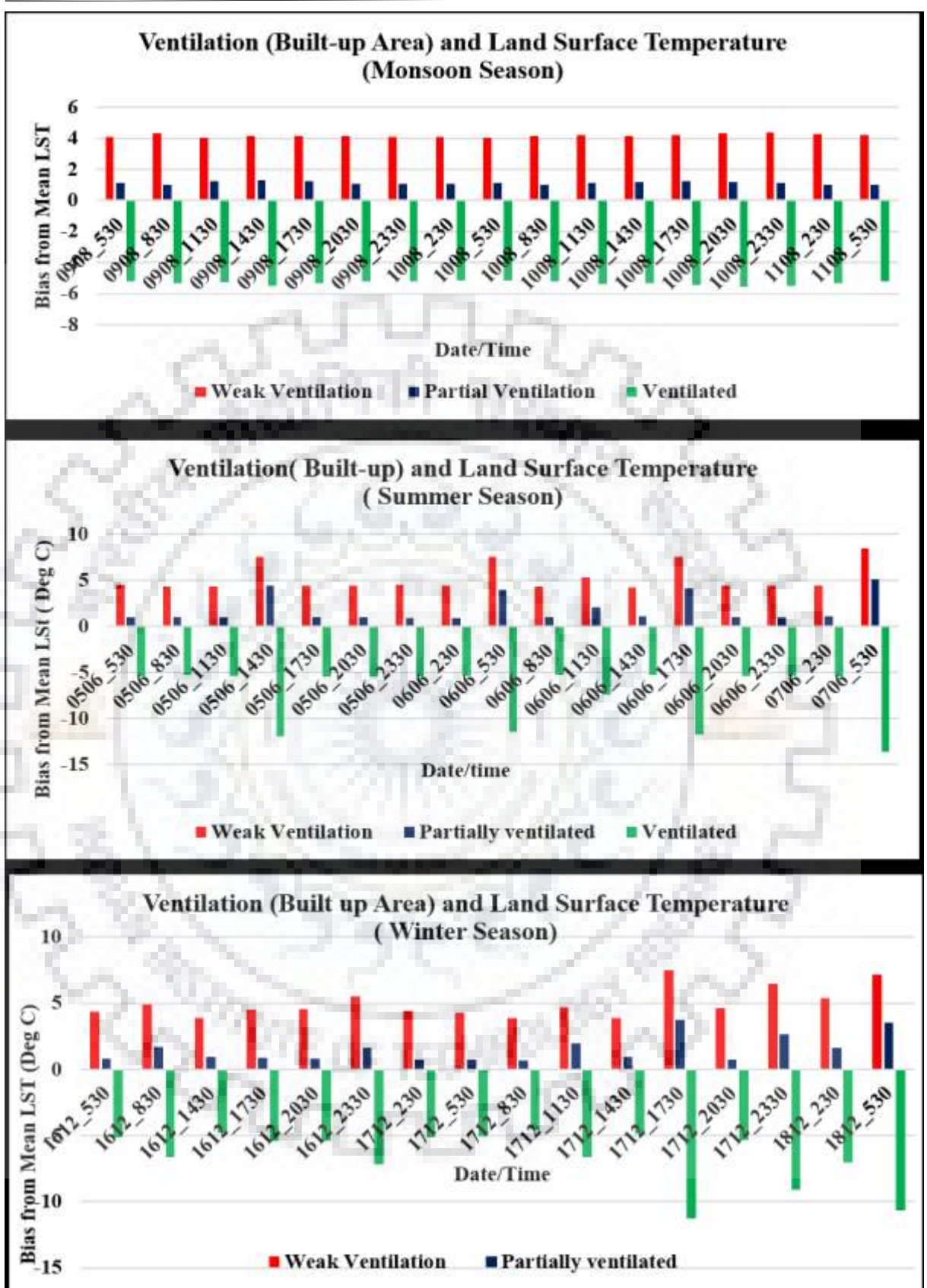


Figure 6-10: Diurnal variability in bias from Mean LST of Ventilation class in urban built-up

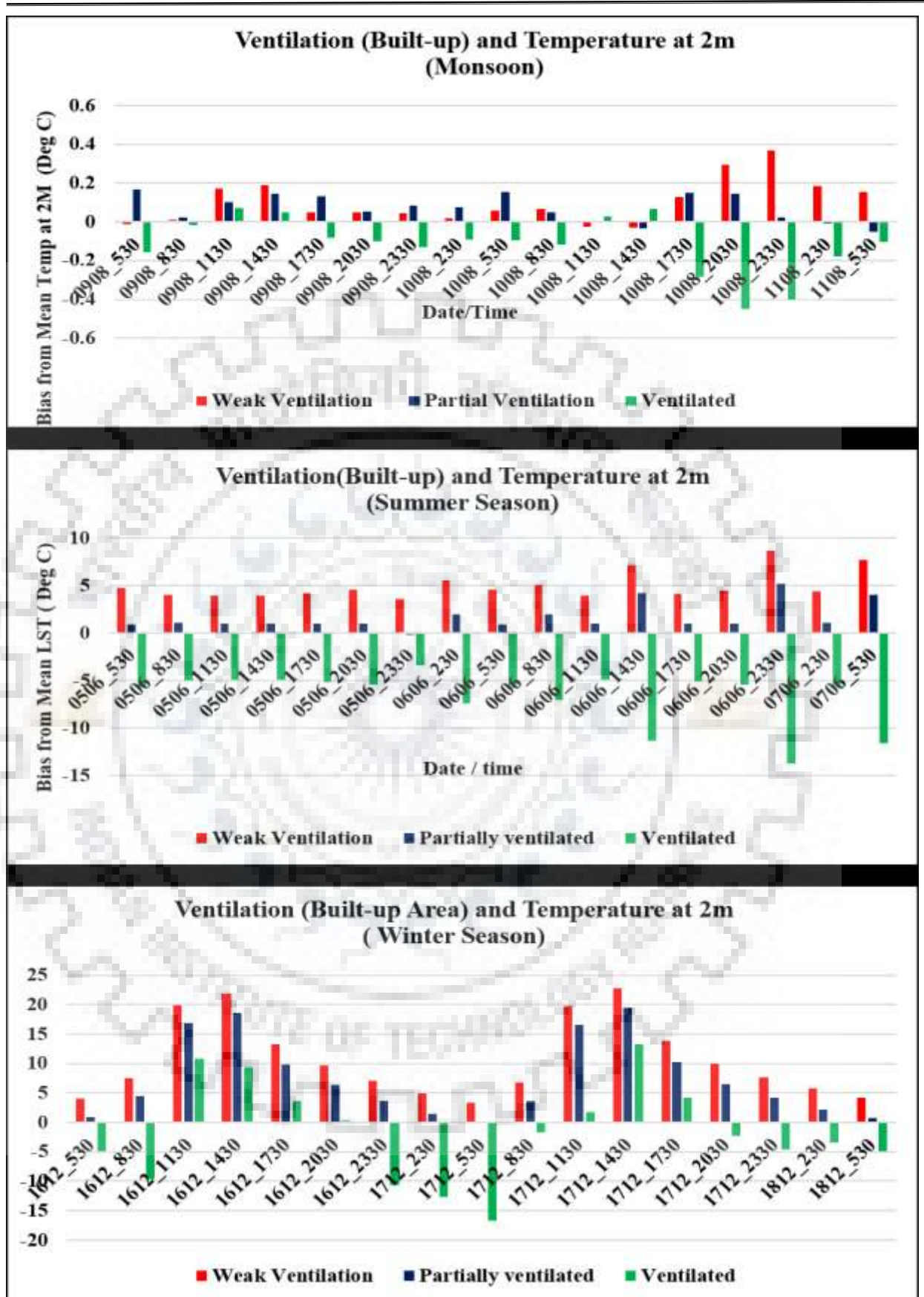


Figure 6-11: Diurnal variability in bias from Temperature at 2m of Ventilation class in urban built-up

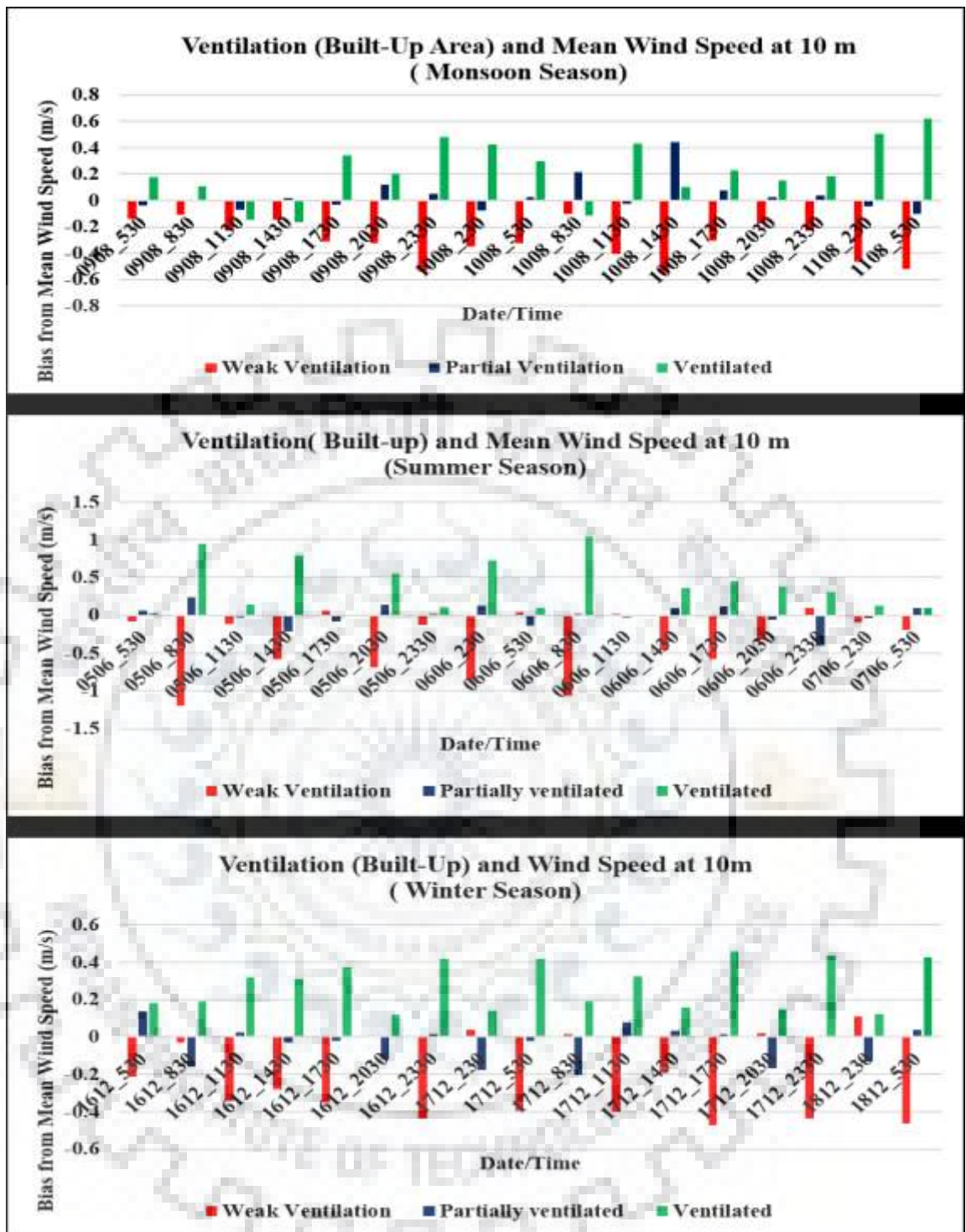


Figure 6-12: Diurnal variability in bias from Wind Speed at 10m of Ventilation class in urban built-up

6.4.4 WUDAPT and GIS based Local Climate Zone

Significant differences can be observed in area statistics of WUDAPT and GIS based LCZ classification (Table 6-3). It may be attributed to differences in spatial resolution of raw satellite data, date and season of acquisition of satellite images and processing algorithms. For example,

low plants LCZ constitutes the dominant LCZ (~55%) in WUDAPT classification, while bare soil is the dominant class in GIS based LCZ. Landsat 8 data which have been used for WUDAPT LCZ, have been acquired in the month of February. During this month wheat crop, which is staple crop of this region, is in full growth stage. Dominance of agriculture vegetation in this season has resulted in high percentage of low plants LCZ which constitutes agriculture and urban park area. The primary input for low plants classification in GIS based LCZ is LULC which have been obtained through supervised classification of Pleiades MX ortho images. These images have varied season and dates of acquisition which posed significant challenges for the classification of LULC as discussed in chapter 4. The variation in season has led to dominance of bare soil class in GIS based LCZ.

The urban LCZ classes (LCZ 1-10) also displayed substantial differences in area statistics of WUDAPT and GIS based LCZ. It is primarily attributed to difference in processing algorithm and criterion ranges. While WUDAPT utilizes random forest classifier which is a pixel based classifier, GIS based LCZ map utilizes the unique distribution of geometric and surface cover properties (UCPs) and modified criterion ranges based on existing conditions in the study region. Besides, use of Landsat 8 (medium resolution data) for WUDAPT results in mixed pixels due to high heterogeneity of urban environment. Mixed pixels poses a major issue in classification with pixel based classifiers (Fisher, 1997). Since, mixed pixels are a combination of reflectance from building, road, vegetation, lawns and water all lump together, pixel based classifiers are known to have low accuracy in urban areas (Epstein, Payne, & KramerE., 2002). Whereas in high resolution (Pleiades) data, proportion of mixed pixels is significantly reduced.

GIS based LCZ classification provided improved accuracy not only in overall classification but also in accuracy of each LCZ as DSM was also included in extraction of building surface area. It shows that in complex and dense urban environment of developing region with high seasonality effect, GIS based classification provides higher and reasonable accuracy than WUDAPT classification. However, the only complexity involved is availability of detailed UCPs information. However, this limitation can be overcome by utilization of sub-meter optical high resolution stereo for the retrieval of UCPs in complex urban environment as discussed and detailed out in this work.

6.4.5 Role of seasonality in LCZ classification

Nearly 64-65% of the study area comprises of low plants and bare soil LCZ classes. The proportion of these class in the study area is dependent on agricultural practices in the region

which is highly dependent on season. The prevalent agriculture practices in the study area primarily has two major cropping season kharif and rabi which falls into monsoon and winter season respectively Hence, the proportion of these two class varies throughout the year. . In summer season, proportion of bare soil is more whereas in monsoon and winter season, proportion of low plants class is higher. Significant differences have been observed in area percentage of bare rock class as it is also highly varied according to season. In monsoon and post monsoon season, availability of moisture promotes growth of vegetation even in the rocky area while in winter and summer season, lack of moisture exposes the rocky outcrop. Hence, it is mandatory to prepare LCZ maps by utilizing the same season images in order to have conclusive comparison.

Initially, training samples for WUDAPT LCZ in Google earth data have been digitized on the data which is displayed by default in GE. However, it has resulted in very poor accuracy of land cover classes. Later on, training samples have been modified by displaying the same season data as of raw Landsat 8 data (February). It shows that seasonal effects needs to be taken care while identification of training samples and ground truthing for better classification results. However, in tropical and semi-tropical region, impact of season requires further investigation by employing classification n different seasons. In future, methodologies for combining LCZ outputs of different seasons may also be explored for a comprehensive LCZ classification.

6.4.6 Relationship of Local Climate Zone Map with Land Surface Temperature

GIS based LCZ map have been analyzed with LST maps generated from Landsat 8 TIRS data (section 5.2.1) for four prominent seasons of the study area. Bias from Mean LST (Figure 6-13) revealed that bare soil LCZ class had shown maximum temperature in summer and post-monsoon season. Whereas in winter season, maximum temperature has been displayed by bare rock or paved class. Out of all built-up LCZ classes, Heavy industry (LCZ 10), Large Low rise(LCZ8) and compact Low rise (LCZ 3) displayed maximum temperatures except in winter season where compact midrise and open midrise and heavy industry showed maximum temperature. It may be attributed to low sun elevation angle of winter sun. Water had shown minimum temperature in all seasons except winter season where low plants exhibited the lowest temperature. In general the open low rise and sparsely built LCZ classes have shown temperature lower than mean LST value. But Other Built-up LCZ classes always displayed temperature more than mean LST. The highest temperature of heavy industry can be attributed to high level of anthropogenic emissions and large concrete structures. The large low rise LCZ class also has more amount of concrete

surfaces which leads to higher temperature. Compact low rise LCZ has high density of population which also contributes to anthropogenic heat emission. Besides, large volume of low albedo and high heat capacity construction material and narrow street canyons store and traps high amount of heat in the urban fabric, which lead to rise in temperature in compact low rise LCZ. Similar relationships of LCZ class with temperature have been observed in Chandigarh, India (Gupta et al., 2017b) where also heavy industry LCZ displayed highest mean temperature in 2008 and 2013.

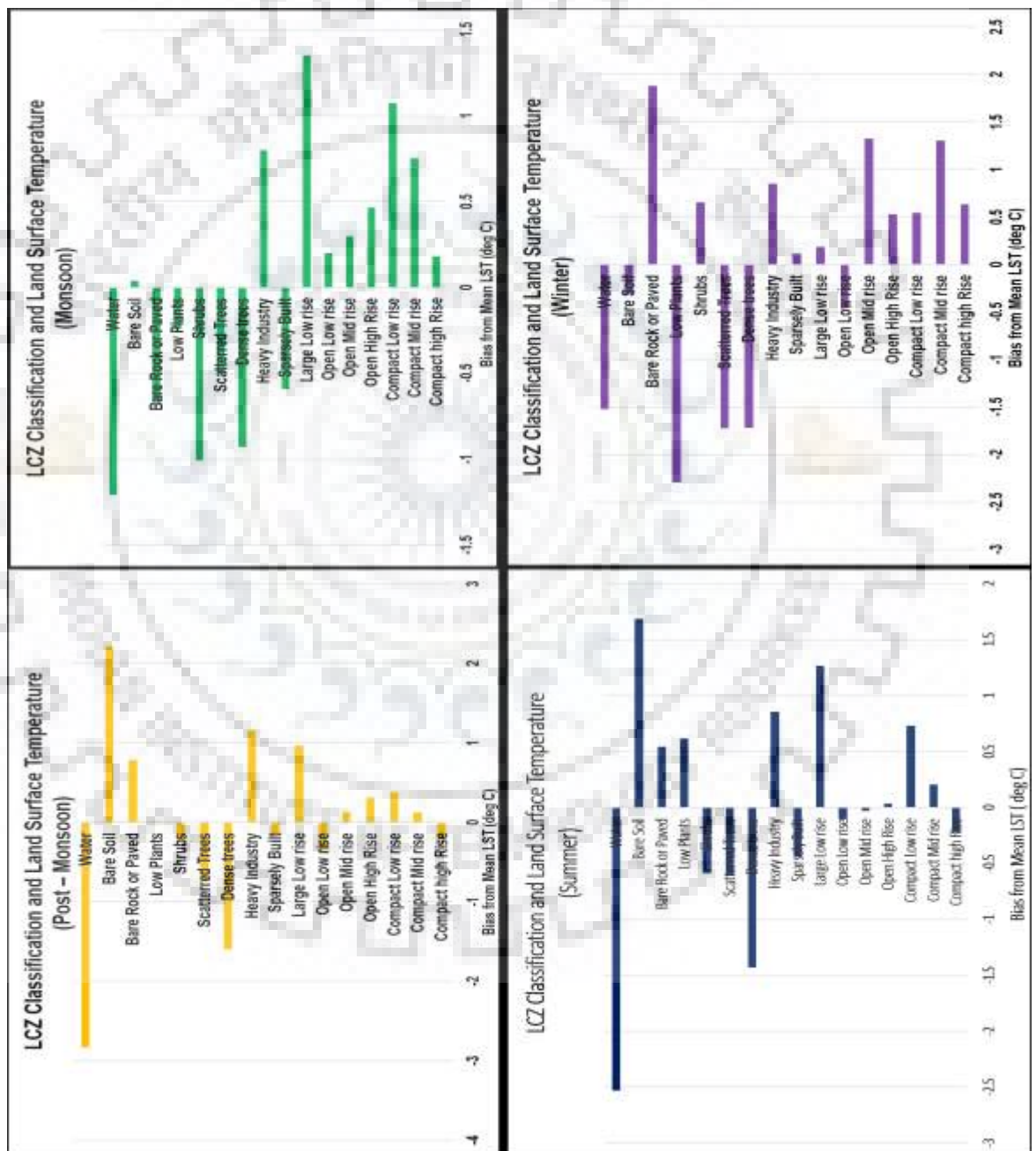


Figure 6-13: Bias from Mean LST of Local Climate Zone classification

6.5 SUMMARY

This chapter presented two application of UCPs such as ventilation assessment and GIS based LCZ map, the studies on which is almost nonexistent in India and very few in developing world. Ventilation assessment map provides an assessment of ventilated and weak ventilation zones. It also provides an insight into the potential ventilation corridors in the study area. The study area exhibits one major ventilation corridor and few of the minor ventilation corridors at city level. The lack of adequate ventilation in the study area may be one of the reason for severe air pollution in the winter season and UHI conditions. However, further investigation and studies are required to assess the effect of street orientation and prevailing wind direction in the study area for improved understanding. The relationship of ventilation path map with climate indicators revealed that in general ventilated zones has lower mean temperature and higher wind speed as compared with weak ventilation areas. This presents an interesting finding and corroborates the fact that ventilation can be an effective measure to mitigate UHI. Relationship of ventilation assessment map with UCPs shows that high density built up areas should not be allowed to have higher FAR in order to restrict the building height and subsequent roughness of the land surface. The weak ventilation zone in the study area in general coincides with those area which have high value of BSF (>0.6). The assessment may be utilized by planners to define zoning, FAR and building regulation for climate sensitive urban planning. The generated ventilation path can be utilized for urban climate map studies in the study region which can be further utilized to define strategies for climate resilient urban environment.

WUDAPT is a worldwide initiative to collect level 0 data on form and function of the cities and employs free data, software and pixel based classifier for LCZ classification. However, in dense and complex urban environment as in study region, it did not yield satisfactory result. The UCPs have also been utilized to generate GIS based LCZ map which has shown significant improvement in accuracy over WUDAPT LCZ. The detailed UCPs generated in this study can be utilized for generating level 1 and level 2 data of WUDAPT as well as for its integration in urban climate models. As discussed earlier that paucity of detailed information on UCPs is considered as one of the major factor for inadequate utilization of recently developed urban canopy models. The retrieved UCPs in this study fill this gap with an immense potential to boost urban climate research and modeling in developing regions.

CHAPTER 7

CONCLUSION, RECOMMENDATIONS AND SCOPE FOR FURTHER RESEARCH

7.1 INTRODUCTION

This chapter summarizes the key findings based on the existing literature review, describes general and specific conclusion based on the findings of the research undertaken, highlights significance of the research, discusses major recommendations for planners and researchers working in the field of urban climate studies and outlines suggestions on scope for further research.

The whole study is segmented into three broad components each one addressing three objectives of the research. First component (Chapter 4) details out the methodologies and results of retrieval and characterization of Urban Canopy Parameters (UCPs) from high resolution optical satellite stereo data. Estimation and modeling of spatially variable urban climate indicators forms second component (Chapter 5) of the study which have been utilized to analyze relationship of spatially variable climate indicators with retrieved UCPs as part of first component. Third and last component (Chapter 6) demonstrates the application of retrieved UCPs (first objective) for urban climate studies i.e. ventilation assessment and GIS based Local Climate Zone (LCZ) mapping and further analysis of their relationship with spatially variable climate indicators.

7.2 KEY FINDINGS AND CONCLUSIONS

General observations have been drawn after the review of existing work relevant to this study highlighting research gaps and need to undertake this research. It also outlines the major research aims. Further, specific findings and conclusions for various aspects of the study such as retrieval of Urban Canopy Parameters (UCPs), challenges faced in the retrieval of UCPs, characterization of UCPs in study area, application of UCPs viz. ventilation assessment and GIS based LCZ, relationship of UCPs, ventilation assessment and GIS based LCZ with spatially variable climate indicators, are presented.

7.2.1 General Observations

Urban areas occupy 3% of ice free land area but they are cumulatively responsible for emission of 75% of Green House Gases (GHGs), therefore contributing significantly in global warming.

It is projected that 90% of future urban growth is likely to happen mainly in developing countries. Population growth pressure coupled with lack of adequate infrastructure and implementation of planned development in these regions are leading to numerous climate and environmental issues. Increased frequency of natural disasters and extreme weather events in these regions calls for scientific understanding of impact of urban areas on climate and vice versa to ensure sustainable development.

UCPs have significant role to play in mapping and studying the micro climatic set up of any urban area. These UCPs are the basic input parameters for understanding the energy interactions at the surface of the earth and how in certain urban environment energy exchange happens. UCPs define those properties of urban built form which has direct or indirect bearing on urban micro climate.

Paucity of information on Urban Canopy Parameters (UCPs) is one of the major constraint for limited urban climate research and modeling studies in complex urban environment of developing regions, hence, information on UCPs is critical for urban climate studies as well as for implementation of recent Urban Canopy Models (UCMs) for scientific understanding of climatic phenomenon in these regions.

3D GIS database obtained either from ground surveys or remote sensing technology (airborne LiDAR, aerial images or high resolution InSAR) have been utilized widely for retrieval of UCPs mostly in developed world. However, non-availability of 3D GIS database and airborne data, resulted in a limited number of studies on UCPs in developing regions.

Not many studies have explored the use of Very High Resolution Satellite (VHRS) optical stereo data for extraction of UCPs, however, the widespread availability, extensive coverage and low cost of very high resolution satellite data needs to be evaluated for generation of UCPs in developing regions.

Thermal remote sensing and numerical model simulations are the methods which can be employed in urban areas for obtaining the high resolution spatially variable information on climate indicators since, large network of ground observation towers is expensive and not feasible in urban areas due to stringent siting requirements.

3D UCPs such as building height, complete aspect ratio, sky view factor etc. has substantial impact on urban micro climate, however, its relationship with spatially variable climate indicators is still largely unexplored, primarily due to unavailability of information on 3D UCPs.

The Delhi Urban Agglomeration (UA), which is the third largest UA of the world and largest UA of the India, has been selected as the study area due to its highly dense, sprawled, highly heterogeneous and complex development characteristics of urban built form, high air pollution levels, high anthropogenic pressure and challenging composite climate.

Hence, this study focused on the utilization of sub-meter VHRS optical stereo images for retrieval and application of UCPs in a highly complex and dense urban environment of Delhi, a city in a developing country, and to understand the relationship of various UCPs with urban climate indicators.

7.2.2 Retrieval of Urban Canopy Parameters

The study developed a novel approach for the retrieval of building height, building surface fraction (BSF) and wall surface area, which are the basic input UCPs for the computation of other UCPs, by utilizing Digital Surface Model (DSM) generated from VHRS stereo data in a highly dense and complex urban environment of Delhi urban region.

The validation of key UCPs derived through VHR optical stereo images have shown good accuracy with ground measurements. The Mean error, RMSE and MAE for building heights has been found to be less than 1 m and Cumulative Random Error (CRE) ranged from 2.5% to 9.9% in high rise to low rise development respectively. The other key UCPs such as Land Use Land cover (Accuracy ~ 85%), Building Surface Fraction (BSF) (Accuracy ~84.27%) and SVF (RMSE-0.046 and correlation-0.94) also displayed reasonable accuracy.

Key UCPs retrieved in this study have been further utilized for the computation of other UCPs such as pervious surface fraction and impervious surface fraction (2D UCPs), Mean and standard deviation of building height in 30m grid cell, Building Volume, Height to Width Ratio, Complete Aspect Ratio, Building Surface Area to Plan Area Ratio, Zero Plane Displacement Height and Surface Roughness Length (3D UCPs). Sky View Factor UCP for the study area has been computed by employing raster based computation on generated DSM for the study area.

7.2.3 Characterization of Urban Canopy Parameters in study region

The characterization of UCPs in the study area revealed highly dense, heterogeneous and sprawled character of the study region which has significant impact on urban climate.

The very high density of built-up is evident from BSF map as ~ 17% of built-up has building density of more than 80% and nearly 35% of building surface area fall under 0.6-1 BSF range. It clearly shows the presence of very high density built-up in study area.

The distribution of building heights obtained through RS data revealed sprawled urban form in the study area in spite of having huge population and development pressure in last few decades. Nearly 58% of built-up area falls under low rise development (< 10m) and 41% area falls under midrise development (10-25 m) with less than 1% area only has high rise development. It may be attributed to easy availability of land being a flat topography, socio economic preferences and restrictions on FAR in the initial years of development in study area.

Most of the high rise development have been found to be in peripheral regions near to NOIDA and Gurgaon and Ghaziabad in sporadic patches. However, development of high-rise development in surrounding peripheral areas may again led to further retardation of wind flow in the study region.

Computation of standard deviation of building heights at 30 m grid resolution have shown high values of standard deviation (>1 in nearly 75% of grid cells) which is indicative of highly heterogeneous urban built form. It is primarily due to large influx of migrant population, plotted development and lack of implementation of planning regulations which have resulted in formation of unauthorized and unplanned urban settlements.

It has been observed that large proportion of vegetation and bare soil (<70%) has high temporal variation in the proportion of vegetation and bare soil across season and years depending on vegetation phenology and cropping patterns. The variation in proportion has profound impact on micro climate, evaporative cooling and energy exchange mechanism.

In general, building volume, zero plane displacement height, Surface Roughness Length, Complete Aspect Ratio (CAR), Height- to- width ratio (H/W ratio) and BSAPAR found to be high in eastern part stretched along River Yamuna and in western part of study area. The high value range of above parameters in highly dense parts of study area presented a remarkable departure from earlier research conducted in developed countries where even in downtown area, values found to be comparatively lower. This also indicates presence of very high density urban built up in the study area.

7.2.4 Challenges faced in the retrieval of Urban Canopy Parameters

The major challenge faced in processing of the UCPs is the huge volume of data (covering more than 2600 sq km), very high density of built-up and multiple scenes (14 Stereo pairs) of different dates.

The huge volume of data (~0.5TB) required high end computing resources as even processing of one scene could not be completed on high end regular workstation. Hence, whole DSM and UCPs processing have been carried out in windows based High Performance Computing (HPC) system of 24 core processor and 128 GB RAM.

The very high density of built-up posed challenges as occlusions and shadow in compact built-up area resulted in poor object based classification to obtain individual building footprint for the generation of 3D cadastral data in study area. Hence, a novel step-by step filtration of non-building pixels on a regular grid have been employed to generate the building height map and subsequent computation of BSF and other UCPs in the study area.

Procurement of archived data have been preferred to reduce cost of data as this is a demonstrative study. However, it resulted in procurement of scenes varying in dates, season and year. To maintain uniformity in outputs, all the stereo pairs were processed individually and further mosaicked to generate final Digital Surface Model (DSM). It also posed challenges in classification of LULC, where each MX ortho have been classified and post classification images have been mosaicked after contextual refinements.

A rule of thumb approach by utilizing mean building height have been employed for computation of surface roughness length in the absence of information on frontal area index. λ_f is one of the key parameter for the computation of surface roughness length. However, its computation by employing available tools in the complex urban environment of study region did not yield satisfactory results.

7.2.5 Application of Urban Canopy Parameters

The study also demonstrated the potential of UCPs for urban climate applications through the generation of ventilation assessment map and GIS based local climate Zone map. The study presented a novel hierarchical methodology for the derivation of GIS based LCZ map by utilizing detailed UCPs and ancillary information of the study region.

The analysis of ventilation map showed merely 17% of built-up area as ventilated area. More than 45% of built-up area falls under weak or blocked ventilation and nearly 38% area is partially ventilated. The ventilation map of Delhi clearly brings out the lack of adequate ventilation in the built-up area which makes the city prone to severe air pollution in winter season and high UHI conditions.

GIS based LCZ maps generated from application of detailed UCPs displayed high accuracy of classification (overall Accuracy >85% and kappa ~0.86) not only for the entire classification but even for each LCZ class. The pixel based classification methodology proposed by World Urban database and Access Portal Tool (WUDAPT), which have been applied worldwide to collect data on urban form and function by utilizing free RS datasets and GIS software, provided poor accuracy (overall accuracy ~49.43% and kappa ~0.46) of LCZ classification in the complex urban environment of study area.

7.2.6 Relationship of UCPs with Spatially variable climate indicators

The study explores the relationship between the UCPs and spatially variable climate indicators. Land Surface Temperature (LST) at 30 m spatial resolution estimated from Landsat 8 and LST, Temperature at 2m and wind speed at 500m spatial resolution obtained from downscaling of met variables in WRF model have been utilized for this purpose.

Validation of WRF outputs (Temperature at 2M, Relative humidity and Wind Speed) revealed reasonable accuracies with strong correlation values for temperature at 2m and relative humidity, however, wind speed have shown weak correlation.

It may be attributed to broad incorporation of roughness characteristics in the model. Urban areas are the roughest surfaces with high heterogeneity in surface roughness in small distances. The approach adopted in this study classifies urban area in three broad urban LULC classes with a single roughness value for each class which is insufficient to represent the urban heterogeneity.

Downscaling of met variables using WRF-urban model at 500m grid resolution provided satisfactory results, but it is still a coarse resolution to match the very high resolution at which the UCPs have been generated.

The primary results of UCPs-LST relationship revealed that 2D UCPs has shown strong correlation and outperformed all other UCPs. While 3D UCPs such as z_d , SVF, CAR, BSAPAR, H/W ratio, building volume except building height and Z_o exhibited poor to moderate correlation

with LST. The weak correlation between 3D UCPs and LST can be attributed to the nadir viewing geometry and over sampling of thermal sensor data from a resolution of 100 m to 30 m.

Strong positive correlation was found with BSF and ISF and strong negative correlations with PSF and VSF, which is a consistent finding with earlier research in this field. In case of few UCPs such as CAR, SVF, H/ W Ratio, correlation with LST also varied from season to season, the phenomenon which needs further investigation in the study area.

The key UCPs which exhibited strong relationship with LST have been utilized to analyze the variability of Surface Urban Heat Island (SUHI) across all four seasons in a year. SUHI intensities was found to be maximum during winter season while lowest during post-monsoon season across all UCPs. BSF and ISF exhibited increasing SUHI intensity with increasing value while PSF and MBH showed decreasing trend of SUHI intensity with increasing value. Zo and SVF in general exhibited negative trend of second polynomial order.

Analysis of diurnal variability of SUHI intensity with WRF simulations for three seasons: summer, winter and monsoon displayed maximum SUHII at 5:30 IST with more SUHII during night time. Whereas, minimum SUHII value were observed during daytime at 11:30 IST and 14:30 IST in both summer and winter season. As a matter of fact, urban area displayed cool island effect at 1130 IST and 1430 IST. It clearly indicates that the study area experiences more intensity of SUHI during night time as compared to day time in summer and winter season.

7.2.7 Relationship of ventilation assessment and GIS based LCZ map with Climate indicators

The analysis of ventilation assessment map with climate indicators (LST at 30 m spatial resolution) has shown higher wind speed and lower temperature in ventilated area as compared to weak ventilation zone. The difference in the mean temperature of both the classes were highest in monsoon season (~5.5 degree Celsius) and minimum in post-monsoon season (0.15 degree Celsius).

The high difference in mean LST of ventilated and weak ventilated zones in monsoon season raises serious concerns regarding the thermal comfort in built-up area. Although, the study area is mostly dry during rest of the year, but, in monsoon season humidity level are more than 80% and slight increase in temperature leads to substantial increase in thermal stress. This phenomenon is responsible for substantial increase in use of air-conditioners in the study area

which further add to the canyon level thermal stress. It again exacerbated by the trapping of heat in narrow canyons and weak ventilation.

The similar results were achieved while analyzing the relationship of ventilation assessment with WRF outputs of LST and temperature at 2m for different seasons. The departure from mean wind speed at 10 m of ventilation classes displayed higher mean wind speed (2m/s) in ventilated zones as compared to weak ventilation zones (0.1 m/s). The finding also endorses the concept that adequate ventilation in urban area assists in mitigating the impact of UHI.

The relationship between ventilation zones and UCPs revealed weak ventilation in built-up area with high value of BSF (>0.6) exhibit. However, the analysis also shows that if buildings have less than 9m in height, it may be possible to maintain proper ventilation in such compact urban built forms.

The distribution analysis of LST in various LCZ classes showed that all built-up LCZ classes except sparsely built and open low rise revealed higher temperature than mean LST value in all seasons. However, heavy industry, compact low rise and large low-mid-rise LCZ revealed highest temperature among all LCZ classes, primarily due to high anthropogenic heat emission, large population concentration and high amount of impervious surfaces in heavy industry, compact low rise and large low rise LCZ respectively. Bare Soil and Bare rock LCZ had also shown highest temperatures among all LCZ classes except monsoon season.

7.3 MAJOR CONTRIBUTIONS OF THE RESEARCH STUDY

Paucity of information on UCPs is considered as one of the major impediment for limited number of studies on urban climate especially in the developing regions. The novel methodologies developed in this study for generation of key UCPs from optical stereo satellite data in a highly dense and complex urban environment of developing region provides an alternate methodology for generating these UCPs using high resolution optical satellites stereo data, which till recent, has not been seriously considered.

The developed methodologies provides the framework for automated retrieval of UCPs with very less percentage of manual editing. This study therefore holds strong significance for urban climate studies in developing regions, as the availability of Airborne LiDAR, Aerial photographs and high resolution InSAR is either expensive or has limited availability in these regions.

The presented methodology to obtain 3D information in urban areas has huge potential to upgrade available 2D geodatabase, which is being generated for 500 cities of India under AMRUT subscheme on GIS based formulation of Master Plans, to 3D GIS database in near future which can be utilized to boost the applications for urban climate research and modeling.

This study also explored the relationship of 3D UCPs with spatially variable climate indicators, the studies on which are almost non-existent in the developing regions. Several studies have been conducted to assess the relationship of 2D UCPs especially vegetation fraction, impervious surface area and LULC. However, the study exploring relationships between 3D UCPs and these climatic indicators remained largely unexplored. This study is first of its own kind in the study area where the spatial variability of climatic indicators have been thoroughly studied in relation to 3D UCPs and found a strong correlation with building heights and surface roughness length.

The study also holds much significance in establishing the relationship between the derived UCPs and spatially variable climatic indicators and showcases the immense utility of these UCPs and their relationships with climatic indicators for use in urban climate models. The study is not just pioneering for the study region but also for the developing regions in semi-arid and arid tropics in development of climate sensitive urban habitations. The input parameters derived from the study and their relationship with climate indicators will help the planners for effective demarcation of climate sensitive zones and also create better FAR and building regulations suitable to the climatic set up of the urban area.

The study has also demonstrated derivation of ventilation assessment and GIS based LCZ maps in the complex and highly dense urban environment of the study region, the studies on which is non-existent. The ventilation path maps generated through this study can be used for climate studies in the study area and can serve as a basic input parameter for defining strategies for development of climate resilient urban environment.

The high accuracy of GIS based LCZ maps thus derived opens up substantial potential for development of LCZ maps which provides a better framework for UHI studies and understanding of contribution of the urban classes on the temperature patterns. It also brought out the fact that pixel based classification as proposed by the WUDAPT do not provide acceptable accuracy in complex urban environment.

7.4 KEY RECOMMENDATIONS

Key recommendations have been drawn and grouped into three broad categories that are urban canopy parameters, implications for urban climate research and modeling and implications for urban planning based on the key findings and conclusions of the study.

7.4.1 Urban Canopy Parameters

The study recommends the use of VHRS optical stereo data for retrieval of UCPs in highly complex urban environment such as present in study region. The reasonable accuracies achieved in extraction of basic input UCPs such as building height, BSF and wall area ratio recommends the use of this data for retrieval of other UCPs as well.

The study has successfully demonstrated that VHRS optical stereo data can be effectively utilized for retrieval of both 2D as well as 3D UCPs in a high density complex urban environment. It renders VHRS optical stereo data a good choice for generation of these parameters especially in an extremely heterogeneous built-up environment.

Developing regions (mostly located in tropical and sub-tropical regions) display high seasonal variability of land cover and heterogeneity of urban built form. These regions are also witnessing the rapid urbanization and quick changes in land surface cover with continuous and fast urban growth. Since the information captured using satellite data provide greater details on continuous monitoring of urban spread and seasonal variability of surface parameters due to its repetitive coverage, use of VHRS data has potential for continuous updation and monitoring of 3D configuration of urban areas as well as to provide information on seasonal variability in surface cover fractions.

Characterization of UCPs in the study region highlights highly dense, sprawled and heterogeneous urban built form of study area, which has significant impact on urban climate in the study region. The study recommends that the understanding gained in this study should be utilized for formulation of appropriate planning guidelines in the study area so as to ensure climate oriented planning in the study region.

Derivation of ventilation assessment map of study region of Delhi have been demonstrated by employing aerodynamic roughness UCPs (Zero Plane Displacement height and Surface Roughness Length) generated in this study. Analysis of ventilation assessment map has brought out lack of adequate ventilation in the study area. It renders the study region prone to severe air

pollution in winter season and high UHI conditions. Hence, study recommends the use of UCPs for derivation of ventilation map and its subsequent utilization for understanding relationship of ventilation zones with UHI.

The study recommends the use of detailed UCPs for the derivation of LCZ map in highly complex and heterogeneous urban environment as GIS based LCZ map provided very high accuracy as compared to pixel based classification.

7.4.2 Implications for urban climate studies, research and modeling

This study unlocks plethora of options for researchers, planners as well as city administrators to consider very high resolution satellite data for derivation of UCPs that are important input for urban climate studies. It opens up new vistas for urban climate research and modeling as unavailability of spatially variable UCPs in the developing region is cited as one of the major reason for limited number of urban climate studies in these regions.

It has further opened up new vistas for conducting detailed studies for urban habitations in tropical and semi tropical regions that are characterized by high seasonal variability. The improved knowledge on urban micro climate in these regions will assist in climate sensitive urban planning and design, improvement in living environment and subsequent mitigation of global climate change.

The information on UCPs thus obtained can be utilized in recently developed Urban Canopy Models (UCMs) for mesoscale and micro scale climate modeling, application of UCPs for urban climate research and for improved understanding of relationship between UCPs and climate indicators in these regions.

Utilization of LST for analyzing the relationship with 3D UCPs posed limitations due to nadir viewing geometry of satellite sensor and oversampling of TIRS data. But, this is the only spatially variable data which is available at such a high spatial resolution (30m) with long duration of temporal data available since 1984. The study finds it highly suitable for carrying out SUHI and inter seasonal variability and correlation studies. It can also be utilized for analyzing long-term trends of SUHI and integration with field observation and numerical modeling for micro scale climate simulations.

The use of WRF model for downscaling the climate variables to 500m grid resolution is also demonstrated in this study with reasonable accuracies. Given the constraints on availability of

spatially variable data for very high resolution climate indicators, the study recommends the use of WRF model simulations for obtaining the spatially variable climate indicators at micro urban scale.

7.4.3 Implications for urban planning

The derived LCZ maps has a substantial potential to be used by the development authorities and profession like architect and planners which may use them for master plan and development plan as they can help in analysing the present climatic condition of an area and provides a framework of classification which can be integrated with planning process.

Similarly, generated ventilation path map and detailed UCPs can be utilized for the preparation of Urban Climate map (UC-map), which can be a tool in the hands of planners to integrate climate knowledge into planning process for climate sensitive urban planning as well as to devise strategies for mitigation and adaptation of recent and future climate change.

The ventilation maps derived from the UCPs generated in this study provided the fundamental understanding of the ventilation zones and also the relationship between the ventilation zones and urban built-up form characteristics, an understanding which can be utilized for devising planning and policy guidelines for enhancing natural ventilation in urban areas

The relationship between ventilation zones and building surface fraction revealed that areas with high value of BSF (>0.6) exhibit weak ventilation. However, the analysis also shows that if buildings less than 9m in height also displayed adequate ventilation. This finding is interesting as compact built forms with high BSF are considered highly suitable for semi-arid and arid tropics where this study area is situated. Narrow street canyon in compact built form restricts the access of solar radiation in urban canyons and hence, considered as one of the effective measure to enhance thermal comfort in these climate zones. This is very helpful for urban planners where they can use these findings to define the zone regulations, FAR and building regulations that are sensitive and responsive to climatic setup of the given urban areas.

The analysis of LCZ maps with LST provided an improved understanding of relationship of various LCZ classes with micro climatic temperature variations. The insights thus obtained can be further utilized for identification of possible mitigation strategies for better living environment in urban areas.

7.5 SCOPE FOR FURTHER RESEARCH

This section highlights the scope for further research in four domain of urban climate studies that includes scope for further research for retrieval and characterization of UCPs, spatially variable climate indicators, application of UCPS for urban climate studies and urban planning and scope for further research in urban climate modeling.

7.5.1 Urban Canopy Parameters

In this study, VHRS optical stereo data have been utilized for the extraction of building heights. However, occlusions, shadows and vegetation poses some limitation in retrieval of very high accuracy building height distribution. In future, fusion of high resolution InSAR and VHRS optical stereo may be carried out to obtain height information in complex urban environment such as in study area. Besides, in future, the available worldwide DSM and DTM with 1 m resolution on cost basis may also be evaluated for retrieval of UCPs in complex urban environment of developing regions.

In this study, Pleiades stereo images have been utilized to extract the building height as tri-stereo Pleiades images were not available in archived data. However, Pleiades has the capabilities to provide tri-stereo images (one nadir and two off nadir). Hence, tri-stereo images with suitable acquisition geometry may be evaluated in future for extraction of building heights.

Acquisition of single season VHRS multi spectral data in future may help in overcoming the challenge posed by the classification of multi-date and season data since, vegetation in tropical and semi-tropical regions has high seasonal variability in land cover and vegetation phenology.

The obtained nDSM from optical satellite stereo data displays surface height variation in roofs. Although the variation is small ($\pm 1.5\text{m}$), the impact of variation in roof heights needs to be investigated further to analyze its impact on computation of various UCPs. Similarly, the height bias has been analyzed for three broad height groups, however impact of height bias on UCPs computation may be evaluated further as part of future research.

The validation of major input parameters for the computation of UCPs i.e. building height, building surface area and LULC have only been carried out in this study due to absence of existing 3D GIS database of study area. However, in future, validation of UCPs may be attempted for a group of buildings in a neighborhood by obtaining 3D information either from secondary sources or through ground based surveys.

The computation of key roughness UCPs such as frontal area index, frontal area density and surface roughness length is direction dependent. Computation of these parameters requires 3D GIS vector database and use of automated tools. The available tools (UMEP and UME) did not yield satisfactory results in highly dense and heterogeneous urban environment of study areas, hence, in future modified approaches or tools may be employed for computation of these key roughness UCPs. In future, vegetation and terrain for the computation of roughness characteristics may also help in extending these methodologies for all kind of terrain and ecological regions.

Unmanned Aerial Vehicles (UAVs) popularly known as drones is an upcoming technology which is capable of providing super high resolution (2-5 cm) optical stereo and very high density LiDAR point cloud due to its low flying height. It may prove to be a potential technology for mapping of core areas having very high density of built-up. It may be able to provide highly detailed characteristics of urban areas which may assist in resolving the narrow street canyons in compact urban built form. It also has capabilities to provide very high resolution (spatial and temporal) information on thermal remote sensing and atmospheric variables which may be utilized for understanding the complex relationship of UCPs with climate indicators.

7.5.2 Choice of Grid Size

In this study, 30 m grid resolution have been applied in order to minimize the averaging effect on building height which is observed in the study area due to highly heterogeneous development. However, it has resulted in depiction of larger buildings in a number of pixels with a BSF value of 1. Hence, in future, computation of UCPs on various grid sizes (coarser to finer) may be attempted to investigate the effect of various grid sizes (coarser to finer) on UCPs especially on 100m grid size to capture local scale characteristics as recommended by WUDAPT (Bechtel et al., 2015).

The WUDAPT recommends use of 100 m grid size in order, however, due to highly heterogeneous development of Delhi , it was found that coarser grid size has strong averaging effect on building heights and most of the high rise building area was converted into mid-rise buildings area. On the other hand, small grid sizes depicts larger objects in more number of pixels. For example, a large size industrial building or shopping mall is covered in more than one pixel. It leads to BSF values of 1 in few of the grids. Although it constitutes a very small fraction of total built up area. The study on the scale effect in Hong Kong revealed that accuracy of urban morphological characteristics increases with the coarser spatial scale(Xu et al., 2017). The study

achieved better fitting accuracy with 500m grid size. However, further investigation is needed in the study area for better understanding of the effect of scale/grid size for the retrieval of UCPs.

7.5.3 Spatially Variable Urban Climate indicators

A temporal study covering the region across multiple dates and years may be carried out in future to establish detailed understanding on UCPs –LST relationship.

The independent assessment of 2D and 3D UCPs would only be possible if temperature of all surfaces which actively take part in modification of micro urban climate is considered. The availability of 3D complete temperature data cube through modeling and simulation may assist in drawing better correlation statistics.

LST obtained through thermal remote sensing has shortcomings as discussed in previous section. It does not provide wall- to-wall complete surface temperature of urban surfaces which is must to understand the relationship of 3D UCPs with temperature variations. LST is not only different from air temperature, it also over represents the horizontal urban surfaces. In future, improved numerical model can be used to obtain complete 3D temperature data cube in future to assess the micro level variations in urban areas and improved understanding of urban thermal environment and correlation with 3D UCPs.

It also brought to attention that UHI is a relative phenomenon which is dependent on surrounding land surface cover. The study region is surrounded by substantial amount of bare soil (~30%), which heats up faster as compared to urban area, while urban area takes time to gain heat due to shading of surfaces and thermal lag time of built-up materials. Various researchers have applied 11:00 AM pass of Landsat satellite to study UHI, however, at this hour especially in summer the built-up area displays less temperature in semi-arid climate zone of study area as compared to surroundings due to low thermal capacity of bare soil. This phenomenon and use of morning pass for UHI studies needs a thorough investigation in future especially in arid and semi-arid regions.

High resolution WRF-urban simulations at sub-km scales are computer resource intensive. In future, with an increase in computational resources, longer duration simulations may also be carried out for long term study of climate variability in urban regions.

Downscaling of the climate indicators in WRF-urban may be improved further by coupling it with high resolution urban climate models and ingestion of detailed UCPs for simulation of high resolution climate variables. Further downscaling of WRF-Urban may also assist in analyzing

the relationship of UCPs with other climate variables other than LST and may also be utilized to investigate intra-urban variations.

7.5.4 Application of Urban Canopy Parameters

The unavailability of proper ventilation corridors retards the air flow within the built-up area resulted in very weak circulation and thereby restricts the continuous flow and exchange of fresh air in these regions. It is recommended to carry out further investigation and explore the relationship between street orientation and prevailing wind direction for better understanding of ventilation zones and their pattern in each of these zones.

The study region of Delhi has composite climate with varied dominant wind directions in different seasons, thus poses varied requirements for enhancing thermal comfort in different seasons. Hence, in future, seasonal impact of wind flow through development of direction specific ventilation path maps may provide better understanding to devise strategies for adequate ventilation in urban areas.

The criteria for identification of ventilation corridor have been adopted from Matzarakis and Mayer 1992 who proposed these guidelines based on VDI 1988 and 1989 developed for Germany. Since Germany has temperate and marine climate and its development pattern is very different from the study area. Investigation of suitable criteria for tropical and semi-tropical countries may be carried out to develop guidelines suited to these climate zones.

7.5.5 Urban climate Research and Modeling

The derived LCZ map can also be ingested in numerical models for improved simulations and forecasting over urban areas. The detailed UCPs generated in this study may also be ingested in the model in near future to evaluate the impact of gridded roughness characteristics on model simulations. UCPs retrieved in this study may also be utilized for generating level 1 and level 2 data of WUDAPT and can be suitably ingested in mesoscale models for urban climate modeling.

Further optimization in WRF model physics, simulation time and computational resources may enhance model capabilities for further high resolution simulations and integration of detailed UCPs in the model. The optimization of model may enhance opportunities for improved simulations, weather forecast and predictions, urban climate maps studies and urban climate research.

The key findings and conclusions of this study recommends the use of VHRS optical stereo data for retrieval of 2D as well as 3D UCPs in complex and heterogeneous urban environment of developing regions. This is the next best suitable alternative available in the absence of Airborne LiDAR and aerial images data in the developing regions. Similarly, study also recommends use of retrieved UCPs for host of applications ranging from ventilation assessment, GIS based LCZ map, UC-map, parameterization of urban characteristics in numerical modeling and so on. Availability of information on UCPs has substantial potential for understanding the climate characteristics of urban areas in developing regions, carrying out urban climate research, improved modeling of urban climate phenomenon and climate oriented urban planning to mitigate climate change impacts and to ensure sustainable development.





BIBLIOGRAPHY

- Adolphe, L. (2001). A Simplified Model of Urban Morphology: Application to an Analysis of the Environmental Performance of Cities. *Environment and Planning B: Planning and Design*, 28(2), 183–200. <https://doi.org/10.1068/b2631>
- Al-Sallal, K. A., & Al-Rais, L. (2012). Outdoor airflow analysis and potential for passive cooling in the modern urban context of Dubai. *Renewable Energy*, 38(1), 40–49. <https://doi.org/10.1016/J.RENENE.2011.06.046>
- Alcoforado, M. J., Andrade, H., Lopes, A., & Vasconcelos, J. (2009). Application of climatic guidelines to urban planning. The example of Lisbon (Portugal). *Landscape and Urban Planning*, 90, 56–65. <https://doi.org/10.1016/j.landurbplan.2008.10.006>
- Alcoforado, M. J., Lopes, A. S., & Andrade, H. (2015). Urban climatic map studies in Portugal: Lisbon. In E. Ng & C. Ren (Eds.), *The Urban Climatic Map: A Methodology for Sustainable Urban Planning* (1st ed., pp. 209–236). <https://doi.org/10.4324/9781315717616>
- Ali-Toudert, F., & Mayer, F. H. (2006). Numerical study on the effects of aspect ratio and orientation of an urban street canyon on outdoor thermal comfort in hot and dry climate. *Building and Environment*, 41, 94–108.
- Anon. (n.d.-a). CISL RDA: ECMWF IFS CY41r2 High-Resolution Operational Forecasts. Retrieved December 24, 2019, from <https://rda.ucar.edu/datasets/ds113.1/>
- Anon. (n.d.-b). SKYVIEW. Retrieved December 24, 2019, from https://www.pcigeomatics.com/geomatica-help/references/pciFunction_r/python/P_skyview.html
- Anon. (2011a). District Census Handbook , Ghaziabad. Retrieved May 21,2019 from http://censusindia.gov.in/2011census/dchb/0909_PART_B_DCHB_GHAZIABAD.pdf
- Anon. (2011b). Haryana Series-07 PART XII-B District Census Handbook Faridabad , Census of India 2011. Retrieved May 21,2019 from http://censusindia.gov.in/2011census/dchb/0620_PART_B_DCHB_FARIDABAD.pdf
- Anon. (2011c). Uttar Pradesh District Census Handbook Gautam Buddha Nagar, Census of India 2011. Retrieved May 21,2019 from http://censusindia.gov.in/2011census/dchb/0910_PART_B_DCHB_GAUTAM BUDDHA NAGAR.pdf
- Anon. (2011d). District Census Handbook, NCT of Delhi. Retrieved May 21,2019 from Directorate of Census Operations, Delhi website: http://censusindia.gov.in/2011census/dchb/0700_PART_A_DCHB_NCT OF DELHI.pdf
- Anon. (2012a). Chapter 1: Introduction. In Economic Survey of Delhi, 2005–2006. Retrieved May 22,2019 from http://delhi.gov.in/wps/wcm/connect/DoIT_Planning/planning/economic+survey+of+delhi/content3/introduction
- Anon.. (2012b). Epidemiological Study on Effect of Air Pollution on Human Health (Adults) in Delhi. Retrieved May 19, 2019 from

- http://cpcb.nic.in/uploads/healthreports/Epidemiological_study_Adult_Peer_2012.pdf reviewed-
- Anon. (2016a). Functional Plan on Drainage for NCR. National Capital Region Planning Board, Min. of Urban Development, Govt. of India.
- Anon. (2016b). Ground Water Year Book. Retrieved May 23,2019 from http://cgwb.gov.in/Regions/GW-year-Books/GWYB-2015-16/GWYB_Delhi_2015-16.pdf
- Arrhenius, S. (1896). On the influence of carbonic acid in the air upon the temperature of the ground. London, Edinburgh, and Dublin. *Philosophical Magazine and Journal of Science*, 41, 237–275.
- Arora M.K. (2010). Land cover classification from Remote Sensing data - Geospatial World. Retrieved May 21, 2019, from Geospatial World website: <https://www.geospatialworld.net/article/land-cover-classification-from-remote-sensing-data/>
- Attri, S. D., & Tyagi, A. (2009). Climate Profile of India. Retrieved April 21,2019 from http://www.indiaenvironmentportal.org.in/files/climate_profile.pdf
- Awrangjeb, M., Zhang, C., & Fraser, C. S. (2015). Building Detection in Complex Scenes Through Effective Separation of Buildings from Trees. *Photogrammetric Engineering & Remote Sensing*, 78(7), 729–745. <https://doi.org/10.14358/pers.78.7.729>
- Babazadeh, M., & Kumar, P. (2015). Estimation of the Urban Heat Island in Local Climate Change and Vulnerability Assessment for Air Quality in Delhi. *European Scientific Journal*, 7881(June), 55–65.
- Bakarman, M. A., & Chang, J. D. (2015). The Influence of Height/width Ratio on Urban Heat Island in Hot-arid Climates. *Procedia Engineering*, 118, 101–108. <https://doi.org/10.1016/J.PROENG.2015.08.408>
- Baklanov, A., Grimmond, C.S.B., Carlson, D., Terblanche, D., Tang, X., Bouchet, V., Lee, B., Langendijk, G., Kolli, R.K., Hovsepyan, A (2018). From urban meteorology, climate and environment research to integrated city services. *Urban Climate*, 23, 330–341. <https://doi.org/10.1016/j.uclim.2017.05.004>
- Barsi, J. A., Lee, K., Kvaran, G., Markham, B. L., & Pedelty, J. A. (2014). The spectral response of the Landsat-8 operational land imager. *Remote Sensing*, 6(10), 10232–10251. <https://doi.org/10.3390/rs61010232>
- Bechtel, B., Alexander, P., Böhner, J., Ching, J., Conrad, O., Feddema, J., Mills, G., See, L., Stewart, I. D. (2015). Mapping Local Climate Zones for a Worldwide Database of the Form and Function of Cities. *ISPRS International Journal of Geo-Information*, 4(1), 199–219. <https://doi.org/10.3390/ijgi4010199>
- Bechtel, B., Demuzere, M., Sismanidis, P., Fenner, D., Brousse, O., Beck, C., Van C., Frieke, Olaf C., Iphigenia, K, Ariane M., Mills, G., Niyogi, D., Otto, M., See, L., Verdonck, Marie-Leen (2017). Quality of Crowdsourced Data on Urban Morphology—The Human Influence Experiment (HUMINEX). *Urban Science*, 1(2), 15. <https://doi.org/10.3390/urbansci1020015>
-

- Bechtel, B., Alexander, P. J., Beck, C., Böhner, J., Brousse, O., Ching, J., Demuzere, M., Fonte, C., Gál, T., Hidalgo, J., Hoffmann, P., Middel, A., Mills, G., Ren, C., See, L., Sismanidis, P., Verdonck, Marie-Leen, Xu, G., Xu, Y. (2019). Generating WUDAPT Level 0 data – Current status of production and evaluation. *Urban Climate*, 27, 24–45. <https://doi.org/10.1016/j.uclim.2018.10.001>
- Berger, C., Rosentreter, J., Voltersen, M., Baumgart, C., Schmuilius, C., & Hese, S. (2017). Spatio-temporal analysis of the relationship between 2D/3D urban site characteristics and land surface temperature. *Remote Sensing of Environment*, 193, 225–243. <https://doi.org/10.1016/j.rse.2017.02.020>
- Bhagwan Sahay, C., Kumharji Members, G., Shanta Vashist, K., Nair, C., Bahl, R. R., & Kumar Vaish, R. (1962). *Master Plan for Delhi, 1962*. Retrieved from www.rgplan.org
- Bhaskaran, S., Paramananda, S., & Ramnarayan, M. (2010). Per-pixel and object-oriented classification methods for mapping urban features using Ikonos satellite data. *Applied Geography*, 30, 650–665. <https://doi.org/10.1016/j.apgeog.2010.01.009>
- Bhavana, M., Gupta, Kshama, Pal P. K. (2018). Improved Urban Parameters for Urban Micro-Climate Modelling Using WRF Model. *Centre for Space Science and Technology Education in Asia-Pacific, Dehradun* (Unpublished Thesis).
- Bhavana, M., Gupta, Kshama, Pal, P. K., Kumar, A. S., & Gummapu, J. (2018). Evaluation of High Resolution Urban LULC for Seasonal Forecasts of Urban Climate using WRF Model. *ISPRS Annals of Photogrammetry, Remote Sensing and Spatial Information Sciences*, IV–5, 303–310. <https://doi.org/10.5194/isprs-annals-IV-5-303-2018>
- Blake, R., Grimm, A., Ichinose, T., Horton, R., Gaffin, S., Jiong, S., Bader, D., & Cecil, L. D. (2011). Urban climate: Processes, trends, and projections. Climate Change and Cities. In Rosenzweig, C., Solecki, W. D., S. A. Hammer, & S. Mehrotra (Eds.), *First Assessment Report of the Urban Climate Change Research Network* (pp. 43–81). Cambridge, UK: Cambridge University Press.
- Bonafoni, S., Baldinelli, G., Rotili, A., & Verducci, P. (2017). Albedo and surface temperature relation in urban areas: Analysis with different sensors. *2017 Joint Urban Remote Sensing Event (JURSE)*, 1–4. <https://doi.org/10.1109/JURSE.2017.7924612>
- Bottema, M. (1997). Urban roughness modelling in relation to pollutant dispersion. *Atmospheric Environment*, 31(18), 3059–3075. [https://doi.org/10.1016/S1352-2310\(97\)00117-9](https://doi.org/10.1016/S1352-2310(97)00117-9)
- Bretar, F., Wagner, W., & Paparoditis, N. (2011). Advances in LiDAR data processing and applications. *ISPRS Journal of Photogrammetry and Remote Sensing*, 66(6), S1. <https://doi.org/10.1016/j.isprsjprs.2011.12.002>
- Brousse, O., Martilli, A., Foley, M., Mills, G., & Bechtel, B. (2016). WUDAPT, an efficient land use producing data tool for mesoscale models? Integration of urban LCZ in WRF over Madrid. *Urban Climate*, 17, 116–134. <https://doi.org/10.1016/j.uclim.2016.04.001>
- Brown, M. J., & Williams, M. D. (1998). *An Urban Canopy Parameterization for Mesoscale Meteorological Models*. Retrieved from <https://permalink.lanl.gov/object/tr?what=info:lanl-repo/lareport/LA-UR-98-3831>

- Burian, Steven J, Velugubantla, S. P., & Brown, M. J. (2002a). Morphological Analyses using 3D Building Databases: Phoenix, Arizona. In *LA-UR-01-4055*.
- Burian, Steven J, Brown, M. J., & Linger, S. P. (2002b). Morphological Analyses using 3D Building Databases: Los Angeles, California. In *LA-UR-02-781*. Retrieved from <https://www.researchgate.net/publication/260286741>
- Burian, SJ, Han, W., & Brown, M. (2003a). Morphological analyses using 3D building databases: Houston, Texas. *Los Alamos National Laboratory*, (November 2003). Retrieved from http://www.researchgate.net/profile/Michael_Brown44/publication/260339606_Morphological_Analyses_Using_3D_Building_Databases_Houston_Texas/links/0deec530d7d3edd075000000.pdf
- Burian, Steven J, & Brown, M. J. (2003b). Morphological analyses using 3D building databases: Oklahoma City. Retrieved from <https://www.researchgate.net/publication/260286743>
- Burian, Steven, Brown, M. J., Ching, J. K. S., Cheuk, M. L., Yuan, M., Han, W., & McKinnon, A. T. (2004a). Urban morphological analysis for mesoscale meteorological and dispersion modeling applications: current issues. *Fifth Symposium on Urban Environment*, 11. Retrieved from <https://ams.confex.com/ams/AFAPURBBIO/webprogram/Paper80276.html>.
- Burian, Steven J, Stetson, Stephen W., Han, W., & Ching, Jason, Byun, D. (2004b). High-Resolution Dataset of Urban Canopy Parameters for Houston, Texas. *Fifth Symposium on the Urban Environment, American Meteorological Society, Vancouver, BC, Canada 23-28 August 2004.*, (August), 1–9. Vancouver, BC, Canada.
- Burian, S. J., & Shepherd, J. M. (2005). Effect of urbanization on the diurnal rainfall pattern in Houston. *Hydrological Processes*, 19, 1089–1103.
- Burian, Steven, & Jason, C. (2009). *Development of Gridded Fields of Urban Canopy Parameters for Advanced Urban Meteorological and Air Quality Models*. Retrieved from http://cfpub.epa.gov/si/si_public_record_report.cfm?dirEntryId=213904
- Campbell, I., Kalanki, A., & Sachar, S. (2018). *Solving the Global Cooling Challenge: How to Counter the Climate Threat from Room Air Conditioners*. Retrieved from www.rmi.org/insight/solving_the_global_cooling_challenge.
- Carter, M., Shepherd, J. M., Burian, S., Jeyachandran, I., (2012). Integration of Lidar Data into a Coupled Mesoscale–Land Surface Model: A Theoretical Assessment of Sensitivity of Urban–Coastal Mesoscale Circulations to Urban Canopy Parameters. *Journal of Atmospheric and Oceanic Technology*, 29(3), 328–346. <https://doi.org/10.1175/2011JTECHA1524.1>
- Central Pollution Control Board. (2016). *Air pollution in Delhi: An Analysis*. Retrieved from [http://cpcbenvi.nic.in/envi_newsletter/Air pollution in Delhi.pdf](http://cpcbenvi.nic.in/envi_newsletter/Air%20pollution%20in%20Delhi.pdf)
- Chakraborty, S. D., Kant, Y., & Mitra, D. (2015). Assessment of land surface temperature and heat fluxes over Delhi using remote sensing data. *Journal of Environmental Management*, 148, 143–152. <https://doi.org/10.1016/j.jenvman.2013.11.034>
- Chakraborty A, Seshasai MVR, Rao. SK, and Dadhwal V.K. (2017). Geo-spatial analysis of

- temporal trends of temperature and its extremes over India using daily gridded ($1^\circ \times 1^\circ$) temperature data of 1969–2005. *Theoretical and Applied Climatology*, 130(1–2), 133–149.
- Chang, S., Jiang, Q., & Zhao, Y. (2018). Integrating CFD and GIS into the development of urban ventilation corridors: A case study in Changchun City, China. *Sustainability (Switzerland)*, 10(6). <https://doi.org/10.3390/su10061814>
- Chapman, L., Thornes, J. E., & Bradley, A. V. (2002). Sky-view factor approximation using GPS receivers. *International Journal of Climatology*, 22, 615–621. <https://doi.org/10.1002/joc.649>
- Chatrath, D., & Pushplata. (2018). *A study of development patterns in peripheral urban areas*. Indian Institute of Technology, Roorkee.
- Chen, F., Kusaka, H., Tewari, M., Bao, J.-W., & Hirakuchi, H. (2004). Utilizing the coupled WRF/LSM/urban modeling system with detailed urban classification to simulate the urban heat island phenomena over the greater Houston area. Retrieved June 12, 2019, from <http://citeseerx.ist.psu.edu/viewdoc/download?doi=10.1.1.568.1067&rep=rep1&type=pdf>
- Chen, F., Kusaka, H., Bornstein, R., Ching, J., Grimmond, C. S.B., Grossman-Clarke, S., Loridan, T., Manning, K. W., Martilli, A., Miao, S., Sailor, David, S., Francisco P, Taha, H., Tewari, M., Wang, X., Wyszogrodzki, A. A, Zhang, C., (2011). The integrated WRF/urban modelling system: Development, evaluation, and applications to urban environmental problems. *International Journal of Climatology*, 31(2), 273–288. <https://doi.org/10.1002/joc.2158>
- Chen, L., & Ng, E. (2011). Quantitative urban climate mapping based on a geographical database: A simulation approach using Hong Kong as a case study. *International Journal of Applied Earth Observations and Geoinformation*, 13, 586–594. <https://doi.org/10.1016/j.jag.2011.03.003>
- Chen, Y., Tong, Z., & Malkawi, A. (2017). Investigating natural ventilation potentials across the globe: Regional and climatic variations. *Building and Environment*, 122, 386–396. <https://doi.org/10.1016/j.buildenv.2017.06.026>
- Ching J., Mills G., Bechtel B., See L., Feddema J., Wang X., Ren C., Brousse O., Martilli A., Neophytou M., Mouzourides P., Stewart I., Hanna A., Ng E., Foley M., Alexander, P., Aliaga D., Niyogi D., Shreevastava A., Bhalachandran P., Masson V., Hidalgo J., Fung J., Andrade M., Baklanov A., Dai W., Milcinski G., Demuzere M., Brunsell N., Pesaresi M., Miao S., Mu Q., Chen F., and Theeuwes N., (n.d.). WUDAPT: An Urban Weather, Climate, and Environmental Modeling Infrastructure for the Anthropocene. *Bulletin of the American Meteorological Society*, 1907-1924, Retrieved June 28, 2019 from <https://journals.ametsoc.org/doi/pdf/10.1175/BAMS-D-16-0236.1>.
- Ching, J., Brown, M., Burian, S., Chen, F., Cionco, R., Hanna, A., Hultgren, T., Mcpherson, T., Sailor, D., Taha, H., Williams, D (2009). National Urban Database and Access Portal Tool. *Bulletin of American Meteorological Society*, (August 2009), 1157–1168. <https://doi.org/10.1175/2009BAMS2675.1>
- Chun, B., & Guldmann, J.-M. (2014). Spatial statistical analysis and simulation of the urban heat island in high-density central cities. *Landscape and Urban Planning*, 125, 76–88. <https://doi.org/10.1016/J.LANDURBPLAN.2014.01.016>
-

- Coeurdevey, L., & Fernandez, K. (2012). *DEFENCE AND SPACE Intelligence Pléiades Imagery User Guide*.
- Conzen, M. P. (2001). The study of urban form in the United States. Retrieved May 11, 2019 from <http://www.urbanform.org/pdf/conzen2001.pdf>
- Counihan, J. (1971). Wind tunnel determination of the roughness length as a function of the fetch and the roughness density of three-dimensional roughness elements. *Atmospheric Environment* (1967), 5(8), 637–642. [https://doi.org/10.1016/0004-6981\(71\)90120-X](https://doi.org/10.1016/0004-6981(71)90120-X)
- Dare, P. M. (2005). Shadow analysis in high-resolution satellite imagery of urban areas. *Photogrammetric Engineering & Remote Sensing*, 71, 169–177.
- Deilami, K., Kamruzzaman, M., & Liu, Y. (2018). Urban Heat Island effect: A systematic review of spatio-temporal factors, data, methods, and mitigation measures. *International Journal of Applied Earth Observation and Geoinformation*, 67, 30–42.
- Demographia World Urban Areas: 2019: Population, Land Area & Urban Densities | Newgeography.com. (n.d.). Retrieved May 19, 2019, from <http://www.newgeography.com/content/006272-demographia-world-urban-areas-2019-population-land-area-urban-densities>
- Deng, C., & Wu, C. (2012). BCI: A biophysical composition index for remote sensing of urban environments. *Remote Sensing of Environment*, 127, 247–259. <https://doi.org/10.1016/j.rse.2012.09.009>
- DESA/UN-WUP. (2018). World Urbanization Prospects: The 2018 Revision. In *Department of Economic and Social Affairs*. Retrieved from <https://population.un.org/wup/Publications/Files/WUP2018-KeyFacts.pdf>
- Dini, G. R., Jacobsen, K., & Heipke, C. (2013). Delineation of Building Footprints from High Resolution Satellite Stereo Imagery using Image Matching and a GIS Database. *International Archives of the Photogrammetry, Remote Sensing and Spatial Information Sciences*, XL-1/W1, 81–85. Retrieved from <https://pdfs.semanticscholar.org/cfae/c7cb3759e160d81eb09c92e9a748234b6679.pdf>
- Dozier, J., & Frew, J. (1990). Rapid Calculation of Terin Parameters For Radiation Modeling From Digital Elevation Data. *IEEE Transactions on Geoscience and Remote Sensing*, 28(5), 963–969. <https://doi.org/10.1109/36.58986>
- Duda, M. (2007). *The WRF Preprocessing System: Overview and Installation*. Retrieved from https://dtcenter.org/events/tutorial07_winter/Presentations/Gill_wps_overview.pdf
- Dupont, V. (2004). Urban Development and Population Redistribution in Delhi: Implications for Categorizing Population. In T. Champion & G. Hugo (Eds.), *New Forms of Urbanization Beyond the Urban-Rural Dichotomy* (pp. 171–193). Retrieved from http://horizon.documentation.ird.fr/exl-doc/pleins_textes/divers17-07/010045617.pdf
- Efe, S. I., & Eyefia, A. O. (2014). Urban Effects on the Precipitation of Benin, Nigeria. *American Journal of Climate Change*, 3, 8–21.
- Ellefsen, R. (1991). Mapping and measuring buildings in the canopy boundary layer in ten U.S. cities. *Energy and Buildings*, 15–16, 1025–1049. Retrieved from

https://www.researchgate.net/publication/256596858_Mapping_and_measuring_buildings_in_the_canopy_boundary_layer_in_ten_US_cities

- Ellefsen, R., & Cionco, R. M. (2002). A method for inventorying urban morphology. *Fourth Symposium on the Urban Environment*. Norfolk: American Meteorological Society.
- Emmanuel, R. (2016). *Urban Climate Challenges in the Tropics*. Imperial College Press, <https://doi.org/10.1142/p1048>.
- Epstein, J., Payne, K., & Kramer E. (2002). Techniques for mapping suburban sprawl. *Photogr. Eng. Remote Sens.*, 63(9), 913–918.
- Erell, E., Pearlmutter, D., & Williamson, T. T. J. (2011). *Urban microclimate: designing the spaces between buildings*. London: Routledge.
- Fisher, P. (1997). The pixel: A snare and a delusion. *International Journal of Remote Sensing*, 18(3), 679–685. <https://doi.org/10.1080/014311697219015>
- Fraser, C. S., Baltasvias, E., & Gruen, A. (2001). 3D building reconstruction from high-resolution ikonos stereo-imagery. In E. P. Baltasvias, A. Grün, & L. Van Gool (Eds.), *Automatic Extraction of Man-Made objects from aerial and space images(III)* (1st ed., pp. 331–344). Ascona: Balkema.
- Gál, T., & Sümeghy, Z. (2007). Mapping the Roughness Parameters in a Large Urban Area for Urban Climate Applications. *Acta Climatologica Et Chorologica*, 40–41, 27–36.
- Gál, T., & Unger, J. (2009a). Detection of ventilation paths using high-resolution roughness parameter mapping in a large urban area. *Building and Environment*, 44(1), 198–206. <https://doi.org/10.1016/j.buildenv.2008.02.008>
- Gál, Tamás, Lindberg, F., & Unger, J. (2009b). Computing continuous sky view factors using 3D urban raster and vector databases: Comparison and application to urban climate. *Theoretical and Applied Climatology*, 95(1–2), 111–123. <https://doi.org/10.1007/s00704-007-0362-9>
- Ganguly, K., Kumar, R., Mruthyunjaya Reddy, K., Jagadeeswara Rao, P., Raj Saxena, M., & Ravi Shankar, G. (2017). Optimization of spatial statistical approaches to identify land use/land cover change hot spots of Pune region of Maharashtra using remote sensing and GIS techniques. *Geocarto International*, 32(7), 777–796. <https://doi.org/10.1080/10106049.2016.1178813>
- Garratt, J. R. (1992). *The Atmospheric Boundary Layer*. Cambridge: University Press, Cambridge.
- Garuma, G. F. (2018). Review of urban surface parameterizations for numerical climate models. *Urban Climate*, 24, 830–851. <https://doi.org/10.1016/j.uclim.2017.10.006>
- Geletič, J., & Lehnert, M. (2016). GIS-based delineation of local climate zones: The case of medium-sized Central European cities. *Moravian Geographical Reports*, 24(3), 2–12. <https://doi.org/10.1515/mgr-2016-0012>
- Georgatou, C., & Kolokotsa, D. (2016). Urban Climate Models. In M. Santamouris & D. Kolokotsa (Eds.), *Urban Climate Mitigation Techniques* (1st ed., pp. 175–194). New York,

New York, USA: Routledge.

- Gharai, B., Rao, P. V. N., & Dutt, C. B. S. (2018). Mesoscale model compatible IRS-P6 AWiFS-derived land use/land cover of Indian region. *Current Science*, 115(12), 2301–2306. <https://doi.org/10.18520/cs/v115/i12/2297-2301>
- Giridharan, R. (2016). Urban climate modeling: challenges in the tropics. In R. Emmanuel (Ed.), *Urban climate challenges in the tropics* (1st ed., pp. 255–304). London: Imperial College Press.
- Givoni, B. (1992). Climatic aspects of urban design in tropical regions. *Atmospheric Environment. Part B. Urban Atmosphere*, 26(3), 397–406. [https://doi.org/10.1016/0957-1272\(92\)90015-K](https://doi.org/10.1016/0957-1272(92)90015-K)
- Givoni, B. (1998). *Climate considerations in building and urban design*. Retrieved from <https://www.wiley.com/en-aw/Climate+Considerations+in+Building+and+Urban+Design-p-9780471291770>
- Global Human Settlement - Data overview - European Commission. (2016). Retrieved June 15, 2019, from European Commission website: <https://ghsl.jrc.ec.europa.eu/data.php>
- Glotfelty, T., Tewari, M., Sampson, K., Duda, M., Chen, F., & Ching, J. (2013). NUDAPT 44 Documentation. Retrieved May 2, 2019, from https://ral.ucar.edu/sites/default/files/public/product-tool/NUDAPT_44_Documentation.pdf
- Griend, A. A. van de., Owe, M., Chang, A. T. C. (Alfred T. C.), & Vugts, H. F. (1992). *Botswana water and surface energy balance research program*. Retrieved from <http://boysen.berry.edu/title/botswana-water-and-surface-energy-balance-research-program-pt-1-integrated-approach-and-field-campaign-results/oclc/769736426>
- Grimmond, C. S. B., & Souch, C. (1994). Surface description for urban climate Studies: a GIS based methodology. *Geocarto International*, 9, 47–59.
- Grimmond, C. S. B., King, T. S., Roth, M., & Oke, T. R. (1998). Aerodynamic roughness of urban areas derived from wind observations. *Boundary-Layer Meteorology*, 89(1), 1–24. <https://doi.org/10.1023/A:1001525622213>
- Grimmond, C. S. B., & Oke, T. R. (1999). Aerodynamic Properties of Urban Areas Derived from Analysis of Surface Form. *Journal of Applied Meteorology*, 38(9), 1262–1292. [https://doi.org/10.1175/1520-0450\(1999\)038<1262:APOUAD>2.0.CO;2](https://doi.org/10.1175/1520-0450(1999)038<1262:APOUAD>2.0.CO;2)
- Grimmond, C.S.B., Roth, M., Oke, T.R., Au, Y.C., Best, M., Betts, R., Carmichael, G., Cleugh, H., Dabberdt, W., Emmanuel, R., Freitas, E., Fortuniak, K., Hanna, S., Klein, P., Kalkstein, L.S., Liu, C.H., Nickson, A., Pearlmutter, D., Sailor, D., Voogt, J. (2010a). Climate and More Sustainable Cities: Climate Information for Improved Planning and Management of Cities (Producers/Capabilities Perspective). *Procedia Environmental Sciences*, 1, 247–274. <https://doi.org/10.1016/J.PROENV.2010.09.016>
- Grimmond, C. S. B., Blackett, M., Best, M. J., Barlow, J., Baik, J-J., Belcher, S. E., Bohnenstengel, S. I., Calmet, I., Chen, F., Dandou, A., Fortuniak, K., Gouvea, M. L., Hamdi, R., Hendry, M., Kawai, T., Kawamoto, Y., Kondo, H., Krayenhoff, E. S., Lee, S-H., Loridan,

- T., Martilli, A., Masson, V., Miao, S., Oleson, K., Pigeon, G., Porson, A., Ryu, Y-H., Salamanca, F., Shashua-Bar, L., Steeneveld, G-J., Tombrou, M., Voogt, J., Young, D., Zhang, N (2010b). The International Urban Energy Balance Models Comparison Project: First Results from Phase 1. *Journal of Applied Meteorology and Climatology*, 49(6), 1268–1292. <https://doi.org/10.1175/2010JAMC2354.1>
- Grimmond, C. S. B., Blackett, M., Best, M. J., Baik, J.-J., Belcher, S. E., Beringer, J., Bohnenstengel, S. I., Calmet, I., Chen, F., Coutts, A., Dandou, A., Fortuniak, K., Gouvea, M. L., Hamdi, R., Hendry, M., Kanda, M., Kawai, T., Kawamoto, Y., Kondo, H., Krayenhoff, E. S., Lee, S.-H., Loridan, T., Martilli, A., Masson, V., Miao, S., Oleson, K., Ooka, R., Pigeon, G., Porson, A., Ryu, Y.-H., Salamanca, F., Steeneveld, G.J., Tombrou, M., Voogt, J. A., Young, D. T., Zhang, N.. (2011). Initial results from Phase 2 of the international urban energy balance model comparison. *International Journal of Climatology*, 31(2), 244–272. <https://doi.org/10.1002/joc.2227>
- Grover, A., & Singh, R. (2015). Analysis of Urban Heat Island (UHI) in Relation to Normalized Difference Vegetation Index (NDVI): A Comparative Study of Delhi and Mumbai. *Environments*, 2(4), 125–138. <https://doi.org/10.3390/environments2020125>
- Guha, S., Govil, H., Dey, A., & Gill, N. (2018). Analytical study of land surface temperature with NDVI and NDBI using Landsat 8 OLI and TIRS data in Florence and Naples city, Italy. *European Journal of Remote Sensing*, 51(1), 667–678. <https://doi.org/10.1080/22797254.2018.1474494>
- Guleria, S., & Gupta, A. K. (2016). *Heat Wave in India*. Retrieved from https://nidm.gov.in/PDF/pubs/heat_wave_18.pdf
- Guo, G., Zhou, X., Wu, Z., Xiao, R., & Chen, Y. (2016). Characterizing the impact of urban morphology heterogeneity on land surface temperature in Guangzhou, China. *Environmental Modelling and Software*, 84, 427–439. <https://doi.org/10.1016/j.envsoft.2016.06.021>
- Gupta, K., & Jain, S. (2005). Enhanced capabilities of IRS P6 LISS IV sensor for urban mapping. *Current Science*, 89(11), 1805–1812.
- Gupta, K., Bhardwaj, A., Kumar, P., & Pushpalata. (2015). Procedural Rule Based 3D City Modeling and Visualization using High Resolution Satellite Data. *International Journal of Advancement in Remote Sensing, GIS and Geography*, 3(2).
- Gupta Kshama, Pushplata, John Sandeep, Bhardwaj Ashutosh, Kumar Pramod, Kumar, A. S. (2017a). Comparative evaluation of Pleiades, Cartosat- 2 and Kompsat-3 Stereo data for DSM and 3D model generation. *38th Asian Conference on Remote Sensing: Space Applications: Touching Human Lives*, 1–7. Retrieved from https://scholar.google.co.in/citations?user=9E_dmkgAAAAJ&hl=en#d=gs_md_cita-d&u=%2Fcitations%3Fview_op%3Dview_citation%26hl%3Den%26user%3D9E_dmkgAAAAJ%26citation_for_view%3D9E_dmkgAAAAJ%3AfQNAKQ3IYiAC%26tzom%3D-330
- Gupta, K., Pushplata, Rajwal, T., Nekkla, S., Kumar, P., & Senthil Kumar, A. (2017b). Investigating the relationship of urban form and function with surface temperature patterns: A case study of Chandigarh. *38th Asian Conference on Remote Sensing - Space Applications: Touching Human Lives, ACRS 2017*, 6. Retrieved from <https://www.scopus.com/inward/record.uri?eid=2-s2.0->

85047431690&partnerID=40&md5=4506b9c8909e70e9393e6bdd77f09ca7%0Ahttps://www.researchgate.net/profile/Kshama_Gupta3/publication/321161074_ Investigating_the_relationship_of_urban_form_and_function_with_sur

- Gupta, N. (1998). *Delhi between two empires, 1803-1931 : society, government and urban growth*. Oxford University Press.
- Gurgaon, T. D. (n.d.). *HARYANA SERIES-07 PART XII-A DISTRICT CENSUS HANDBOOK Census of India 2011*. Retrieved from http://censusindia.gov.in/2011census/dchb/DCHB_A/06/0618_PART_A_DCHB_GURGAON.pdf
- Gurjar, B. R., Jain, A., Sharma, A., Agarwal, A., Gupta, P., Nagpure, A. S., & Lelieveld, J. (2010). Human health risks in megacities due to air pollution. *Atmospheric Environment*, *44*(36), 4606–4613. <https://doi.org/10.1016/J.ATMOENV.2010.08.011>
- Hammerberg, K., Brousse, O., Martilli, A., & Mahdavi, A. (2018). Implications of employing detailed urban canopy parameters for mesoscale climate modelling: a comparison between WUDAPT and GIS databases over Vienna, Austria. *International Journal of Climatology*, *38*, e1241–e1257. <https://doi.org/10.1002/joc.5447>
- Hämmerle, M., Gál, T., Unger, J., & Matzarakis, A. (2011). Introducing A Script for Calculating the Sky View Factor used for Urban Climate Investigations. *Acta Climatologica Et Chorologica*, *44–45*, 83–92. Retrieved from <https://pdfs.semanticscholar.org/e536/7135863131e634b2cd35b8c31d657f81ab17.pdf>
- Hanna, S. R., & Chang, J. C. (1992). Boundary-layer parameterizations for applied dispersion modeling over urban areas. *Boundary-Layer Meteorology*, *58*(3), 229–259. <https://doi.org/10.1007/BF02033826>
- Heiden, U., Segl, K., Roessner, S., & Kaufmann, H. (2007). Determination of robust spectral features for identification of urban surface materials in hyperspectral remote sensing data. *Remote Sensing of Environment*, *111*(4), 537–552. <https://doi.org/10.1016/j.rse.2007.04.008>
- Herold, M., & Roberts, D. A. (2010). The spectral dimension in urban remote sensing. In R. Tarek & C. Jürgens (Eds.), *Remote Sensing and Digital Image Processing* (Vol. 10, pp. 47–65). https://doi.org/10.1007/978-1-4020-4385-7_4
- Herold, M., Roberts, D. A., Gardner, M. E., & Dennison, P. E. (2004). Spectrometry for urban area remote sensing-Development and analysis of a spectral library from 350 to 2400 nm. *Remote Sensing of Environment*, *91*, 304–319. <https://doi.org/10.1016/j.rse.2004.02.013>
- Hong-Mei, Z., Xiao-Ling, C., Ping-Xiang, L., & Zhi-Yong, Y. (2006). Remote sensing image-based analysis of the relationship between urban heat island and land use/cover changes. *Remote Sensing of Environment*, *104*(2), 133–146. <https://doi.org/10.1016/j.rse.2005.11.016>
- Howard, L. (1820). The Climate of London. Retrieved from http://www.urban-climate.org/documents/LukeHoward_Climate-of-London-V1.pdf
- Huff, F. A., & Changnon, S. A. J. (1973). Precipitation Modification by Major Urban Areas.

Bulletin of American Meteorological Society, 54(12), 1220-1232.

- Hussain, M., & Lee, B. (1980). *An investigation of wind forces on three dimensional roughness elements in a simulated atmospheric boundary layer flow. Part II : flow over large arrays of identical roughness elements and the effect of frontal and side aspect ratio variations*. Retrieved from https://www.researchgate.net/publication/293155980_An_investigation_of_wind_forces_on_three_dimensional_roughness_elements_in_a_simulated_atmospheric_boundary_layer_flow_Part_II_flow_over_large_arrays_of_identical_roughness_elements_and_the_effect_of
- IPCC. (2007). *Fourth Assessment Report of the Intergovernmental Panel on Climate Change*.
- Iyer, U. S., & Ernest Raj, P. (2013). Ventilation coefficient trends in the recent decades over four major Indian metropolitan cities. *Journal of Earth System Science*, 122(2), 537–549. <https://doi.org/10.1007/s12040-013-0270-6>
- Jain, Rajul. (2009). Delhi Development Plan: Citizen Appraisal. Working paper 216. Centre for Civil Society. New Delhi: 1-45.
- Jensen, J. R. (2007). *Remote sensing of the environment : an earth resource perspective* (2nd ed.). Retrieved from https://books.google.co.in/books/about/Remote_Sensing_of_the_Environment.html?id=A6YsAQAAMAAJ&redir_esc=y
- Jeyachandran, I., Burian, S. J., & Stetson, S. W. (2010). Estimating urban canopy parameters using synthetic aperture radar data. *Journal of Applied Meteorology and Climatology*, 49(4), 732–747. <https://doi.org/10.1175/2009JAMC2075.1>
- Jhaldiyal, A., Gupta, K., Gupta, P. K., Thakur, P., & Kumar, P. (2018). Urban Morphology Extractor: A spatial tool for characterizing urban morphology. *Urban Climate*, 24, 237–246. <https://doi.org/10.1016/J.UCLIM.2018.04.003>
- Jiang, J., & Tian, G. (2010). Analysis of the impact of Land use/Land cover change on Land Surface Temperature with Remote Sensing. *Procedia Environmental Sciences*, 2, 571–575. <https://doi.org/10.1016/j.proenv.2010.10.062>
- Jiang, L., Lu, L., Jiang, L., Qi, Y., & Yang, A. (2014). Impact of a Detailed Urban Parameterization on Modeling the Urban Heat Island in Beijing Using TEB-RAMS. *Advances in Meteorology*, 2014, 1–11. <https://doi.org/10.1155/2014/602528>
- Jiménez-Muñoz, J.-C.; Sobrino, J. A. (2008). Split-window coefficients for land surface temperature retrieval from low-resolution thermal infrared sensors. *IEEE Geoscience and Remote Sensing Letters*, 5(4), 806–809.
- Jiménez-Muñoz, J.C.; Sobrino, J. A. (2010). A single-channel algorithm for land-surface temperature retrieval from ASTER data. *IEEE Geoscience and Remote Sensing Letters*, 7(1), 176–179.
- Johnson, G. T., & Watson, I. D. (1984). The Determination of View-Factors in Urban Canyons. *Journal of Climate and Applied Meteorology*, 23(2), 329–335. [https://doi.org/10.1175/1520-0450\(1984\)023<0329:TDOVFI>2.0.CO;2](https://doi.org/10.1175/1520-0450(1984)023<0329:TDOVFI>2.0.CO;2)

- Jun, M.-J., Kim, J.-I., Kim, H.-J., Yeo, C.-H., & Hyun, J.-Y. (2017). Effects of Two Urban Development Strategies on Changes in the Land Surface Temperature: Infill versus Suburban New Town Development. *Journal of Urban Planning and Development*, 143(3), 04017010. [https://doi.org/10.1061/\(ASCE\)UP.1943-5444.0000396](https://doi.org/10.1061/(ASCE)UP.1943-5444.0000396)
- Kak, S. (2013). *The Mahabharata and the Sindhu-Sarasvati Tradition*. Retrieved from <http://www.ece.lsu.edu/kak/MahabharataII.pdf>
- Kaplan, G., Avdan, U., & Yigit Avdan, Z. (2018). *Urban Heat Island Analysis using the Landsat 8 Satellite Data: A Case Study in Skopje, Macedonia*. 5171. <https://doi.org/10.3390/ecrs-2-05171>
- Kaspersen, P. S., Fensholt, R., & Drews, M. (2015). Using Landsat vegetation indices to estimate impervious surface fractions for European cities. *Remote Sensing*, 7(6), 8224–8249. <https://doi.org/10.3390/rs70608224>
- Kato, S., & Huang, H. (2009). Ventilation efficiency of void space surrounded by buildings with wind blowing over built-up urban area. *Journal of Wind Engineering and Industrial Aerodynamics*, 97(7,8), 358–367.
- Kent, Christoph w., Grimmond, CSB, Gatey, D., Barlow, J.F., Kotthaus, S., Lindberg, F., Halios, C., Lee, K., Ward, H.C., Hong, J.W., Hong, J., H. K. (2018). Urban Aerodynamic Roughness and Wind Speed Estimation. *Urban Climate News*, 67, 13–18. Retrieved from www.urban-climate.org
- Kent, C. W., Grimmond, S., & Gatey, D. (2017). Aerodynamic roughness parameters in cities: Inclusion of vegetation. *Journal of Wind Engineering and Industrial Aerodynamics*, 169, 168–176. <https://doi.org/10.1016/j.jweia.2017.07.016>
- Kikon, N., Singh, P., Singh, S. K., & Vyas, A. (2016). Assessment of urban heat islands (UHI) of Noida City, India using multi-temporal satellite data. *Sustainable Cities and Society*, 22, 19–28.
- Kirthiga, S. M., & Patel, N. R. (2018). Impact of updating land surface data on micrometeorological weather simulations from the WRF model. *Atmósfera*, 31(2), 165–183. Retrieved from <https://www.revistascca.unam.mx/atm/index.php/atm/article/view/ATM.2018.31.02.05/46615>
- Kondo, J., & Yamazawa, H. (1986). Aerodynamic roughness over an inhomogeneous ground surface. *Boundary-Layer Meteorology*, 35(4), 331–348. <https://doi.org/10.1007/BF00118563>
- Kotharkar, R., Bahadure, P., Sarda, N., Kotharkar, R., Bahadure, P., & Sarda, N. (2014). Measuring Compact Urban Form: A Case of Nagpur City, India. *Sustainability*, 6(7), 4246–4272. <https://doi.org/10.3390/su6074246>
- Kotharkar, R., Ramesh, A., & Bagade, A. (2018). Urban Heat Island studies in South Asia: A critical review. *Urban Climate*, 24, 1011–1026. <https://doi.org/10.1016/J.UCLIM.2017.12.006>
- Kotharkar, R., & Surawar, M. (2016). Land Use, Land Cover, and Population Density Impact on

- the Formation of Canopy Urban Heat Islands through Traverse Survey in the Nagpur Urban Area, India. *Journal of Urban Planning and Development*, 142(1), 04015003. [https://doi.org/10.1061/\(ASCE\)UP.1943-5444.0000277](https://doi.org/10.1061/(ASCE)UP.1943-5444.0000277)
- Kumar, S., & Panwar, M. (2017). Urban Heat Island Footprint Mapping of Delhi using Remote Sensing. *International Journal on Emerging Technologies*, 8(1), 80–83.
- Kutzbach, J. (1961). *Investigations of the wind profiles by artificially controlled surface roughness*. University of Wisconsin, Madison.
- Lalitha, A., Gupta, K., & Rao, M. J. (2018). *Multi-City Urban Weather Simulation using WRF Model*. Andhra University(Unpublished Thesis).
- Lall, A. B., Pandit, M., & Appasamy, P. (1990). Climate and Housing Form : a Case Study of New Delhi. *Energy and Buildings*, 16, 837–849.
- Landsberg, H. E. (1972). *The Urban Climate*. Academic Press Inc. New York
- Lankao, P. R. (2008). *Urban Areas and Climate Change: Review of Current Issues and Trends*. Retrieved from http://www.ral.ucar.edu/staff/prlankao/GRHS_2011_IssuesPaperfinal.pdf
- Li, D., & Bou-Zeid, E. (2013). Synergistic Interactions between Urban Heat Islands and Heat Waves: The Impact in Cities is Larger than the Sum of Its Parts. *Journal of Applied Meteorology and Climatology*, 52, 2051–2064. <https://doi.org/10.1175/JAMC-D-13-02.s1>
- Li, H., Zhou, Y., Li, X., Meng, L., Wang, X., Wu, S., & Sodoudi, S. (2018). A new method to quantify surface urban heat island intensity. *Science of the Total Environment*, 624, 262–272. <https://doi.org/10.1016/j.scitotenv.2017.11.360>
- Li, Z.-L., Tang, B.-H., Wu, H., Ren, H., Yan, G., Wan, Z., Trigo, I.F., Sobrino, J.A. (2013). Satellite-derived land surface temperature: Current status and perspectives. *Remote Sensing of Environment*, 131, 14–37. <https://doi.org/10.1016/J.RSE.2012.12.008>
- Lindberg, F., Holmer, B., & Thorsson, S. (2008). SOLWEIG 1.0 – Modelling spatial variations of 3D radiant fluxes and mean radiant temperature in complex urban settings. *International Journal of Biometeorology*, 52(7), 697–713. <https://doi.org/10.1007/s00484-008-0162-7>
- Lindberg, F., Grimmond, C. S. B., & Martilli, A. (2015). Sunlit fractions on urban facets - Impact of spatial resolution and approach. *Urban Climate*, 12, 65–84. <https://doi.org/10.1016/j.uclim.2014.11.006>
- Lindberg, F., Grimmond, C.S.B., Gabey, A., Huang, B., Kent, C. W., Sun, T., Theeuwes, N. E., Järvi, L., Ward, H. C., Capel-Timms, I., Chang, Y., Jonsson, P., Krave, N., Liu, D., Meyer, D., Olofson, K., Frans G. Tan, J., Wästberg, D., Xue, L., Zhang, Z. (2018). Urban Multi-scale Environmental Predictor (UMEP): An integrated tool for city-based climate services. *Environmental Modelling & Software*, 99, 70–87. <https://doi.org/10.1016/J.ENVSOFT.2017.09.020>
- Liu, P., Jia, S., Han, R., & Zhang, H. (2018). Landscape Pattern and Ecological Security Assessment and Prediction Using Remote Sensing Approach. *Journal of Sensors*, 2018, 1–14. <https://doi.org/10.1155/2018/1058513>
- Liwen Huang, Shen, H., Wu, P., Zhang, L., & Zeng, C. (2015). Relationships Analysis of Land

- Surface Temperature with Vegetation Indicators and Impervious Surface Fraction by Fusing Multi-Temporal and Multi-Sensor Remotely Sensed Data. *2015 Joint Urban Remote Sensing Event (JURSE)*, 1–4. <https://doi.org/10.1109/JURSE.2015.7120459>
- Loridan, T., & Grimmond, C. S. B. (2012). Characterization of Energy Flux Partitioning in Urban Environments: Links with Surface Seasonal Properties. *Journal of Applied Meteorology and Climatology*, 219–241. <https://doi.org/10.1175/JAMC-D-11-038.1>
- Lundgren, K., & Kjellstorm, T. (2013). Sustainability Challenges from Climate Change and Air Conditioning Use in Urban Areas. *Sustainability*, 5, 3116–3128.
- M., P., Nain, S., Kumar, A., Singh, B. P., Kumar, K., & K., J. V. (2014). Analysis of Temperature Variability Over Northwest Part of India for The Period 1970-2000. *Natural Hazards*, 75(1). <https://doi.org/DOI:10.1007/s11069-014-1352-8>
- M, S., S, M., & Dadhwal, V. (2015). Automatic Conversion of DSM to DTM by Classification Techniques using Multi-date Stereo Data from Cartosat-1. *Journal of the Indian Society of Remote Sensing*, 43(3), 513–520.
- Macdonald, R. W., Griffiths, R. F., & Hall, D. J. (1998). An Improved Method for The Estimation of Surface Roughness of Obstacle Arrays. *Atmospheric Environment*, 32(11), 1857–1864. [https://doi.org/10.1016/S1352-2310\(97\)00403-2](https://doi.org/10.1016/S1352-2310(97)00403-2)
- Maji, S., Ahmed, S., & Siddiqui, W. A. (2015). Air Quality Assessment and Its Relation to Potential Health Impacts in Delhi, India. *Current Science*, 109(5), 902–909. <https://doi.org/10.18520/v109/i5/902-909>
- Martilli, A., Clappier, A., & Rotach, M. W. (2002). An Urban Surface Exchange Parameterisation for Mesoscale Models. *Boundary-Layer Meteorology*, 104(2), 261–304. <https://doi.org/10.1023/A:1016099921195>
- Masson, V., Champeaux, Jean-Louis, Chauvin, F., Meriguet, C., Lacaze, R., (2003). A Global Database of Land Surface Parameters at 1-km Resolution in Meteorological and Climate Models. *Journal of Climate*, 16(9), 1261–1282. <https://doi.org/10.1175/1520-0442-16.9.1261>
- Mather, P. M., & Koch, M. (2011). *Computer Processing of Remotely-Sensed Images: An Introduction*. Wiley-Blackwell.
- Matzarakis, A., & Mayer, H. (2008). *Dependence of the thermal urban climate on morphological variables*. Freiburg. Project: RayMan Model retrieved from https://www.researchgate.net/publication/228514161_Dependence_of_the_thermal_urban_climate_on_morphological_variables
- Matzarakis, Andreas, & Mayer, H. (1992). Mapping of urban air paths for planning in Munich. *Wissenschaftliche Berichte Institut für Meteorologie Und Klimaforschung*, 16, 13–22.
- Middel, A., Häb, K., Brazel, A. J., Martin, C. A., & Guhathakurta, S. (2014). Impact of urban form and design on mid-afternoon microclimate in Phoenix Local Climate Zones. *Landscape and Urban Planning*, 122, 16–28. <https://doi.org/10.1016/j.landurbplan.2013.11.004>
- Middel, A., Lukasczyk, J., Maciejewski, R., Demuzere, M., & Roth, M. (2018). Sky View Factor

- footprints for urban climate modeling. *Urban Climate*, 25, 120–134. <https://doi.org/10.1016/J.UCLIM.2018.05.004>
- Mills, G., Cleugh, H., Emmanuel, R., Endlicher, W., Erell, E., McGranahan, G., Ng, E., Nickson, A., Rosenthal, J., Steemer, K. (2010). Climate Information for Improved Planning and Management of Mega Cities (Needs Perspective). *Procedia Environmental Sciences*, 1, 228–246. <https://doi.org/10.1016/J.PROENV.2010.09.015>
- Mills, G., Bechtel, B., Ching, J., See, L., Feddema, J., Foley, M., Alexander, P. O'connor, M (2015). An Introduction to the WUDAPT project. *Proceedings of the ICUC9. Meteo France*. Retrieved from <http://landsat.usgs.gov/landsat8.php>
- Mirzaei, P. A. (2015). Recent challenges in modeling of urban heat island. *Sustainable Cities and Society*, 19, 200–206. <https://doi.org/10.1016/J.SCS.2015.04.001>
- Mitraka, Z., Del Frate, F., Chrysoulakis, N., & Gastellu-Etchegorry, J.-P. (2015). Exploiting Earth Observation data products for mapping Local Climate Zones. *2015 Joint Urban Remote Sensing Event (JURSE)*, 1–4. <https://doi.org/10.1109/JURSE.2015.7120456>
- Mohammad Awrangjeb, Mehdi RavanBakhsh, Fraser, O. S. (2010). Automatic detection of residential buildings using LIDAR data and multispectral imagery. *ISPRS Journal of Photogrammetry and Remote Sensing*, 65, 457–467.
- Mohan, M., & Bhati, S. (2011). Analysis of WRF Model Performance over Subtropical Region of Delhi, India. *Advances in Meteorology*, 2011, 1–13. <https://doi.org/10.1155/2011/621235>
- Mohan, M., Kandya, A., & Battiprolu, A. (2011). Urban Heat Island Effect over National Capital Region of India: A Study using the Temperature Trends. *Journal of Environmental Protection*, 02(04), 465–472. <https://doi.org/10.4236/jep.2011.24054>
- Mohan, M., Kikegawa, Y., Gurjar, B. R., Bhati, S., Kandya, A., & Ogawa, K. (2009). Assessment of urban heat island intensities over delhi. *The Seventh International Conference on Urban Climate*, Yokohama, Japan, (July), 3–6.
- Molnar, G., Gal, T., & Gyongyosi, A. Z. (2018). Evaluation of WRF-LCZ system in simulating urban effects under non-ideal synoptic patterns. *Acta Climatologica*, 51(52), 57–73.
- Moonen, P., Defraeye, T., Dorer, V., Blocken, B., & Carmeliet, J. (2012). *Urban Physics : effect of the micro-climate on comfort , health and energy demand*. 2050, 1–50.
- Naeem, S., Cao, C., Waqar, M. M., Wei, C., & Acharya, B. K. (2018). Vegetation role in controlling the ecoenvironmental conditions for sustainable urban environments: a comparison of Beijing and Islamabad. *Journal of Applied Remote Sensing*, 12(01), 1. <https://doi.org/10.1117/1.JRS.12.016013>
- Narain, S. (2016). Sustainable cities are inclusive cities: urban growth in the South has to be affordable and so sustainable. Retrieved May 21, 2019, from Centre for Science and environment, New Delhi website: http://ecoinsee.org/lib_docs/conference-2016/Keynote_Addresses/INSEE_Conf_2016_Keynote_Sunita_Narain.pdf
- Ndossi, M. I., & Avdan, U. (2016). Application of open source coding technologies in the production of Land Surface Temperature (LST) maps from Landsat: A PyQGIS plugin. *Remote Sensing*, 8(5). <https://doi.org/10.3390/rs8050413>
-

- Neophytou, M., Mouzourides, P., Kyprianou, A., Choudhary, R., & Ching, J. (2015). Sensitivity of mesoscale models to scale dependent UCP inputs: an example from urban energy demand. *9th International Conference on Urban Climate*, 6. Retrieved from http://www.meteo.fr/icuc9/LongAbstracts/nomtm11-4-7021409_a.pdf
- Ng, E., Yuan, C., Chen, L., Ren, C., & Fung, J. C. H. (2011). Improving the wind environment in high-density cities by understanding urban morphology and surface roughness: A study in Hong Kong. *Landscape and Urban Planning*, 101(1), 59–74. <https://doi.org/10.1016/J.LANDURBPLAN.2011.01.004>
- Ng, E. (2015). The Urban Climate Map- A methodology for Sustainable planning, *Taylor and Francis*, London, 528. <https://doi.org/10.4324/9781315717616>
- Ng, E. (2016). Urban air ventilation in High-Density Cities in the Tropics. In R. Emmanuel (Ed.), *Urban climate challenges in the tropics* (1st ed., pp. 79–110). London: Imperial College Press.
- Odunuga, S., & Badru, G. (2015). Landcover Change, Land Surface Temperature, Surface Albedo and Topography in the Plateau Region of North-Central Nigeria. *Land*, 4(2), 300–324. <https://doi.org/10.3390/land4020300>
- Oke, T. R. (1981). Canyon geometry and the nocturnal urban heat island: Comparison of scale model and field observations. *Journal of Climatology*, 1(3), 237–254. <https://doi.org/10.1002/joc.3370010304>
- Oke, T. R. (1987). *Boundary Layer Climate* (Second). London: Routledge.
- Oke, T. R. (1988). Street design and urban canopy layer climate. *Energy and Buildings*, 11(1–3), 103–113. [https://doi.org/10.1016/0378-7788\(88\)90026-6](https://doi.org/10.1016/0378-7788(88)90026-6)
- Oke, T. R. (2008). *Guide to Meteorological Instruments and Methods of Observation* (No. WMO-No. 8.). Retrieved from www.wmo.int.
- Oke, T. R., & Stewart, I. D. (2012). Local Climate Zone for Urban Temperature Studies. *Bulletin of the American Meteorological Society*, 93(93), 1879–1900. <https://doi.org/10.1175/BAMS-D-11-00019.1>
- Oke, T. R., Mills, G., Christen, A., & Voogt, J. A. (2017). *Urban Climates*. <https://doi.org/10.1017/9781139016476>
- Otte, T. L., Lacser, A., Dupont, S., & Ching, J. K. S. (2004). Implementation of an Urban Canopy Parameterization in a Mesoscale Meteorological Model. *Journal of Applied Meteorology*, 1648–1665. Retrieved from <http://citeseerx.ist.psu.edu/viewdoc/download?doi=10.1.1.174.2893&rep=rep1&type=pdf>
- Pan, J. (2015). Analysis of human factors on urban heat island and simulation of urban thermal environment in Shanghai, China. *Journal of Applied Remote Sensing*, 9(1), 22.
- Pandey, A. K., Kumar, D., Singh, S., Pandey, P., Prakash, A., Berwal, S., Lodhi, N., Maithani, S., Jain, V. K., Kumar, K. (2014). Spatio - temporal variations of Urban Heat Island over Delhi. *Urban Climate*, 10, 119–133.
- Park, C., Ha, J., & Lee, S. (2017). Association between Three-Dimensional Built Environment

- and Urban Air Temperature: Seasonal and Temporal Differences. *Sustainability*, 9(8), 1338.
- Patz, J. A., Diarmid, C.-L., Holloway, T., & Foley, J. A. (2005). Impact of regional climate change on human health. *Nature*, 438(17), 310–317.
- Perera, N. G. R., & Langappuli, B. L. T. (2013). Surface Fraction as a variable for Urban Heat Island Amelioration in Colombo. *Faculty of Architecture Research Symposium*, (December 2013).
- Petersen, R. L., & Parce, D. K. (1994). *Development and testing of methods for estimating surface roughness length at refineries*. Ft. Collins, CO.
- Poli, D., Remondino, F., Angiuli, E., & Agugiaro, G. (2015). Radiometric and geometric evaluation of GeoEye-1, WorldView-2 and Pléiades-1A stereo images for 3D information extraction. *ISPRS Journal of Photogrammetry and Remote Sensing*, 100, 35–47. <https://doi.org/10.1016/J.ISPRSJPRS.2014.04.007>
- Qin, Z., Karnieli, A., & Berliner, P. (2001). A mono-window algorithm for retrieving land surface temperature from Landsat {TM} and its application to the Israel-Egypt border region. *Int. J. Rem. Sens.*, 18(18), 3719–3746.
- Raasch, S., & Schröter, M. (2001). PALM - A large-eddy simulation model performing on massively parallel computers. *Meteorologische Zeitschrift*, 10(5), 363–372. <https://doi.org/10.1127/0941-2948/2001/0010-0363>
- Rajpriya, N., Vyas, A., & Sharma, S. (2014). Generation of 3D Model for Urban area using Ikonos and Cartosat-1 Satellite Imageries with RS and GIS Techniques. *The International Archives of Photogrammetry, Remote Sensing and Spatial Information Sciences*, 40(8), 899.
- Rasul, A., Balzter, H., Smith, C., Remedios, J., Adamu, B., Sobrino, J.A., Srivani, M., Weng, Q. (2017). A Review on Remote Sensing of Urban Heat and Cool Islands. *Land*, 6(2), 38. <https://doi.org/10.3390/land6020038>
- Ratti, C., Di Sabatino, S., & Britter, R. (2006). Urban texture analysis with image processing techniques: Winds and dispersion. *Theoretical and Applied Climatology*, 84(1–3), 77–90. <https://doi.org/10.1007/s00704-005-0146-z>
- Raupach, M. R. (1992). Drag and drag partition on rough surfaces. *Boundary-Layer Meteorology*, 60(4), 375–395. <https://doi.org/10.1007/BF00155203>
- Raupach, M. R. (1994). Simplified expressions for vegetation roughness length and zero-plane displacement as functions of canopy height and area index. *Boundary-Layer Meteorology*, 71(1–2), 211–216. <https://doi.org/10.1007/BF00709229>
- Raupach, M. R., Antonia, R. A., & Rajagopalan, S. (1991). Rough-Wall Turbulent Boundary Layers. *Applied Mechanics Reviews*, 44(1), 1–25. <https://doi.org/10.1115/1.3119492>
- Ren, C., Ng, E., & Kaztschner, L. (2009). *Review Of Worldwide Urban Climatic Map Study And Its Application In Planning*. The seventh International Conference on Urban Climate, 29 June -3 July, 2009Yokohama Japan, Available online: http://www.ide.titech.ac.jp/~icuc7/extended_abstracts/pdf/374213-3-090516013120-003.pdf, Last Accessed June 28, 2019

- Ren, C., Ng, E. Y., & Katzschner, L. (2011). Urban climatic map studies: a review. *International Journal of Climatology*, 31(15), 2213–2233. <https://doi.org/10.1002/joc.2237>
- Ren, C., Wang, R., Cai, M., Xu, Y., Zheng, Y., & Ng, E. (2016). The accuracy of LCZ maps generated by the World Urban Database and Access Portal Tools (WUDAPT) Method: A Case Study of Hong Kong. *The Fourth International Conference on Countermeasure to Urban Heat Islands*, (June), 1–11. <https://doi.org/10.1093/mnras/stv403>
- Revi, A., Satterthwaite, D. E., Aragón-Durand, F., Corfee-Morlot USA, Jan, K., Robert BR, da Silva, Jo, Dodman, David, Maskrey, Andrew, Pahwa G., Sumetee, Balbus, John, Cardona, Omar-Dario, Sverdlik, Alice, Barros, VR, Dokken, DJ, Mach, KJ, Bilir, Te, Chatterjee, M, Ebi, KL, Estrada, Yo, Genova, RC, Girma, B, Kissel, Es, Levy, An, MacCracken, S. (2014). *Urban Areas, AR5 Climate Change 2014: Impacts, Adaptation, and Vulnerability*. Retrieved from William Solecki website: https://www.ipcc.ch/site/assets/uploads/2018/02/WGIAR5-Chap8_FINAL.pdf
- Rich, P. M., Wood, J., Vieglais, D. A., Burek, K., & Webb, N. (1996). *HemiView Version 2.1 Notes: HemiView Manual Revision Number: 2.1*. Retrieved from https://www.delta-t.co.uk/wp-content/uploads/2017/02/hv2um2_1.2.pdf
- Ridd, M. K. (1995). Exploring a V-I-S (vegetation-impervious-soil) model for urban ecosystem analysis through remote sensing: comparative anatomy for cities. *International Journal of Remote Sensing*, 16(12), 2165–2185. Retrieved from https://geog.sdsu.edu/Research/Projects/IPC/publication/Ridd_1995_VIS.pdf
- Rotach, M. W. (1994). Determination of the zero plane displacement in an urban environment. *Boundary-Layer Meteorology*, 67(1–2), 187–193. <https://doi.org/10.1007/BF00705513>
- Roth, M., Oke, T. R., & Emery, W. J. (1989). Satellite-derived urban heat islands from three coastal cities and the utilization of such data in urban climatology. *International Journal of Remote Sensing*, 10(11), 1699–1720. <https://doi.org/10.1080/01431168908904002>
- Salamanca, F., Martilli, A., Tewari, M., Chen, F. (2011). A Study of the Urban Boundary Layer Using Different Urban Parameterizations and High-Resolution Urban Canopy Parameters with WRF. *Journal of Applied Meteorology and Climatology*, 50(5), 1107–1128. <https://doi.org/10.1175/2010JAMC2538.1>
- Salleh, S. A., Latif, Z. A., Pradhan, B., Wan Mohd, W. M. N., & Chan, A. (2014). Functional relation of land surface albedo with climatological variables: a review on remote sensing techniques and recent research developments. *Geocarto International*, 29(2), 147–163. <https://doi.org/10.1080/10106049.2012.748831>
- Scarano, M., & Sobrino, J. A. (2015). On the relationship between the sky view factor and the land surface temperature derived by Landsat-8 images in Bari, Italy. *International Journal of Remote Sensing*, 36(19–20), 4820–4835. <https://doi.org/10.1080/01431161.2015.1070325>
- Sharma, A., Fernando, H. J. S., Hamlet, A. F., Hellmann, J. J., Barlage, M., & Chen, F. (2017). Urban meteorological modeling using WRF: a sensitivity study. *International Journal of Climatology*, 37(4), 1885–1900. <https://doi.org/10.1002/joc.4819>
- Sharma, N., Taneja, S., Sagar, V., & Bhatt, A. (2018). Forecasting air pollution load in Delhi
-

- using data analysis tools. *Procedia Computer Science*, 132, 1077–1085. <https://doi.org/10.1016/j.procs.2018.05.023>
- Shen, G., Ibrahim Abdoul, N., Zhu, Y., Wang, Z., & Gong, J. (2017). Remote sensing of urban growth and landscape pattern changes in response to the expansion of Chongming Island in Shanghai, China. *Geocarto International*, 32(5), 488–502. <https://doi.org/10.1080/10106049.2016.1156166>
- Shishegar, N. (2013). Street Design and Urban Microclimate: Analyzing the Effects of Street Geometry and Orientation on Airflow and Solar Access in Urban Canyons. *Journal of Clean Energy Technologie*, 1(1), 52–56. <https://doi.org/10.7763/JOCET.2013.V1.13>
- Singh, M. (2015). Urban Development Patterns and Entrenched Heat Island – A Distinctive Approach to Study Heat Island Intensity, GRIHA Council, The Energy and Resources Institute (TERI), Delhi, India. *Proceedings of Building Simulation 2015, 14th Conference of International Building Performance Simulation Association, Hyderabad, India, Dec. 7-9, 2015*. (Mohan, 1047–1053. Hyderabad, India.
- Sismanidis, P., Keramitsoglou, I., Bechtel, B., & Kiranoudis, C. (2016). Improving the Downscaling of Diurnal Land Surface Temperatures Using the Annual Cycle Parameters as Disaggregation Kernels. *Remote Sensing*, 9(1), 23. <https://doi.org/10.3390/rs9010023>
- Small, C., & Naumann, T. (2001). The global distribution of human population and recent volcanism. *Environmental Hazards*, 3(3), 93–109. <https://doi.org/10.3763/ehaz.2001.0309>
- Sobrino, J. A., Jiménez-Muñoz, J. C., & Paolini, L. (2004). Land surface temperature retrieval from LANDSAT TM 5. *Remote Sensing of Environment*, 90(4), 434–440. <https://doi.org/10.1016/j.rse.2004.02.003>
- Sohn, G., & Dowman, I. (2007). Data fusion of high-resolution satellite imagery and LiDAR data for automatic building extraction. *ISPRS Journal of Photogrammetry and Remote Sensing*, 62(1), 43–63. <https://doi.org/10.1016/j.isprsjprs.2007.01.001>
- Souch, C., & Grimmond, S. (2006). Applied climatology: urban climate. *Progress in Physical Geography*, 30(2), 270–279. <https://doi.org/10.1191/0309133306pp484pr>
- Srivanit, M., & Kazunori, H. (2011). The influence of urban morphology indicators on summer diurnal range of urban climate in Bangkok Metropolitan area, Thailand. *International Journal of Civil & Environmental Engineering*, 11(5), 34–46.
- Srivastava, P. K., Majumdar, T. J., & Bhattacharya, A. K. (2010). Study of land surface temperature and spectral emissivity using multi-sensor satellite data. *Journal of Earth System Science*, 119(1), 67–74. <https://doi.org/10.1007/s12040-010-0002-0>
- Stewart, I. D., & Oke, T. R. (2012). Local climate zones for urban temperature studies. *Bulletin of the American Meteorological Society*, 93(12), 1879–1900. <https://doi.org/10.1175/BAMS-D-11-00019.1>
- Steyn, D. G. (1980). The calculation of view factors from fisheye-lens photographs: Research note. *Atmosphere-Ocean*, 18(3), 254–258. <https://doi.org/10.1080/07055900.1980.9649091>
- Stocker, T.F., Qin, D., Plattner, G.-K., Tignor, M., Allen, S.K., Boschung, J., Nauels, A., Xia, Y., Bex, V., Midgley, P.M. (2013). *Fifth Assessment Report of the Intergovernmental Panel on*
-

Climate Change.

- Stout, G. E. (1962). *Some observations of cloud initiation in industrial areas: In Air Over Cities.* Washington, DC.
- Suder, A., & Szymanowski, M. (2014). Determination of Ventilation Channels In Urban Area: A Case Study of Wrocław (Poland). *Pure and Applied Geophysics*, 171(6), 965–975. <https://doi.org/10.1007/s00024-013-0659-9>
- Surawar, Meenal; Kotharkar, R. (2017). Assessment of Urban Heat Island through Remote Sensing in Nagpur Urban Area Using Landsat 7 ETM+ satellite images. *International Journal of Urban and Civil Engineering*, 11(7), 868–874. Retrieved from <http://waset.org/publications/10007350>
- Tack, F., Buyuksalih, G., & Goossens, R. (2012). 3D building reconstruction based on given ground plan information and surface models extracted from spaceborne imagery. *ISPRS Journal of Photogrammetry and Remote Sensing*, 67, 52–64. <https://doi.org/10.1016/J.ISPRSJPRS.2011.10.003>
- Taha, H., Chang, S.-C., & Akbari, H. (2000). *Meteorological and Air Quality Impacts of Heat Island Mitigation Measures in Three U.S. Cities.* Retrieved from https://www.epa.gov/sites/production/files/2014-08/documents/3_cities.pdf
- Takkanon, P., & Chantarangul, P. (2019). Effects of urban geometry and green area on thermal condition of urban street canyons in Bangkok. *Architectural Science Review*, 62(1), 35–46. <https://doi.org/10.1080/00038628.2018.1534724>
- Tang, H.-T., & Lee, Y.-M. (2016). The making of Sustainable Urban Development: A synthesis framework. *Sustainability*, 8, 492.
- Theurer, W. (1999). Typical building arrangements for urban air pollution modelling. *Atmospheric Environment*, 33(24–25), 4057–4066. [https://doi.org/10.1016/S1352-2310\(99\)00147-8](https://doi.org/10.1016/S1352-2310(99)00147-8)
- Thiele, A., Cadario, E., Schulz, K., Thonnessen, U., & Soergel, U. (2007). Building Recognition From Multi-Aspect High-Resolution InSAR Data in Urban Areas. *IEEE Transactions on Geoscience and Remote Sensing*, 45(11), 3583–3593. <https://doi.org/10.1109/TGRS.2007.898440>
- Tse, R. O. C., Gold, C., & Kidner, D. (n.d.). *3D City Modelling from LIDAR Data.* 161–175. Retrieved June 28, 2019 from <http://www.gdmc.nl/projects/rgi-otb/3dtopo/documents/RGI-011-142.pdf>.
- Tv, R., Aithal, B. H., & Sanna, D. D. (2012). Insights to urban dynamics through landscape spatial pattern analysis. *International Journal of Applied Earth Observation and Geoinformation*, 18, 329–34383. <https://doi.org/10.1016/j.jag.2012.03.005>
- Unger, J., Lelovics, E., & Gál, T. (2014). Local Climate Zone mapping using GIS methods in Szeged. *Hungarian Geographical Bulletin*, 63(1), 29–41. <https://doi.org/10.15201/hungeobull.63.1.3>
- USGS. (2018). *Landsat 8 Data Users Handbook.* Retrieved from <https://prd-wret.s3-us-west-2.amazonaws.com/assets/palladium/production/atoms/files/LSDS->
-

1574_L8_Data_Users_Handbook_v4.0.pdf

- Voogt, J. A., Oke, T. R. (1997). Complete Urban Surface Temperatures. *Journal of Applied Meteorology*, 36(9), 1117–1132. [https://doi.org/10.1175/1520-0450\(1997\)036<1117:CUST>2.0.CO;2](https://doi.org/10.1175/1520-0450(1997)036<1117:CUST>2.0.CO;2)
- Voogt, J., & Oke, T. (2003). Thermal remote sensing of urban climates. *Remote Sensing of Environment*, 86(3), 370–384. [https://doi.org/10.1016/S0034-4257\(03\)00079-8](https://doi.org/10.1016/S0034-4257(03)00079-8)
- Vyas, A., Shastri, B., & Y, J. (2014). Spatio-Temporal Analysis of UHI using Geo-Spatial Techniques: A case study of Ahmedabad. *The International Archives of Photogrammetry, Remote Sensing and Spatial Information Sciences*, 40(8), 997.
- Wang, Xi, & Gong, Y. (2010). The impact of an urban dry island on the summer heat wave and sultry weather in Beijing City. *Chinese Science Bulletin*, 55(16), 1657–1661. <https://doi.org/10.1007/s11434-010-3088-5>
- Wang, Xuemei, Dai, W., & Dai, J. (2017). Developing Fine-scale Urban Canopy Parameters in Guangzhou City and its Application in the WRF-Urban model. *World, 9000*, Retrieved from http://www.meteo.fr/icuc9/LongAbstracts/gd5-2-3221289_a.pdf
- Wei, C., & Blaschke, T. (2018). Pixel-Wise vs. Object-Based Impervious Surface Analysis from Remote Sensing: Correlations with Land Surface Temperature and Population Density. *Urban Science*, 2(2), 14. <https://doi.org/10.3390/urbansci2010002>
- Wendall Cox. (2011). The Evolving Urban Form: Delhi | Newgeography.com. Retrieved May 19, 2019, from <http://www.newgeography.com/content/002545-the-evolving-urban-form-delhi>
- Weng, Q. (2014). On the issue of scale in urban remote sensing. In Q. Weng (Ed.), *Scale Issues in remote Sensing* (1st ed., pp. 61–78). New Jersey: John Willey & Sons.
- Weng, Q., Lu, D., & Liang, B. (2006). Urban Surface Biophysical Descriptors and Land Surface Temperature Variations. *Photogrammetric Engineering & Remote Sensing*, 72(11), 1275–1286. Retrieved from <http://isu.indstate.edu/qweng/PERS2006.pdf>
- Wicht, M., Wicht, A., & Osińska-Skotak, K. (2017). Detection of ventilation corridors using a spatio-temporal approach aided by remote sensing data. *European Journal of Remote Sensing*, 50(1), 254–267. <https://doi.org/10.1080/22797254.2017.1318672>
- Wicht, M., & Wicht, A. (2018). LiDAR-Based Approach for Urban Ventilation Corridors Mapping. *IEEE Journal of Selected Topics in Applied Earth Observations and Remote Sensing*, 11(8), 2742–2751. <https://doi.org/10.1109/JSTARS.2018.2791410>
- Wieringa, J. (1992). Updating the Davenport roughness classification. *Journal of Wind Engineering and Industrial Aerodynamics*, 41–44, 357–368. Retrieved from <https://s3.amazonaws.com/academia.edu.documents/31539898/DAVENPORT.pdf?AWSAccessKeyId=AKIAIWOWYYGZ2Y53UL3A&Expires=1556861150&Signature=Gsdyv%2B%2BawjD7mgDISuL5ChJpCt8%3D&response-content-disposition=inline%3Bfilename%3DDAVENPORT.pdf>
- Wisner, B., & Adams, J. (2002). *Environmental health in emergencies and disasters : A practical guide*. Retrieved from
-






https://www.who.int/water_sanitation_health/hygiene/emergencies/em2002intro.pdf







- Wong, M. S., Nichol, J. E., To, P. H., & Wang, J. (2010a). A simple method for designation of urban ventilation corridors and its application to urban heat island analysis. *Building and Environment*, 45(8), 1880–1889. <https://doi.org/10.1016/j.buildenv.2010.02.019>
- Wong, M. S., Nichol, J. E., Y Ng, E. Y., Guilbert, E., Kwok, K. H., To, P. H., & Wang, J. Z. (2010b). GIS technique for mapping urban ventilation using frontal area index and least cost path analysis. *International Archives of the Photogrammetry, Remote Sensing and Spatial Information Sciences*, 38, 586–591. Retrieved from <https://www.isprs.org/proceedings/xxxviii/part2/presentations/S15/Wong.pdf>
- Wong, M. S., Nichol, J., & Ng, E. (2011). A study of the “wall effect” caused by proliferation of high-rise buildings using GIS techniques. *Landscape and Urban Planning*, 102(4), 245–253. <https://doi.org/10.1016/j.landurbplan.2011.05.003>
- Wong, M. S., & Nichol, J. E. (2013). Spatial variability of frontal area index and its relationship with urban heat island intensity. *International Journal of Remote Sensing*, 34(3), 885–896. <https://doi.org/10.1080/01431161.2012.714509>
- Wu, C., & Yuan, F. (2011). *Remote sensing of High resolution urban impervious surfaces, Urban Remote Sensing: Monitoring, Synthesis and modeling in urban environment* (first; X. Yang, Ed.). West Sussex, UK: John Wiley & Sons, Ltd.
- Xu, Y., Ren, C., Ma, P., Ho, J., Wang, W., Kevin, K., Lin, H., & Ng, E. (2017). Urban morphology detection and computation for urban climate research. *Landscape and Urban Planning*, 167, 212–224. <https://doi.org/10.1016/J.LANDURBPLAN.2017.06.018>
- Y., Y. (2007). Measures to mitigate urban heat Islands. *Global Change and Sustainable Development*, 1(2), 18–46.
- Yang, L., & Li, Y. (2011). Thermal conditions and ventilation in an ideal city model of Hong Kong. *Energy and Buildings*, 43(5), 1139–1148.
- Yin, C., Yuan, M., Lu, Y., Huang, Y., & Liu, Y. (2018). Effects of urban form on the urban heat island effect based on spatial regression model. *Science of The Total Environment*, 634, 696–704. <https://doi.org/10.1016/J.SCITOTENV.2018.03.350>
- Yom, J.-H., & Oh, J. (2011). Automatic Building Reconstruction with Satellite Images and Digital Maps; Automatic Building Reconstruction with Satellite Images and Digital Maps. *ETRI Journal*, 33(4), 537–546. <https://doi.org/10.4218/etrij.11.1610.0020>
- Yong, X., Peifeng, M., Hui, L., & Edward, N. (2015). Fusion of World-view2 stereo and TerraSAR-X images for 3D building extraction in urban areas. *9th International Conference on Urban Climate*. Retrieved from http://www.meteo.fr/icuc9/LongAbstracts/gd8-4-4671275_a.pdf
- Yu, X., Guo, X., & Wu, Z. (2014). Land surface temperature retrieval from landsat 8 TIRS-comparison between radiative transfer equation-based method, split window algorithm and single channel method. *Remote Sensing*, 6(10), 9829–9852. <https://doi.org/10.3390/rs6109829>
- Yuan, C., Ren, C., & Ng, E. (2014). GIS-based surface roughness evaluation in the urban
-

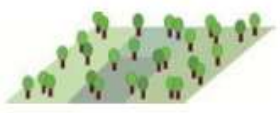
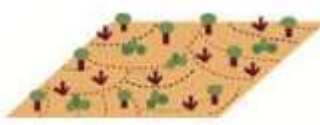




- planning system to improve the wind environment - A study in Wuhan, China. *Urban Climate*, 10(P3), 585–593. <https://doi.org/10.1016/j.uclim.2014.06.005>
- Yue, W., Liu, Y., Fan, P., Ye, X., & Wu, C. (2012). Assessing spatial pattern of urban thermal environment in Shanghai, China. *Stochastic Environmental Research and Risk Assessment*, 26(7), 899–911.
- Zhang, C., Awrangjeb, M., & Fraser, C. S. (2011). *Effective Separation of Trees and Buildings for Automated Building Detection*. Retrieved from https://www.researchgate.net/profile/Mohammad_Awrangjeb/publication/290042838_Effective_separation_of_trees_and_buildings_for_automated_building_detection/links/5698514008ae34f3cf1f4bad.pdf
- Zhou, D., Xiao, J., Bonafoni, S., Berger, C., Deilami, K., Zhou, Y., Frohling, S., Yao, R., Qiao, Z., Sobrino, J. A. (2019). Satellite remote sensing of surface urban heat islands: Progress, challenges, and perspectives. *Remote Sensing*, 11(1), 1–36. <https://doi.org/10.3390/rs11010048>
- Zhou, Q.-Y., & Neumann, U. (2008). Fast and extensible building modeling from airborne LiDAR data. *Proceedings of the 16th ACM SIGSPATIAL International Conference on Advances in Geographic Information Systems - GIS '08*, 1. <https://doi.org/10.1145/1463434.1463444>



Appendix A: Description of Local Climate Zone

Description of Local Climate Zone (Source: Stewart and Oke, 2012)			
Urban built-up LCZ	Graphical Representation	LCZ	Definition
Compact High-rise		LCZ 1	Compact High-Rise represents the dense tall building to tens of stories. Building free-standing, closely spaced. Sky View from street level significantly reduced. Building are usually made up of steel, concrete, and glass construction. Land cover is mostly paved; few or no trees. High space heating/ cooling demand and Heavy traffic flow. The function of the class is for commercial and residential uses and will be found in the core or peripheral part of the city.
Compact midrise		LCZ 2	Its represents the building from 3-9 stories which are mainly separated by narrow streets and inner courtyards. Building uniform in height, sky view from street significantly reduced. Land cover is mostly paved and the construction material used is stone, brick, tile and concrete. The function of these classes is for residential, commercial and industrial.
Compact Low rise		LCZ 3	Attached or closely spaced building with 1-3 stories tall. Buildings small and tightly packed along the narrow streets, often without discernible alignment. Moderate spacing heating/cooling demand and low to moderate traffic flow. Used for residential and commercial purpose. Can be located in old cities and towns.
Open high-rise		LCZ 4	Buildings ten of stories and more tall set in open, geometric arrangement. Buildings uniform in heights, width and spacing. Abundance of open space and pervious land cover. Material used for construction is stone, brick, tile and concrete. The use is for residential purpose and can be found on the periphery or densely populated cities.
Open midrise		LCZ 5	Open arrangements of mid-rise building with 3-9 stories. Enough amount of pervious surface with small plants and scattered trees. Used for residential,

			institutional and commercial purpose and can be located on the periphery.
Open low-rise		LCZ 6	Small building with 1-3 stories tall or an open arrangement of low-rise buildings. The construction material used is wood, brick, stone, tile and concrete. Function is for residential and commercial, can be located in medium density city, periphery or in commuter town.
Lightweight low-rise		LCZ 7	Represents dense storey small buildings, attached or closely spaced and separated by narrow roads and alleys. With a little or no consolidated infrastructure. Construction material used is wood, thatch, corrugated materials. And may have few or no trees. Function is for residential, squatter settlements, slums. Can be found on the periphery or near to extended metropolitan cities.
Large low-rise		LCZ 8	Large low-rise 1-3 stories separated by extensive paved surfaces. With few or no trees and land cover mostly paved. Construction material used is steel, metal. Concrete and stone. Function for light industrial complex, commercial or transportation hub. Can be located on periphery.
Sparsely built		LCZ 9	Sparse arrangements of medium or small sized buildings in a natural setting. Abundance of pervious land cover. Function is for residential, commercial, institutional, agriculture, farms and country estate. Can be located on periphery, extended region of metropolitan region.
Heavy industry		LCZ 10	These are the large low-rise and mid-rise industrial structures with few or no trees. Land cover is mainly paved or hard packed. Construction material is metal, steel and concrete. Function is industries and can be located in city or Industrial Model Township.
Land Cover types	Graphical representation	LCZ	Definition
Dense trees		LCZ A	Heavily wooded landscape of deciduous and/or evergreen trees. Land cover mostly pervious (low plants). Zone function is natural forest, tree cultivation, or urban park.

Scattered trees		LCZ B	Lightly wooded landscape of deciduous and/or evergreen trees. Land cover mostly pervious (low plants). Zone function is natural forest, tree cultivation, or urban park
Bush, scrub		LCZ C	Open arrangement of bushes, shrubs, and short, woody trees. Land cover mostly pervious (bare soil or sand). Zone function is natural scrubland or agriculture.
Low plants		LCZ D	Featureless landscape of grass or herbaceous plants/crops. Few or no trees. Zone function is natural grassland, agriculture, or urban park
Bare rock or paved		LCZ E	Featureless landscape of rock or paved cover. Few or no trees or plants. Zone function is natural desert (rock) or urban transportation.
Bare soil or sand		LCZ F	Featureless landscape of soil or sand cover. Few or no trees or plants. Zone function is natural desert or agriculture.
Water		LCZ G	Large, open water bodies such as seas and lakes, or small bodies such as rivers, reservoirs, and lagoons.



Appendix B: Bio Data of Candidate

A. Personal Information

Name of Candidate: Kshama Gupta
Course: Ph D Research Scholar
Department: Department of Architecture and Planning
Institute: Indian Institute of Technology, Roorkee
Enrollment No. 12910002

B. Contact Information

Postal Address:

Scientist/ Engr. SF,
Urban and Regional Studies Department,
Indian Institute of Remote Sensing,
4, Kalidas Road,
Dehradun-248001

Contact:09219021565

email: kshama@iirs.gov.in / gupta.kshama@gmail.com

c. Academic Qualification:

- M. Tech. (Urban Planning) (1999- 2001), School of Planning and Architecture, New Delhi (67%)
- B. Architecture (1993-1998), MNIT, Jaipur (67.7%)
- Senior Secondary School (1992), Board of Secondary Education, Rajasthan (77.3%)
- Secondary School Examination (1990), Board of Secondary Education, Rajasthan (83.6%)

D. Professional Profile:

- 18 Years of experience as researcher in the field of Remote Sensing, Digital Image Processing and GIS specialist at Indian Space Research organization, Dehradun (Since Nov 2001).
- Approx. One year of working experience as Urban Manager in the field of urban development at Intercontinental Consultants and Technocrats, New Delhi (2001).
- One year of working experience in the field of Architecture as Assistant Architect (1998-99).
- Research Interest: Urban Microclimate, Urban 3D modeling, LiDAR, Urban Green Spaces



Appendix C: List of Publications

JOURNAL

Gupta Kshama, Bhardwaj Ashutosh, Kumar Pramod, Pushpalata, 2015, Procedural rule based 3D city modeling and visualization using high resolution satellite data, *International Journal of Advancement in Remote Sensing, GIS and Geography*, 3(2), 16-25. (*Open Access Journal, Impact Factor- 0.994*)

INTERNATIONAL CONFERENCES

Kshama Gupta, Pushplata, Sandeep John, Ashutosh Bhardwaj, Pramod Kumar, A. Senthil Kumar, Comparative evaluation of Pleiades, Cartosat- 2 and Kompsat-3 Stereo data for DSM and 3D model generation, Asian Conference on Remote Sensing, October 23-27, 2017, Delhi.

Kshama Gupta, Pushplata, Tanya Rajwal, Sandeep Nekkla, Pramod Kumar, A. Senthil Kumar, Investigating the relationship of urban form and function with surface temperature patterns, Asian Conference on Remote Sensing, October 23-27, 2017, Delhi.

Kshama Gupta, Prasun Kumar Gupta, Alok Jhaldiyal, Pushplata, WRF-UME for computation of urban canopy parameters for weather research forecasting model, International Tropical Meteorology Symposium for advancements in Space based earth observations and services for Weather and climate, November, 7-10, 2017, Ahmedabad, India.

Gupta K., Bhardwaj A., Kumar P., Pushpalata, Krishna Murthy Y.V.N., 2013, 3D visualization and modeling of urban areas using Airborne LiDAR data, Joint international workshop of ISPRS WG VIII/1 and WG IV/4 on 'Geospatial data for Disaster and Risk Reduction' from November 21-22, 2013 at Hyderabad, India.



Appendix D: Answers to the Examiners' comments

S. No.	Remarks	Answers
External Examiner 1: Foreign Examiner		
Comments		
<ul style="list-style-type: none"> • Outstanding PhD Thesis • Represents well the size of analysis, data processing and simulation • More than enough for a standard PhD research 		
Observations		
1	The candidate mentioned the WRF is used in 500m resolution. This resolution is the gray zone of the model since there are some physical processes (e.g. convection, cloud processes etc.) which are included using parameterization. In this resolution these processes have to be regarded not as parameterization but physical calculation. The current state of WRF is not ensure that all of the simulation is realistic in this resolution. In Figure 5-10 the strange patterns (mostly in the south eastern part) in the wind field may be the sign of numerical instability caused by the too fine resolution.	Reference to the other research work of Author has been added (p123). An uncertainty analysis of WRF simulations at 1 km resolution and 0.5 km resolution has already been carried out with respect to ground based observations, wherein it has been found that 0.5 km grid resolution shows comparatively less mean error and similar RMSE values for temperature as compared to 1 km domain size. Hence, it was concluded that both domain 0.5 km as well as 1 km domain provided stable results. The pattern in Figure 5-10 may be due to the normalization of the roughness in that area in WRF.
2	In chapter 4.3.4. , there are only a short description about the SVF calculation. Since there is no reference of the applied software tool, it is impossible to be sure about the correctness of the obtained SVF values. In the same chapter there is only a sentence about the validation, but it is unclear how the fish eye photographs were processed.	Reference appended (p74). Fish eye photographs have been processed in Hemi view canopy analysis software tool, which processes hemispherical photographs to compute the fraction of visible sky. Detailed explanation added (p74).
3	In chapter 4.3.5.3 the candidate describe how the flyovers and elevated metro network was eliminated. It is correct, however in the aspect of radiation balance these urban object may have an important role as important like the buildings or tress. If these objects are rare in the study area than it is not a problem,	These objects have been included in the Impervious Surface Fraction (ISF) as recommended by Stewart and Oke, 2012 and Oke, 2017 (Table 2-2, p23). The ISF layer has been analyzed and also used as an input for GIS based LCZ classification.

S. No.	Remarks	Answers
	but, if these objects are widely spread in the urban area, then it has to be included somehow to the analysis.	
4	In the case of the calculation of the mean building parameters a 30 m resolution grid was applied. This size is too fine in case of climate parameters- surface parameter comparison, since in urban areas the air temperature is affected by a ~500 sized source area. The justification of the selected size is missing from the documents. Section 4.5.4 give some information about the choice of grid size. I understand it but do not agree. The 100m resolution recommended by the WUDAPT is the minimum spatial size for urban climate analysis. In case at this size the high rise building will be shaded than it means that few tall building have insignificant effect on urban areas in climatology aspect.	The 30 m grid size has been chosen after few experiments carried out at coarser grid sizes to minimize strong averaging effect on building heights (Section 4.5.4). However, the choice of grid size further can be optimized in future at different grid resolutions to investigate the effect of high-rise if they can be ignored (p 202).
5	In chapter 4.3.8 the volumetric average height is calculated using a 60 m filter. It is not clear why. Chapter 4.3.9 and 4.3.10 – it is not clear how the neighboring and merged walls of the different buildings were handled during the calculation.	In this study a gridded approach have been employed to compute the parameters. The input layers for the computation of volumetric averaged height have been computed at 30m. Since, the parameter needed computation of volume and then averaging of height with respect to volume, 60 m grid encompassing 4 number of 30 m grid have been utilized to compute the volumetric averaged height. The explanation is appended in the section 4.3.8 (p 78). Effect of neighboring and merged walls have been ignored in calculation.
6	Chapter 4.3.17 the surface roughness length depends on the wind direction since the frontal area are different in different aspect. It is not clear how this feature were handled during the calculation.	The effect of frontal area in a particular wind direction could not be taken into account as existing software tools such as UMEP and UME for computation of frontal area did not yield satisfactory results in the complex urban environment of Delhi UA. Further improvement in these tools for automated

S. No.	Remarks	Answers
	<p>What is the reason that there are several straight line (and elevation difference) in the northern part of the study area in fig 4-9?</p> <p>Is this measurement error affected the key results of the thesis?</p>	<p>computation of λ_f may improve computation of z_o (p 108).</p> <p>The several straight lines in the northern part are mainly due to road network which has lower elevation, hence lower roughness length value.</p> <p>This does not affect the key results as it is not a measurement error.</p>
7	<p>About Section 5.2 WRF is weather model and output is called climate indicator. In the research 3 day long simulations were applied. It is contradictory because for the calculation of climate indicators 30 or at least multiyear climate datasets are necessary.</p>	<p>To carry out the short term forecasts of WRF model at high grid resolution, GFS forecast data of 0.25 degree have been utilized as initial and boundary conditions which is forecasted using long term climate data. As model forecast indirectly includes long term data, it is considered as climate indicator.</p>
8	<p>Chapter 5.4 the relationship of SUHI and UCLHI were evaluated in seasonal aspect. Since UCLHI was simulated only for a couple of days these conclusions are not entirely established.</p>	<p>Due to limitation of computational resources, the requirement of which is very high at 500m grid resolution, the simulations have been carried out only for 3 days. However, an increase in computational resources available may assist in carrying out the simulations for longer duration in future research (p 10 and 203).</p>
9	<p>About Chapter 6.2.2.1 Post classification filtering is skipped in WUDAPT method. Without it the LCZ map will be fragmented with multiple small 100 m sized patches. Since it is “Local climate “zones, the map should represent the local scale climate features.</p> <p>The GIS LCZ mapping method is promising. However it has the same error in case of below local scale patches on the map. Since the evaluation of urban area based on 50 m grid size the proper explanation for this is micro climate zones. Some post classification filtering like in WUDAPT method would help the result of GIS method.</p>	<p>Post classification filtering applied and methodology appended (p162).</p> <p>Post classification filtering have already been applied to GIS LCZ mapping method.</p>

S. No.	Remarks	Answers
10	<p>Chapter 1 (Introduction) is unnecessarily detailed. There are several not so important information what is repeated in this chapter (e.g. urbanization, climate change).</p> <p>Chapter 1.6 and 1.8 is unnecessary.</p>	<p>Modified as suggested.</p> <p>Generally used format in the institute have been followed.</p>
11	<p>On several occasions the paragraphs are too long. It does not properly separate the sub-information for a given topic. This feature makes the thesis hardly readable.</p>	<p>Corrections have been carried out as suggested.</p>
12	<p>A summary of a main chapter is unnecessary (e.g. chapter 2.11, 3.6 etc.)</p>	<p>Summary of each chapter has been provided to highlight the key findings of the chapter.</p>
13	<p>In my point of view, the style of citations is not convenient. However, the thesis uses consistent style.</p>	<p>The style of citations have been modified to alphabetical order.</p>
14	<p>In chapter 1.3 the candidate states that the best available resolution of climate indicators in free domain is 12.5 km. Without any citation it is hard to evaluate this statement.</p>	<p>Citation appended (p6).</p>
15	<p>In chapter 1.6 the candidate introduce several parameters without any citations.</p> <p>It is not appropriate that the citations are not separated by space from the last word of the sentences. In case the citation is inside the sentences, there are space.</p>	<p>Citations added (p8).</p> <p>Spacing corrected.</p>
16	<p>Page 34: References are missing. Various methods such as fish eye photographs [132], scaled models, evaluation of GPS signals and 3D urban database had been applied for computation of SVF”.</p>	<p>All citation have been appended (p35).</p>
17	<p>Page 64: There are no reference Pleiades Satellite data source.</p>	<p>Citation added (p66).</p>
18	<p>Page 72: There are no reference for the Geomatica SVF calculator tool.</p>	<p>Citation appended (p74).</p>
19	<p>Typing Errors</p> <p>The measure are usually not separated from the value (e.g. 500 m), but several occasions there are space (e.g. 2.5 m).</p>	<p>All errors corrected.</p>

S. No.	Remarks	Answers
	Page 2, 8, 9, 18, 24, 30, 32,35, 43,46,49, 83, 123, 129, 145, Table 2.1 equations are unreadable and several parts equation are missing in row 5.	The formatting of Table 2-1 changed to make the equations readable (p 20).
20	On page 58 the candidate states “Winters are cold and dry and continues from the month of December to January”. Next paragraph presents that the temperature ranges from 10 to 25. At Global scale this temperature is hard to be regarded as cold.	The paragraph have been modified to make it clearer(p 58)
21	In figure 3-9 there is only one category in the high resolution part. In this case high resolution has no additional information.	Figure modified (p 59).
22	The legend and the colors in figure 4-24, 4-28 and 4-29 do not help to evaluate the buildings in the study area.	The legend has been modified with fewer classes to make it clearer. (p 95, 98, 99).
23	Local Climate Zonation (LCZ) scheme is Local Climate Zone (LCZ) scheme.	Modified as suggested.
External Examiner 2 : Indian Examiner 1		
Comments		
<ul style="list-style-type: none"> • Study is a significant contribution in the area • Research questions well formulated. • Adequate review of Literature. • The processing steps are explained adequately. • Study is a good approach to link urban parameters, RS derived geophysical parameters and a modeling framework. • Well planned, executed and written work 		
Observations		
1	Graphical Summary of meteorological observations in Delhi	Graphical Summary provided(p 60)
2	i. Accuracy of DTM, especially as it influences building height? ii. Surface height variation of roofs and their influence on various UCP?	i. The accuracy table of DTM added (Section 4.5.1, p105, Table 4-12). ii. In this study, Surface height variation of roofs obtained at 1m resolution has been aggregated at 30 m spatial resolution. Hence, it was considered that their influence on UCPs computation is minimal.

S. No.	Remarks	Answers
	<p>iii. Effect of choice of spatial aggregation on UCP (30 m has been adopted)?</p> <p>iv. Calibration/validation of some of the surface parameters for model houses?</p> <p>v. Evaluation of height bias with height of building and its impact on UCP?</p>	<p>iii. The 30 m grid size has been chosen after few experiments carried out at coarser grid sizes to minimize strong averaging effect on building heights. However, the choice of grid size further can be analyzed in future at different grid resolutions to investigate its impact on UCPs (p 202).</p> <p>iv. Since, no existing 3D GIS database was available for the study area, the validation of computed UCPs was not envisaged as part of this study. However, the study has already been taken up as part of future research and same has been integrated in the further scope of the research (p 202).</p> <p>v. Evaluation of height bias have been carried out in three broader groups (Pl refer Table 4-13 p 105). Since, the bias in building height found to be sub-meter level in all height groups, effect of bias has not been considered in this study.</p>
3	<p>i. Are 3-day periods sufficient to explore the relation?</p> <p>ii. Is LST valid parameter to test the relationship, given unknown accuracy of LST retrieval in a complex condition of urban landscape?</p> <p>iii. WRF ability to capture urban climate at 500m resolution is not explicitly demonstrated in the study?</p>	<p>i. Ideally longer duration should be used for exploring the relationship. However, high resolution simulation (500m grid resolution) with WRF model is computer resource intensive, hence only few days simulation could only be carried out. In future, with the increasing computational resources, the simulations may be carried out for longer durations (p 203).</p> <p>ii. LST derived from thermal remote sensing data is the only data which provides the spatially variable temperature data at highest possible resolution which is not possible to obtain through ground based in-situ observations.</p> <p>iii. At 500 m resolution, WRF model is able to pick up meso-scale variations such as diurnal variation of SUHII, UCLHII and</p>

S. No.	Remarks	Answers
		variation in different ventilation classes. However, the grid resolution of 500 m have been found still too coarse for analyzing the relationship with UCPs and among various urban built form classes. Further downscaling of WRF simulations as part of future research work by coupling it with high resolution urban climate models may assist to analyze intra-urban variations. (p 203).
4	Alphabetical order for reference	Implemented
External Examiner 3 : Indian Examiner 2		
Observations		
1	The study has multiple components UCP, UCP n LST relationship, WRF simulations, LCZ mapping with WUDAPT and RS based methods, modification of LCZ criterion, LCZ n LST, Ventilation assessment maps. The study fails to link them properly and conclude comprehensively. It would have been a good contribution if the scholar had restricted to only UCP or only WRF i.e. any one or two components.	Linkages between different components of the study have been mentioned (p 7, 189).
2	Methodology is very brief and does not include the sub-methodologies (?) mentioned in various chapters (Ref. chapter 4, 5, 6)	Methodology provided in the first chapter provides overview of methodology adopted to carry out this study. Sub-methodologies adopted to undertake various aspects of an objective have been explained in one chapter along with results and discussions for better clarity and continuity which would not have been so if all methodologies adopted for different aspects of all objectives would have been explained in the beginning.
3	The objectives have no mention of LCZ but LCZ is being discussed and analyzed. Why?	LCZ being one of the application of retrieved UCPs have been discussed and further demonstrated as part of broader objective (Objective 3).

S. No.	Remarks	Answers
4	<p>Urban Canopy Parameters (UCP) should be defined properly.</p> <p>What is the criteria for the selection of UCPs (for the study)?</p>	<p>The definition have already been given in Section 2.5(p 18).</p> <p>Retrievability of UCPs from Optical Satellite VHRS stereo have been the criteria for selection of UCPs.</p>
5	<p>Table 2-1: Whether the source given here is for all listed parameters description or just for one parameter description?</p> <p>What is parameter description?</p> <p>Are there sub-parameters (If I may say so) defining or describing the parameter or different descriptions or definitions of the same parameter?</p>	<p>Sources given for one parameter group is for all parameters in that group.</p> <p>Parameter description is the name of the parameter. Heading in the table have been modified to avoid the ambiguity (Table 2-1).</p> <p>Definitions and implication of different parameters on urban climate have been presented in Table 2-2.</p>
6	<p>Section no. 2.6: Why is this being discussed?</p> <p>What do you mean by “methods for spatially variable urban climate indicators”?</p>	<p>Study of advantages and disadvantages of various methods has been done to identify the most suitable method compatible with current geospatial technologies in order to provide spatially variable information on UCPs.</p> <p>Method for spatially variable urban climate indicators meant the methods which provides spatially variable information on urban climate indicators which is not available from sparse in-situ measurements.</p>
7	<p>Section 4.3.1.6</p> <p>How is the accuracy assessment done?</p> <p>Please give the accuracy matrix.</p>	<p>Accuracy assessment of building heights has referred to validation of building heights. The title have been modified accordingly (p 72).</p> <p>The results of the validation of building heights have been explained in Section 4.5.1 p 105.</p>
8	<p>Section 4.3.4</p> <p>How many samples were chosen for accuracy assessment?</p>	<p>40 randomly distributed samples of Fish eye photographs have been obtained from ground for the accuracy assessment of Sky View Factor (SVF) (p 74).</p>

S. No.	Remarks	Answers
9	Fig 4-7 Why is building Height map being considered as part of surface cover computation when it doesn't get mentioned in section 4.3.6.	Building height map have been utilized to extract building surface area as pixels more than 2 m in height only been considered as Building Surface, already mentioned in section 4.3.6.1(p 76).
10	Building material and anthropogenic are very critical to UHI studies. Why these parameters are not considered in the study?	Building material extraction needs use of very high resolution hyperspectral remote sensing data while Anthropogenic heat assessment is done using very high resolution thermal remote sensing data and both these datasets (VHRS hyperspectral and thermal) were not available, hence, these are not considered in this study.
11	How many scenes are being used for LST computation n why?	4 scenes have been utilized for computation of LST to analyze the seasonal variation in 4 prevailing seasons of study area. (p 119).
12	What is date and time of the scene? If only one scene is being used then how do you draw such major conclusions on the basis of just one scene?	The date and time of the scenes is given in Table 5-2 (p117). 4 scenes have been utilized for analysis. The analysis provides information on intra-class variation, which has relative variation. However, more number of scenes spreading over a duration may also be studied in future(p 117).
13	Fig 5-16 onwards_ color scheme and interval should have been kept uniform.	Color Scheme have been modified as suggested. However, interval was defined based on the characteristics displayed by every parameter (p 145-146).
14	Why LCZ based study being considered as part in this research when it is being done in isolation?	LCZ based study have been carried out to demonstrate the application of computed UCPs through demonstration of GIS based LCZ map. WUDAPT map has only been used to highlight significant improvement in accuracy of GIS based LCZ map after employing the computed UCPs from Optical VHRS stereo data.
15	Section 6.1- Last paragraph. What does it mean?	The last paragraph mentions what all have been studies/discussed in the chapter thereafter.
16	Section 6.2.2.2Is it GIS based or RS based LCZ map.	The classification has been called as GIS based LCZ as the integration of RS derived

S. No.	Remarks	Answers
		layers and ground based information have been carried out in GIS. Some of the inputs such as heavy industry, large low rise, road network have been obtained and refined with the help of ground knowledge, published maps and master plan documents. Hence, it is called as GIS based LCZ classification.
17	Section 6.2.2.2 and Section 6.3.3 have same title.	Section 6.2.2.2 explains the methodology to generate GIS based LCZ classification while section 6.3.3 presents the results of the classification and intermediate steps.
18	<p>Section 6.3.3.1: Why should the LCZ criteria should be modified?</p> <p>What is the basis of modification?</p> <p>The criteria range in LCZ original have been evolved based on a logic. What is the logic or basis for modification?</p>	<p>Only the range of the LCZ criteria have been modified not the criteria itself.</p> <p>The modifications in the LCZ criteria range have been carried out with respect to ground truth collected during filed survey.</p> <p>The original LCZ criteria have been evolved based on the study conducted in cities of developed regions which shows considerable variations in case of cities in developing regions especially in Indian context. Therefore, the criteria range are modified to address the conditions in the Indian context.</p>
19	Table no. 6.4: the modified values for BSF original LCZ is in the range of 50-90, 75-95and 90-100. Please explain. How can they all fall in compact category?	Original values of BSF for LCZ 1, 2, 3 is given for compact category. Modified range is higher than original range, hence they all fall in compact category.
20	<p>What is the major conclusion of the overall study?</p> <p>The research scholar is asked to revise the last chapter with the addition of overall conclusions.</p>	<p>Major conclusion of the study states that Optical VHRS stereo data can be recommended for retrieval of UCPs which can be further utilized effectively for urban climate modeling and research studies. Key findings of the study already have been mentioned in section 7.2(p 189),</p> <p>The application of UCPs have been discussed in section 2.10 and two</p>

S. No.	Remarks	Answers
	<p>What are the applications of a study like this?</p> <p>Are they generic or city specific?</p>	<p>applications have been demonstrated in Chapter -6.</p> <p>The methodologies developed in the study are generic, however, the characterization and analysis is city specific.</p>
21	<p>The research scholar should explain how chapter no. 04, 05 and 06 are linked and what are the conclusion from their linkage?</p>	<p>The relationship derived/explained in Chapter 5 is based on analysis of relationship with UCPs derived in Chapter 4. While Chapter 6 presents the results of application of UCPs (LCZ and ventilation assessment) retrieved in Chapter 4 and also analyses the relationship of LCZ and ventilation assessment with spatially variable climate indicators modeled in Chapter 5 (p 7, 65, 189).</p> <p>It concludes that Optical VHRS Stereo data can be utilized for computation of UCPs in complex urban environment which can be further employed successfully for various aspects of studies on urban climate research and modeling.</p>